

University of Southampton Research Repository ePrints Soton

Copyright © and Moral Rights for this thesis are retained by the author and/or other copyright owners. A copy can be downloaded for personal non-commercial research or study, without prior permission or charge. This thesis cannot be reproduced or quoted extensively from without first obtaining permission in writing from the copyright holder/s. The content must not be changed in any way or sold commercially in any format or medium without the formal permission of the copyright holders.

When referring to this work, full bibliographic details including the author, title, awarding institution and date of the thesis must be given e.g.

AUTHOR (year of submission) "Full thesis title", University of Southampton, name of the University School or Department, PhD Thesis, pagination

UNIVERSITY OF SOUTHAMPTON

FACULTY OF ENGINEERING AND THE ENVIRONMENT

**Experimental Study, Mathematical Modelling and Dynamical Analysis of
Magnetorheological Elastomer Materials and Structures for Vibration Control**

by

Guanghong Zhu

Thesis for the degree of Doctor of Philosophy

August 2015

UNIVERSITY OF SOUTHAMPTON

ABSTRACT

FACULTY OF ENGINEERING AND THE ENVIRONMENT

Thesis for the degree of Doctor of Philosophy

EXPERIMENTAL STUDY, MATHEMATICAL MODELLING AND DYNAMICAL ANALYSIS OF MAGNETORHEOLOGICAL ELASTOMER MATERIALS AND STRUCTURES FOR VIBRATION CONTROL

Guanghong Zhu

As a smart material, magnetorheological elastomer (MRE) is composed of magnetisable particles dispersed in a non-magnetic medium. Because the mechanical properties of MRE can be continuously, rapidly and reversibly controlled by adjusting magnetic field in a pre-yield regime, there has been increasing research on MRE for mitigation of unwanted vibrations, and yet the application and commercialisation in various fields are still on a very early stage. Considering the dependence of mechanical properties on strain, frequency and magnetic field the current research on mathematical modelling for MRE is still insufficient to provide guidelines for engineering applications.

In this study, the dynamical properties of MRE were studied by means of shear tests under different driving frequencies (1-80Hz), strain amplitudes (0-6.0%) and magnetic fields (0-500mT). The experimental results have shown that the storage modulus of MRE increases as the frequency increases, but the loss modulus initially increases with frequency (<10Hz) up to a maximum value and then decreases with further increasing frequencies; both the storage modulus and loss modulus decrease with an increase of strain, and they increase with increasing magnetic flux densities until the magnetic saturation occurs. With the full use of gathered information on mechanical property characterisation of MRE, a nonlinear mathematical model is established to describe the complex behaviour of MRE for the dynamical analysis of vibration systems, and a methodology of modelling is proposed for materials to continuously describe the dynamic behaviour in certain region of strain and frequency with a benefit of low requirement for the calculation on parameter identification. A structure of MRE is developed with a high bearing capacity and a good controllability of stiffness to benefit vibration control systems. The dynamical properties of this structure are predicted with the dynamic design and the mathematical modelling, and the results are examined through dynamic tests to validate that the extension of this mathematical model in MRE structures. Furthermore, dynamical analysis is presented for a two-stage vibration isolation system, a vibration absorption system and an isolation system consists of a continuous beam and an MRE isolator to examine the efficiency of MRE absorbers and isolators. Results show that a reduction of the vibration amplitude, the force transmissibility or the power flow transmissibility can be achieved by properly designing dynamical systems and considering the excitation frequency ranges. Comparing with conventional absorbers and isolators, MRE devices can locally and globally improve the performance of vibration control significantly from the perspective of dynamical behaviour, transmissibility or vibratory energy transmission.

Contents

Chapter 1 Introduction	1
1.1 Background	1
1.2 Aims and objectives	2
1.3 Novelty	3
1.4 Thesis structure	5
Chapter 2 Mechanical properties, modelling and applications of MRE	7
2.1 Fabrication of MRE	7
2.1.1 Selection of matrix and particles.....	7
2.1.2 Influence of magnetisation.....	8
2.1.3 Influence of coupling agents.....	10
2.2 Mechanical properties of MRE	10
2.2.1 Payne effect	10
2.2.2 Mullin effect	12
2.2.3 MR effect	12
2.3 Dependences of MRE	15
2.3.1 Frequency dependence.....	15
2.3.2 Temperature dependence	16
2.4 Mathematical modelling of MRE.....	16
2.4.1 Linear models	16
2.4.2 Nonlinear models.....	20
2.5 Applications of MRE	24
2.5.1 MRE based vibration absorber	24
2.5.2 MRE based vibration isolator	26
2.5.3 MR structures.....	29

2.5.4	Feasibility study of MRE	31
2.6	Motivation for current work	33
Chapter 3 Experimental setup for dynamical property characterisation of MRE.....		35
3.1	Introduction	35
3.2	Experimental setup	35
3.2.1	MRE samples preparation	35
3.2.2	Dynamic test apparatus	37
3.2.3	Data process method	39
3.3	The influence of microstructure on MRE mechanical properties	40
3.3.1	The influence of magnetisable particles	40
3.3.2	The influence of magnetic field	43
3.3.3	The influence of coupling agents	50
3.4	Summary	53
Chapter 4 Mechanical properties of MRE		55
4.1	Introduction	55
4.2	Dependence on magnetic field	55
4.3	Dependence on strain	60
4.4	Dependence on frequency	63
4.5	Conclusions	67
Chapter 5 Mathematical modelling for MRE		69
5.1	Introduction	69
5.2	Modelling for dynamical properties of MRE	70
5.2.1	Modelling method for MRE	70
5.2.2	Nonlinear analysis on MRE modelling	74
5.3	Mathematical modelling for MRE structure	76
5.3.1	Dynamic design for MRE structure	76
5.3.2	Experimental validation of dynamic design	77

5.4	Summary	81
Chapter 6	Two-stage Nonlinear MRE Vibration Isolation Systems	83
6.1	Introduction	83
6.2	Equations of motion	83
6.2.1	Standard form of equations of motion	83
6.2.2	Steady state response of system	87
6.3	Efficiency analysis of vibration isolation system	91
6.3.1	Analysis of dynamical characteristic	91
6.3.2	Analysis of isolation characteristic	93
6.4	Numerical results and discussions	94
6.4.1	Influence of linear parameters	94
6.4.2	The influence of non-linearity	97
6.5	Summary	102
Chapter 7	MRE Vibration Absorption Systems	105
7.1	Introduction	105
7.2	Equations of motion	105
7.2.1	Standard form of equations of motion	105
7.2.2	Steady state response of system	108
7.3	Efficiency analysis of vibration absorption system	111
7.3.1	Analysis of dynamical characteristic	111
7.3.2	Analysis of absorption characteristic	112
7.4	Numerical results and discussions	113
7.4.1	Influence of linear parameters	113
7.4.2	The influence of non-linearity	116
7.5	Summary	122
Chapter 8	Nonlinear MRE Isolation Systems with a Flexible Base	125
8.1	Introduction	125

8.2	Equation of motion.....	126
8.2.1	Standard form of equations of motion	126
8.2.2	Steady state response of system.....	128
8.3	Efficiency analysis of vibration isolation system.....	131
8.3.1	Analysis of isolation characteristics.....	131
8.3.2	Power flow analysis	131
8.4	Numerical results and discussions.....	133
8.4.1	The influence of linear parameters.....	133
8.4.2	The influence of non-linearity.....	140
8.5	Summary	148
Chapter 9	Conclusions	151
9.1	Mechanical properties of MRE	151
9.2	Mathematical modelling for MRE	152
9.3	Applications for vibration control	153
Chapter 10	Recommendations for future work	155
	List of Publications.....	157
	References	159
	Appendices	169
	Appendix I	169
	Appendix II.....	171
	Appendix III.....	172
	Appendix IV	173
	Appendix V.....	174

List of Figures

Figure 2.1 SEM images of (a) isotropic MREs and (b) anisotropic MRE.....	9
Figure 2.2 The sketch of mechanism of MR elastomers under magnetic field.	9
Figure 2.3 Experimental result of filled rubber: (a) storage modulus and (b) loss modulus at different amplitudes and frequencies	11
Figure 2.4 Storage modulus and loss modulus of MRE under different strain amplitudes.	11
Figure 2.5 Stress-strain plots of MRE with different magnetic field at a fixed strain amplitude of 0.2% and a driving frequency of 5 Hz	13
Figure 2.6 Dependence of storage modulus and loss modulus of isotropic MRE with different concentrations of 40 μm iron particles in silicone on the magnetic flux density	14
Figure 2.7 Storage modulus and loss modulus by oscillatory tests under different driving frequency.....	15
Figure 2.8 (a) Temperature-dependent modulus of MRE and (b) Stress-strain curve of MRE at different temperatures.	16
Figure 2.9 Stress-strain plot for linear viscoelastic material under sinusoidal actuating loading and the relationship between geometry and dynamic properties.	17
Figure 2.10 Kelvin-Voigt model for MRE.	19
Figure 2.11 Three-parameter Kelvin viscoelastic model for MRE.....	21
Figure 2.12 Three-parameter Maxwell viscoelastic model for MRE	21
Figure 2.13 Four-parameter viscoelastic model for MRE	22
Figure 2.14 General Maxwell viscoelastic model for MRE.	22
Figure 2.15 Stress–strain relationships with various magnetic fields at strain amplitude of 10%.	23

Figure 2.16 ATVA (a) Sketch: 1. Oscillator: 2. MR elastomers: 3. Magnetic conductor: 4. Coils; (b) Photograph.....	25
Figure 2.17 (a) A compact MR elastomer ATVA: 1. Cover, 2. Guide rod, 3. Linear bearing, 4. Magnetic conductor, 5. Shear plate, 6. MREs, 7. Base, 8. Electromagnet, 9. Mounting shell. (b) Schematic of a compact squeeze MRE absorber.....	26
Figure 2.18 The MRE ATVA (a) schematic diagram and (b) photograph: (1) mounting shell; (2) MRE; (3) helical spring; (4) shear block; (5) magnetic conductor; (6) guide rod; (7) connector of the voice coil motor and the shell; (8) voice coil motor; (9) flange; (10) base.....	26
Figure 2.19 Schematic diagram of the MRE seat isolator	28
Figure 2.20 Laminated MRE based isolator. (a) Schematic diagram (b) Prototype of the isolator....	29
Figure 2.21 (a) Cross-section of the MRE base isolator (b) Typical laminated rubber isolator.	29
Figure 2.22 Diagrams of (a) an MRE-based composite wall supporting equipment and (b) an MRE-based composite floor supporting equipment.....	30
Figure 2.23 Schematic diagram of sample with holes of MRF and MRG.....	31
Figure 2.24 Microscopic structures of PCL-blended MRE where (a) before the preforming configuration, (b) and (c) after the preforming configuration, respectively, corresponding to the two states when the temperature is below and above PCL melting point, and (d) and (e) are the enlarged views of the distribution of particles in the matrix corresponding to (b) and (c).....	31
Figure 2.25 Relationship between MR effect and number of cycles for structured MRE with (a) 60%, (b) 70%, and (c) 80% iron particles by mass, under various fatigue strain amplitudes.	33
Figure 2.26 (a) Stress amplitude versus log cycles to failure and (b) Stress softening behaviour in an engineering stress controlled fatigue test.....	33
Figure 2.27 (a) Modulus after cyclic loading and (b) Relationship between MR effect and cycle numbers.....	33
Figure 3.1 Shear test rigs for MRE samples with circular disc magnets.	37
Figure 3.2 (a) MRE samples. (b) Experimental setup.	38

Figure 3.3 Stress-strain plot for MRE material under harmonic load.....	39
Figure 3.4 Storage modulus of (a) silicone rubber and (b) isotropic MRE with different strain amplitude and loading frequency.....	41
Figure 3.5 Loss modulus of (a) silicone rubber and (b) isotropic MRE with different strain amplitude and loading frequency.....	42
Figure 3.6 Loss factor of (a) silicone rubber and (b) isotropic MRE with different strain amplitude and loading frequency.....	43
Figure 3.7 Storage modulus of (a) isotropic MRE and (b) anisotropic MRE with different strain amplitude and loading frequency.....	44
Figure 3.8 Storage modulus of (a) isotropic MRE and (b) anisotropic MRE at 10 Hz with different strain amplitude and magnetic field.	45
Figure 3.9 Loss modulus of (a) isotropic MRE and (b) anisotropic MRE with different strain amplitude and loading frequency.....	46
Figure 3.10 Loss modulus of (a) isotropic MRE and (b) anisotropic MRE at 10 Hz with different strain amplitude and magnetic field.	47
Figure 3.11 Loss factor of (a) isotropic MRE and (b) anisotropic MRE with different strain amplitude and loading frequency.....	48
Figure 3.12 Loss factor of (a) isotropic MRE and (b) anisotropic MRE at 10 Hz with different strain amplitude and magnetic field.	49
Figure 3.13 Storage modulus of anisotropic MRE (a) without silicone oil and (b) with silicone oil at different strain amplitude and magnetic field.....	50
Figure 3.14 Loss modulus of anisotropic MRE (a) without silicone oil and (b) with silicone oil at different strain amplitude and magnetic field.	51
Figure 3.15 Loss factor of anisotropic MRE (a) without silicone oil and (b) with silicone oil at different strain amplitude and magnetic field.	52
Figure 4.1 Stress-strain plot with varying magnetic flux densities under quasi static loading for (a) isotropic MRE and (b) anisotropic MRE.	56
Figure 4.2 Stress-strain plot at 10Hz with different magnetic flux densities for (a) isotropic MRE and (b) anisotropic MRE.....	57

Figure 4.3 Dependence of storage modulus on magnetic field at 10Hz.	58
Figure 4.4 Dependence of loss modulus on magnetic field at 10Hz.....	58
Figure 4.5 Dependence of loss factor on magnetic field at 10Hz.	59
Figure 4.6 Dependence of relative MR effect on magnetic field at 10Hz.	59
Figure 4.7 Stress-strain plot at 10Hz with different strain amplitudes of (a) isotropic MRE and (b) anisotropic MRE.	61
Figure 4.8 Dependence of storage modulus on strain amplitude at 10Hz.	62
Figure 4.9 Dependence of loss modulus on strain amplitude at 10Hz.....	62
Figure 4.10 Dependence of loss factor on strain amplitude at 10Hz.	63
Figure 4.11 Dependence of relative MR effect on strain amplitude at 10Hz.	63
Figure 4.12 Stress-strain plot at 1.5% strain amplitude with varying frequencies for (a) isotropic MRE and (b) anisotropic MRE.	64
Figure 4.13 Dependence of storage modulus on frequency at 1.5% strain amplitude.....	65
Figure 4.14 Dependence of loss modulus on frequency at 1.5% strain amplitude.	66
Figure 4.15 Dependence of loss factor on frequency at 1.5% strain amplitude.....	66
Figure 4.16 Dependence of relative MR effect on frequency at 1.5% strain amplitude.....	67
Figure 5.1 Force-displacement hysteresis curves for anisotropic MRE with 30 vol.% of iron particles with different magnetic field strength values ^[110]	70
Figure 5.2 Kelvin-Voigt model of MRE.....	71
Figure 5.3 The equivalent stiffness of anisotropic MRE sample (a) when $B = 0$, (b) when $B = 160\text{mT}$	74
Figure 5.4 The equivalent damping of anisotropic MRE sample (a) when $B = 0$, (b) when $B = 160\text{mT}$	75
Figure 5.5 A schematic of MRE structure.	76
Figure 5.6 The designed stiffness of MRE structure (a) when $B = 0$, (c) when $B = 160\text{mT}$ and the designed damping of MRE structure (b) when $B = 0$, (d) when $B = 160\text{mT}$	78

Figure 5.7 Experimental setup for MRE structure.....	79
Figure 5.8 The experimental results of structural stiffness (a) when $B = 0$, (c) when $B = 160\text{mT}$ and the experimental results of structural damping (b) when $B = 0$, (d) when $B = 160\text{mT}$	79
Figure 5.9 The error between the predicted values and experimental results of stiffness for MRE structure (a) when $B = 0$, (c) when $B = 160\text{mT}$; and the error between the predicted values and experimental results of damping for MRE structure (b) when $B = 0$, (d) when $B = 160\text{mT}$	80
Figure 6.1 Two-stage vibration isolation system with MRE isolators.....	84
Figure 6.2 Experimental results of storage modulus when (a) $B = 0$, (b) $B = 500\text{mT}$	86
Figure 6.3 Experimental results of loss modulus when (a) $B = 0$, (b) $B = 500\text{mT}$	86
Figure 6.4 Response of the system	88
Figure 6.5 Poincare maps of the system	88
Figure 6.6 The influence of M_2 on natural frequencies of system.....	92
Figure 6.7 The effect of stiffness K_2 on the amplitude of vibration response.....	95
Figure 6.8 The effect of mass M_2 on the amplitude of vibration response.	96
Figure 6.9 The effect of stiffness K_2 on the transmissibility of system	96
Figure 6.10 The effect of mass M_2 on the transmissibility of system.....	97
Figure 6.11 The vibration responses of different systems.	98
Figure 6.12 The vibration response of system with MRE isolators.....	99
Figure 6.13 The vibration response of different systems.....	99
Figure 6.14 The force transmissibility of different systems	100
Figure 6.15 The transmissibility of system with MRE isolators	101
Figure 6.16 The force transmissibility of different systems	102
Figure 7.1 Vibration system with an MRE absorber.	106
Figure 7.2 Response of the system.	108

Figure 7.3 Poincare maps of the system.	108
Figure 7.4 The influence of M_I on natural frequencies of this composite system.	111
Figure 7.5 The effect of mass M_I on the amplitude of vibration response	114
Figure 7.6 The effect of damping C_I on the amplitude of vibration response	115
Figure 7.7 The effect of mass M_I on the transmissibility	115
Figure 7.8 The effect of damping C_I on the transmissibility	116
Figure 7.9 The vibration responses of different systems	117
Figure 7.10 The vibration responses of MRE absorption systems	118
Figure 7.11 The vibration responses of different systems.	119
Figure 7.12 The transmissibility of different systems.	120
Figure 7.13 The transmissibility of MRE absorption systems.....	121
Figure 7.14 The transmissibility of different absorption systems.....	121
Figure 8.1 Dynamic interaction system comprising a machine, an isolator and a beam.	126
Figure 8.2 Response of different systems.	134
Figure 8.3 Amplitude Spectrum of $Y_1(t)$	135
Figure 8.4 (a) The influence of base on the vibration amplitude of Y_2 and (b) the vibration amplitude of Y_1	136
Figure 8.5 The influence of base on the transmissibility	136
Figure 8.6 The influence of base on the input power	137
Figure 8.7 The influence of base on the power transmission	138
Figure 8.8 The influence of base on the isolated vibratory power.....	138
Figure 8.9 Response of Y_1 in different systems (a) at 20 Hz and (b) at 23 Hz, (c) response of Y_2 at different frequencies.....	139
Figure 8.10 The vibration amplitude of (a) Y_1 and (b) Y_2 in different vibration systems.	141
Figure 8.11 The vibration amplitude of (a) Y_1 and (b) Y_2 in MRE isolation systems	141

Figure 8.12 The vibration amplitude of (a) Y_1 and (b) Y_2 in different isolation systems.	142
Figure 8.13 The transmissibility in different vibration systems	143
Figure 8.14 The transmissibility in different MRE isolation systems	143
Figure 8.15 The transmissibility in different isolation systems	144
Figure 8.16 (a) The input power and (b) the isolated power in different vibration systems.....	145
Figure 8.17 The power transmitted to the base in different isolation systems	146
Figure 8.18 (a) The input power and (b) the isolated power in different MRE vibration systems ...	146
Figure 8.19 The power transmitted to the base in different MRE isolation systems.....	147
Figure 8.20 (a) The input power and (b) the isolated power in different vibration systems.....	148
Figure 8.21 The power transmitted to the base in different isolation systems	148

List of Tables

Table 3.1 Fabrication of small-sized samples.....	36
Table 3.2 Pot lives and curing times at various temperatures.....	36
Table 3.3 Test apparatus for small-sized samples	38
Table 5.1 Experimental parameters in expressions of storage modulus and loss modulus.	72
Table 5.2 Parameters for the expressions of spring force and the damper force.	77
Table 6.1 Parameters of stiffness and damping	87
Table 7.1 Parameters of designed stiffness and damping.	107
Table 8.1 Parameters of designed stiffness and damping	134

Declaration of Authorship

I, *Guanghong Zhu*, declare that this thesis and the work presented in it are my own and has been generated by me as the result of my own original research.

Experimental Study, Mathematical Modelling and Dynamical Analysis of Magnetorheological Elastomer Materials and Structures for Vibration Control

I confirm that:

1. This work was done wholly or mainly while in candidature for a research degree at this University;
2. Where any part of this thesis has previously been submitted for a degree or any other qualification at this University or any other institution, this has been clearly stated;
3. Where I have consulted the published work of others, this is always clearly attributed;
4. Where I have quoted from the work of others, the source is always given. With the exception of such quotations, this thesis is entirely my own work;
5. I have acknowledged all main sources of help;
6. Where the thesis is based on work done by myself jointly with others, I have made clear exactly what was done by others and what I have contributed myself;
7. Parts of this work have been published as listed in publications.

Signed:

Date:

Acknowledgements

Firstly, I gratefully acknowledge the invaluable help from my supervisors Associate Prof. Yeping Xiong, Prof. Stephen Daley and Prof. Ajit R Shenoi. Without your advice, encouragement and patience, this thesis would not reach its present level. Another special acknowledgement goes to Yeping for all the suggestions on my project work during my PhD study.

I would like to thank my colleague Ms Kyriaki Sapouna who gave me kind encouragement and helpful instructions through the design of experiments. I would also like to express my gratitude to colleagues in this research group, Dr. Jian Yang, Mr Pengfei Xiong and Mr Yuan Li for the helpful discussions. The help from technicians Mr Peter Sellen and Mr Dave Beckett is also appreciated.

The financial support from the Faculty of Engineering and the Environment (FEE), the Lloyd's Register Educational Trust (LRET), and the China Scholarship Council is gratefully acknowledged. I would extend my sincere thanks to Yeping for her encouragement and great help to my applications for these scholarships.

Finally I would like to thank my husband, my parents and my sister for their love and great encouragement through all these years.

Thank you all very much!

Guanghong

Nomenclature

Symbol	Meaning	Units
A	cross sectional area	m^2
B	magnetic field strength	tesla
C	damping coefficient	$\text{N}\cdot\text{s}/\text{m}$
D	thickness	m
E	Young's modulus	Pa
EI	bending stiffness	$\text{N}\cdot\text{m}^2$
G	shear modulus	Pa
K	stiffness	N/m
M'	storage modulus	Pa
M''	loss modulus	Pa
S	displacement	m
T	period	s
γ	shear strain	-
ε	normal strain	-
ρ	mass density per unit length	kg/m
σ	normal stress	Pa
τ	shear stress	Pa
ω	angular frequency	rad/s

Abbreviation

Abreviation	Full version
ATVA	Adaptive tuned vibration absorber
MRE	Magnetorheological elastomer
MRF	Magnetorheological fluid
SDOF	Single degree of freedom
TVA	Tuned vibration absorber

Chapter 1 Introduction

1.1 Background

In order to avoid the problems due to vibration as much as possible in engineering applications, it is necessary to develop vibration control techniques all the time. The vibration control technique is widely used to suppress vibrations either locally for flexible structures or globally for rigid structures in various fields, such as civil engineering, automotive industry, aircraft industry and watercraft industry. As a conventional approach, passive vibration control is advantageous for its simplicity and ease of implementation; however, the limitation of adaptability makes it fail to satisfy advanced requirements. Considering that many practical systems have time-varying vibration sources or wide vibration bandwidth, active control is an ideal strategy for great vibration control performance, but it has drawbacks such as power requirement, cost and complexity. Because of the combination of the versatility of active control and reliability of passive control, semi-active (adaptive-passive) vibration control has attracted considerable attention over the past decades. Semi-active vibration control systems can adjust their resonance frequencies without consuming extra energy in real time, Therefore they have potential in engineering applications where high level of vibration control is required^[1,2].

Various smart materials, such as piezoelectric materials, shape memory alloys, controllable fluids and elastomers, have been used to tackle vibration problems as smart elements with different control schemes, because they have adjustable abilities for sensors, actuators and controllers by adding secondary sources such as thermal, magnetic or electric energy^[3]. Therefore, increasing effort has been devoted to making semi-active vibration control devices more utilizable by incorporating smart materials. Since 1948 the discovery of the magneto-rheological (MR) phenomenon by Rabinow^[4], MR materials have proven to be well suited to many applications. Numerous applications are based on MRF because of its MR effect, the dynamic yield stress can be continuously, rapidly and reversely controlled by the applied magnetic field^[5]. Such applications have been commercialised and industrialised in various fields such as motor damping, vehicle's suspension and earthquake resistance^[6,7,8]. Compared with the MRF, the application and commercialisation of MRE are still on an exploratory stage and the solid state of MRE can overcome many shortcomings of MRF including lower yield

stress, sensitivity to impurities, relatively high voltage supplies, liquid leakage and particle residue^[9]. The stiffness and damping properties of MRE can be continuously, rapidly and reversibly adjusted within its pre-yield zone by controlling an applied magnetic field, making this material suitable for semi-active vibration control systems^[10]. However, most of research on mathematical modelling for MRE is limited to presenting its linear mechanical properties which is not accurate due to the dependences on frequency, strain and field^[10,11]. Therefore, aiming at expediting the application and commercialisation of MRE, progressive research should spare no effort to develop mathematical models for precisely describing its dynamical properties.

This research is concerned with experimental characterisation of the dynamical properties of MRE. As a starting point, MRE samples are investigated in shear mode, but the methodology and results are expandable to compression mode because of the relationship between elastic modulus and shear modulus. In compression the elastic modulus is comparatively larger, so the relative change of elastic modulus resulting from the application of magnetic field is smaller than the relative change of shear modulus. Based upon the experimental research of mechanical properties for MRE a mathematical model is established to describe its dynamical behaviour and this mathematical model is employed to evaluate the efficiency of various MRE devices for vibration control in different dynamical systems. A challenge arises from precise description of the dynamical behaviour of MRE associated with frequency and strain dependences. To address this, a nonlinear mathematical model is proposed as an appropriate polynomial expression of frequency and strain. Another challenge arises from examining the vibration control effectiveness of MRE devices, and here various MRE devices are investigated to take dynamical behaviour, transmissibility and vibratory energy transmission into account in the selected dynamical systems.

1.2 Aims and objectives

The aims of this PhD project are: investigate the mechanical properties of MRE, propose a mathematical model to predict the dynamic behaviour of this material and apply this material to dynamical systems to control vibration transmissions adaptive to the changing operational conditions. The principal objectives are accordingly:

1. Mechanical property characterisation for MRE

The mechanical properties, including storage and loss moduli, are examined under dynamic loading conditions by designing and setting up a reliable measuring system. Firstly, the Instron E1000 Electro Plus in the Transport Systems Research Laboratory is employed to

perform dynamic loading tests, so as to obtain the experimental data for mechanical property characterisation of MRE. Secondly, the experimental data is processed following the Dynamic Mechanical Analysis directions for Instron E1000 ElectroPlus measurements to analyse the mechanical properties of MRE.

2. Mathematical modelling for MRE

A nonlinear mathematical model is proposed to predict the dynamic behaviour of MRE under different loading conditions. Firstly, based on the experimental results of mechanical property characterisation a model is established mathematically to describe the dependences of MRE on frequency and strain. Secondly, the nonlinear model is developed into a polynomial of frequency and strain to investigate the efficiencies of MRE absorbers and isolators in various vibration control systems.

3. Dynamic design of MRE structure

An MRE structure is designed to provide a good bearing capacity and a pronounced controllability of stiffness, and the mechanical properties of the MRE structure are predicted by the dynamical design and examined through the experimental research. Firstly, the MRE structure is designed based upon the experimental results of mechanical properties characterisation for MRE. Afterwards, the experimental research on the mechanical properties of the MRE structure is compared with the theoretical prediction through the dynamic design to verify the extension of all analytical discussion on the MRE.

4. Efficiency analysis for MRE isolators and absorbers

Different dynamic systems are selected to explore the performance evaluation on vibration control for MRE absorbers and isolators and provide guidelines for parameter selection in the dynamic design of MRE vibration control systems. Firstly, the dynamic designs for MRE absorbers and isolators are proposed on the basis of the dynamic design for MRE structures. Secondly, numerical simulation is carried out in Matlab to investigate the vibration characteristics of respective systems, and the efficiencies of vibration isolators and absorbers are evaluated from the perspective of dynamical behaviour, transmissibility and vibratory energy transmission.

1.3 Novelty

Due to the Payne effect, the Mullin effect and MR effect, the MRE is a nonlinear viscoelastic material with dependences of mechanical property on strain, frequency and magnetic field.

There are lots of experimental results on the stiffness properties of MRE, including the dependence of stiffness on frequency, strain and magnetic field; in this project the damping properties of MRE are also investigated to attain an integral research and model the dynamical behaviour for this material. Dynamic tests in shear mode are carried out to study the dependence of MRE, the mechanical properties are studied in a frequency range of 1 ~ 80Hz, a strain range of 1 ~ 5% and a magnetic field strength range of 0 ~ 500mT.

Accurate models to describe the complex dynamical behaviour are essential to step towards the industrialisation and commercialisation of MRE. Currently, most modelling on MRE material has focused on the linear dynamical behaviour, and there are a few models to describe the influence of magnetic field, driving frequency and strain amplitude on the dynamical behaviour. However, MRE material displays a non-linear strain-stress relationship, and there is still a lot of work to do on mathematical modelling. The majority of the research on modelling of dynamical properties of MRE focuses on the hysteretic behaviour of this material, which is effective for describing the effects of loading history on the dynamic response of MRE, but considering time-varying vibration sources in reality it is hard to apply these models in a wide bandwidth because the influence of loading history varies with frequencies. There are also many researchers who modelled the dependence of mechanical properties on magnetic fields for MRE, but these models are limited to static loading conditions. In this project, the comprehensive experimentation research enables a nonlinear mathematical model to represent the dynamic behaviour of MRE. In this model the spring force and the damping force is expressed in the form of polynomials, and the frequency and strain are independently continuous variables. Due to the low requirement of calculation on parameter identification with the full use of gathered information on mechanical properties, this methodology of modelling can be also applied to other materials to describe the dynamic behaviour in a certain range continuously.

The current investigation on dynamical properties of MRE on a large scale, which is essential for the application of MRE, is still deficient. Possessive research should spare no effort to develop a theoretical model to offer valid dynamical analysis of MRE structure and accurate evaluation of its vibration control efficiency. This study develops an MRE structure with a high bearing capacity and good controllability of stiffness, which can benefit vibration control systems. The stiffness and damping of this MRE structure are predicted by combining the dynamic design and the mathematical model. Subsequently this MRE structure is examined through dynamic tests in a frequency range of 1 ~ 60Hz, a strain range of 1 ~ 5% and a

magnetic field strength range of 0 ~ 160mT. Lastly the predictions are compared with the experimental results to validate that the mathematical model of MRE can be extended to MRE structures.

Comparing with the industrialisation and commercialisation of MRF the current application of MRE on vibration control is still at a very exploratory stage. In this project, the nonlinear mathematical model of MRE is used to evaluate the efficiency of vibration control in dynamical systems. Herein a two stage isolation system, an absorption system and an isolation system with a flexible base are presented. Aiming at providing guidelines for parameter selection in the dynamic design of MRE vibration control systems, the effective evaluation of vibration control is investigated from the perspectives of dynamical behaviour, transmissibility and vibratory energy transmission in selected dynamical systems. The control efficiency of MRE devices are compared with traditional devices and the influence of non-linearity on vibration control is also analysed.

1.4 Thesis structure

The thesis begins with a general overview of the current research of MRE. The fabrication, classification, fundamental mechanics, theoretical models and applications of MRE are reviewed to exhibit the research background and significance of this project. It is shown that the majority of current research on mathematical modelling of MRE is insufficient in the integration of nonlinearities due to the dependence of mechanical properties on strain, frequency and magnetic field, and the application of MRE in vibration control is on a very early stage because both the valid mathematical model and the experimental research on a large scale are deficient for accurately describing the dynamical behaviour of MRE vibration systems.

Chapter 3 elaborates the manufacturing of MRE samples and a methodology to characterise the dynamical properties of MRE in shear mode. The influences of ferromagnetic particle, magnetic field and coupling agent during solidification on mechanical properties of MRE are also discussed, respectively.

Chapter 4 investigates the dependences of mechanical properties on frequency, strain and magnetic field to provide useful information for mathematical modelling of MRE. The storage modulus and loss modulus in shear mode are examined in a range of frequencies from 1Hz to 80Hz, a range of strain amplitudes from 1% to 6% and a range of magnetic field intensities of 0 to 0.5T.

Chapter 5 proposes a mathematical model to continuously describe the dynamical behaviour of MRE. This nonlinear model is developed from the Kelvin Voigt model and based on the experimental results of mechanical property characterisation. An MRE structure is graphically designed and experimentally tested to examine the extendibility of this nonlinear model on a large scale, where the dependence on strain and frequency is utilised as inputs in the research on MRE vibration systems.

Chapter 6 analyses the effectiveness of MRE isolators within the context of a two-stage vibration system. The steady state response is obtained by formulating the motion equations, and the transmissibility of the isolation system is investigated by comparing different isolation systems. Reductions in the vibration response and isolation transmissibility can be obtained by properly selecting the parameters, which will provide guidelines for the dynamic design of two-stage MRE isolation systems. The numerical results show that when comparing with traditional isolators the isolation characteristic can be improved with MRE isolators by applying magnetic field at frequencies in the required regime.

Chapter 7 studies the dynamics of a vibration system with an MRE absorber. The motion equations are formulated to obtain the steady state response of system and the absorption characteristics are analysed for different parameters to evaluate the efficiency of vibration control. The results reveal that the vibration response and transmissibility can be effectively reduced with a proper parameter selection; thereby, this study is instructional for the dynamic design of MRE absorbers. The comparison of numerical results between traditional absorbers and MRE absorbers also displays that an improved absorption performance can be obtained with an adaptive MRE absorber by adjusting the applied magnetic field.

Chapter 8 investigates the performance evaluation on vibration control for MRE isolators within a dynamical system comprising a flexible beam. The steady state response of the system is analysed by formulating the motion equations, and the numerical results of transmissibility and vibratory power are discussed to assess the effectiveness of vibration control. The isolation characteristics of the system are evaluated and compared for different parameters from perspective of dynamical behaviour, force transmissibility and vibratory energy transmission. The results provide useful guidelines for the dynamic design of this vibration system. By comparing with traditional isolators, the effectiveness of vibration control can be improved with adaptive MRE isolators through adjusting the applied magnetic field.

Chapter 2 Mechanical properties, modelling and applications of MRE

2.1 Fabrication of MRE

2.1.1 Selection of matrix and particles

MRE is a kind of multi-functional composite material, where typically magnetisable particles are suspended in a non-magnetic elastomer. For matrix material, having good mechanical properties and high mechanical strength is very important. There are many elastomers and gels which might be used as the matrix of a MRE, such as natural rubber^[12], silicon elastomer^[13], polystyrene^[12], gelatin^[14], polyurethane sealant^[15]. Generally speaking, hard matrix materials have high zero-field modulus, and soft matrix provides small resistance to particles aligning in the direction of magnetic field; therefore softer matrix materials may show a greater MR effect^[16] which is the difference between the zero-field modulus and the modulus measured under external magnetic field. Additional plasticizers have proven to be effective in reducing zero-field modulus and improving the MR effect^[12,17], but too much plasticizer will also undermine the ability of materials to sustain load.

This implies that the gel based MRE have high MR effects, but they are ill-suited for load bearing applications due to low mechanical strength and reduced fatigue life, meanwhile the elastomer based MRE has good bearing capacity, although their applications are limited by their low MR effect. Basically the obvious aging phenomenon of natural rubber-based MRE makes it difficult to possess excellent resistance to chemical or mechanical degradation. Therefore within natural rubber matrix the magnetisable particles have to be coated, which complicates the manufacture procedure of MRE material. As a kind of synthetic material, silicone elastomer is a suitable candidate because of good elasticity and temperature resistance. Furthermore silicone elastomer based MRE can be cured at room temperature, which simplifies the fabrication of MRE material.

Magnetisable particle of MRE need to have good magnetic permeability, high saturation magnetisation and low remnant magnetisation. Good magnetic permeability and high saturation

magnetisation can provide high attraction between magnetisable particles, and thereby a high MR effect which is recommended. Low remnant magnetization is also an important characteristic^[18], which guarantees that the dependent properties of MRE can be adjusted continuously, rapidly and reversibly by an applied magnetic field. This is because when the magnetic field is switched off high remnant particles tend to stick together and prevent a completely reversible MR effect. Magnetisable particles of MRE are usually made of soft ferromagnetic materials. And the most commonly used magnetisable particles are carbonyl iron powders, because of their good magnetic permeability, high saturation magnetisation and low remnant magnetisation.

The size and shape of the particles are also very important factors that influence the behaviour of MRE. Comparing with the shape, the average size of particles is more important. Basically, larger particles can improve the MR effect because stronger dipole–dipole action results in aligning in the direction of the magnetic field more easily^[19]. MRE with large particles also has high elastic modulus and poor interactions between particles and matrix, which may cause poor mechanical properties^[20].

Experiments reveal that high concentration of magnetisable particles can increase elastic modulus and MR effect. But above a threshold, further increase of particle volume concentration causes an elastic modulus drop of MRE, whilst at the same time the linear viscoelastic region gradually disappears with increasing filler content. Because when the elastomer is not sufficient for filling all the voids between particles, the mechanical properties of the composite will deteriorate, which is a general characteristic of filled rubber compounds^[21]. It is believed that the critical volume concentration for magnetisable particle is 30%; higher than this threshold the mechanical properties, stability and inoxidisability of MRE material will deteriorate with increasing volume concentration of particles^[22].

2.1.2 Influence of magnetisation

The interaction between the non-magnetic matrix and the magnetisable particles can be either strong or weak and it influences its mechanical and rheological properties; especially in the linear viscoelastic range these are highly affected by the microstructure of composite. Firstly magnetisable particles are embedded in the uncured non-magnetic matrix and then the mixture is cured. There are two kinds of MRE due to the different ways in which the particles are dispersed in the matrix namely, anisotropic MRE which have a directed particle orientation attributed to the application of magnetic field during curing procedure and isotropic MRE which can be characterized by a random distribution of magnetisable particles because of the curing

without magnetic field^[23]. In the curing process, an applied magnetic field forces the magnetisable particles to form in chains; thus the particles are fixed after the matrix solidification, which is called anisotropic MRE. Otherwise, isotropic MRE is cured without a magnetic field thereby can be considered as homogeneous materials^[24]. In Figure 2.1, the SEM images display the microstructures of anisotropic MRE and isotropic MRE.

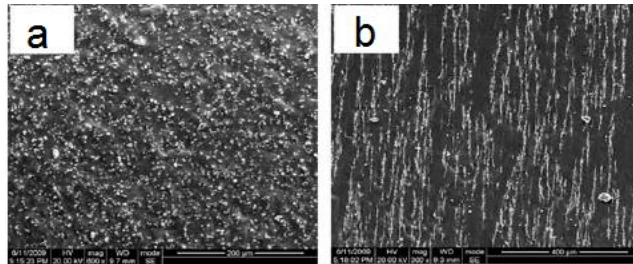


Figure 2.1 SEM images of (a) isotropic MREs and (b) anisotropic MRE^[15].

The mechanism of magnetorheological (MR) effect: when a magnetic field is applied to MRE materials, the particles inside tend to align in the direction of magnetic flux, thereby the elastic matrix is also deformed, as shown in Figure 2.2. As a result MRE materials become stiffer with the application of external magnetic field, and the field-induced change in elastic modulus is commonly used to describe the measurement of MR effect. When the particles are magnetically saturated the maximum change of elastic modulus occurs, and when the applied magnetic field is parallel to the particle alignment in conjunction with the direction of stress the greatest MR effect can be found^[25].

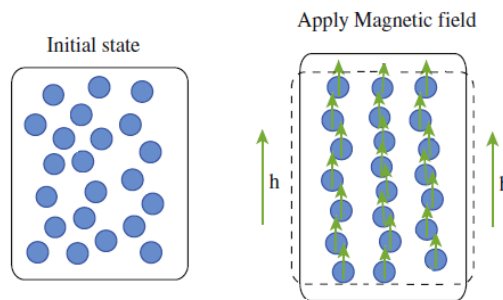


Figure 2.2 The sketch of mechanism of MR elastomers under magnetic field^[43].

Therefore, anisotropic MRE material displays a more significant MR effect compared with isotropic MRE material. Additionally, anisotropic MRE always possesses higher zero-field elastic modulus and shear modulus than isotropic MRE with the same composition, which can be explained by the fact that the clusters or chains of magnetisable particles enhance the

interactions and resist the compressing force or shearing force, and friction occurs between the particles^[26].

2.1.3 Influence of coupling agents

The mechanical properties of MRE are strongly dependent on its microstructure and the interaction between magnetisable particles and non-magnetic matrix is relatively important^[30]. Good wetting of particles is essential to form a continuous structure, because loose agglomerates are believed to be potential failure initiation sites^[27]. Besides when gaps exist between matrix and particles, magnetic energy will be lost, thereby the microstructure will not change appreciably with the application of magnetic field, which destroys the rheological properties of MRE and reduces the MR effect. The coupling agent can effectively enhance the interaction between magnetisable particles and non-magnetic matrix in various ways, which may improve the MR effect^[28]. According to Wang's research vinytriethoxysilane improved the tensile strength of MRE by 77% and MR effect by 37%^[29]. In Wu's study diisooctyl phthalate allowed carbonyl iron particles to align more easily in the matrix as a result the composite owned greater MR effect. However, the thermal stability and compressive strength are undermined^[15]. The research of Li and Sun showed that multi-walled carbon nanotubes could be also added to MRE as a coupling agent^[31], where a layer of nanocomposite could wrap the particles and form a district interface to improve the bonding between magnetisable particles and matrix. This composite could combine the outstanding properties of both the smart material and the carbon nanotubes, and exhibited both higher zero-field stiffness and larger absolute MR effect.

2.2 Mechanical properties of MRE

2.2.1 Payne effect

The Payne effect can be observed when filler-reinforced rubber is subjected to cyclic loading with small strain amplitudes, and it can also be manifested as a dependence of the modulus on the applied strain amplitude^[32]. The Payne effect can be physically attributed to deformation induced changes in microstructure, such as the breakage and recovery of weak physical bonds linking adjacent filler clusters. The Payne effect of MRE can be defined as the decrease of storage modulus and loss modulus with increasing amplitude of the applied harmonic load^[33], as shown in Figure 2.3. It is reported that the Payne effect increases with increasing filler concentration in the composite material^[34].

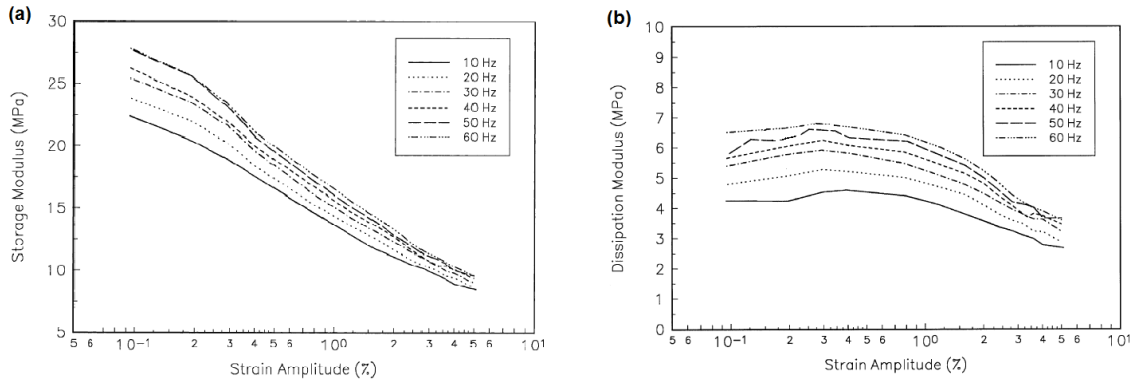


Figure 2.3 Experimental result of filled rubber: (a) storage modulus and (b) loss modulus at different amplitudes and frequencies^[33].

As a kind of filler-reinforced rubber, MRE also performs a transient behaviour of the Payne effect, namely when the amplitude of applied harmonic deformation is increasing, the storage modulus decreases from a high level to a low plateau while the loss modulus also decreases^[35], as shown in Figure 2.4.

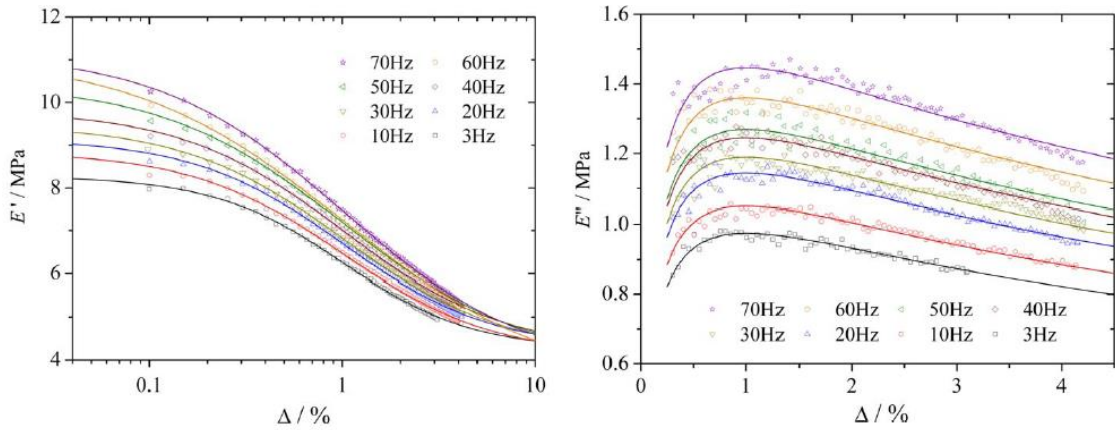


Figure 2.4 Storage modulus and loss modulus of MRE under different strain amplitudes^[35].

Additionally, anisotropic MRE has a more pronounced Payne effect than isotropic MRE. At the same time, the applied strain amplitude is also relative to the MR effect because the magnetic forces are dependent on the distance between the particles. Therefore, the maximum MR effect can be obtained at relatively small strain amplitudes when the interaction between the particles is strong^[36], and the MR effect decreases gradually with increasing amplitude of applied harmonic deformation, because the MR effect will diminish when the particle chains start to yield^[37].

2.2.2 Mullin effect

The Mullins effect is a particular phenomenon of the dynamic response in filled rubbers where the stress–strain curve depends on the maximum loading previously encountered. MRE also has Mullin effect which can be described as the composite becoming softer with the loading cycles until the composite comes to a stable point after certain number of cycles^[38]. So the same applied strain, during the first loading cycles will result in lower and lower stress, which is due to the breakdown of original firm binding structure between the filler particles and the rubber matrix^[39]. If the material is left unloaded for a period this firm binding will start forming again and the material will partly recover its original stiffness. Additionally the recovery procedure can be speeded up when the material is heated. However, whether materials can recover totally to their original state depends on the strain they are loaded to^[40].

2.2.3 MR effect

As a kind of resilient material, MRE has rheological properties which can be changed with the action of an applied magnetic field, which is called the MR effect. The effect is taking place on a micron scale when filler particles interact with elastomer molecules, which can be called the elastomer-filler mesophase. Elastomer compounds are highly complex polymer systems where various solid ingredients are dispersed in an elastomer matrix, especially when the elastomer exhibits a viscoelastic character by nature^[41].

MRE is commonly operated in the linear viscoelastic region with small deformations, where its field-dependent modulus can be continuously, rapidly and reversibly controlled in the pre-yield regime through adjusting an external magnetic field. MR effect enables the rheological properties of MRE to be varied by magnetic field, as shown in Figure 2.5, which is known as the relative change of the effective modulus when the magnetic field intensity increases from 0T to a value. MR effect can be defined as

$$\frac{M_B - M_0}{M_0} \times 100\% \quad (2.1)$$

where M_0 is the effective modulus when magnetic flux density is 0T and M_B is the effective modulus when magnetic flux density is a maximum.

It is suggested that the magnetic force between magnetisable particles inside the composite is relevant to the modulus of MRE. When a magnetic field is exerted, the filler particles will get magnetised and interact with surrounding particles^[42]. Therefore, even the

isotropic MRE belongs to anisotropic materials in essence. In MRE material, the stiffness of composite depends on the number of particle chains per unit cross section and the stiffness of particle chains is sensitive to the amount of polymer in the gaps between the magnetisable particles. The application of magnetic field can effectively increase the stiffness of particle chains, so MR effect is a kind of temporary reinforcement. When applying an external magnetic field, the MRE will slightly deform without any mechanical loads. Thus, isotropic MRE will expand in the direction of the magnetic field, while anisotropic MRE will compress; additionally the magnetically induced deformations are related to the applied field strength when the magnetic field is parallel to the oriented structure^[43]. The deformation of anisotropic MRE driven by external magnetic field is smaller than that of isotropic MRE with the same volume fraction, which coincidences with the fact that anisotropic MRE is stiffer than isotropic MRE in the chain direction^[44].

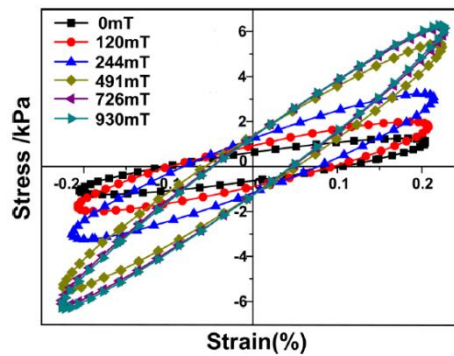


Figure 2.5 Stress-strain plots of MRE with different magnetic field at a fixed strain amplitude of 0.2% and a driving frequency of 5 Hz^[52].

Magnetic flux density is very important among all the factors relevant to the magnetic force, and the magnetic force grows with increasing magnetic field intensity thus the modulus of MRE also grows. As show in Figure 2.6, both storage modulus and loss modulus of MRE increase with magnetic flux density. When saturation occurs, the magnetization of each particle will remain constant and the magnetic force between the particles will stop increasing with magnetic field^[45]. Therefore, the moduli of MRE change very little with increasing magnetic flux density within such a regime, and the modulus of anisotropic MRE seems to be more sensitive to magnetic field intensity, which also indicates that the MR effect of anisotropic MRE is greater than isotropic ones^[46].

At present, the broad industrial application of MRE is limited due to the MR effect not being large enough. In previous studies, the MR effect as a function of particle magnetisation,

and the maximum possible field-induced change in modulus occurs when the aligned particles are magnetically saturated, which explains why it is useful to select active particles with high magnetic permeability and saturation magnetization.

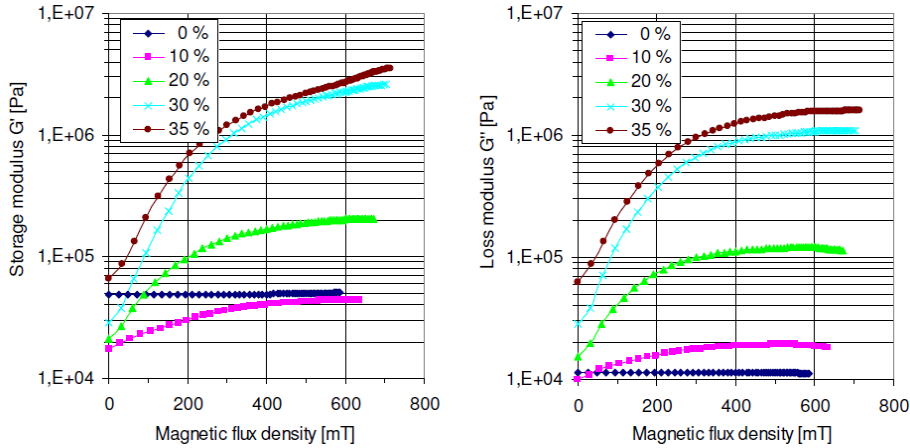


Figure 2.6 Dependence of storage modulus (left) and loss modulus (right) of isotropic MRE with different concentrations of 40 μm iron particles in silicone on the magnetic flux density^[45].

The MR effect can be improved by several factors which can be deduced from the mechanism. Firstly, the larger dipole-dipole action between magnetisable particles will make it easier to align in the direction of the magnetic field; and thus obtain higher MR effect. Increasing the amount and size of magnetisable particles is an effective way to enhance this interaction. However, too large concentration and size of particles will result in a high zero-field modulus M_0 and then a low relative MR effect. Additionally, the mechanical properties, stability and inoxidizability of MRE will also deteriorate with increasing the amount or size of magnetisable particles. It is reported that for a required particle volume fraction the employment of an appropriate mixture of large particles and small particles (of 7.9 μm and 1.25 μm diameters) can effectively increase the field induced modulus of MRE without a concomitant increase of the zero-field modulus^[47]. According to the mathematical modelling of Jolly and the finite element calculation of Davis, the highest MR effect is believed to take place when the particle volume fraction is 30% and the zero-field shear modulus of anisotropic MRE is larger than the isotropic materials with the same composition^[48,49].

Secondly, the soft matrix material leads to a low zero-field modulus M_0 , which offers a potential opportunity for high relative MR effect. Simultaneously the softer matrix has smaller resistance to magnetisable particles getting aligned along the magnetic field lines, which also indicates that softer matrix materials may show a greater relative MR effect. The addition of

plasticizer has proven to be effective in enhancement for relative MR effect by decreasing the zero-field modulus. However, too much plasticizer will result in too soft matrix, and MRE based on soft elastomer matrices are usually ill-suited for most load-bearing applications because of low strength and reduced fatigue life.

Thirdly, the interaction between magnetisable particles and non-magnetic matrix is also helpful in improving the MR effect. Because magnetic energy will be lost when gaps exist between particles and matrix, then the microstructure of MRE cannot be changed much with the magnetic field, thus the modulus cannot be changed much either. Han found that magnetisable particles in wavy chains are more effective in improving the MR effect in both shear and tension/compression than magnetisable particles in straight chains^[50].

2.3 Dependences of MRE

2.3.1 Frequency dependence

In previous studies, most researchers employed the relationship between the known sinusoidal excitation frequency and its responses to evaluate the modulus of MRE, and the experimental research reveals that the storage modulus G' and the loss factor $\tan\delta$ also change with the applied driving frequency, as shown in Figure 2.7. The storage modulus increases with the increment of driving frequency, whilst the loss factor decreases with increasing frequency and the relationship between them can be considered linear^[51].

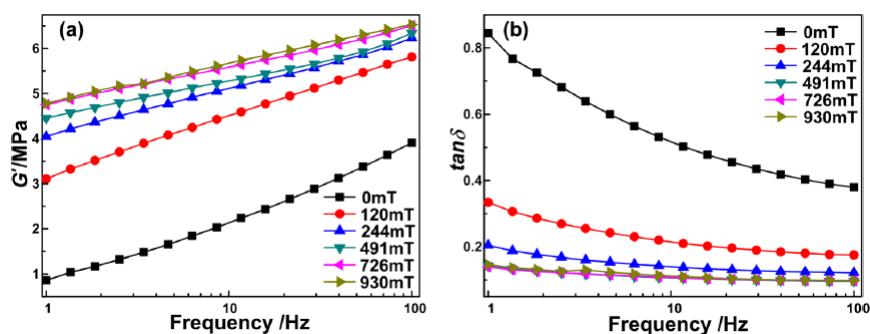


Figure 2.7 Storage modulus and loss modulus by oscillatory tests under different driving frequency^[51].

Actually, the dependences on frequency are determined by the matrix material, or we can say MRE inherits the dependences on frequency from the matrix material. Noticeably, it is difficult to excite MRE material over 100Hz, because fixing MRE samples with high excitation frequency causes their viscoelasticity to vanish^[52].

2.3.2 Temperature dependence

It is reported that temperature can also influence the mechanical properties of MRE, and experimental research reveals that both storage modulus and loss modulus decrease with increasing temperature^[53]. As shown in Figure 2.8, the storage modulus decreases by 50% from 20°C to 80°C. It is worth pointing out that the electromagnets will produce thermal impact on MRE material while generating magnetic field and the increasing temperature will cause unreliable experimental results. Basically there are two main factors that influence the MR effect due to increment of temperature: (i) the magnetisation of particles decreases, which can reduce the maximum change of normal force, and (ii) the modulus of matrix decreases with increasing temperature, which can benefit the movement of the magnetisable particles inside and enhance the interaction between particles^[54].

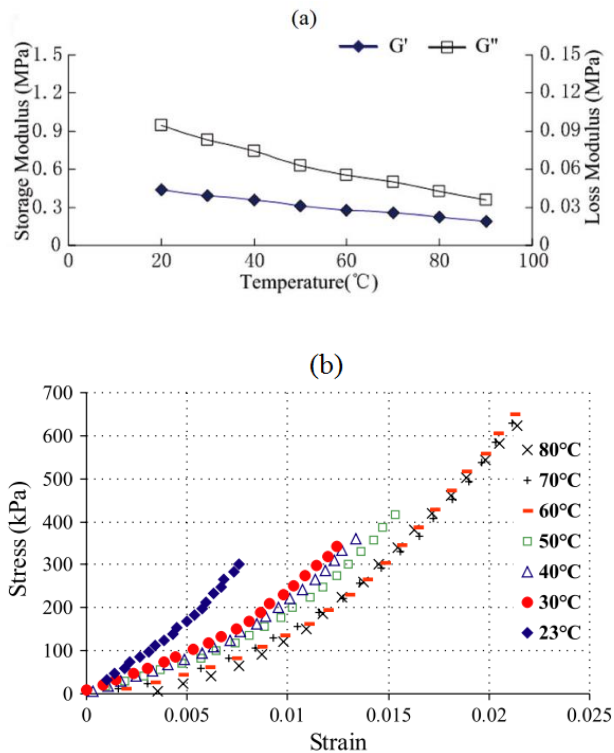


Figure 2.8 (a) Temperature-dependent modulus of MRE^[53] and (b) Stress-strain curve of MRE at different temperatures^[55].

2.4 Mathematical modelling of MRE

2.4.1 Linear models

The MRE exhibits linear viscoelastic characterisation within a certain range of frequency and strain where the microstructure of material does not change; thus, tiny strain excitations will

result in linear responsive stresses in this linear viscoelastic region. Although considerable destruction of microstructure has great influence on the dynamic performance of MRE material, it is still believed that it remains linear viscoelastic if the microstructure is only slightly destroyed. The dynamic behaviour of MRE under an applied harmonic load can be described by linear models developed with respect to its elastic hysteresis. When sinusoidal loads are applied to linear viscoelastic materials, the responsive stress will be a sinusoidal function with the same angular frequency neither exactly in phase with the applied strain nor totally out of phase^[56]. The stress $\sigma(\omega t)$ and strain $\varepsilon(\omega t)$ can be expressed in sinusoidal form:

$$\begin{aligned}\varepsilon &= \varepsilon_0 \sin \omega t \\ \sigma &= \sigma_0 \sin(\omega t + \varphi) = \sigma_0 \cos \varphi \sin \omega t + \sigma_0 \sin \varphi \cos \omega t\end{aligned}\quad (2.2)$$

where σ_0 and ε_0 are amplitudes of stress and strain, respectively, ω is the angular frequency, t is cycle time and φ is the loss angle whose range is $0^\circ < \varphi < 90^\circ$. In viscoelastic materials, some of the deformation energy can be stored and recovered, whilst the remainder is dissipated as heat during each cycle. The first term on the right of Equation (2.2) represents the elastic component and the second item indicates the viscous component. It is obvious that the shape of the stress-strain curves for linear viscoelastic material under sinusoidal load is elliptical as shown in Figure 2.9.

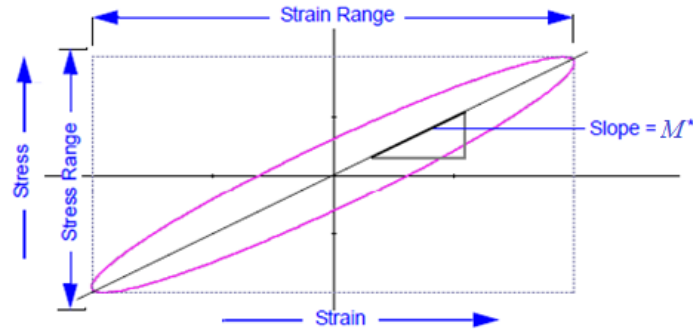


Figure 2.9 Stress-strain plot for linear viscoelastic material under sinusoidal actuating loading and the relationship between geometry and dynamic properties^[52].

The storage modulus M' represents the ability of viscoelastic material to store the energy due to deformation, which contributes to the material stiffness. The loss modulus M'' indicates the ability of viscoelastic material to dissipate the energy of deformation. They can be defined as:

$$\sigma = \varepsilon_0 (M' \sin \omega t + M'' \cos \omega t) \quad (2.3)$$

where M can be either the shear modulus G or the Young's modulus E . It is usually convenient to express the modulus as a complex quantity. Then the dependence of the in-phase and out-of-phase stress on the strain can be presented using the complex modulus M^* :

$$M^* = M' + iM'' . \quad (2.4)$$

The ratio between the loss and storage moduli is another widely used term for viscoelastic materials:

$$\tan \varphi = \frac{M''}{M'} \quad (2.5)$$

where $\tan \varphi$ is called the loss factor, which can be used for describing the efficiency of damping caused by the viscoelastic material.

Based on the relationship between the geometry of stress-strain curve and dynamic properties of viscoelastic material in Figure 2.9, the complex modulus M^* can be obtained by calculating the slope of the line from the maximum strain to the minimum strain, and the loss angle φ is relevant to the energy dissipation per volume within an oscillatory cycle which is the area enclosed by the hysteresis loop. The storage modulus M' and loss modulus M'' can be expressed with the loss angle φ and the magnitude of modulus $|M^*|$:

$$M' = |M^*| \cos \varphi \quad M'' = |M^*| \sin \varphi \quad (2.6)$$

where $|M^*| = \sqrt{M'^2 + M''^2}$.

Experimental research demonstrates that MRE behave with linear viscoelastic properties when the strain amplitude is within 10%, and then the hysteresis curve of response stress and input strain can be simplified as elliptical loops. There are already several linear viscoelastic models to process the stiffness and damping capability of MRE, and the Kelvin-Voigt model is the simplest among all the models. As shown in Figure 2.10, this is a parallel combination of a dash-pot and a spring. When the load is not too high, the Kelvin-Voigt model can represent creep in materials very well, because it predicts the material to deform at a decreasing rate with a constant stress and approach asymptotically the steady-state strain as time increases to infinity. But this model is not good with modelling relaxation in materials when the stress is released.

In Figure 2.10 γ^* is input strain and τ^* is response stress, both of them in complex form. The corresponding parameters are defined with reference to Equation (2.6).

$$M' = k, \quad M'' = c\omega \quad (2.7)$$

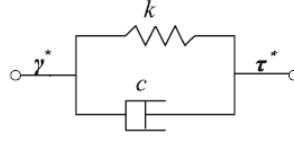


Figure 2.10 Kelvin-Voigt model for MRE^[56].

Damping dissipates energy in vibrating systems, as a process it happens when the damping force is proportional to the vibrational velocity and has dimensions of force per unit velocity. When the system is subject to an external impulse, the smallest amount of damping for no oscillation occurs in free vibration response, and is defined as the critical damping. In practice, damping is usually smaller than the critical value. For MRE material, the damping can be considered as a viscous characteristic, and the constant describes the damping rate of the material. Subjecting the system to forced or free oscillations, damping can be studied when it is on a subcritical level, which can be obtained from the dynamic equilibrium equation of viscoelastic motion for a single degree of freedom (SDOF) system, namely.

$$m\ddot{x}(t) + c\dot{x}(t) + kx(t) = F_0 e^{i\omega t} \quad (2.8)$$

where F_0 is the external oscillating force, m the effective mass, $x(t)$ the displacement and k the spring constant of the system. However, the value of the viscous damping constant c is dependent on the dimensions of the specimen. Thus the dimensionless damping ratio ξ , of actual damping to the critical damping, is often used instead of the damping constant c . The critical viscous damping constant is defined as $c_c = 2m\omega_0$, where ω_0 is the natural frequency of the vibrating system, respectively. The damping ratio is defined as

$$\xi = \frac{c}{c_c} = \frac{c}{2m\omega_0}. \quad (2.9)$$

Damping has only a minor influence on the response of system in the frequency regions either well below or well above the resonance frequency, but it is of great importance near the resonance frequency. In the range of $\omega \ll \omega_0$ the vibration is almost the same as produced by the static action of force, and in the range of $\omega \gg \omega_0$ the high frequency disturbing force practically produces no forced vibrations and damping has only a secondary effect on the value of magnification factor. In these regions, the effect of damping can be neglected. But in the case of resonance where the magnification factor can be quite large, the damping becomes very

important and it cannot be disregarded as the magnification factor is very sensitive to the changes in damping^[57].

2.4.2 Nonlinear models

Within the pre-yield regime, the modulus of MRE is dependent on not only the applied magnetic field but also the applied strain amplitude and the driving frequency. Additionally interfacial slippages also occur between the matrix and particles. As a result, the relationship between applied strain amplitude and the response stress amplitude is nonlinear^[58]. However, until now most of research has focused on the linearity when it comes to theoretical problems and the nonlinearity of MRE has not been systematically investigated.

Several theoretical models have been proposed to describe the magneto-rheological properties of MRE. The first dipole model was developed by Jolly in 1996 which is basically quasi-static and one-dimensional^[47], and the saturated field-induced shear modulus was given by

$$G_J = \frac{\varphi J_s^2}{2\mu_p \mu_0 h^3} \quad (2.10)$$

where h is the space between two adjacent particles, φ is the volume fraction of magnetisable particles, J_s is the saturation magnetization, μ_0 is the permeability of ferrum and μ_p is the relative permeability of medium.

In 1999 Davis proposed another chain model to deduce the field induced shear modulus^[59], which differed by a numerical factor of 1.2 due to isolated chains, and the optimum particle volume fraction was predicted to be 27%. This was expressed as

$$G_D = \frac{3\varphi J_s^2}{5\mu_p \mu_0 h^3}. \quad (2.11)$$

Chen came up with a column model in 2007 to calculate the field induced shear modulus^[60], namely

$$G_C = \frac{(\mu_{\parallel} - \mu_{\perp}) H_0^2 \sin \gamma \cos \gamma}{\gamma} \quad (2.12)$$

where γ is the shear strain, H_0 is the applied magnetic field strength, μ_{\parallel} the permeability of the block parallel to the column axes and μ_{\perp} the permeability of the block perpendicular to the column axes.

There are also several viscoelastic models that have been proposed in previous research to describe the frequency and strain dependent properties of MRE. Based on classical Kelvin-Voigt model a three-parameter viscoelastic model was developed, as shown in Figure 2.11, with spring k_1 used to improve the efficiency when the model is subject to sudden load. The corresponding parameters are defined by Equation (2.13)^[61]

$$M' = \frac{k_1 k_2 (k_1 + k_2) + k_1 (c\omega)^2}{(k_1 + k_2)^2 + (c\omega)^2}, \quad M'' = \frac{k_1^2 c\omega}{(k_1 + k_2)^2 + (c\omega)^2}. \quad (2.13)$$

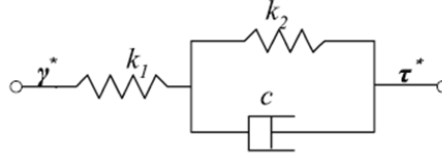


Figure 2.11 Three-parameter Kelvin viscoelastic model for MRE^[61].

Figure 2.12 shows a standard linear solid model for MRE, which combines aspects of the Maxwell model and Kelvin-Voigt model to describe the overall behaviour of a system, and Equation (2.14) defines the corresponding parameters. This model is capable of describing the general features of viscoelastic relaxation, but the model lacks the ability to model the relaxation over the full range^[62].

$$M' = k_1 + \frac{k_2 (c\omega)^2}{k_2^2 + (c\omega)^2}, \quad M'' = \frac{k_2^2 (c\omega)}{k_2^2 + (c\omega)^2} \quad (2.14)$$

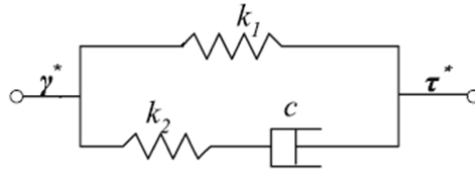


Figure 2.12 Three-parameter Maxwell viscoelastic model for MRE^[62].

As shown in Figure 2.13, a four-parameter viscoelastic model for MRE was proposed and the corresponding parameters^[63] are defined by Equation (2.15).

$$M' = \frac{(k_0 k_1 + k_0 k_2 + k_1 k_2) \left[(k_1 + k_2)^2 + (c\omega)^2 \right] + k_1^2 (c\omega)^2}{(k_1 + k_2) \left[(k_1 + k_2)^2 + (c\omega)^2 \right]}, M'' = \frac{k_1^2 c\omega}{(k_1 + k_2)^2 + (c\omega)^2} \quad (2.15)$$

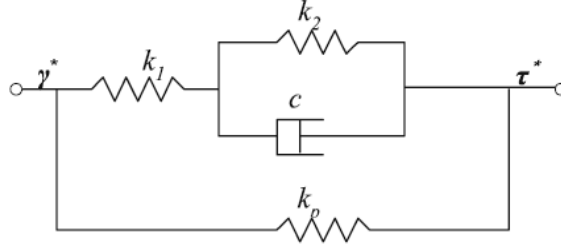


Figure 2.13 Four-parameter viscoelastic model for MRE^[63].

Furthermore, a general Maxwell viscoelastic model^[64] for MRE was developed as shown in Figure 2.14, and the corresponding parameters are defined by Equation (2.16), as

$$M' = k_0 + \sum_{i=1}^n \frac{k_i (c_i \omega)^2}{k_i^2 + (c_i \omega)^2}, M'' = \sum_{i=1}^n \frac{k_i^2 (c_i \omega)}{k_i^2 + (c_i \omega)^2}. \quad (2.16)$$

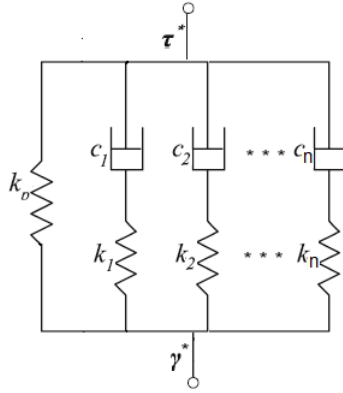


Figure 2.14 General Maxwell viscoelastic model for MRE^[64].

Once large strain amplitude causes the destruction of microstructure, the nonlinearity will take place within MRE material. In that case the response stress of a sinusoidal strain loading can be expressed by a Fourier series of odd harmonics^[65], where the higher harmonics of the driving frequency are due to the nonlinearity of viscoelastic material, namely

$$\begin{aligned} \varepsilon &= \varepsilon_0 \sin \omega t \\ \sigma &= \sum_{n=1, \text{odd}}^N \sigma_n \sin(n\omega t + \varphi_n) \end{aligned} \quad (2.17)$$

It can be observed in Equation (2.17) that when the classical model is under a sinusoidal loading, the nonlinearity will give rise to a non-elliptic stress-strain curve due to harmonic distortion^[62], as shown in Figure 2.15. The high order terms generally have no explicit physical meaning, thus are of little help in further understanding the complex nonlinear behaviour.

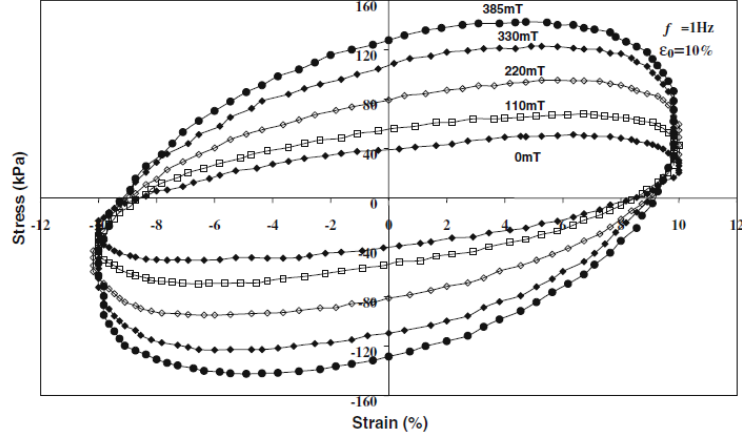


Figure 2.15 Stress–strain relationships with various magnetic fields at strain amplitude of 10%^[62].

Jun-Tao Zhu proposed another model^[66], where ε is assumed to be the input strain and σ is the output stress, with the stress–strain relationship is described by

$$\sigma(\omega) = G_0 \varepsilon(\omega) + G_0 \tau^\alpha (i\omega)^\alpha \varepsilon(\omega). \quad (2.18)$$

Notably, in this model α is an arbitrary order derivative, including fractional order. As for modelling the response of MRE material, it is a major challenge to capture the strain stiffening in force-displacement loops and the nonlinear relationship between velocity and force.

Jian Yang proposed a new phenomenological model to portray this unique behaviour^[67]. This model incorporates a Bouc–Wen component, which is combined with a spring and a damper to portray the unique strain stiffening property, and a Voigt element to describe hysteresis loops and solid-material behaviour, respectively.

For each hysteresis loop of stress-strain curve, an equivalent storage modulus G'_{equ} and an equivalent loss modulus G''_{equ} can be calculated by Equation (2.6). In comparison with non-linear models, this equivalent method avoids discussing the high order issues which have no explicit physical meanings. Therefore, to some extent, the equivalent dynamic mechanical properties are valuable for characterisation of the stiffness and the energy dissipation.

2.5 Applications of MRE

2.5.1 MRE based vibration absorber

In engineering applications tuned vibration absorbers (TVA) are widely employed to suppress vibrations, either locally for flexible structures or globally for rigid structures. TVAs can be divided into passive TVAs, active TVAs and semi-active TVAs. The generic passive TVAs are typically composed of an oscillator, a spring element and a damping element. A passive TVA can effectively suppress the monotone vibrations in the dynamical system by designing appropriate stiffness and damping. A vibration system with a TVA mounted on can be modelled as a two-DOF dynamical system, where the vibration system can be idealised as an equivalent one-DOF mass-spring system. However, the passive TVA is only functional over a very narrow frequency range. Nevertheless because of its effectiveness, a passive TVA has to be precisely tuned to the compressor self-induced harmonic disturbance for its optimum performance; otherwise a detuned or mistuned TVA could decrease its effectiveness in vibration suppression and even amplify it. Therefore, passive TVAs might lose their function in many practical systems due to time-varying vibration sources and wide vibration frequency range, especially in large scale interconnected structures. An active TVA can be considered as a TVA with a feedback or feed-forward control system, which makes it possible for the active TVA to vary its natural frequency to suit uncertain or time-varying excitation frequencies. Regardless of good vibration absorption ability, it has much energy consumption due to the wide distribution of sensors and actuators^[68]. Even worse is that the active TVA may lose its function and potentially aggravate the primary structure when the control algorithm fails to work.

The above mentioned problems can be overcome with a semi-active TVA, which is also called the adaptive tuned vibration absorber (ATVA). An ATVA can adjust its natural frequency in accordance with the varying conditions by changing its mass or stiffness in real time. Moreover, it consumes less energy because an activation force is no more necessary. So ATVAs are used more widely and the promising dynamical characteristics of MRE make it a suitable candidate as a controllable element for ATVAs. The vibration control mechanism of MRE absorbers is that the elastic modulus can be adjusted rapidly, continuously and reversibly by controlling an external magnetic field, which results in a controllable resonant frequency; hence, the vibration response can be minimised over a broader frequency range^[69].

Ginder and co-workers designed the first MRE TVA and evaluated its absorption efficiency. Their experimental results demonstrated that MRE based TVAs have good capacity

to shift resonance away from the excitation frequency^[7,70,71]. This TVA itself was a closed magnetic circuit, which comprised two MRE slabs, a metallic part and a wired coil. Aiming at improving the frequency shifting capacity, Deng developed MRE TVA with two coils^[72,73], as shown in Figure 2.16, and designed a compact shear mode AVTA using an MR elastomer as shown in Figure 2.17 (a). The electromagnets and magnetic conductor form a closed magnetic path, whilst also serving as a dynamic mass. In this way, the device has a more compact configuration than previous ones. The squeeze mode MR elastomer absorber can also be designed in a more compact manner, as shown in Figure 2.17 (b). Magnetic coils and steel components form a dynamic mass and were placed on top of the MRE samples. Lerner employed MRE material to construct ATVAs in three modes, namely shear mode, longitudinal mode and squeeze mode. The absorbers may adaptively operate over a relatively wide bandwidth without consuming any extra energy and the basic components are absorber mass, base mass MRE slabs and wire coils^[75]. Hoang proposed a MRE ATVA for powertrain vibration mitigation, where the rotational part consisted of an outer ring, an inner ring and MRE samples between the rings^[76].

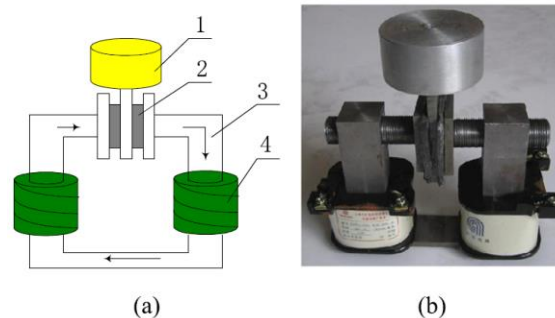


Figure 2.16 ATVA (a) Sketch: 1. Oscillator: 2. MR elastomers: 3. Magnetic conductor: 4. Coils; (b) Photograph^[72].

Gong's research group did pioneer work on the development of ATVAs based on MRE and improved the vibration absorption capacity, as shown in Figure 2.18. Both calculation results and experimental results showed that MRE ATVAs possessed better absorption capacity than traditional TVAs^[72,77,78]. Recently Kim and colleagues developed the continuous control algorithm of MRE ATVAs and the experimental results showed that the MRE ATVA was able to robustly suppress the vibration even when the resonant frequency was changed substantially from the initial frequency^[79]. However, the damping coefficient of ATVAs which employ MRE as smart spring is relatively large, which significantly influences the absorption performance.

Xu attempted to attach a voice coil motor to an MRE ATVA to counteract the damping force, which seemed to be a potential way to solve this problem^[80].

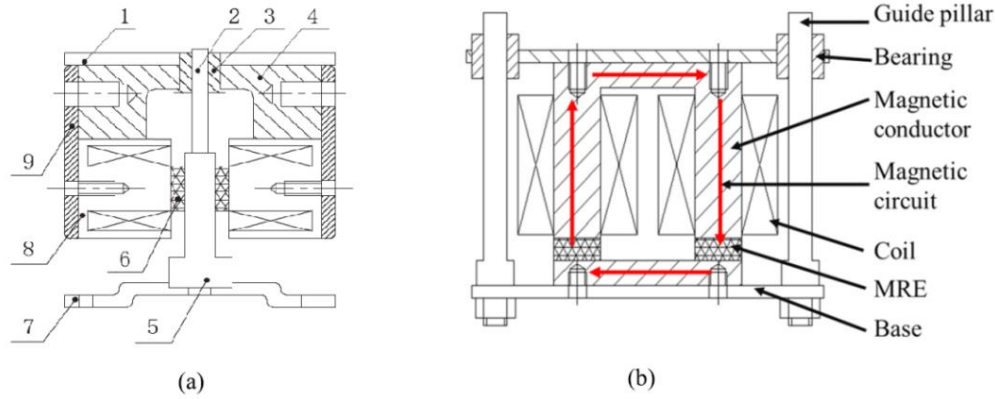


Figure 2.17 (a) A compact MR elastomer ATVA: 1. Cover, 2. Guide rod, 3. Linear bearing, 4. Magnetic conductor, 5. Shear plate, 6. MREs, 7. Base, 8. Electromagnet, 9. Mounting shell. (b) Schematic of a compact squeeze MRE absorber^[74].

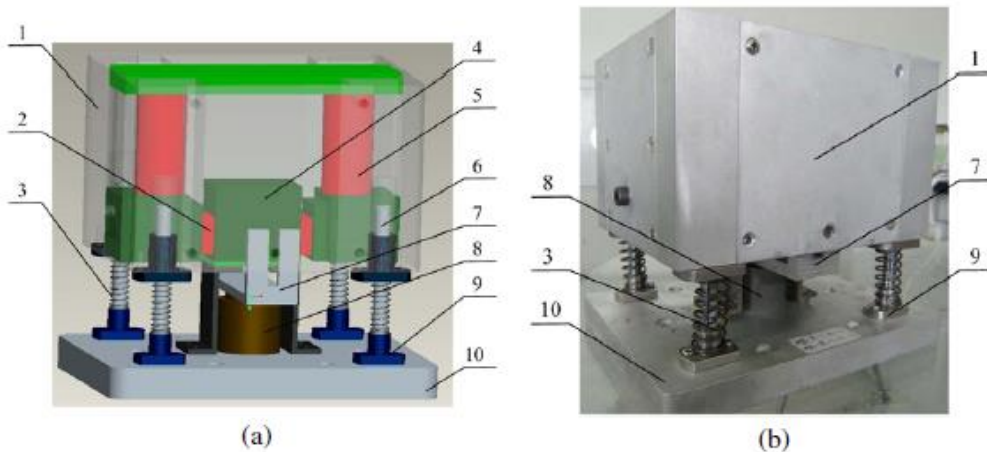


Figure 2.18 The MRE ATVA (a) schematic diagram and (b) photograph: (1) mounting shell; (2) MRE; (3) helical spring; (4) shear block; (5) magnetic conductor; (6) guide rod; (7) connector of the voice coil motor and the shell; (8) voice coil motor; (9) flange; (10) base^[78].

2.5.2 MRE based vibration isolator

A simple linear isolator can attenuate transmitted vibrations at frequencies which exceed the value of $\sqrt{2}\omega_0$ where ω_0 is the natural frequency of the isolator. The transmitted force F_t reaches a value less than the excitation force F_0 at an excitation frequency $\Omega > \sqrt{2}\omega_0$ and the ratio of F_t to F_0 is known as the transmissibility. In resonance damping exerts a beneficial effect on isolation transmissibility, but when $\Omega/\omega_0 > \sqrt{2}$ high damping should be avoided to successfully reduce the transmitted force. Therefore, the effectiveness of any isolator can be

improved by lowering its natural frequency and its damping ratio^[81], which explains why softer restoring force and lower natural frequency can result in better isolation characteristics. Energy dissipation and resilient load-supporting means are the two essential constituents of an isolator. In some isolators the functions of energy-dissipation and load-supporting can be performed by a single element, such as natural rubber and synthetic rubber. In other isolators, the resilient load-supporting means, such as metal springs, may fail to possess sufficient energy dissipation, thus a distinct energy dissipation source need to be provided.

Conventional linear isolators are only functional when their natural frequencies are well below the excitation frequency, which limits them to such engineering applications as moderate environmental disturbances. The spectrum of severe environmental disturbances, such as shocks, random ground motion and impact loads, may contain dangerous low-frequency components. In such cases the linear isolator may experience excessive deflections causing over-stress or even damage to the system^[82]. At very low frequencies, vibration isolation characteristics can be improved by active control systems such as feedback or feed-forward control systems. However, the more effective isolation performance is obtained at the expense of extra energy for providing activation force. What is even worse, the active control system may fail to work even cause damage to the primary structure when the control algorithm loses its function^[83]. A better vibration isolation performance can be obtained by semi-active vibration isolators without consuming any extra energy, because its resonant frequency can be adjusted to minimise the response by changing dynamical properties such as mass, damping or stiffness in real time^[84].

The mechanism of MRE isolators is that the elastic modulus can be controlled by adjusting the magnetic field, which leads to changes of the resonant frequency of the dynamic system. Therefore, at low frequencies, where active vibration control is employed traditionally and passive vibration control is ineffective, the vibration response can be minimised by increasing dynamic stiffness. Semi-active control systems can be considered as hybrid control systems which combine the advantages of both passive ones and active ones.

In 1997, Watson designed a suspension bushing with MRE which enable the patent to vary its stiffness^[85]. Very recently, Hitchcock and Marur also applied patents for MRE vibration isolator and vehicle suspension, respectively^[86,87]. In 2011, Behrooz investigated an integrated system with two MRE isolators by using shaking table tests, and the change in natural frequency of the dynamical system showed that the proposed variable stiffness and damping isolators were capable of isolating structures from the ground vibration^[88]. Du presented a control strategy of vehicle seat suspension by using MRE isolator as shown in Figure 2.19, and

the results showed that the proposed continuous variable stiffness control achieves better isolation performance than conventional on-off control considering the driver body acceleration response^[89]. Opie also proposed an MRE isolator, which enables the device to have a fail-safe operation in the event of a power failure^[90]. Until now, the majority of research on MRE based isolation systems focused on characterisation, numerical evaluations and design of MRE isolators and the experimental tests were limited to simple structure models. However, the applicability to large structures has not been properly studied yet because of the challenge of numerically evaluating the complex behaviour of MRE based isolators and conducting experiments with large-size structures. Eem did pioneer work on the development of MRE isolators and designed a laminated rubber bearing to apply MRE in large scale by inserting aluminium plate layer in the elastomer block, as shown in Figure 2.20. The proposed a smart base isolation system had adaptability to various ground excitations and outperformed passive base isolation systems in terms of reducing the response of the structure^[91,92]. In 2013, Li came up with a seismic isolator, as shown in Figure 2.21. The structure of thin steel and MRE layers ensured a low lateral stiffness and very high vertical stiffness simultaneously. The ideal performance of this new MRE based isolator implied that the design of real-time adaptive base isolation systems would be capable of combatting any type of earthquake with efficiency^[8,67,93].

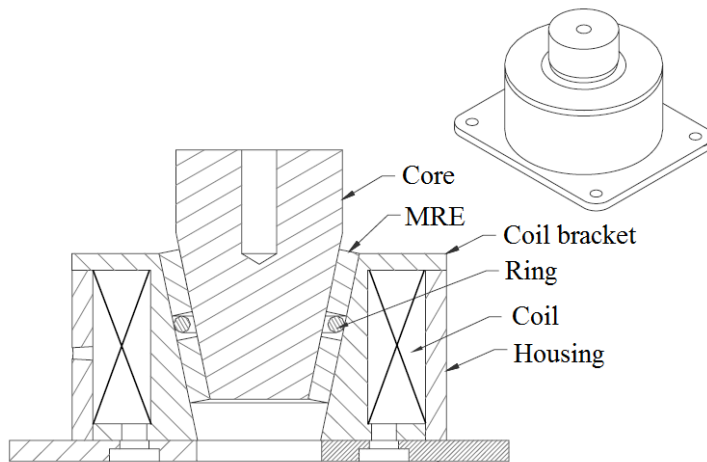


Figure 2.19 Schematic diagram of the MRE seat isolator^[89].

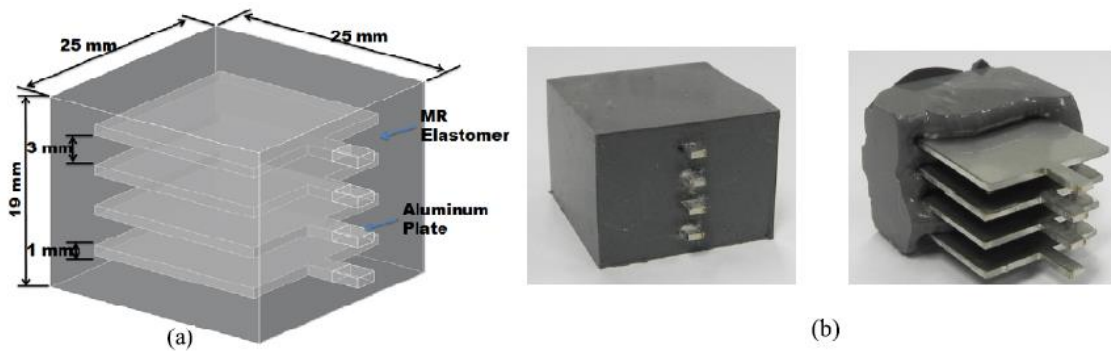


Figure 2.20 Laminated MRE based isolator. (a) Schematic diagram (b) Prototype of the isolator^[92].

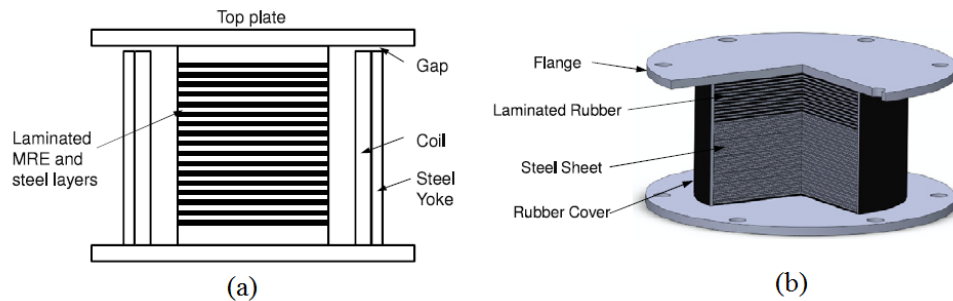


Figure 2.21 (a) Cross-section of the MRE base isolator (b) Typical laminated rubber isolator^[93].

2.5.3 MR structures

As an ideal candidate for smart element in vibration control systems, MRE can be used to tackle vibration problems with various control schemes for automotive industry, ship structures and civil engineering. In engineering practice, ship structures are subject to different kinds of dynamical loads exciting vibrations, which not only affect the operation and health of crew on board but also cause damage to the cargo. Due to their ability to change elastic modulus with the magnetic field, MRE materials can be used in dynamic structures to adjust natural frequency, which is determined by the stiffness and mass of the structure. As elastic modulus increases, the natural frequency of the structure shifts to higher frequencies. The structure can be protected from attaining the resonance phenomena by adjusting its natural frequency.

Choi investigated a core sandwich beam with MRE embedded between steel skins. The MR effects were studied at 0.3 Tesla by comparing simply supported beams with clamped beams. The experimental results showed that the resonance frequency increased by 12% and resonance peak decreases by about 10dB at simply supported conditions; the resonance frequency increased by 15% and the resonance peak decreased by about 8dB at clamped

condition^[94]. Yalcintas studied homogeneous sandwich beams with MR materials between two elastic layers. Both theoretical and experimental results show that for simply supported boundary condition the application of MR adaptive beam resulted in a reduction of 20dB in the vibration amplitudes and a shift of 30% in natural frequencies^[95]. Ni investigated the micro-vibration control efficiency of both MRE based composite wall and MRE based composite floor, as shown in Figure 2.22. The analytical results of velocity response showed that the composite structure incorporating MRE material possessed great micro-vibration suppression capability for support motion excitation of varying frequency^[96]. Dwivedy presented a symmetric three-layered beam with conductive skins and MRE patch between two soft viscoelastic patches in the core layer. From the research when the sandwich beam was subject to periodic axial load, the stability of the system could be significantly improved by the MRE material^[97,98].

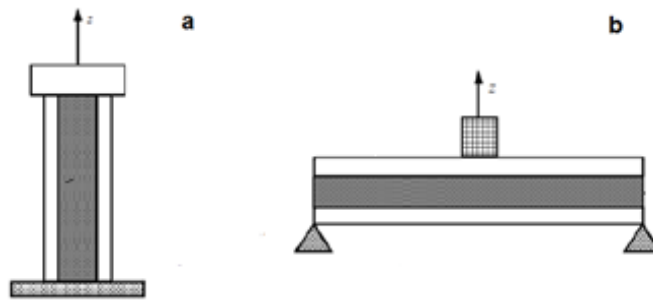


Figure 2.22 Diagrams of (a) an MRE-based composite wall supporting equipment and (b) an MRE-based composite floor supporting equipment^[96].

Aiming at high performance of MR materials, MR fluid-elastomer (MRF-E) has been studied to combine the advantages of MRF material and MRE material. Wang proposed a MR mount with MRF encapsulated in an elastomer; as a result the mount was capable of adjusting dynamic stiffness and damping. The results showed that MRF-E structure enlarged the capacity of changing damping and stiffness with the application of magnetic field^[99]. Similar to the MRF-E mounts, the stiffness of MRF-E vibration isolator changed with the displacement amplitude and magnetic field strength, which made the new isolator have potential in applications where tuning vibration characteristics were desired^[100]. Anderson designed a new isolator consisting of MRF contained within an MRE jacket. The isolator possessed the ability of adjusting its response to stochastic shock and vibratory disturbances^[101]. Zhang studied MRE embedded with MR fluids and MR gels, as shown in Figure 2.23. The experimental results showed that the MR effect was enlarged with the structure and the mechanical properties of MR material was improved^[102]. MRE can be also developed using temperature-controllable materials. Gong studied the damping properties of MRE with polycaprolactone (PCL) as the

temperature-controllable component, which can be transformed from semi crystalline solid into liquated soft material through increasing the temperature above the melting point, as shown in Figure 2.24. This research indicated that when the temperature was above the PCL melting point, the influence of applied magnetic field on the loss factor was enlarged. In addition, when the temperature was below the PCL melting point, great enhancements took place in the strain and frequency dependence of the loss factor^[103].

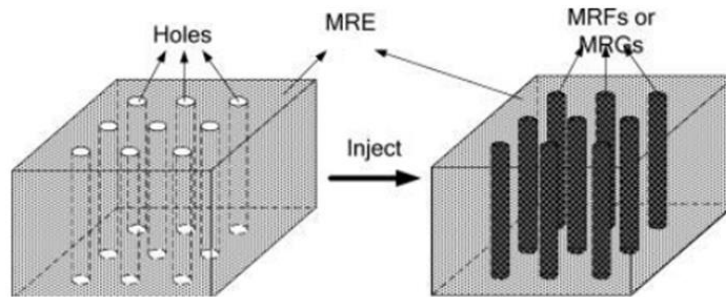


Figure 2.23 Schematic diagram of sample with holes of MRF and MRG^[102].

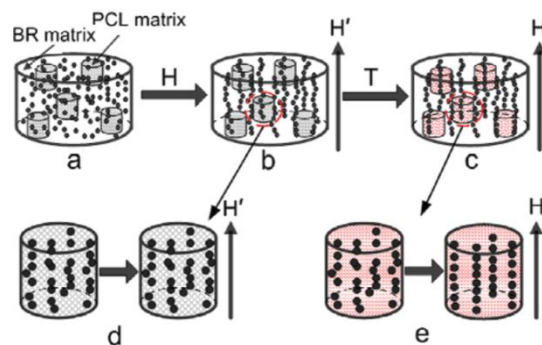


Figure 2.24 Microscopic structures of PCL-blended MRE where (a) before the preforming configuration, (b) and (c) after the preforming configuration, respectively, corresponding to the two states when the temperature is below and above PCL melting point, and (d) and (e) are the enlarged views of the distribution of particles in the matrix corresponding to (b) and (c)^[103].

2.5.4 Feasibility study of MRE

MR effect is a result of change in the mechanical properties of material as the magnetic field strength changes. Since the discovery in 1948 of the magneto-rheological (MR) phenomenon by Rabinow^[4], MRF has been industrialized and commercialized based on its variation capability of yield stress within a post-yield regime under applied magnetic field. Considering MRF comprises of magnetically polarisable particles suspended in viscous fluids, MRE can be taken as the structural solid analogue of MRF, because MRE is composed of polarisable particles dispersed in a polymer medium. Compared with MRF the MR effect of MRE is the field-

dependent elastic modulus within a pre-yield regime and the application of MRE is still on an exploratory stage. But MRE is a good solution to overcome the defects which are latent in the applications of MRF, such as deposition, environmental contamination and sealing problems^[9]. Because of a stable microstructure, compared with common organic polymers, MRE has a relatively higher heat resistance, flame retardancy and chemical stability and also provides better electrical insulation. Take silicone rubber based MRE as an example, which are not flammable, toxic or volatile, and the microstructure is considered to be stable in a broad temperature range between -100 °C and 250 °C^[104]. Additionally silicone rubber based MRE have good resistance to aging and oxidation, so they can work for several decades under natural environment^[105].

At present, the mechanical properties of MRE require an in-depth study, such as Mullin effect, Payne effect, temperature influence, frequency dependence and fatigue mechanism. According to Zhang's study, the storage modulus and loss modulus of MRE with mass fraction 60% of iron particles were almost independent of the strain amplitudes and number of cycles, whilst the storage modulus and loss modulus of MRE with 80% iron particles by weight were strongly dependent on the strain amplitudes and number of cycles, as shown in Figure 2.25^[106]. Zhou investigated the equi-biaxial fatigue properties of MRE within a dynamical bubble inflation system at various stress amplitudes ranging from 0.75 to 1.4 MPa. The stress-strain relationship and S-N curves of MRE, from the experimental results, can be seen in Figure 2.26. The fatigue lives decreased with the stress and stress softening continued with the accumulation of cycles, especially the softening behaviour was more pronounced in the first 100 cycles^[107]. As shown in Figure 2.27, Zhang studied the durability properties of MRE materials based on a series of matrices mixed with cis-polybutadiene rubber (BR) and natural rubber (NR). Both the storage and loss moduli decreased with increasing number of cycles and the MR effect increased after cyclic loading^[108].

Most applications of MRE are limited by its lower MR effect. Lower zero-field elastic modulus usually results in a greater relative MR effect. However, it is usually ill-suited for load-bearing applications due to the low strength and reduced fatigue life. Therefore, the research of MRE is still on a very early stage of commercial and industrial applications. The mechanical properties of MRE are dependent on strain, frequency, temperature, humidity, microstructure and magnetic field. Among these dependent properties, strain dependence limits MRE materials for load bearing applications, because the elastic modulus decreases with increasing strain.

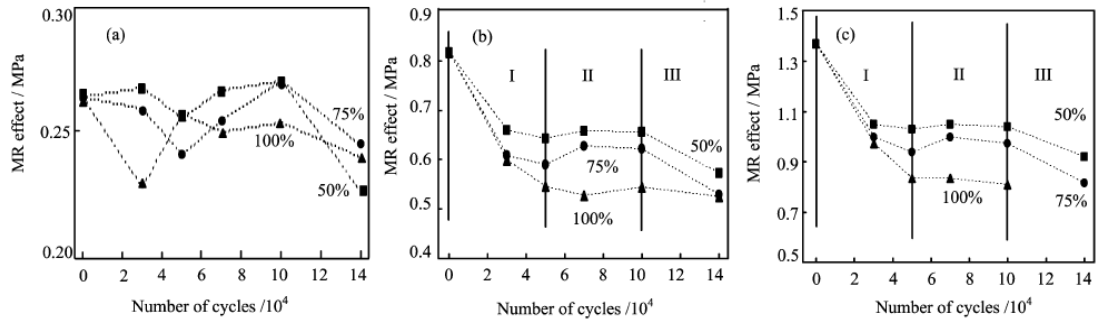


Figure 2.25 Relationship between MR effect and number of cycles for structured MRE with (a) 60%, (b) 70%, and (c) 80% iron particles by mass, under various fatigue strain amplitudes^[106].

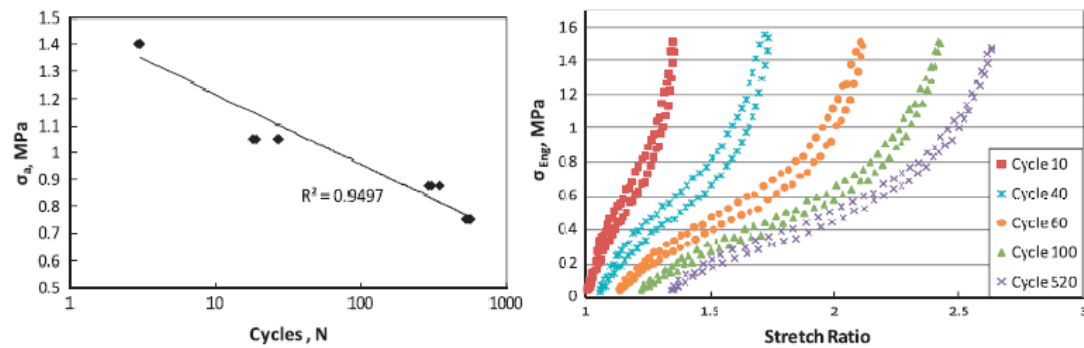


Figure 2.26 (a) Stress amplitude versus log cycles to failure and (b) Stress softening behaviour in an engineering stress controlled fatigue test^[107].

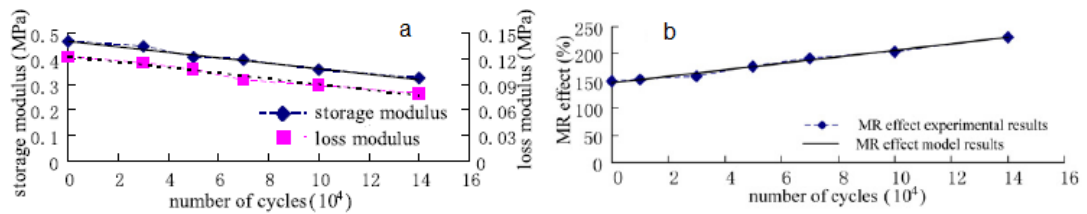


Figure 2.27 (a) Modulus after cyclic loading and (b) Relationship between MR effect and cycle numbers^[108].

2.6 Motivation for current work

In a summary, current research on the engineering application of MRE is still in its infancy. Lots of experimental results are reported on the stiffness properties of MRE, but there are a lot of work undone to understand the dependence of damping properties on frequency, strain and magnetic field. In addition, because of time-varying vibration sources in reality current mathematical models for describing the dynamical behaviour of MRE are deficient to support related applications for vibration control. Considering effectiveness and economy, a

valid methodology of performance evaluation without manufacturing and testing MRE devices is important for the dynamic design of vibration control devices.

To achieve deeper and more comprehensive understanding of the mechanical properties of MRE material and structure forms the foundational motivation of this PhD project. The overall objective is to apply MRE material in vibration control systems, as part of this project. This thesis mainly focuses on the aspects associated with the dynamical analysis of MRE, including:

1. Characterising the mechanical properties of MRE experimentally to investigate the influence of frequency, strain and magnetic field on the dynamical behaviour.
2. Establishing a nonlinear model mathematically with all the above dependences taken into account to describe the dynamical behaviour of MRE material and structure.
3. Analysing the vibration response, transmissibility and vibratory energy transmission of dynamical systems with MRE structure to evaluate the vibration control efficiency.

Chapter 3 **Experimental setup for dynamical property characterisation of MRE**

3.1 Introduction

The mechanical properties of MRE material have been studied by many researchers both theoretically and experimentally, but there is still much work to be done for the commercialisation and industrialisation of its application. MRE has field dependent modulus which can be controlled by adjusting an external magnetic field, and the microstructure of MRE affects its mechanical properties and dependences on magnetic fields, strains and frequencies. At present we can learn the stiffness properties with current experimental studies, but more investigations on the loss modulus are necessary for understanding the damping properties.

This chapter mainly focuses on the experimental setup for dynamic load testing and the characterisation of mechanical properties. Firstly, the preparation of MRE samples is briefly introduced with respect to its composition, categories and fabrication. And then the test apparatus and data processing method are illustrated. Secondly, a series of experiments are carried out in shear mode to investigate the influence of microstructure on the mechanical properties of MRE, especially the influence of magnetisable particles, magnetic fields and coupling agents. Therefore, this chapter offers the preparation and methodology for dynamic mechanical analysis of MRE in the following sections.

3.2 Experimental setup

3.2.1 MRE samples preparation

The simplified manufacturing procedure can be illustrated as follows: firstly Elastosil A is mixed with Elastosil B, according to the instructions (Appendix I) the mixing ratio of these two compounds was 10:1 by weight. Silicone oil is chosen based on the discussion in Section 2.1 and can be also added into the mixture under the guidance of Appendix II to improve the interaction between magnetisable particles and non-magnetic matrix, such as the MRE samples in Section 3.3.3. Then the carbonyl iron powders sized up to 9 μm are added with reference to an identified optimal particle volume concentration of about 30%^[22], which is considered to be

able to generate the maximum MR effect; secondly, after stirring thoroughly, the mixture is placed in a vacuum chamber for about 30 minutes at room temperature to remove air bubbles entrapped inside; finally the mixture is put into square prism aluminium moulds $21.8 \times 21.8 \times 6.5 \text{ mm}^3$ and left to solidify.

The shape and dimensions of the MRE samples are designed by referring to the BS ISO 4664-1:2011 (Appendix III) for shear tests and the basic parameters of small-sized samples are given in Table 3.1. For the curing of anisotropic samples, the moulds with mixture inside are placed between two permanent magnets producing a stable uniform magnetic field. In this study, the MRE is assumed to be homogeneous on the considered length scale and non-aging under isothermal conditions at room temperature. Without the application of magnetic field the isotropic MRE is perfectly isotropic but the anisotropic MRE is not. In Table 3.2, the pot lives and curing times of MRE processing are listed at various temperatures. As instructed in Appendix I, the pot lives indicate the time required for the mixture to attain a viscosity of 150 Pa·s and curing times apply to a layer thickness of 1cm. It can be seen that as the curing temperature increases the required time for MRE casting reduces.

Table 3.1 Fabrication of small-sized samples

Iron particle size, μm	6 ~ 9
Shape	Rectangular column
Dimensions, mm^3	$22.0 \times 22.0 \times 6.5$
Magnetic flux density, mT	0. 290

Table 3.2 Pot lives and curing times at various temperatures

Temperature $^{\circ}\text{C}$	Pot lives	Curing times
5	6 hr	
23	90 min	15 hr
30	40 min	4 hr
60		2 hr
100		15 min

3.2.2 Dynamic test apparatus

The experiments for the mechanical property characterisation were performed by Instron E1000 Electro plus in Transport Systems Research Laboratory. During dynamic tests, displacement and force are the main tracking channels. The strain amplitude and the excitation frequency can be controlled by the channels of displacement and time, and the resulting stress can be calculated by measuring the force channel. In this study circular disc magnets are used to carry out dynamic tests for MRE by varying the external magnetic field. As shown in Figure 3.1, the diameter of the circular disc magnets is 40mm. By adding the applied circular disc magnets, the magnetic flux density can be increased by several discrete values. With permanent magnets the magnetic field intensity can be only changed in discrete values and the low requirement of magnetic field makes low costs of permanent magnets preferable for the experiments of mechanical property characterisation. Comparatively expensive electro-magnets are capable to continuously control the magnetic field intensity, which is essential for the adaptive MRE devices to improve the effectiveness of vibration control.

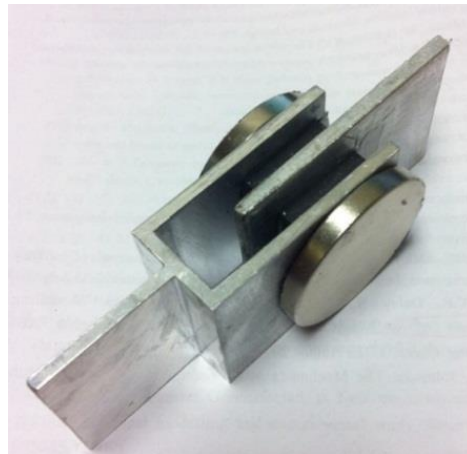


Figure 3.1 Shear test rigs for MRE samples with circular disc magnets.

As shown in Figure 3.2, two rectangular MRE blocks are bonded to the surfaces of stainless aluminium rigs using Araldite Standard adhesive. Before the loading tests, the MRE samples are preloaded and unloaded for at least five times until 20% in strain because of Mullins effect, which is a phenomenon where the stiffness decreases with the loading cycles until the material comes to a stable point after certain cycles (usually 3-5)^[38]. As a kind of filled rubber, the same applied strain will result in lower and lower stress in MRE during the first loading cycles, which can be idealised for many purposes as an instantaneous and irreversible softening of the stress–strain curve that occurs whenever the load increases beyond the

maximum value it encountered previously^[39]. When strains applied to anisotropic MRE samples, the mode of testing we attain with this apparatus is not pure shear. But in this thesis the applied strains are small, so it is assumed that the related errors can be neglected to have pure shear states for anisotropic MRE samples during testing.

According to BS ISO 4664-1:2011 (Appendix III), the shear property characterisation of MRE was performed under static and dynamic loading conditions in certain range of frequencies, strain amplitudes and magnetic flux densities, as shown Table 3.3.

Table 3.3 Test apparatus for small-sized samples

Frequency, Hz	1, 5, 10, 20, 30, 40, 50, 60, 70, 80
Strain amplitude, %	0, 1, 2, 3, 4, 5
Magnetic flux density, mT	0, 160, 260, 400, 500

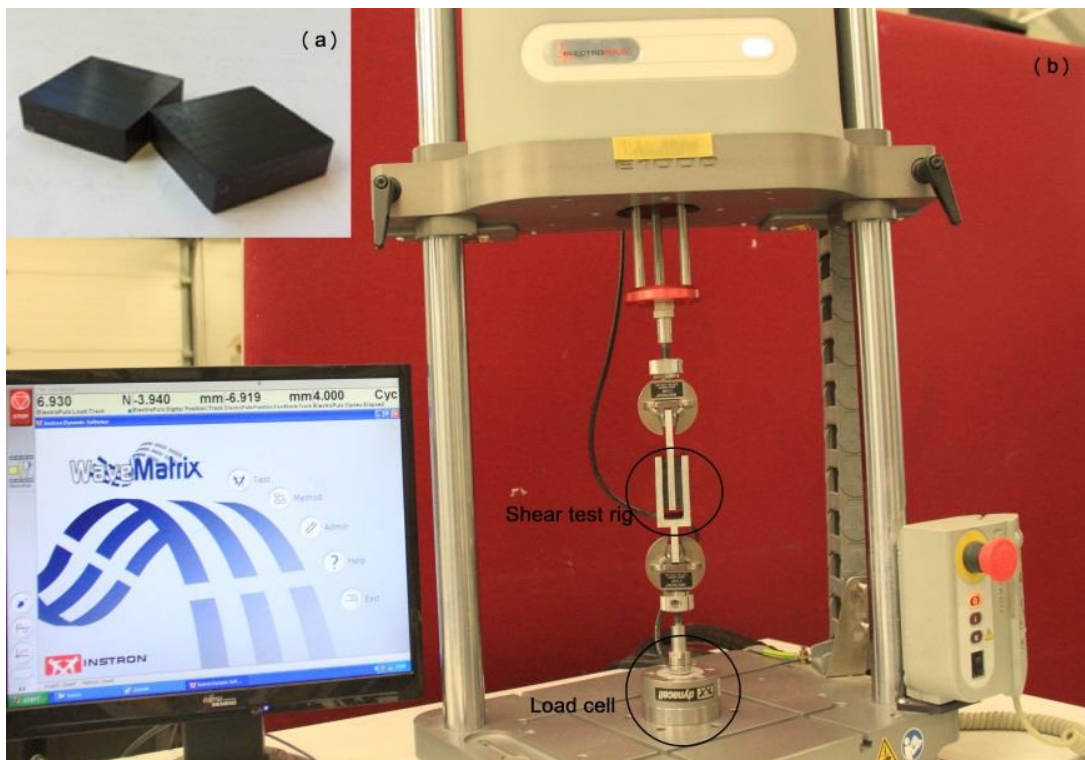


Figure 3.2 (a) MRE samples. (b) Experimental setup.

3.2.3 Data process method

The experimental data of frequency, load and position channels are recorded to obtain the force-displacement curves for MRE samples. The dynamic tests are performed for a range of frequencies from 0 to 80Hz, strain amplitudes from 0 to 5% and magnetic field intensities from 0 to 0.5 T. The storage and loss moduli of MRE can be calculated following the directions of the manual of Instron E1000 Electro plus for Dynamic Mechanical Analysis measurements (Appendix IV). In order to attain a good reliability, each set of tests are carried out with three pairs of samples independently, every test is repeated twice for each pair of samples and the experimental data are averaged to present the curve or surface. During testing we noticed that the experimental data change very little for the same samples when the dynamic tests are repeated, there are small differences in the experimental data between different pairs of samples in the same set, and the six experimental results in the same set have the same trends in the range of strain, frequency and magnetic field for testing.

As a kind of rubber material, the MRE cannot respond instantaneously when a sinusoidal strain is applied because of its viscosity; hence the resultant stress will lag the input with a loss angle or factor, as shown in Figure 3.3.

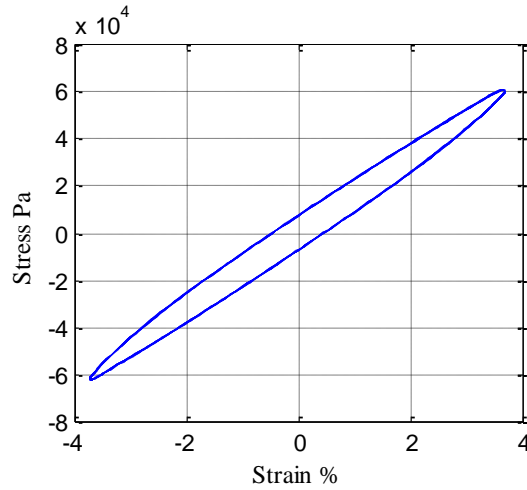


Figure 3.3 Stress-strain plot for MRE material under harmonic load.

To take this situation into consideration, mathematically the modulus of MRE is considered to be a complex number comprising a real elastic component and an imaginary viscous component, namely the storage modulus and loss modulus

$$M^* = M' + iM'' \quad (3.1)$$

where M^* can be either the Young's modulus E or the shear modulus G , M' and M'' denote the storage modulus and the loss modulus, respectively. The complex modulus M^* can be obtained by calculating the ratio of the stress range to the strain range. The loss angle φ is relevant to the energy dissipation per volume within an oscillatory cycle, which is the area enclosed by the hysteresis loop and can be calculated following the Dynamic Mechanical Analysis directions of the manual for Instron E1000 ElectroPlus measurements in this study. The complex modulus M^* , storage modulus M' , loss modulus M'' and loss angle φ can be defined as follows:

$$\begin{aligned}
M' &= M^* \cos \varphi \\
M'' &= M^* \sin \varphi \\
M^* &= A_{stress} / A_{strain} \\
\varphi &= \arcsin \frac{E_{loop}}{\pi A_{strain} A_{stress}}
\end{aligned} \tag{3.2}$$

where E_{loop} is the energy enclosed by the hysteresis loops, A_{strain} denotes the strain amplitude and A_{stress} the stress amplitude.

3.3 The influence of microstructure on MRE mechanical properties

3.3.1 The influence of magnetisable particles

In Figure 3.4 we can see the influence of microstructure on storage modulus due to the presence of magnetisable particles, and the blue dots on the surface indicate experimental data of silicone rubber and isotropic MRE. It can be seen from Figure 3.4 (a) that in the dynamic tests the storage modulus of silicone rubber decrease with the increasing strain amplitude and increases as the driving frequency increases. From 1Hz to 80Hz, the storage modulus increases dramatically at the beginning, higher than 20Hz it increases slowly and reaches the highest storage modulus of 0.76MPa. From Figure 3.4 (b) we can see that the storage modulus of isotropic MRE shows a similar dependence on frequency and strain as silicone rubber in the vibration tests. The storage modulus decreases as the strain amplitude increases. When the driving frequency goes up from 1Hz to 80Hz, the storage modulus increases obviously at the beginning, higher than 20Hz the increase slows down and the highest storage modulus is 1.25MPa at 80Hz. Comparing Figure 3.4 (a) with Figure 3.4 (b), it is obvious that the presence of magnetisable particles, in agreement with the previous discussion in [45], improve the storage modulus of the elastomer by approximately 70%. But it does not change the dependence on frequency and strain, because the two fitting surfaces have similar shapes.

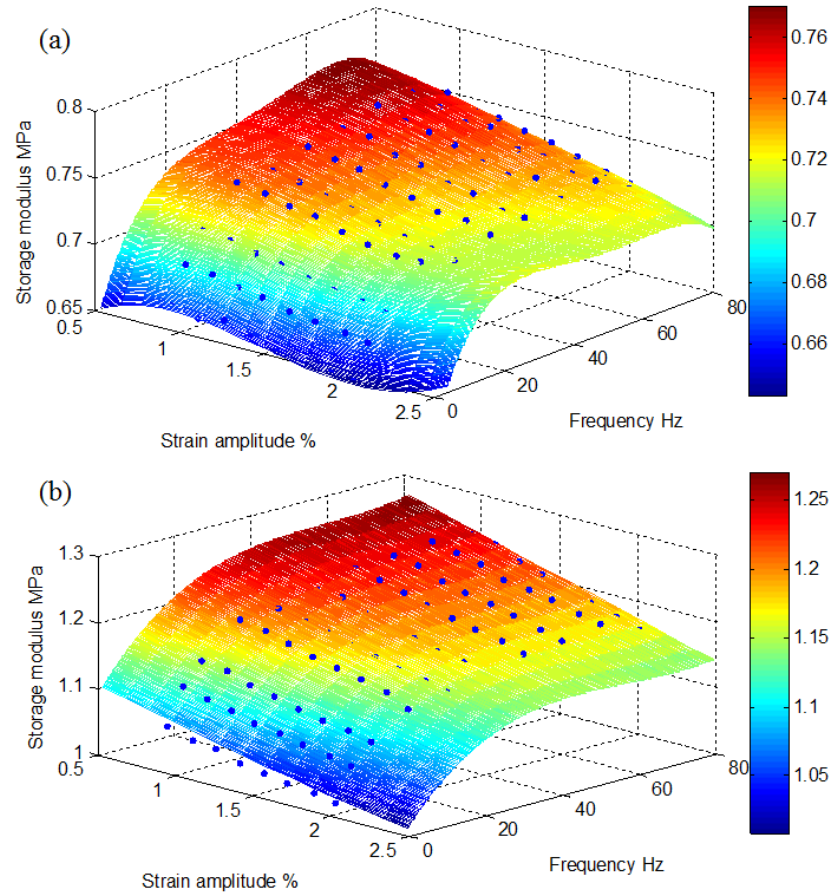


Figure 3.4 Storage modulus of (a) silicone rubber and (b) isotropic MRE with different strain amplitude and loading frequency.

The influence of microstructure on loss modulus due to the presence of magnetisable particles can be seen in Figure 3.5, and experimental measurements of silicone rubber and isotropic MRE are denoted by the blue dots. Figure 3.5 (a) shows that in the vibration tests the loss modulus of silicone rubber does not change with the strain amplitude. As the driving frequency increases from 1Hz to 80Hz, the loss modulus increases at the beginning, at 10Hz it reaches a maximum of 46 kPa and starts to decrease with further increase of frequency. It can be seen from Figure 3.5 (b) that the loss modulus of isotropic MRE shows a similar dependence on frequency and strain as silicone rubber in the dynamic tests. The loss modulus barely decreases with increasing strain amplitude. The loss modulus also increases with the driving frequency at the beginning, reaching a maximum of 89 kPa at 10Hz and starts to decrease with further increasing frequencies. From the comparison of Figure 3.5 (a) and Figure 3.5 (b), we can see that the presence of magnetisable particles, in agreement with the observations in [45], improves the loss modulus of the elastomer by approximately 100%. As the two fitted surfaces have similar shapes, so it does not change the dependence on frequency and strain.

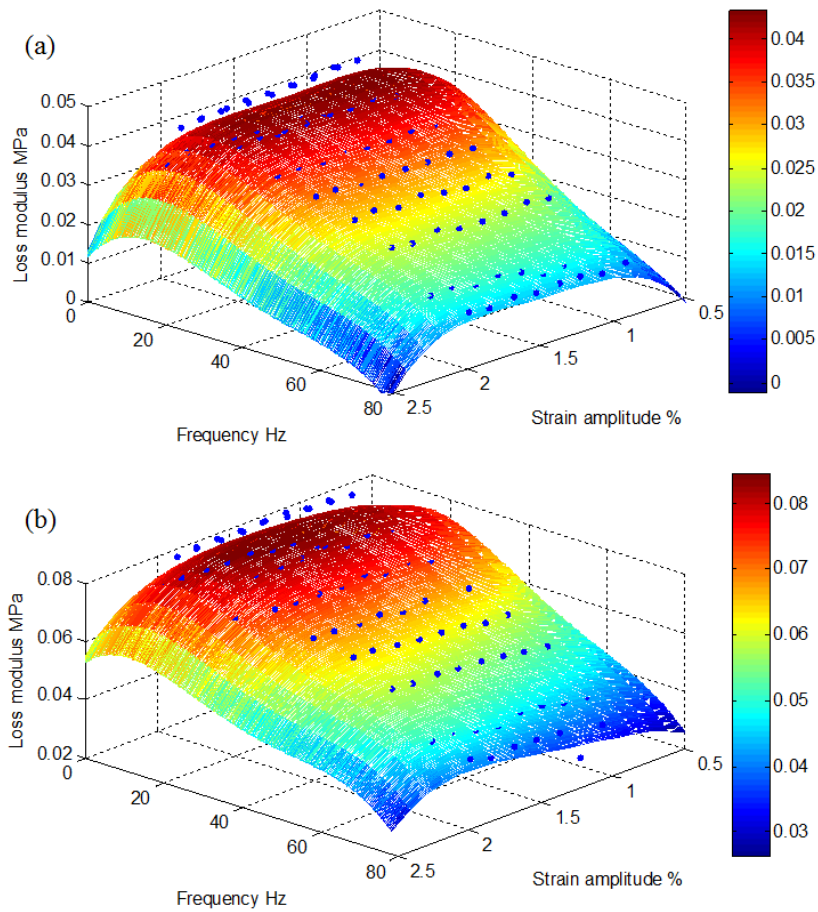


Figure 3.5 Loss modulus of (a) silicone rubber and (b) isotropic MRE with different strain amplitude and loading frequency.

Figure 3.6 illustrates the influence of microstructure on loss factor due to the presence of magnetisable particles, and the blue dots indicate experimental data of silicone rubber and isotropic MRE. It can be seen from Figure 3.6 (a) that in the dynamic tests the loss factor of silicone rubber does not change with the strain amplitude. As the driving frequency goes up from 1Hz to 80Hz, the loss factor increases at the beginning, reaches a maximum of 0.06 at 10Hz and starts to dramatically decrease at higher frequencies. Figure 3.6 (b) shows that the loss factor of isotropic MRE has the same dependence on frequency and strain as silicone rubber in vibration tests. The loss factor changes little with the strain amplitude; meanwhile it increases with the driving frequency at the beginning, reaches a maximum of 0.08 at 10Hz and begins to decrease with further increasing frequencies. By comparing Figure 3.6 (b) with Figure 3.6 (a) we can see that the presence of magnetisable particles improves the loss factor of the elastomer by about 20%. However, it changes the dependence on frequency and strain very little, because the two fitted surfaces have the same shapes.

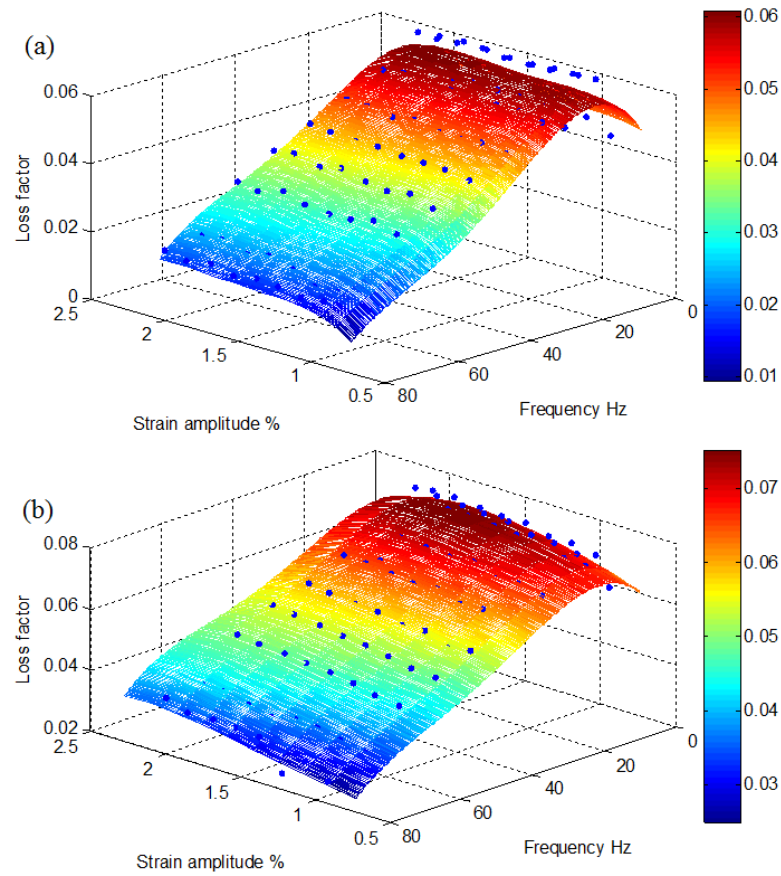


Figure 3.6 Loss factor of (a) silicone rubber and (b) isotropic MRE with different strain amplitude and loading frequency.

3.3.2 The influence of magnetic field

In this section, the solidification of anisotropic MRE samples is attained with a magnetic field of 290mT. In Figure 3.7 we can see the influence of microstructure on storage modulus due to the presence of magnetic field and the experimental measurements of isotropic MRE and anisotropic MRE by the blue dots. Figure 3.7 (a) shows that the storage modulus of isotropic MRE decrease with the strain amplitude and increases with the driving frequency. From 1Hz to 80Hz, the storage modulus increases obviously at the beginning, higher than 20Hz it slows down and reaches 1.25MPa at 80Hz. From Figure 3.7 (b) we can see that the storage modulus of anisotropic MRE shows a similar dependence on frequency and strain as the isotropic MRE. The storage modulus decreases with the strain amplitude. As the frequency increases from 1Hz to 80Hz, the storage modulus increases dramatically at the beginning, higher than 20Hz the increase is slow and the maximum of storage modulus is 2.1MPa. The comparison between Figure 3.7 (a) and Figure 3.7 (b) shows that with the same particle volume concentration the presence of a magnetic field about 290mT during the solidification can improve the storage

modulus of the elastomer by about 65% and also enhance the dependence of storage modulus on frequency and strain at the same time.

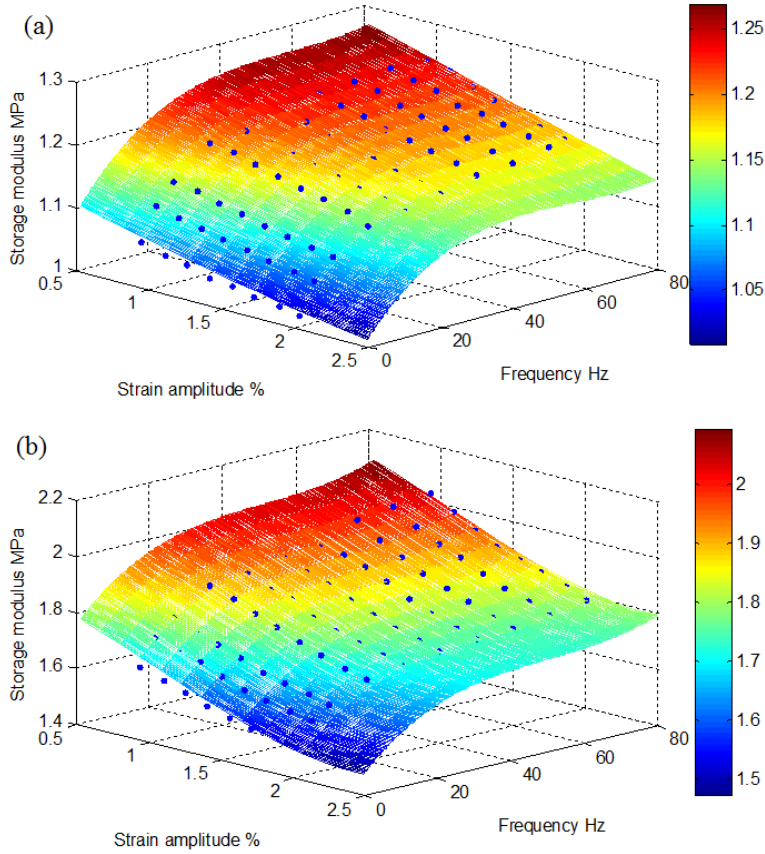


Figure 3.7 Storage modulus of (a) isotropic MRE and (b) anisotropic MRE with different strain amplitude and loading frequency.

Figure 3.8 illustrates the influence of microstructure on storage modulus due to the presence of magnetic field, and the blue dots indicate experimental results of isotropic MRE and anisotropic MRE. From Figure 3.8 (a) it can be seen that at 10Hz the storage modulus of the isotropic MRE increases with magnetic field intensity, and decreases with the increasing strain amplitude. The storage modulus reduces to 1.1MPa when the strain amplitude is 2%. With an external magnetic field of 400mT the storage modulus reaches as high as 1.28MPa when the strain amplitude is 0.9%. In Figure 3.8 (b) the dependence of anisotropic MRE on strain and field is similar to the isotropic MRE in the dynamic tests. When the loading frequency is 10Hz, the application of external magnetic field increases the storage modulus of the anisotropic MRE, but the strain amplitude reduces the storage modulus. Without any external magnetic field, the storage modulus is 1.9MPa when the strain amplitude is 2%; and with an external magnetic field of 400mT, the storage modulus can be as high as 2.8MPa when the strain amplitude is

0.9%. Comparing Figure 3.8 (b) with Figure 3.8 (a), it is obvious that with the same loading frequency of 10Hz and the same particle volume concentration of 30%, the presence of a magnetic field about 290mT during the curing progress can increase the storage modulus of MRE by approximately 100% and also enhance the dependence on magnetic field and strain.

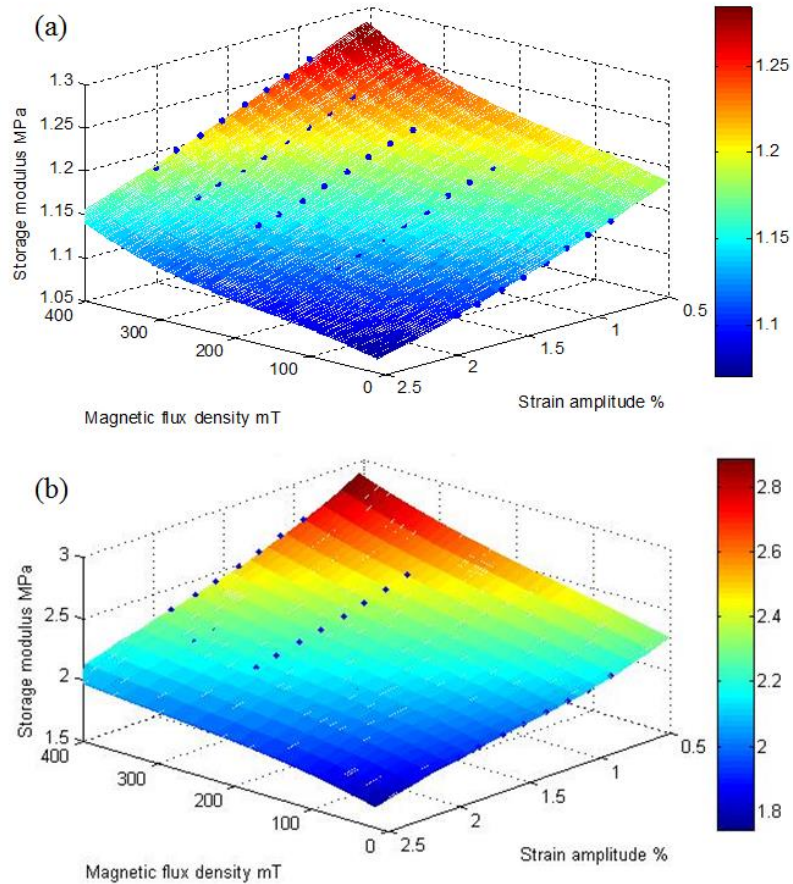


Figure 3.8 Storage modulus of (a) isotropic MRE and (b) anisotropic MRE at 10 Hz with different strain amplitude and magnetic field.

In Figure 3.9 the influence of microstructure on loss modulus due to the presence of magnetic field during curing is shown, and the blue dots are experimental measurements of isotropic MRE and anisotropic MRE. It is shown in Figure 3.9 (a) that without the application of external magnetic field the loss modulus of isotropic MRE decreases slightly with the strain amplitude. As the driving frequency goes up from 1Hz to 80Hz, the loss modulus increases at the beginning, reaches a maximum of 89 kPa at 10Hz and starts to decrease with further increase of driving frequency. From Figure 3.9 (b) we can see that without the application of external magnetic field the loss modulus of anisotropic MRE shows a similar dependence on frequency and strain as isotropic MRE in vibration tests. The loss modulus decreases with the

strain amplitude but more than isotropic MRE. From 1Hz to 80Hz the loss modulus increases initially, reaches a maximum of 240 kPa at 10Hz and decreases with further increasing frequencies. By comparing Figure 3.9 (b) with Figure 3.9 (a), it can be seen that with the same particle volume concentration of 30% the presence of a magnetic field about 290mT during solidifications can increase the loss modulus of the elastomer by about 300% and also enhance its dependence on frequency and strain.

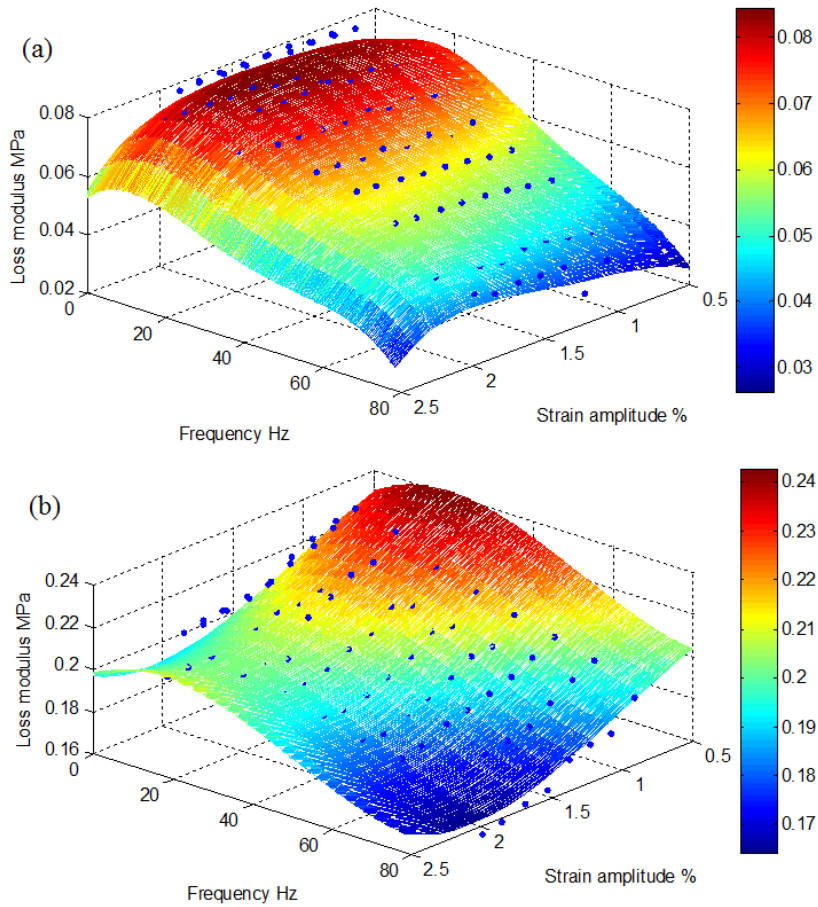


Figure 3.9 Loss modulus of (a) isotropic MRE and (b) anisotropic MRE with different strain amplitude and loading frequency.

From Figure 3.10 we can see the influence of microstructure on loss modulus due to the presence of magnetic field and experimental data of isotropic MRE and anisotropic MRE are denoted with the blue dots on the surface. Figure 3.10 (a) shows that when the loading frequency is 10Hz the loss modulus of isotropic MRE increases with the magnetic flux density and decreases when the strain amplitude increases. Without any external magnetic field, the loss modulus of isotropic MRE is 80 kPa when the strain amplitude is 2%; with an external magnetic field of 400mT the loss modulus is 0.1MPa when the strain amplitude is 0.9%. In Figure 3.10 (b)

it is shown that at 10Hz the loss modulus of anisotropic MRE has a similar dependence on strain and magnetic field as the isotropic MRE in dynamic tests. The application of external magnetic field increases the loss modulus of anisotropic MRE; however, the increasing strain amplitude reduces the loss modulus. Without any external magnetic field, when the strain amplitude is 2% the loss modulus of anisotropic MRE is 0.22MPa; with an external magnetic field of 400mT the loss modulus is 0.32MPa when the strain amplitude is 0.9%. From the comparison of Figure 3.10 (a) and Figure 3.10 (b), we can see that when the loading frequency is 10Hz, the presence of a magnetic field about 290mT during curing can improve the loss modulus of MRE with the same composition by approximately 300% and also enhance the dependence of loss modulus on magnetic field and strain.

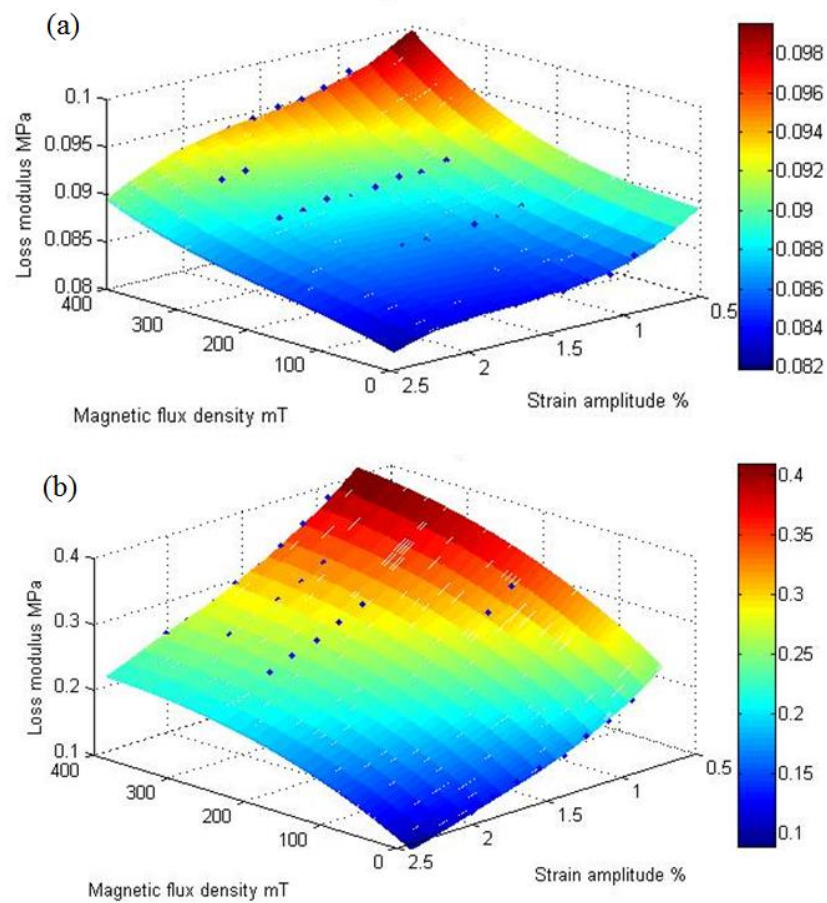


Figure 3.10 Loss modulus of (a) isotropic MRE and (b) anisotropic MRE at 10 Hz with different strain amplitude and magnetic field.

Figure 3.11 shows the influence of microstructure on loss factor due to the presence of magnetic field, and the blue dots indicate experimental measurements of isotropic MRE and anisotropic MRE. From Figure 3.11 (a) it can be seen that without any external magnetic field

the loss factor of isotropic MRE changes little with the strain amplitude. As the frequency increases from 1Hz to 80Hz, the loss factor initially increases, reaches a maximum of 0.08 at 10Hz and starts to decrease at higher frequencies. In Figure 3.11 (b), without the application of magnetic field the loss factor of anisotropic MRE shows the same dependence on frequency and strain as the isotropic MRE. The loss factor changes very little with the strain amplitude. From 1Hz to 80Hz, the loss factor increases at the beginning, reaches a maximum of 0.13 at 10Hz and stops to decrease with further increasing frequencies. Comparing in Figure 3.11 (a) and (b) we can see that with the same particle volume concentration the presence of a magnetic field about 290mT during the solidification can increase the loss factor of MRE by approximately 80%, however, it does not change the dependence on frequency and strain as the two fitted surfaces have similar shapes.

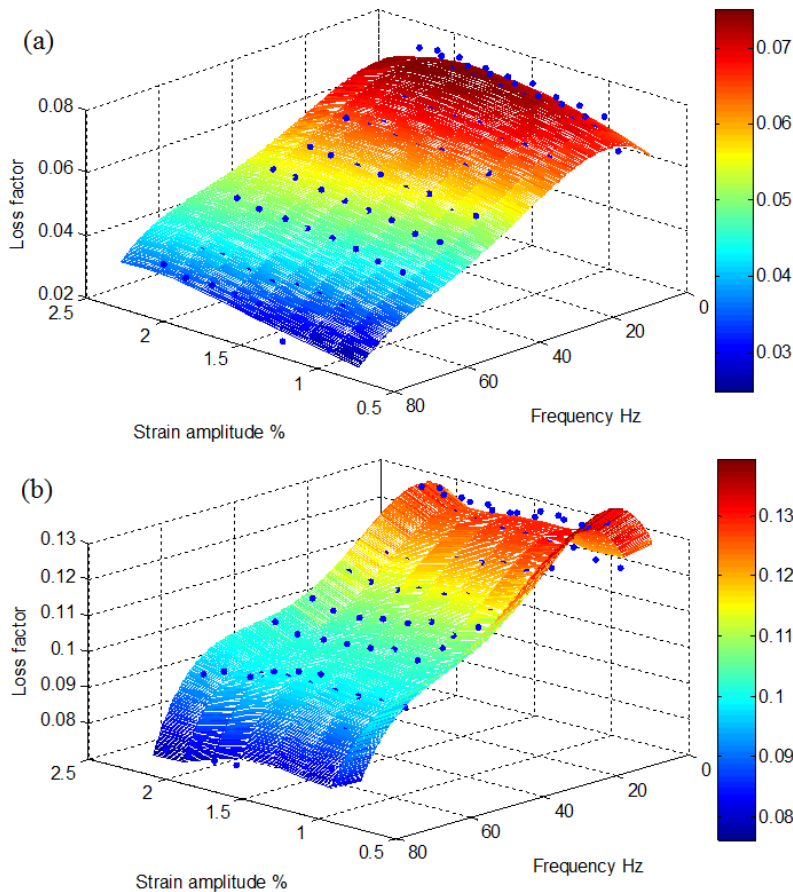


Figure 3.11 Loss factor of (a) isotropic MRE and (b) anisotropic MRE with different strain amplitude and loading frequency.

The influence of microstructure on loss factor due to the presence of magnetic field can be seen in Figure 3.12, and the experimental measurements of isotropic MRE and anisotropic

MRE are indicated with blue dots. It is shown in Figure 3.12 (a) that when the frequency is 10Hz the loss factor of isotropic MRE increases with the magnetic field intensity and decreases with the strain amplitude. Without any external magnetic field, the loss factor of isotropic MRE is as low as 0.074; with an external magnetic field of 400mT the loss factor is 0.082. From Figure 3.12 (b) it can be seen that at 10Hz the loss factor of anisotropic MRE also increases with the magnetic field density and decreases with the strain amplitude. An application of 400mT magnetic field increases the loss factor of anisotropic MRE from 0.11 to 0.135. From the comparison between Figure 3.12 (b) and Figure 3.12 (a) it is obvious that with the same particle volume concentration of 30% and the loading frequency of 10Hz, the presence of a magnetic field about 290mT can improve the loss factor of MRE by about 65% and also enhance the dependence on magnetic field and strain.

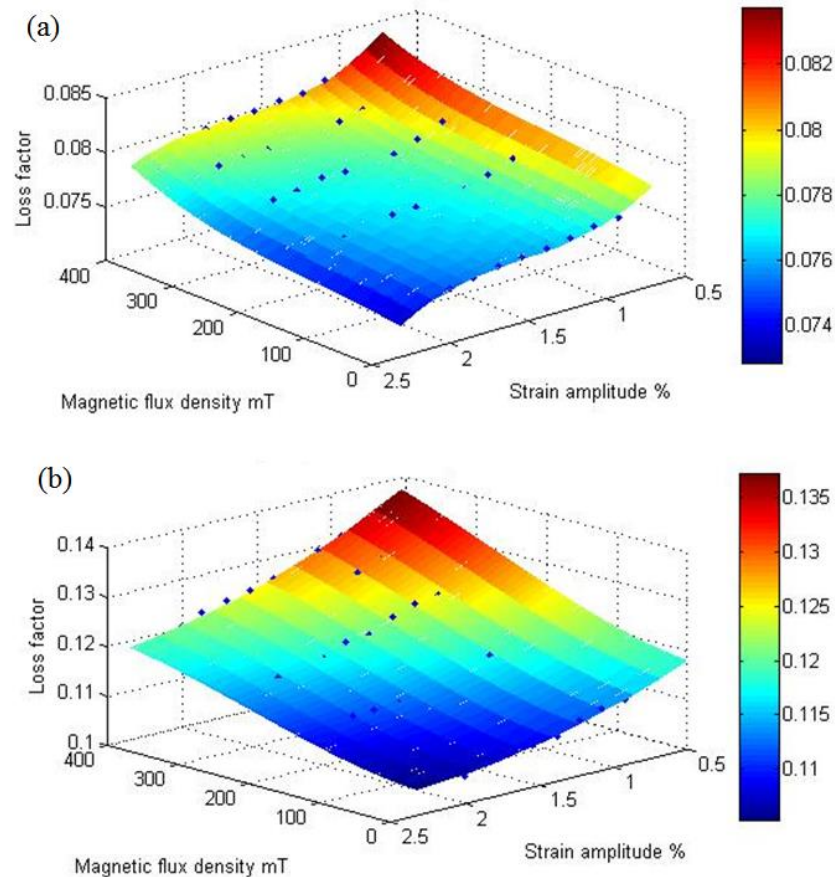


Figure 3.12 Loss factor of (a) isotropic MRE and (b) anisotropic MRE at 10 Hz with different strain amplitude and magnetic field.

3.3.3 The influence of coupling agents

In this section, a group of anisotropic MRE samples are fabricated in the same magnetic field with a coupling agent to investigate its influence on the mechanical properties of MRE. Silicone oil volume concentration is 20%, silicone rubber volume concentration is 50% and carbonyl iron particle volume concentration stays at 30%.

Figure 3.13 shows the influence of microstructure on storage modulus due to the application of coupling agent, and the blue dots indicate experimental measurements of the anisotropic MRE with and without coupling agent.

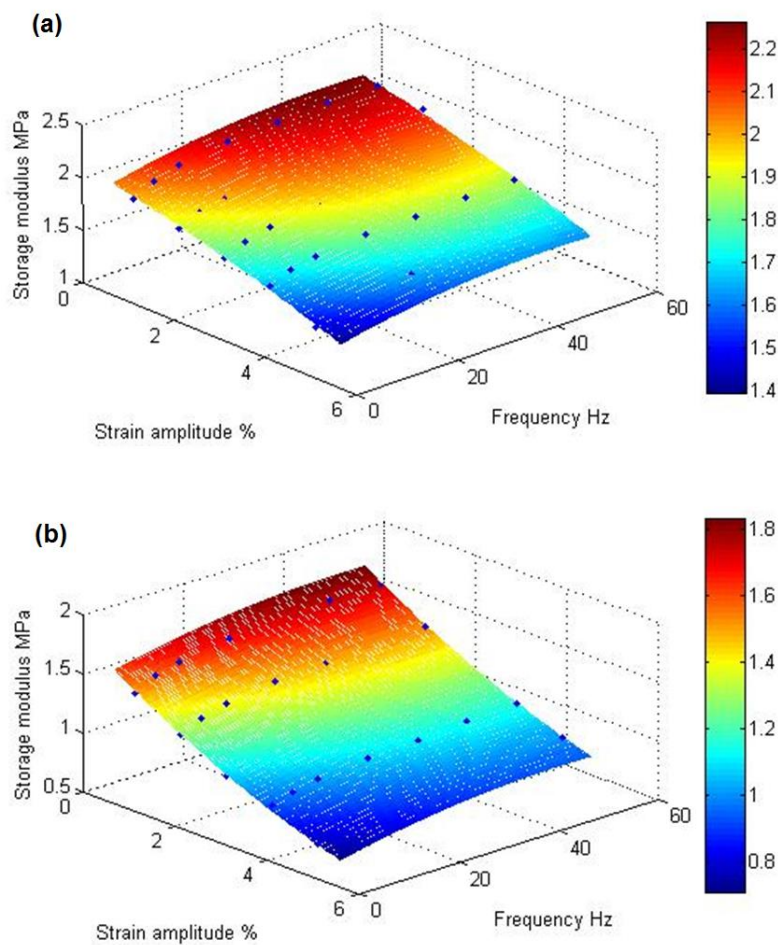


Figure 3.13 Storage modulus of anisotropic MRE (a) without silicone oil and (b) with silicone oil at different strain amplitude and magnetic field.

We can see from Figure 3.13 (a) that in vibration tests the storage modulus of anisotropic MRE increase slightly with the driving frequency and decreases as the strain amplitude increases. From 1% to 6%, the storage modulus decreases obviously 2.2MPa to 1.4MPa.

Figure 3.13 (b) shows that when silicone oil is included, similarly the storage modulus also increases slightly with the driving frequency, and as the strain amplitude increases the storage modulus decreases from 1.7MPa to 0.8MPa. By comparing Figure 3.13 (b) with Figure 3.13 (a), we can see the presence of silicone oil reduces the storage modulus of MRE by approximately 30%, but adding silicone oil into anisotropic MRE does not change the dependence of storage modulus on frequency and strain as the two fitted surfaces have similar shapes.

The influence of microstructure on loss modulus due to the application of coupling agent is shown in Figure 3.14, and the experimental results of the anisotropic MRE with and without coupling agent are illustrated by the blue dots on surfaces.

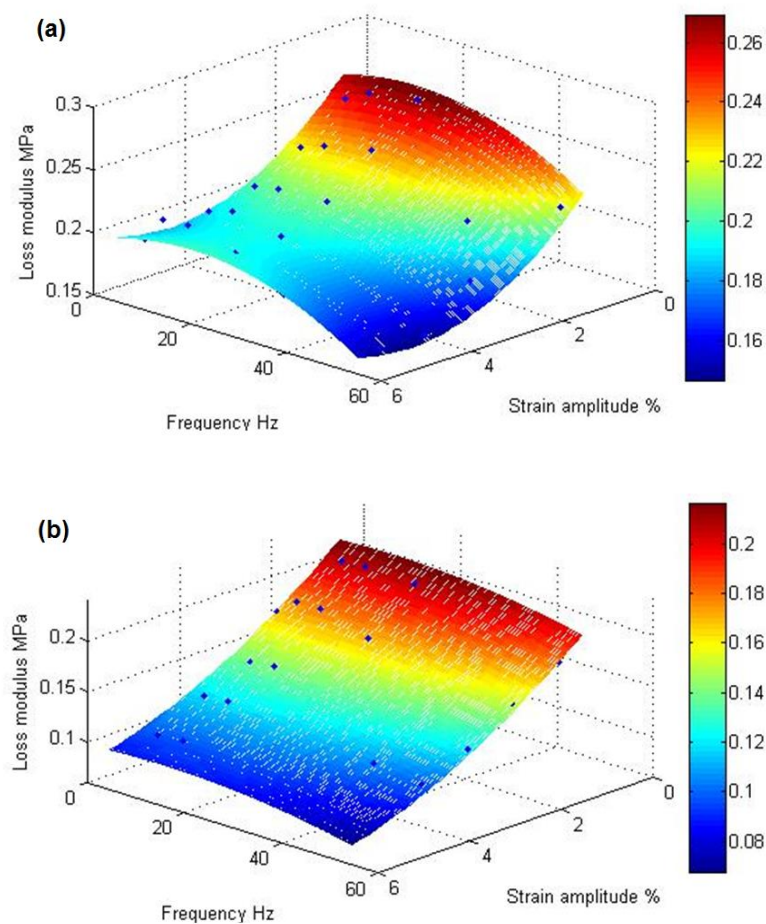


Figure 3.14 Loss modulus of anisotropic MRE (a) without silicone oil and (b) with silicone oil at different strain amplitude and magnetic field.

It can be seen from Figure 3.14 (a) that in the dynamic tests the loss modulus of anisotropic MRE decreases with the strain amplitude. As the driving frequency increases from 1Hz to 60Hz, the loss modulus increases at the beginning, at 10Hz it reaches a maximum of

0.26MPa and starts to decrease with a further increase of frequency. In Figure 3.14 (b) the loss modulus decreases with the increase of strain amplitude. As the driving frequency increases from 1Hz to 60Hz, the loss modulus initially increases, reaches a maximum of 0.2Mpa at 10Hz and decreases with higher frequencies. It can be seen from the comparison of Figure 3.14 (a,b) that the presence of silicone oil reduces the loss modulus of MRE by approximately 30%. But it does not change the dependence on frequency and strain as the two fitted surfaces have similar shapes, but improves the mechanical properties as the fitting surface is smoothed.

In Figure 3.15 we can see the influence of microstructure on loss factor due to the application of coupling agent and the experimental measurements of the anisotropic MRE with and without coupling agent, both denoted by the blue dots.

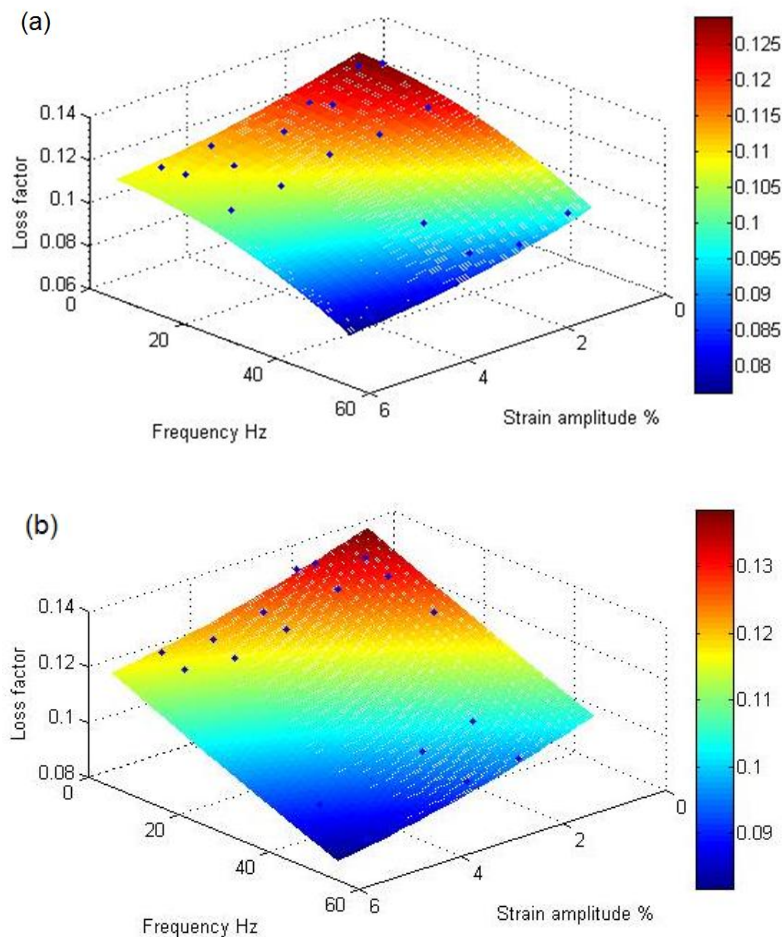


Figure 3.15 Loss factor of anisotropic MRE (a) without silicone oil and (b) with silicone oil at different strain amplitude and magnetic field.

Figure 3.15 (a) shows that in vibration tests the loss factor of anisotropic MRE decreases with the strain amplitude and increases with the driving frequency. From Figure 3.15 (b) it can

be seen that adding silicone oil into anisotropic MRE does not change the loss factor very much. Comparing Figure 3.15 (b) with Figure 3.15 (a), it can be seen that the presence of silicone oil barely has any influence on the loss factor of MRE.

3.4 Summary

The preparation of MRE samples is introduced in this chapter including component selections and manufacture progresses. Good mechanical properties are the most important characteristics for matrix material of MRE, and high magnetic permeability, high saturation magnetisation and low remnant magnetisation are the key characteristics for particles of MRE. For these reasons silicone rubber and carbonyl iron powders are the most commonly used selections. The optimisation particle volume concentration is 30% to ensure the mechanical properties and rheological properties of MRE. As a composite material, MRE can be categorised with respect to the way in which magnetisable particles are embedded in the matrix material: isotropic MRE with a uniform particle distribution and anisotropic MRE with a directed particle orientation.

Test apparatus and data processing for the mechanical property characterisation of MRE are also briefly introduced, and the influence of microstructure on mechanical properties is discussed as well. A series of dynamic tests are carried out to analyse the influence of magnetisable particles, magnetic fields and coupling agents. The presence of magnetisable particles in composition can substantially increase the modulus of elastomer but the dependence does not change appreciably. The application of magnetic field in solidification can effectively enable anisotropic MRE to have higher modulus than isotropic MRE with the same composition and simultaneously enhance the dependence of anisotropic MRE on magnetic fields, strains and frequencies. Adding coupling agents in curing progress can improve the mechanical properties and stability characteristics of MRE, at the same time also reduce the modulus, as a result the composite becomes softer which can potentially allow the material to own higher MR effect.

Chapter 4 **Mechanical properties of MRE**

4.1 Introduction

As a kind of composite material, MRE material behaves like other traditional filled rubbers and displays the Mullin and Payne effects under cyclic loading. All MR materials, including fluids, elastomers and foams, have rheological properties, thus possess the ability to change mechanical properties with a controllable magnetic field. The stiffness of MRE can be adjusted continuously, rapidly and reversibly in the pre-yield region; hence, it is a suitable candidate as a smart spring for vibration control.

In Section 3.3 we can see the overall dependence of mechanical properties on magnetic field, strain and frequency, and in this chapter dynamic tests in shear mode are conducted to investigate the dependence of mechanical properties on magnetic field, strain and frequency, respectively^[9]. The MR effect enables the shear modulus of MRE to increase with the magnetic field intensity and the Payne effect causes the shear modulus to decrease with the loaded strain. In this chapter, the anisotropic MRE samples are cured under a magnetic field of 450mT which is stronger than the magnetic field employed in Chapter 3. As a result the difference of experimental results between isotropic MRE and anisotropic MRE is enhanced to be obvious in the following figures. The dynamic tests carried out are independently repeated twice by three independent pair of MRE samples respectively to attain a good reliability, and all the measurements are taken by averaging the experimental data for dynamic mechanical analysis of MRE. This chapter provides the experimental evidence which is the basis of modelling for MRE to describe its dynamical behaviour in the following chapters.

4.2 Dependence on magnetic field

The stress-strain relationships under quasi static loading for isotropic MRE and anisotropic MRE are shown in Figure 4.1 (a) and Figure 4.1 (b), respectively. It can be seen that the shear modulus of isotropic MRE changes very little with magnetic fields. On the other hand the anisotropic MRE obviously becomes stiffer with magnetic intensity, which can be observed from the slope of the stress strain curve increasing with increasing magnetic flux density.

Comparing Figure 4.1 (a) with Figure 4.1 (b), it is noticeable that anisotropic MRE is stiffer than isotropic MRE with the same composition.

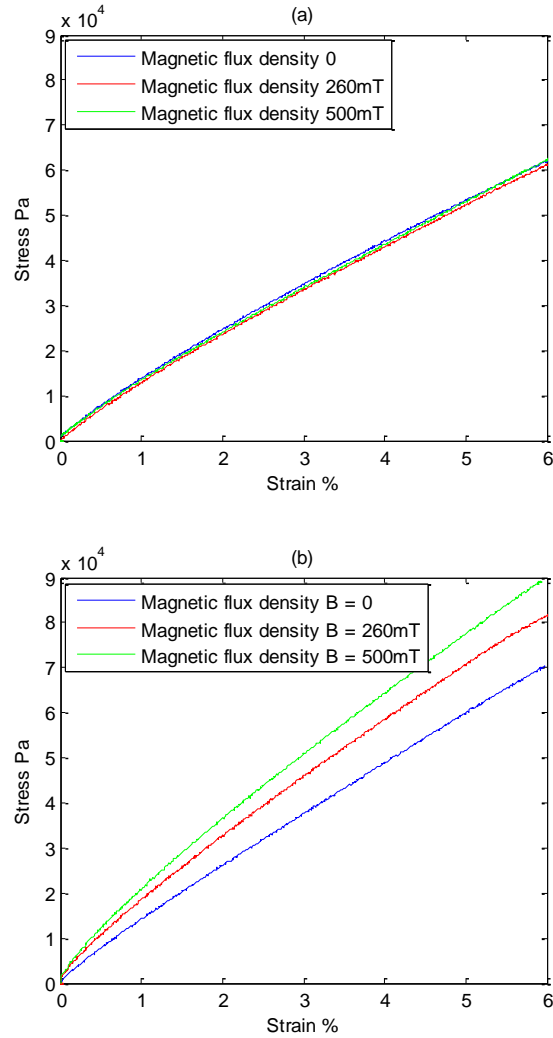


Figure 4.1 Stress-strain plot with varying magnetic flux densities under quasi static loading for (a) isotropic MRE and (b) anisotropic MRE.

Figure 4.2 (a) and Figure 4.2 (b) show the stress-strain hysteresis loops of isotropic MRE and anisotropic MRE at different magnetic intensities, respectively. Based on the stress-strain hysteresis loops, the complex modulus can be obtained from the slope of the line from the point of minimum strain to the point of maximum strain, the loss angle can be calculated from the area within the hysteresis loop and the storage and loss moduli can be obtained from Equation (3.2). We can see that both of the isotropic MRE and the anisotropic MRE show that the complex modulus increases with an increase of magnetic flux density, because the slope of hysteresis loop moves up with magnetic field strength. From the comparison between Figure 4.2

(a) and Figure 4.2 (b) it can be seen that anisotropic MRE possesses higher storage modulus and higher loss modulus than the isotropic MRE with the same composition, for both the slope and the area of stress-strain hysteresis loops for anisotropic MRE are greater than isotropic MRE.

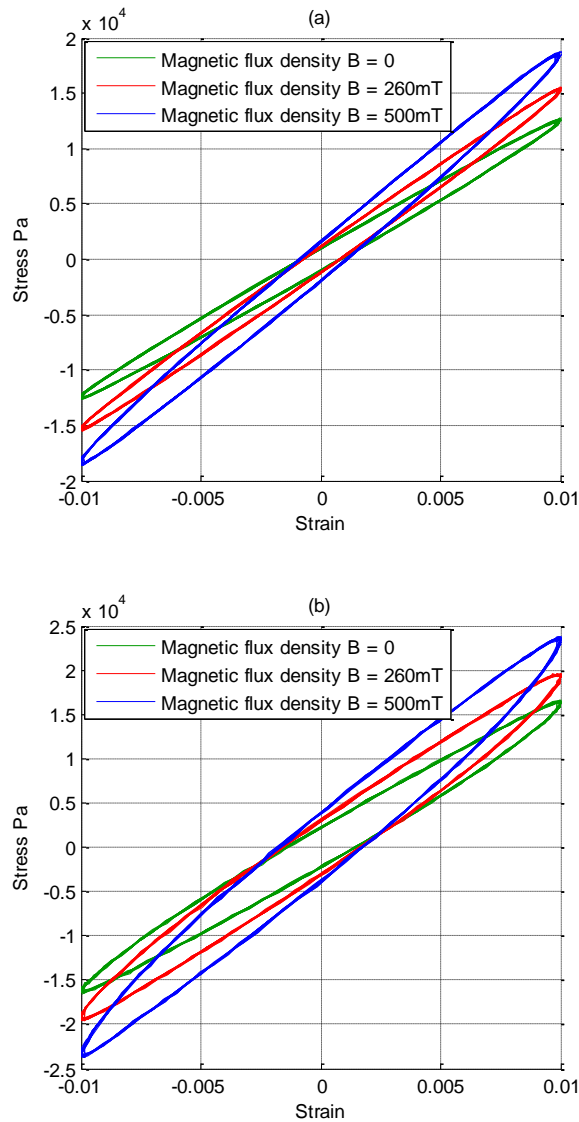


Figure 4.2 Stress-strain plot at 10Hz with different magnetic flux densities for (a) isotropic MRE and (b) anisotropic MRE.

Figure 4.3 shows that the storage modulus increases with magnetic flux densities for both isotropic MRE and anisotropic MRE. For the same strain amplitudes and magnetic flux density the anisotropic MRE has higher storage modulus than the isotropic MRE with identical composition, and the strain amplitude does not change the dependence of storage modulus on magnetic field as the curves for different strain amplitude show similar trends. It can be also noted that the dependence of storage modulus on magnetic field for anisotropic MRE is greater

than that of isotropic MRE with the same composition, because the storage modulus of anisotropic MRE increases more with magnetic field strength.

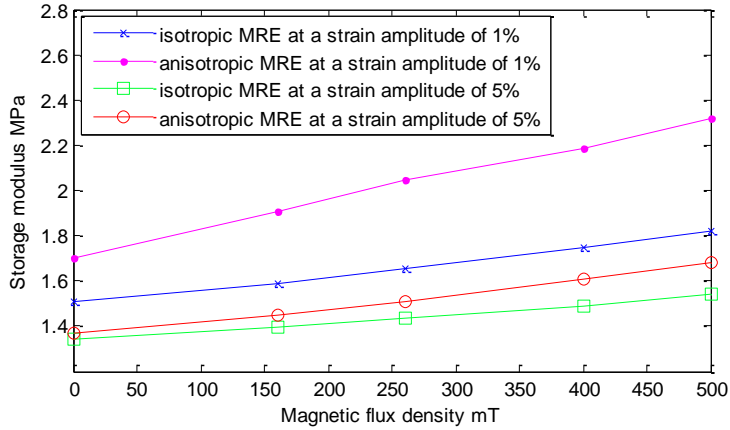


Figure 4.3 Dependence of storage modulus on magnetic field at 10Hz.

From Figure 4.4 we can see that the loss modulus also increases with magnetic flux density for both isotropic MRE and anisotropic MRE, and the dependence of loss modulus on strain is independent of the dependence on magnetic field. Similarly, the loss modulus of anisotropic MRE is always higher than the isotropic MRE with the same composition at the same strain amplitude and magnetic flux density. The loss modulus of anisotropic MRE also displays a more obvious dependence on magnetic field than isotropic MRE with the same composition.

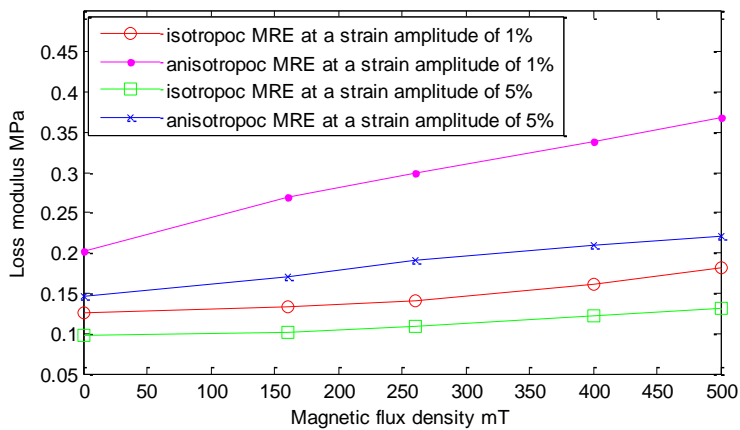


Figure 4.4 Dependence of loss modulus on magnetic field at 10Hz.

It can be seen from Figure 4.5 that the loss factor shows an increase with magnetic flux densities. However, in comparison with the isotropic MRE with the same composition, the loss

factor of anisotropic MRE increases more with magnetic intensity. Similarly the dependence of loss factor on strains is independent from the dependence on magnetic fields, and for the same strain amplitude and magnetic flux density the anisotropic MRE has greater loss factor than the isotropic MRE with the same composition.

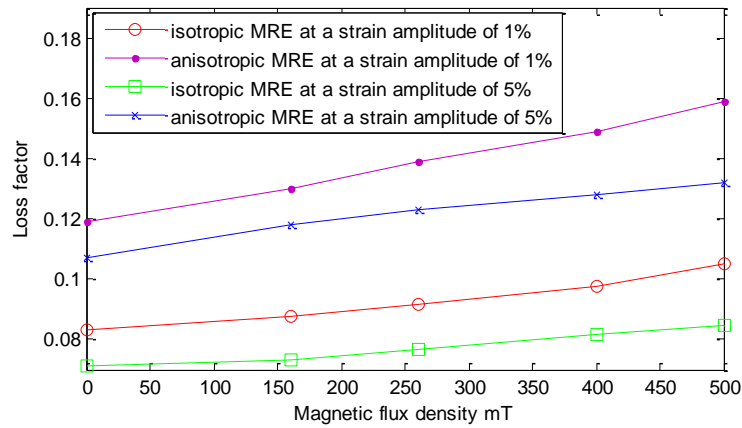


Figure 4.5 Dependence of loss factor on magnetic field at 10Hz.

Because the application of MRE is mainly based the controllability of stiffness, the MR effect is defined as the relative change of the storage modulus in Equation (2.1). Figure 4.6 shows that the MR effect increases with increasing magnetic flux density for both isotropic MRE and anisotropic MRE, and for the same strain amplitude and the same magnetic flux density the anisotropic MRE has a greater MR effect than the isotropic MRE with the same composition, this is in agreement with the results reported in [46]. Similarly, the increase of the MR effect with magnetic intensity for anisotropic MRE is comparatively more obvious.

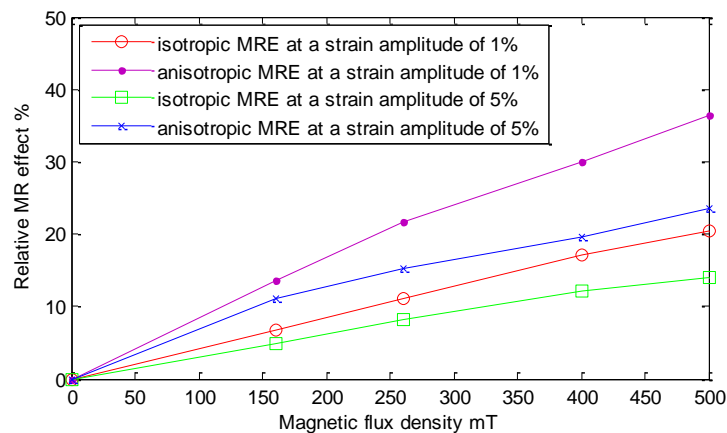


Figure 4.6 Dependence of relative MR effect on magnetic field at 10Hz.

As iterated previously the modulus of MRE is affected by the magnetic force between the particles, amongst all factors influencing this interaction the magnetic intensity is essential. Both storage modulus and loss modulus increase with magnetic flux density and when saturation occurs these moduli will remain constant with the maximum magnetic force between magnetisable particles. Consequently, the MR effect increases with magnetic flux density at the beginning and reaches a maximum at some point; then the MR effect will stay constant with further increases in magnetic field strength. Most experimental research on MRE shows that the increase of MR effect with magnetic intensity is prevalent when the magnetic flux density is below 500 mT, higher than 500 mT the increase of MR effect gradually slows down with magnetic field strength, and above about 800 mT magnetic saturation occurs in the composite there is no more increase of MR effect with further increasing magnetic intensities^[45]. Considering the consumption of electricity for controlling required magnetic fields, the magnetic field below 500 mT is cost-effective, as much more electric energy is required to generate strong magnetic fields of above 500 mT, especially when the resulting increment of MR effect is shrinking.

4.3 Dependence on strain

The dynamic tests of each MRE sample are carried out without magnetic field and under a magnetic field of 500mT. The Payne effect of MRE material can be observed in terms of the dependence of modulus on the amplitude of applied strain, namely both the storage and loss moduli decrease with increasing amplitude of the shown applied harmonic load. Based on the hysteresis loops of isotropic MRE and anisotropic MRE, in Figure 4.7 (a) and Figure 4.7 (b), respectively, we can see that the slope of hysteresis loop decreases with increasing strain amplitudes, indicating that the storage modulus decreases with the strain amplitude. Because the complex modulus can be calculated by the slope of the stress-strain hysteresis loop, the loss angle is relevant to the energy dissipation per volume within an oscillatory cycle, hence the storage and loss moduli can be obtained from Equation (3.2). Comparing Figure 4.7 (b) with Figure 4.7 (a), it is obvious that anisotropic MRE has both higher storage modulus and higher loss modulus than isotropic MRE with the same composition.

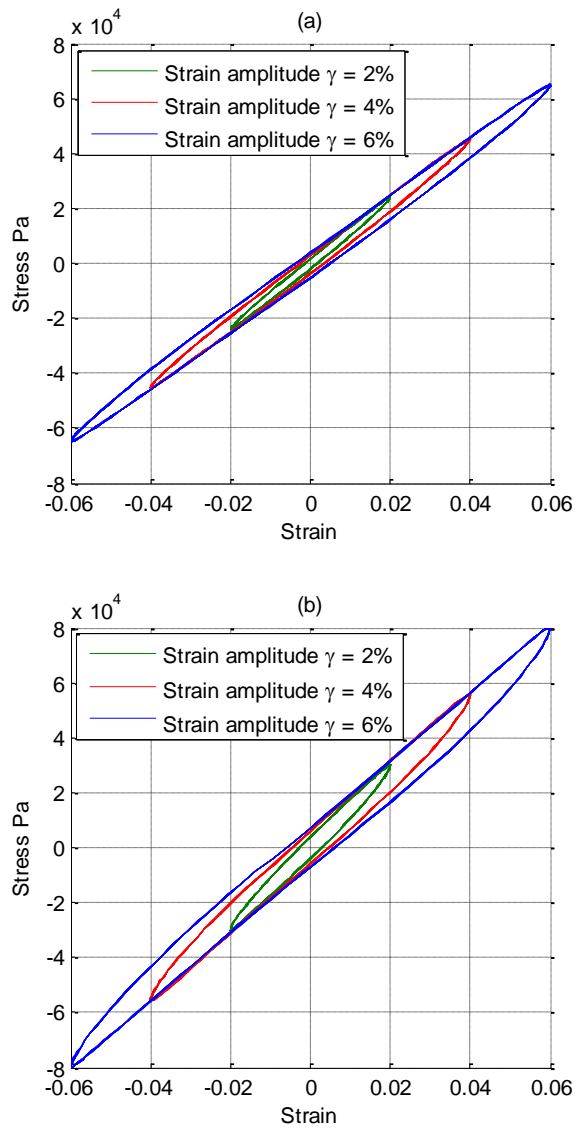


Figure 4.7 Stress-strain plot at 10Hz with different strain amplitudes of (a) isotropic MRE and (b) anisotropic MRE.

Figure 4.8 reveals that the storage modulus decreases with increasing strain amplitude for MRE both without and with the application of external magnetic field; hence the dependence of storage modulus on strains is independent of the dependence on magnetic fields. Under the same strain amplitude and magnetic flux density the anisotropic MRE owns higher storage modulus than the isotropic MRE with the same composition. The storage modulus of anisotropic MRE displays a more obvious dependence on strains than the storage modulus of isotropic MRE because the decrease of the storage modulus with increasing strain amplitudes for anisotropic MRE is greater than that for the isotropic MRE with the same composition in the same magnetic fields.

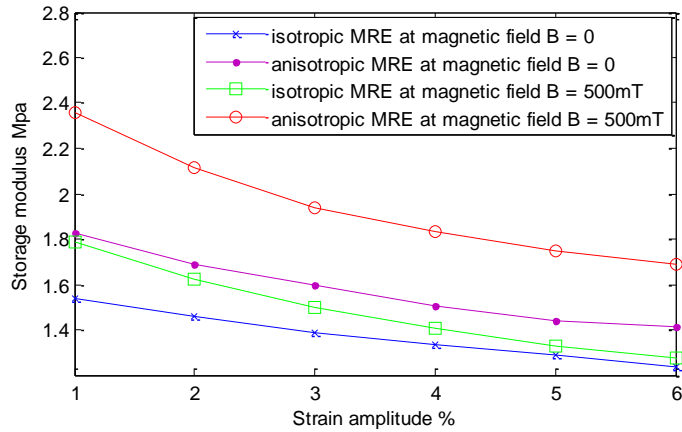


Figure 4.8 Dependence of storage modulus on strain amplitude at 10Hz.

It can be seen from Figure 4.9 that the loss modulus of MRE also decrease with increasing strain amplitudes and the application of magnetic fields does not change the dependence of loss modulus on strains. It is obvious that the loss modulus of anisotropic MRE is higher than the isotropic MRE with the same composition at the same strain amplitude and magnetic flux density, and the decrease of loss modulus with strain amplitude for anisotropic MRE is more obvious than that for isotropic MRE with the same composition, which indicates anisotropic MRE has greater dependence on strain amplitudes than isotropic MRE.

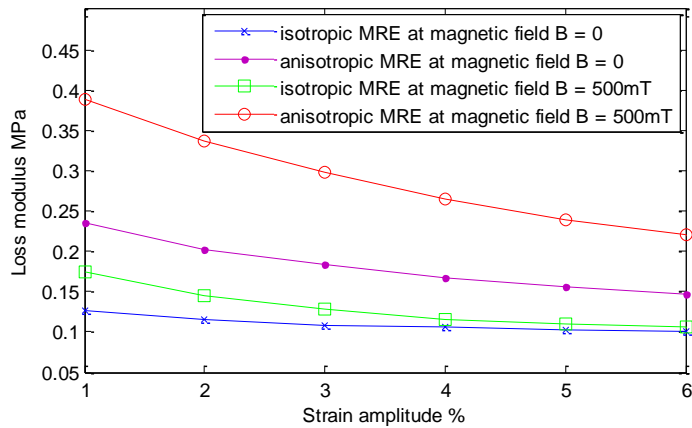


Figure 4.9 Dependence of loss modulus on strain amplitude at 10Hz.

From Figure 4.10 we can see that the loss factor of MRE also decreases with strain amplitude, without and with the application of external magnetic fields; hence, the dependence of loss factor on magnetic fields is independent from the dependence on strains. Similarly, under the same strain amplitude and magnetic flux density the loss factor of anisotropic MRE is

always greater than the isotropic MRE with the same composition, and the loss factor of anisotropic MRE also displays a more pronounced dependence on strain amplitudes than the isotropic MRE as the loss factor of anisotropic MRE decrease with increasing strain amplitude more obviously than the isotropic MRE with the same composition.

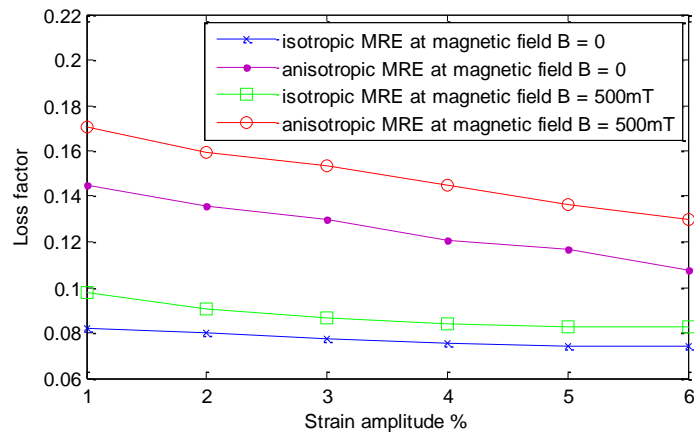


Figure 4.10 Dependence of loss factor on strain amplitude at 10Hz.

Figure 4.11 shows that the MR effect decreases with increasing strain amplitudes for both anisotropic MRE and isotropic MRE. It is also shown that for the same strain amplitudes, the anisotropic MRE has greater MR effects than the isotropic MRE with the same composition.

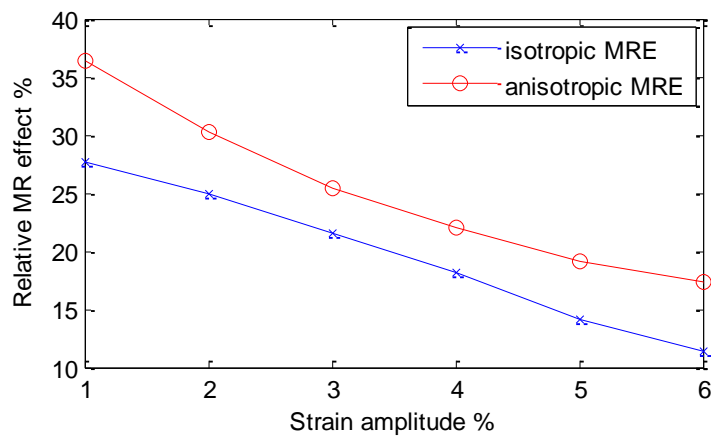


Figure 4.11 Dependence of relative MR effect on strain amplitude at 10Hz.

4.4 Dependence on frequency

From the stress-strain hysteresis loops of isotropic MRE and anisotropic MRE, shown in Figure 4.12 (a) and Figure 4.12 (b), respectively, the complex modulus can be obtained by the

slope of hysteresis loop and the loss angle can be obtained by the area within the hysteresis loop, and then the storage modulus and loss modulus can be calculated by the relationship in Equation (3.2). It can be seen that the storage modulus increases with frequency for both isotropic MRE and anisotropic MRE, as the slope of hysteresis loop increases with frequency. When comparing Figure 4.12 (b) with Figure 4.12 (a), it is noticeable that anisotropic MRE has both higher storage modulus and higher loss modulus than isotropic MRE, because both the slope and the area of hysteresis loop for anisotropic MRE are greater than those of isotropic MRE with the same composition.

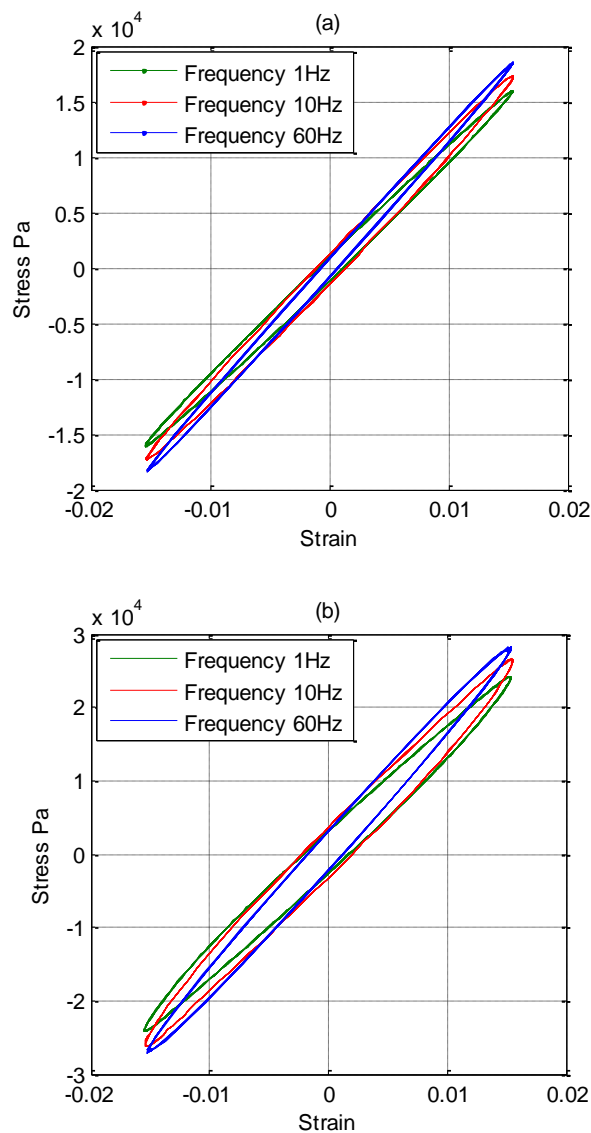


Figure 4.12 Stress-strain plot at 1.5% strain amplitude with varying frequencies for (a) isotropic MRE and (b) anisotropic MRE.

It can be seen from Figure 4.13 that the storage modulus, in agreement with the results reported in [51], increases with frequency and the dependence of storage modulus on frequency does not change with magnetic fields. At the same frequency and under the same magnetic field the anisotropic MRE always possess higher storage modulus than the isotropic MRE with the same composition. Furthermore, the anisotropic MRE shows greater dependence on frequency than the isotropic MRE because the change of storage modulus with increasing frequency for anisotropic MRE is more obvious than the isotropic MRE.

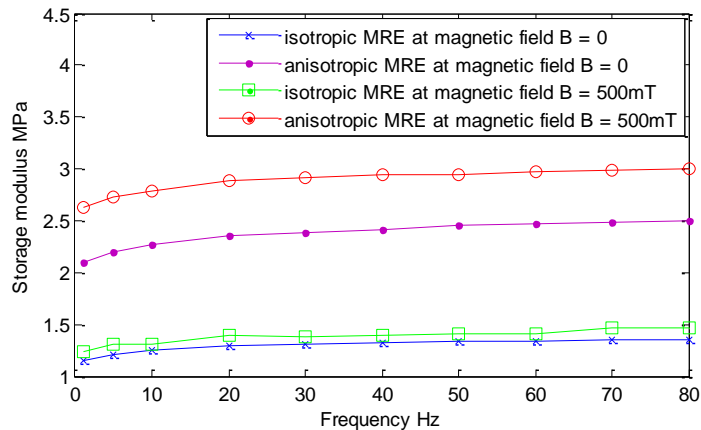


Figure 4.13 Dependence of storage modulus on frequency at 1.5% strain amplitude.

From Figure 4.14 we can see that the loss modulus initially increases with frequency, reaches a maximum at 10Hz and starts to decrease with further increasing frequency either without and with application of external magnetic fields. Similarly, the dependence of loss modulus on frequency is independent from the dependence on magnetic field and the loss modulus of anisotropic MRE is always greater than that for the isotropic MRE with the same composition at the same frequency and in the same magnetic field. The loss modulus of anisotropic MRE changes more obviously with driving frequency, thus, displays greater dependence on frequency than isotropic MRE with the same composition.

Figure 4.15 shows that the dependence of loss factor on magnetic field does not change the dependence on frequency: the loss factor initially increases with frequency until 10Hz, above 10Hz the loss factor decrease with further increasing frequency. Thus at high frequencies the experimental results are in agreement with the research in [51]. Furthermore at the same frequency and magnetic intensity, the anisotropic MRE always has higher loss factors than the isotropic MRE with the same composition. However, the loss factors of the anisotropic MRE and the isotropic MRE display almost the same variation with increasing frequency, which is in

line with the conclusions in Sections 3.3.1 and 3.3.2, namely that the dependence of loss factor on frequency is mainly determined by the matrix material and the magnetisable particles contribute very little to the dependence on frequency.

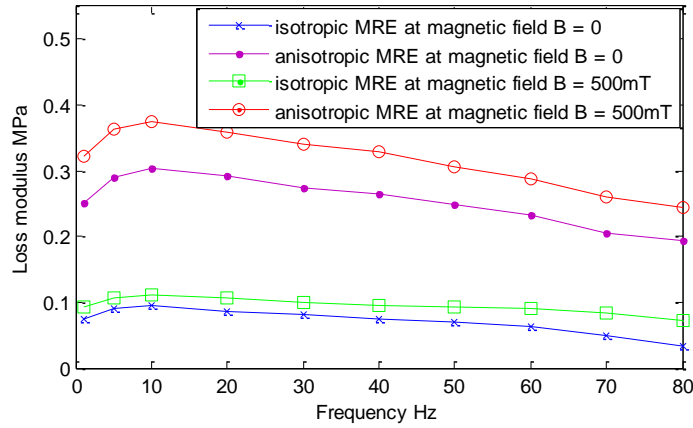


Figure 4.14 Dependence of loss modulus on frequency at 1.5% strain amplitude.

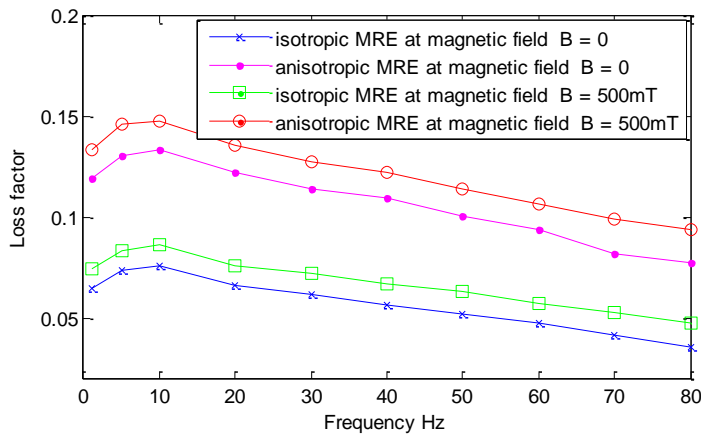


Figure 4.15 Dependence of loss factor on frequency at 1.5% strain amplitude.

From Figure 4.16, it can be seen that the relative MR effect of isotropic MRE changes very little with frequencies. However, the decrease of relative MR effect with increasing frequency for anisotropic MRE is very obvious. At the same frequency, the MR effect of anisotropic MRE is much greater than that for the isotropic MRE with the same composition.

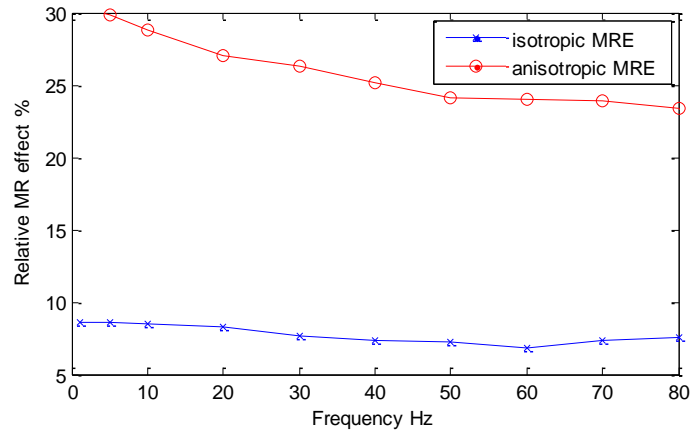


Figure 4.16 Dependence of relative MR effect on frequency at 1.5% strain amplitude.

4.5 Conclusions

This chapter investigates the dependence of mechanical properties of MRE, mainly including the dependence of storage modulus and loss modulus on strain, frequency and magnetic field. The experimental results reveal that both the storage modulus and loss modulus increase with magnetic flux density and decrease with strain amplitude for both anisotropic MRE and isotropic MRE. Furthermore the storage modulus increases with frequencies, but the dependence of loss modulus on frequency is determined by the matrix material. The loss modulus initially increases with frequency, reaches a maximum at 10Hz and then stops to decrease with further increasing frequencies for both anisotropic MRE and isotropic MRE.

Under the same loading conditions, the anisotropic MRE have higher storage modulus, loss modulus and loss factor than the isotropic MRE with the same composition. Furthermore, the anisotropic MRE also shows greater dependence on magnetic field, strain and frequency than the isotropic MRE with the same composition. The MR effect decreases with strain amplitude and frequency, as the increasing strain destroys the interactive force between magnetisable particles and the modulus increases with frequencies. The MR effect increases with the magnetic field strength until magnetic saturation; then the MR effect will remain constant afterwards with further increasing magnetic field intensities. The MR effect can reach as high as 36% under an external magnetic field of 500mT.

Chapter 5 **Mathematical modelling for MRE**

5.1 Introduction

Because of the dependence of mechanical properties on strain and frequency, the MRE material is governed by a non-linear stress-strain relationship. In addition the dependence of MRE on magnetic field can be selected and tuned by adjusting the magnetic field; thus, it is highly suitable for vibration control systems. As an important step towards the application of MRE in engineering practice, accurate mathematical modelling to describe the dynamic behaviour is very essential. Most of the research on mathematical modelling for MRE focuses on either the hysteretic behaviour of this material or the field dependent properties. The former is effective to describe the effects of loading history on dynamic response. However, in reality it is difficult to apply in a wide bandwidth when considering time-varying vibration sources, as the influence of loading history varies with frequency. The latter is limited to static loading conditions, which is inadequate in MRE vibration systems. Considering the dependence of mechanical properties on strain and frequency, current research on modelling for MRE is still insufficient for providing guidelines for engineering applications.

The aim is to propose a non-linear mathematical model for MRE, which is developed from a classic model, based on the experimental research on mechanical property characterisation and capable of representing the dependence of MRE on strain and frequency^[113]. In this model the restoring force and the damping force are expressed in polynomials of frequency and strain as independently continuous variables. This chapter provides a mathematical model for the dynamical analysis of MRE vibration systems and a methodology to establish models for materials to continuously describe the dynamic behaviour in certain region of strain and frequency. The focus is on low requirement of calculation on parameter identification, with full use of gathered information on mechanical properties.

This chapter develops an MRE structure with a high bearing capacity and a good controllability of stiffness to benefit vibration control systems. The stiffness and damping of this structure are predicted by combining the dynamic design and the mathematical modelling, and the results are examined through dynamic tests of this MRE structure to validate the extension of this mathematical model in MRE structures.

5.2 Modelling for dynamical properties of MRE

5.2.1 Modelling method for MRE

When a sinusoidal strain is applied to MRE material, instead of responding instantaneously the resultant stress will lag the input strain with a loss angle. To mathematically represent this behaviour the elastic modulus is commonly considered as a complex number comprising a real elastic element and an imaginary viscous element. A phase difference between input strain and resultant stress implies that part of the energy is put into MRE during loading cannot be recovered during unloading, which leads to a strain-stress hysteresis loop^[109]. The area in hysteresis loops can indicate the amount of energy lost during loading and unloading; hence, it is an indicator of the damping capability of the material. The mechanical properties of MRE depend on strain amplitude, loading frequency, magnetic field and temperature. Under dynamic loading, the force-displacement curves are not exact ellipses, but they are deformed by the amplitude of the applied loading^[110]. For example Figure 5.1 illustrates the force-displacement curves for anisotropic MRE in compression mode studied by Kallio.

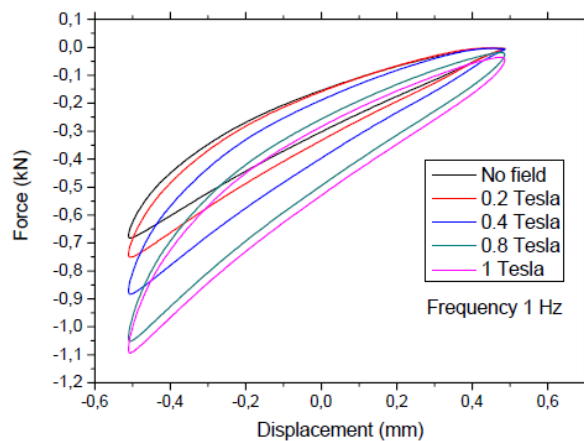


Figure 5.1 Force-displacement hysteresis curves for anisotropic MRE with 30 vol.% of iron particles with different magnetic field strength values^[110].

It has been reported that the effective modulus or the equivalent stiffness decreases with the increasing amplitudes of applied strain. Under cyclic loading conditions with small strain we can observe the Payne effect, which is commonly manifested as a dependence of modulus on the strain amplitudes. As a particular feature of dynamic behaviour, the effect occurs especially in filled rubbers. According to the experimental research MRE also exhibits this feature. The Payne effect can be attributed to deformation-induced changes in the microstructure of material, such as the breakage and recovery of weak physical bonds linking adjacent filler clusters.

The simplest model for MRE is the Kelvin-Voigt model, which can be represented by a viscous damper connected in parallel with an elastic spring as shown in Figure 5.2, where γ^* is assumed to be the input strain and τ^* the output stress.

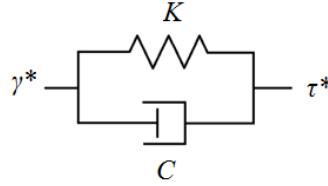


Figure 5.2 Kelvin-Voigt model of MRE.

Because of the dependence of mechanical properties on strain and frequency, both the storage modulus and loss modulus of MRE change with the strain amplitude and frequency. The storage modulus and loss modulus of MRE can be modelled as functions of loading strains and driving frequencies. Based upon the experimental research in Section 4.2, the surface fitting can be carried out with strain amplitude γ and angular frequency ω as independent variables shown in Equation (5.1), namely.

$$\begin{aligned} G'(\gamma, \omega) &= G_0' + G_1' \omega + G_2' \omega^2 + G_3' \gamma + G_4' \gamma^2 \\ G''(\gamma, \omega) &= G_0'' + G_1'' \omega + G_2'' \omega^2 + G_3'' \gamma + G_4'' \gamma^2 \end{aligned} \quad (5.1)$$

where G_0' , G_1' , G_2' , G_3' , G_4' , G_0'' , G_1'' , G_2'' , G_3'' and G_4'' are the parameters that depend on experimental results of mechanical property characterisation.

From the influence of microstructure on mechanical properties in Section 3.3, we can see the anisotropic MRE has higher shear modulus than the isotropic MRE with identical composition which can benefit the bearing capacity of structures. From the dependence of mechanical properties on magnetic fields in Section 4.2, it can be also seen that under the same loading conditions the anisotropic MRE exhibits greater MR effects than the isotropic MRE with the same composition which can contribute to the controllable variability of structures.

For the reasons above, the anisotropic MRE is selected to design vibration control devices, and the relative experimental research is used for the dynamic design of MRE structures. Based on the surface fitting of storage and loss moduli for MRE material in Figure 3.7 (b) and Figure 3.9 (b), the experimental parameters are listed in Table 5.1 and these parameters will be used to predict the equivalent stiffness and damping of MRE structures in the following sections.

Table 5.1 Experimental parameters in the expressions of storage modulus and loss modulus.

G_0' , Pa	G_1' , Pa·s	G_2' , Pa·s ²	G_3' , Pa	G_4' , Pa
1675590	1414.14	-2.97170	-15417040	138352000
G_0'' , Pa	G_1'' , Pa·s	G_2'' , Pa·s ²	G_3'' , Pa	G_4'' , Pa
255039	462.676	-2.12152	-2974230	19367100

When MRE material experiences sinusoidal excitations, the resultant displacement s can be expressed as Equation (5.2).

$$s(\omega, t) = s_0 \sin(\omega t + \theta) \quad (5.2)$$

where s_0 is the amplitude of vibration response. In a simplified mass-spring-damper system, when the spring constant is K and the damping coefficient is C , the equivalent restoring and damping forces can be obtained, as

$$\begin{aligned} F_{spring} &= Ks(\omega, t) \\ F_{damper} &= C\dot{s}(\omega, t) \end{aligned} \quad (5.3)$$

Substituting the displacement and the velocity in Equation (5.2) into Equation (5.3), we have the oscillatory force and the viscous drag,

$$\begin{aligned} F_{spring} &= Ks_0 \sin(\omega t + \theta) \\ F_{damper} &= C\omega s_0 \cos(\omega t + \theta) \end{aligned} \quad (5.4)$$

According to strain theory, the shear strain of MRE material can be expressed.

$$\gamma(\omega, t) = \frac{s_0 \sin(\omega t + \theta)}{D} \quad (5.5)$$

where D is the thickness of MRE samples in shear tests. The restoring force and the damping force can be expressed, considering the stress theory as

$$\begin{aligned} F_{spring} &= G'A\gamma(\omega, t) \\ F_{damper} &= iG''A\gamma(\omega, t) \end{aligned} \quad (5.6)$$

where A is the actual contact area of MRE samples in shear tests. Substituting the shear strain in Equation (5.5) into Equation (5.6), we can obtain the oscillatory force and the viscous drag as

$$\begin{aligned}
F_{spring} &= \frac{G'As_0}{D} \sin(\omega t + \theta) \\
F_{damper} &= i \frac{G''As_0}{D} \sin(\omega t + \theta)
\end{aligned} \tag{5.7}$$

Combining the expressions of Equation (5.4) and Equation (5.7), the equivalent stiffness K and the equivalent damping C can be calculated as

$$\begin{aligned}
K &= \frac{G'A}{D} \\
C &= \frac{G''A}{D\omega}
\end{aligned} \tag{5.8}$$

According to the expressions in Equation (5.1), a non-linear model can be built up based on the Kelvin-Voigt model to describe the dynamical behaviour of MRE. Combining with the dimensions of MRE samples and the setup of dynamic tests, the restoring force and the damping force are, thus, represented by

$$\begin{aligned}
F_{spring}(s, \omega) &= s(K_0 + K_1\omega + K_2\omega^2 + K_3s + K_4s^2) \\
F_{damper}(s, \omega) &= \dot{s}(C_0 + C_1\omega + C_2\omega^2 + C_3s + C_4s^2) / \omega
\end{aligned} \tag{5.9}$$

where s and \dot{s} are relative displacement and velocity, ω is the angular frequency. $K_0, K_1, K_2, K_3, K_4, C_0, C_1, C_2, C_3$ and C_4 are introduced as parameters of stiffness and damping. Because the mathematical modelling is based on the experimental results of mechanical property characterisation for MRE, it is limited to the range of strain $\gamma < 6\%$ and frequency $\omega < 80$ Hz.

With the expressions of equivalent restoring force and equivalent damping force, this model is capable of describing the steady response of MRE material under harmonic loading conditions. Because this mathematical modelling focuses on the effects of strain and frequency on mechanical properties, the hysteretic behaviour of MRE is not taken into account; hence, this model is inadequate for taking into account the influence of loading history on dynamic response. Although it has its limitation under time varying loadings, this model is effective for continuously describing the dynamic behaviour of MRE in certain region of strain and frequency. In comparison with other mathematical models considering the hysteretic behaviour of MRE, this model is more efficient for parameters identification with full use of gathered information on mechanical properties.

5.2.2 Nonlinear analysis on MRE modelling

Based upon the experimental results of storage modulus and loss modulus, the equivalent stiffness and equivalent damping can be obtained when the mechanical properties of MRE are represented by the Kelvin-Voigt model.

From the surface fitting in Figure 5.3 it can be seen that the equivalent stiffness of MRE samples is not constant, similar to the experimental results of storage modulus in Section 3.3. It also depends on displacement and frequency. The equivalent stiffness decreases with increasing amplitude; however, it increases with increasing angular frequency. Within the frequency range of 1 Hz ~ 60 Hz and the displacement range of 1 μm ~ 400 μm , it can be seen that the equivalent stiffness of MRE can be changed by as much as 37 %.

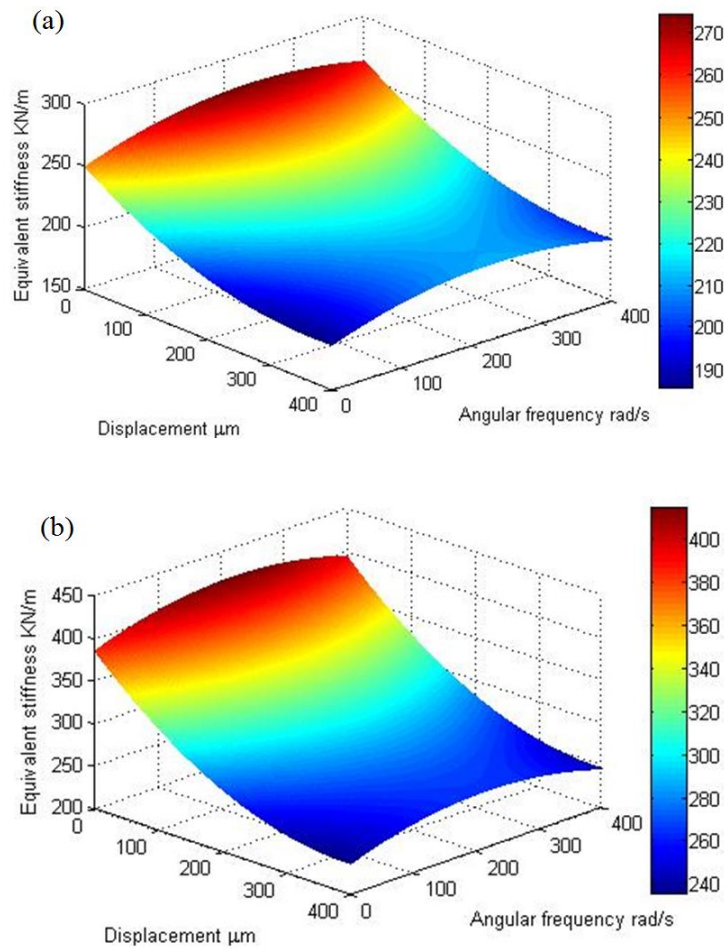


Figure 5.3 The equivalent stiffness of anisotropic MRE sample (a) when $B = 0$, (b) when $B = 160\text{mT}$.

According to the Kelvin-Voigt model and the experimental setup, the equivalent damping of MRE samples can be also calculated from the experimental results of loss modulus in Section 3.3. Figure 5.4 shows that the equivalent damping of MRE samples cannot be simplified as constants. It also depends on the displacement amplitude and the angular frequency. At low frequencies the equivalent damping is quite high and as the frequency increases the equivalent damping decreases, especially at frequencies below 10 Hz it decreases dramatically. On the other hand, the equivalent damping does not change much with the vibration amplitude. It can be seen that within the range of frequency 1 Hz ~ 60 Hz and displacement 1 μm ~ 400 μm , the equivalent damping of MRE can be changed by as high as 1500 %.

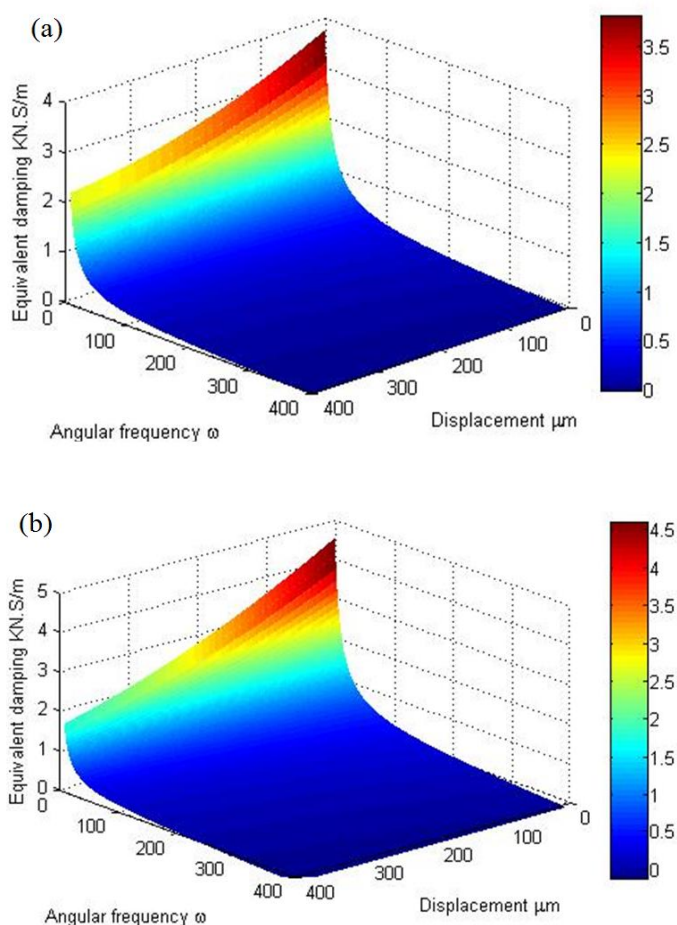


Figure 5.4 The equivalent damping of anisotropic MRE sample (a) when $B = 0$, (b) when $B = 160\text{mT}$.

The surface fitting in this section directly results from the experimental results in Chapter 3, where the experimental data are almost on the fitted surfaces. Because no further fitting

process is induced, the errors generated during fitting are at the same level as they are in Chapter 3. In Appendix V, the maximum error for equivalent stiffness is 4.00% and average error is 1.29%, and the maximum error for equivalent damping is 9.70% and average error is 4.36%, details can be referred to Appendix V.

5.3 Mathematical modelling for MRE structure

5.3.1 Dynamic design for MRE structure

Aiming at a good performance of vibration control, it is important for the dynamic design of MRE structures to effectively improve the bearing capacity and at the same time ensure a substantial variability in equivalent stiffness with magnetic field. In comparison with series connections, parallel connections are more effective for MRE structures for obtaining good load capacities and the two connections are comparable from the perspective of the controllable variability of structural stiffness. Therefore, the parallel connection is adopted for the dynamic design of MRE structures to obtain the good effectiveness of vibration control. As shown in Figure 5.5, the configuration comprises several slices of MRE and two aluminium gratings, allowing flexibility in the vertical direction through shear deformations of MRE material and by applying external magnetic field, the equivalent stiffness of MRE structures can be adaptively controlled. In this dynamic design, the load capacity can be improved by connecting MRE slices in parallel without sacrificing any variability of shear modulus with magnetic field^[111].

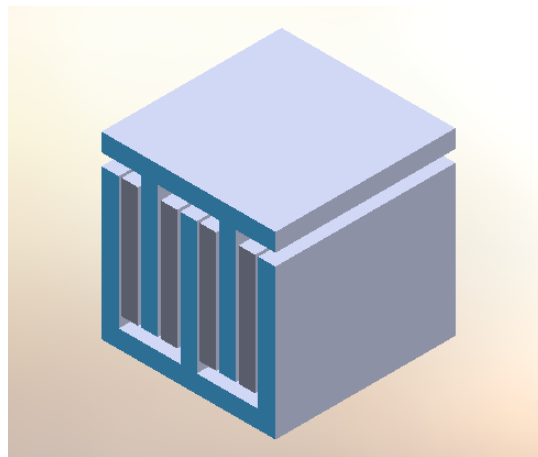


Figure 5.5 A schematic of MRE structure.

In this dynamic design, shown in Figure 5.5 the upper and lower aluminium gratings mesh successfully with MRE elements bonded to their surfaces through Araldite Standard adhesive. The dimension of this device are $60 \times 60 \times 60 \text{ mm}^3$ and for both MRE elements and

aluminium elements the thickness is 6mm and the length is 60mm, the height of MRE elements is 40 mm. The spaces between the MRE elements and the aluminium bases enable the structure to have a maximum deformation of 4 mm in the vertical direction, which equates to a maximum allowable shear strain of 67%. Considering fitting to obtain the parameters in the expressions for the storage modulus and the loss modulus of MRE in Table 5.1, the equivalent stiffness and the equivalent damping of this structure can be obtained by combining the geometric dimensioning of dynamic design with the material properties of MRE, which is similar to the process in previous section, see Equation (5.8). Then the restoring force and the damping force can be represented by Equation (5.10) and the parameters are listed in Table 5.2. Thus

$$\begin{aligned}
F_{spring}(S, \Omega)\Big|_{B=0} &= (K_{00} + K_{10}\Omega + K_{20}\Omega^2 + K_{30}S + K_{40}S^2)S \\
F_{spring}(S, \Omega)\Big|_{B=0.16T} &= (K_{0m} + K_{1m}\Omega + K_{2m}\Omega^2 + K_{3m}S + K_{4m}S^2)S \\
F_{damper}(S, \Omega)\Big|_{B=0} &= \dot{S}(C_{00} + C_{10}\Omega + C_{20}\Omega^2 + C_{30}S + C_{40}S^2)/\Omega \\
F_{damper}(S, \Omega)\Big|_{B=0.16T} &= \dot{S}(C_{0m} + C_{1m}\Omega + C_{2m}\Omega^2 + C_{3m}S + C_{4m}S^2)/\Omega
\end{aligned} \quad (5.10)$$

Table 5.2 Parameters for the expressions of spring force and the damper force.

K_{00} , N/m	K_{10} , N·s/m	K_{20} , N·s ² /m	K_{30} , N/m ²	K_{40} , N/m ³
2680940	2262.62	-4.75472	-24667300	221363000
K_{0m} , N/m	K_{1m} , N·s/m	K_{2m} , N·s ² /m	K_{3m} , N/m ²	K_{4m} , N/m ³
3259500	2579.58	-5.29688	-38567500	331072000
C_{00} , N·s/m	C_{10} , N·s ² /m	C_{20} , N·s ³ /m	C_{30} , N·s/m ²	C_{40} , N·s/m ³
408062	740.282	-3.39443	-4758770	30987400
C_{0m} , N·s/m	C_{1m} , N·s ² /m	C_{2m} , N·s ³ /m	C_{3m} , N·s/m ²	C_{4m} , N·s/m ³
509587	804.920	-3.77984	-7730770	56415200

5.3.2 Experimental validation of dynamic design

As shown in Figure 5.6, the designed stiffness and damping of this MRE structure can be expressed through Equation (5.10) and the parameters are listed in Table 5.2. From Figure 5.6 (a) and Figure 5.6 (c), the bearing capacity for safety can be calculated with the geometric dimensioning of dynamic design and the mechanical properties of MRE. For this MRE structure the static load capacity of bearing is 65kg. The dynamic load capacity of bearing decreases with

the static load exerted on the smart structure and when the static load is close to zero the dynamic load capacity of bearing is 75kg. Furthermore with the application of a magnetic field at 160 mT the dynamic load capacity of bearing can reach 100kg. It can be seen from Figure 5.6 (b) and Figure 5.6 (d) that the damping of this MRE structure declines dramatically at low frequencies below 10 Hz and at high frequencies the damping diminishes and approaches zero.

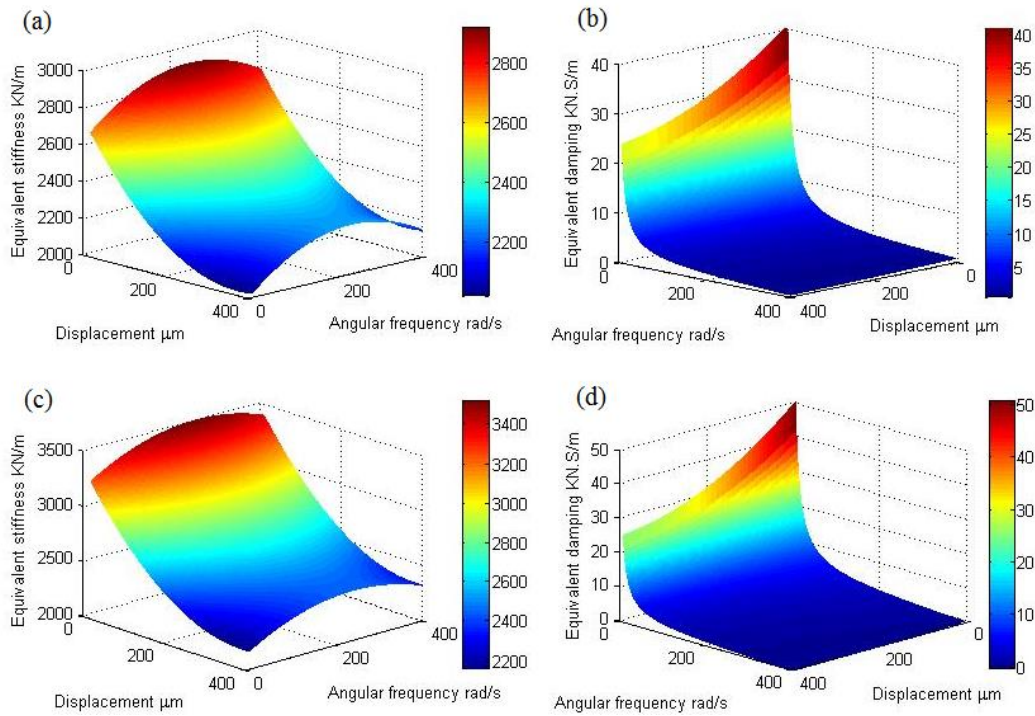


Figure 5.6 The designed stiffness of MRE structure (a) when $B = 0$, (c) when $B = 160\text{mT}$ and the designed damping of MRE structure (b) when $B = 0$, (d) when $B = 160\text{mT}$.

The dynamic test of this MRE structure is conducted to obtain the mechanical properties. As shown in Figure 5.7, the fixtures are made of aluminium and MRE samples are bonded to the metal surfaces with Araldite Standard adhesive. There are eight pieces of MRE prepared in dimensions of $60 \times 40 \times 6 \text{ mm}^3$ for the dynamic tests. Consequently this structure can be examined with two independent sets of four MRE samples, each set of MRE samples are tested twice respectively, and the experimental results are obtained by averaging the four sets of experimental data.

Figure 5.8 shows the experimental results of stiffness and damping by examining the MRE structure. The bearing capacity for safety of this MRE structure can be obtained from Figure 5.8 (a) and Figure 5.8 (c). We can see the stiffness of structure reduces with the vibration amplitude, and this tendency is in agreement with the predictions on the stiffness of this MRE

structure. The static load capacity and the dynamic load capacity are almost the same as the calculation in dynamic design of MRE structure. In Figure 5.8 (b) and Figure 5.8 (d) we can see that the damping of the structure decreases with frequency, especially at frequencies below 10Hz, and is close to zero at high frequencies, which is consistent with the discussion for Figure 5.6 (b) and Figure 5.6 (d).

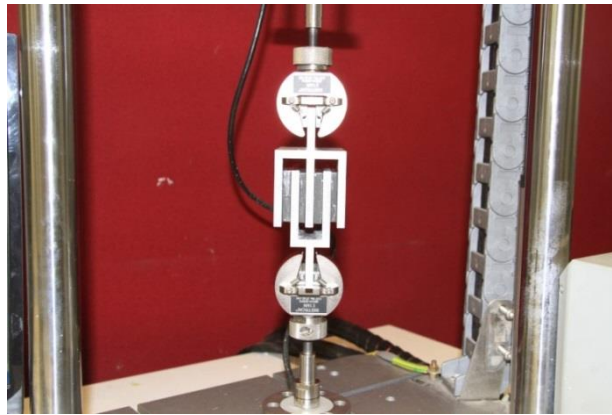


Figure 5.7 Experimental setup for MRE structure.

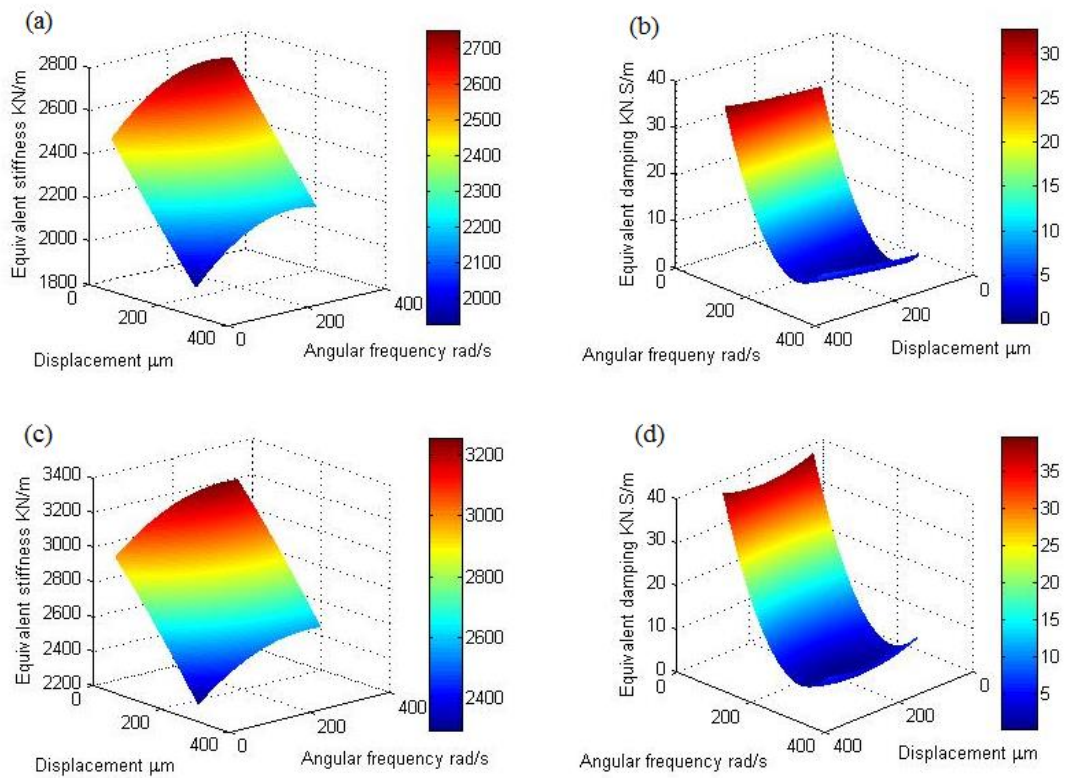


Figure 5.8 The experimental results of structural stiffness (a) when $B = 0$, (c) when $B = 160\text{mT}$ and the experimental results of structural damping (b) when $B = 0$, (d) when $B = 160\text{mT}$.

From Figure 5.9 we can see the errors of predicted values for the stiffness and the damping of MRE structure. In Figure 5.9 (a), (c) and (d) the errors are within 5% which is acceptable, but in Figure 5.9 (b) the errors of equivalent damping when $B = 160\text{mT}$ are a bit higher. Acceptable errors indicate the mathematical model of MRE material can be extended to MRE structures within the used range of displacements and frequencies. However, the mathematical model of MRE is limited to loading conditions of dynamic tests, as the errors of prediction can be mitigated when the working condition is well in the region of strain and frequency of mechanical property characterisation for MRE. In the dynamic tests for MRE materials and MRE structures in shear mode, bonding technology is a reason for creating errors. Overall, within the displacement range of $S < 400\ \mu\text{m}$ and the frequency range of $\Omega < 60\text{Hz}$, the mathematical model is valid for describing the dynamical behaviour of this MRE structure.

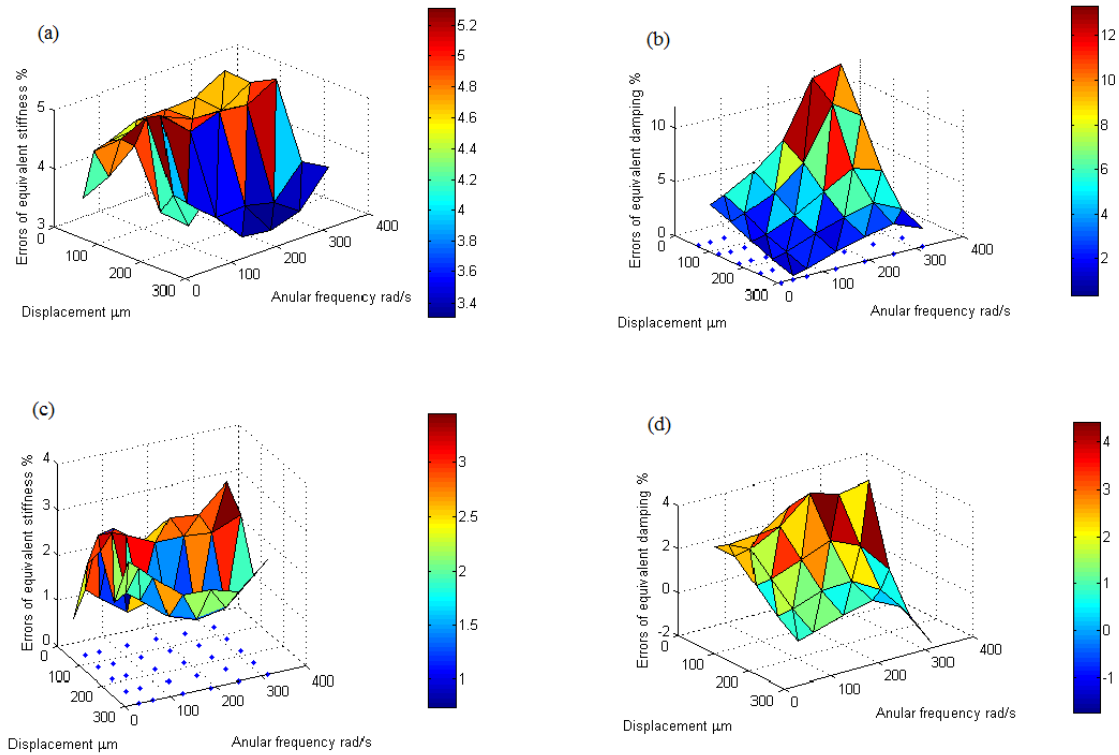


Figure 5.9 The error between the predicted values and experimental results of stiffness for MRE structure (a) when $B = 0$, (c) when $B = 160\text{mT}$; and the error between the predicted values and experimental results of damping for MRE structure (b) when $B = 0$, (d) when $B = 160\text{mT}$.

5.4 Summary

Experimental results confirm the importance of nonlinearities in equivalent stiffness and equivalent damping, which are a consequence of the dependence of storage modulus and loss modulus on frequency and strain, and results in relative differences of 37% and 1500% respectively. This evidence indicates the necessity to consider the nonlinearity in the mechanical properties of MRE for an effective dynamic design in vibration systems.

Based upon the experimental research on the dependence of mechanical properties on frequency and strain in the chapters Chapter 3 and Chapter 4, herein presents a nonlinear mathematical model for MRE material to describe the dynamic behaviour under cyclic loadings. The non-linear mathematical model is developed from the Kelvin-Voigt model, and the restoring force and the damping force are expressed in polynomials of frequency and strain as independently continuous variables. A dynamic design of MRE structure is taken as an example to evaluate the effectiveness of this mathematical model. The geometric dimensioning of dynamic design and the mechanical properties of MRE enable predictions for the structural stiffness and the structural damping within a region of strain and frequency used in the dynamic tests of mechanical property characterisation for MRE. Dynamic tests are conducted for this MRE structure to examine this mathematical model and error analysis is accordingly carried out to assess the efficiency of its extension in structures. The discussion shows that the errors between the predicted values and the experimental results are acceptable. Therefore, the mathematical model is reliable for describing the dynamic behaviour of MRE structures in the range of strain and frequency where mechanical properties are characterised for MRE.

The mathematical model provided in this chapter is essential for the dynamical analysis of MRE vibration systems, and the methodology of building up mathematical models also provides guidelines for materials to continuously describe the dynamic behaviour in the required region of strain and frequency with a low requirement of calculation on parameter identification and full use of gathered information on mechanical properties.

Chapter 6 Two-stage Nonlinear MRE Vibration Isolation Systems

6.1 Introduction

Since the discovery in 1948 of the MR phenomenon by Thomas Rabinow^[4], MR materials such as MR fluids, MR elastomers and MR foams have proven to be suited to vibration mitigation. Numerous applications are based on MRF because the dynamic yield stress can be continuously, rapidly and reversely controlled by the applied magnetic field. Comparing with MRF, the rheological property of MRE is the field-dependent modulus, and the microstructure and mechanical properties of MRE are also relatively stable^[5]. The applications of MRE mainly involve vibration isolators^[8,69,93] and adaptive vibration absorbers^[10,69,75].

Because the mechanical properties of MRE depend on strain, frequency and magnetic field, it is essential for the application to describe the dynamical behaviour with a valid mechanical model. The aim of this chapter is to study the dynamics of a two-stage isolation system with MRE isolators. Firstly, the motion equations are formulated to obtain the overall steady state response of the system and this is followed by dynamical analysis of the resulting system using originally derived analytical expressions. Secondly, the force transmissibility is evaluated and compared for different vibration isolation systems. The numerical results show that a reduction in the vibration response and transmissibility can be obtained by applying a magnetic field to MRE isolators in a proper range of excitation frequency, which will provide useful guidelines for the dynamic design of two-stage MRE vibration isolation systems^[112].

6.2 Equations of motion

6.2.1 Standard form of equations of motion

The two-stage nonlinear isolation system can be considered as a two degree of freedom (DOF) vibration system, as shown in Figure 6.1. X_1 and X_2 are displacements of the two compressors, M_1 and M_2 are corresponding masses supported by non-linear dampers and non-linear springs, the nonlinear damping force and the nonlinear restoring force are expressed by Equation (5.9).

F_0 and Ω are the amplitude and angular frequency of harmonic excitation, respectively. It is assumed that the masses in this system only have vertical displacements.

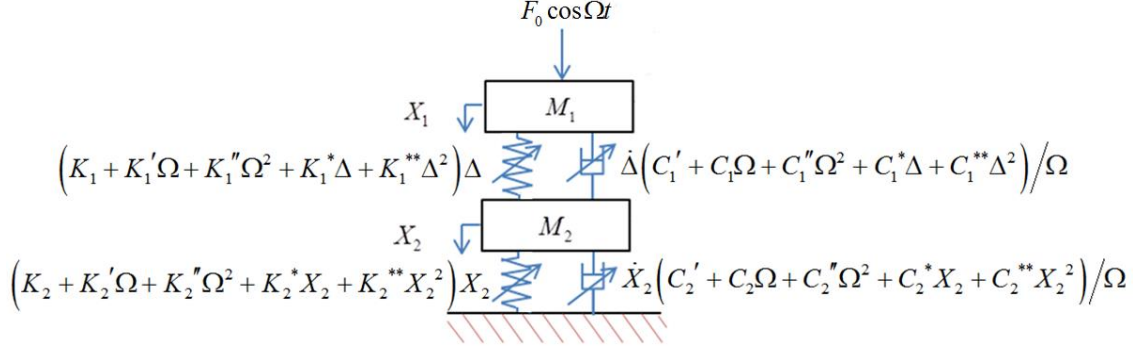


Figure 6.1 Two-stage vibration isolation system with MRE isolators.

Considering the nonlinearity of MRE models in Section 5.3, the governing differential equations are

$$\begin{aligned}
 & M_1 \ddot{X}_1 + \left(C_1 + \frac{C_1'}{\Omega} + C_1'' \Omega + \frac{C_1^*}{\Omega} \Delta + \frac{C_1^{**}}{\Omega} \Delta^2 \right) \dot{\Delta} + \left(K_1 + K_1' \Omega + K_1'' \Omega^2 + K_1^* \Delta + K_1^{**} \Delta^2 \right) \Delta \\
 & = F_0 \cos \Omega t + M_1 g \\
 & M_2 \ddot{X}_2 + \left(C_2 + \frac{C_2'}{\Omega} + C_2'' \Omega + \frac{C_2^*}{\Omega} X_2 + \frac{C_2^{**}}{\Omega} X_2^2 \right) \dot{X}_2 + \left(K_2 + K_2' \Omega + K_2'' \Omega^2 + K_2^* X_2 + K_2^{**} X_2^2 \right) X_2 \\
 & = M_2 g + \left(C_1 + \frac{C_1'}{\Omega} + C_1'' \Omega + \frac{C_1^*}{\Omega} \Delta + \frac{C_1^{**}}{\Omega} \Delta^2 \right) \dot{\Delta} + \left(K_1 + K_1' \Omega + K_1'' \Omega^2 + K_1^* \Delta + K_1^{**} \Delta^2 \right) \Delta
 \end{aligned} \tag{6.1}$$

where $\Delta = X_1 - X_2$ is the relative displacement of mass M_1 with respect of mass M_2 and $\dot{\Delta}$ is the relative velocity, $C_{1,2}$ and $K_{1,2}$ are the linear damping and stiffness of the isolators, respectively; $K_{1,2}'$, $K_{1,2}''$ are coefficients of stiffness which proportionally and quadratically depend on frequency, respectively; $K_{1,2}^*$, $K_{1,2}^{**}$ are coefficients of stiffness which proportionally and quadratically depend on strain, respectively; $C_{1,2}'$, $C_{1,2}''$ are coefficients of damping which anti-proportionally and proportionally depend on frequency, respectively; $C_{1,2}^*$, $C_{1,2}^{**}$ are coefficients of damping which proportionally and quadratically depend on strain, respectively.

Equation (6.1) can be rewritten in matrix form:

$$\mathbf{M}\ddot{\mathbf{x}} + \mathbf{C}\dot{\mathbf{x}} + \mathbf{K}\mathbf{x} = \mathbf{F} \tag{6.2}$$

where

$$\ddot{\mathbf{x}} = \begin{bmatrix} \ddot{X}_1 \\ \ddot{X}_2 \end{bmatrix}, \dot{\mathbf{x}} = \begin{bmatrix} \dot{X}_1 \\ \dot{X}_2 \end{bmatrix}, \mathbf{x} = \begin{bmatrix} X_1 \\ X_2 \end{bmatrix}.$$

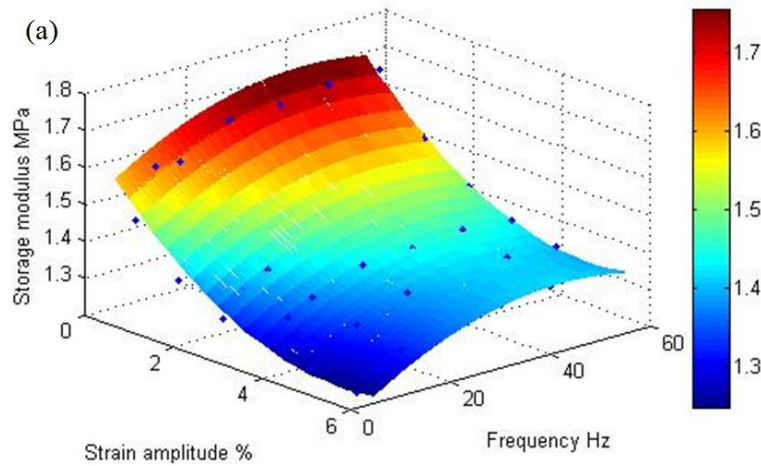
The mass, damping and stiffness matrices are expressed by

$$\mathbf{M} = \begin{bmatrix} M_1 & 0 \\ 0 & M_2 \end{bmatrix}, \mathbf{C} = \begin{bmatrix} C_1 & -C_1 \\ -C_1 & C_1 + C_2 \end{bmatrix}, \mathbf{K} = \begin{bmatrix} K_1 & -K_1 \\ -K_1 & K_1 + K_2 \end{bmatrix}$$

respectively, and the force vector is

$$\mathbf{F} = \begin{bmatrix} F_0 \cos \Omega t + M_1 g - \frac{C_1'}{\Omega} \dot{\Delta} - C_1'' \Omega \dot{\Delta} - \frac{C_1^*}{\Omega} \Delta \dot{\Delta} - \frac{C_1^{**}}{\Omega} \Delta^2 \dot{\Delta} - K_1' \Omega \Delta - K_1'' \Omega^2 \Delta - K_1^* \Delta^2 - K_1^{**} \Delta^3 \\ M_2 g + \frac{C_1'}{\Omega} \dot{\Delta} + C_1'' \Omega \dot{\Delta} + \frac{C_1^*}{\Omega} \Delta \dot{\Delta} + \frac{C_1^{**}}{\Omega} \Delta^2 \dot{\Delta} + K_1' \Omega \Delta + K_1'' \Omega^2 \Delta + K_1^* \Delta^2 + K_1^{**} \Delta^3 \\ -\frac{C_2'}{\Omega} \dot{X}_2 - C_2'' \Omega \dot{X}_2 - \frac{C_2^*}{\Omega} X_2 \dot{X}_2 - \frac{C_2^{**}}{\Omega} X_2^2 \dot{X}_2 - K_2' \Omega X_2 - K_2'' \Omega^2 X_2 - K_2^* X_2^2 - K_2^{**} X_2^3 \end{bmatrix}$$

In this system, M_1 is 30kg and F_0 is 300N. The stiffness and damping can be designed as the discussion in Section 5.3, and the parameters can be obtained by combining the geometrical design of structure and the dynamical properties of material. The limitation of shear strain for static load is defined as 2% for the mechanical property characterisation of MRE material, and the static load capacity can be determined for the safe dynamic design of MRE isolator. According to Equation (5.8), the calculation of equivalent stiffness and damping are based upon experimental results of storage modulus and loss modulus for MRE material, as shown in Figure 6.2 and Figure 6.3. The parameters of designed stiffness and designed damping are listed in Table 6.1, with the application of magnetic field at $B = 500\text{mT}$ the parameters change as the discussion in Section 5.2.



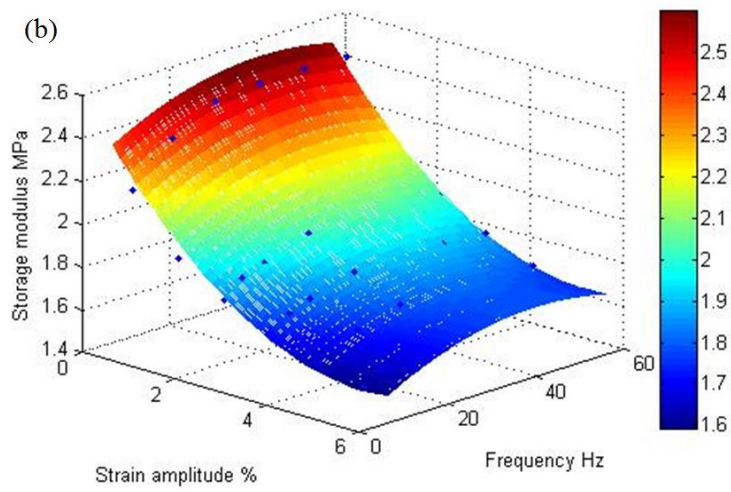


Figure 6.2 Experimental results of storage modulus when (a) $B = 0$, (b) $B = 500\text{mT}$.

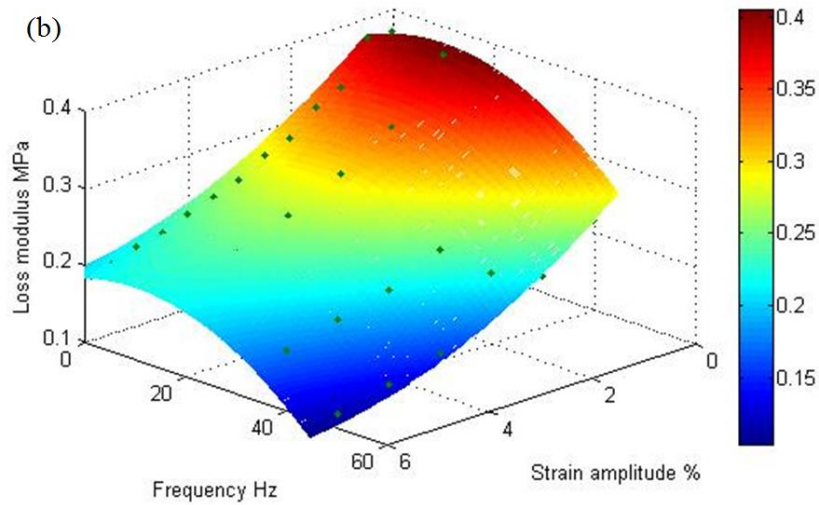
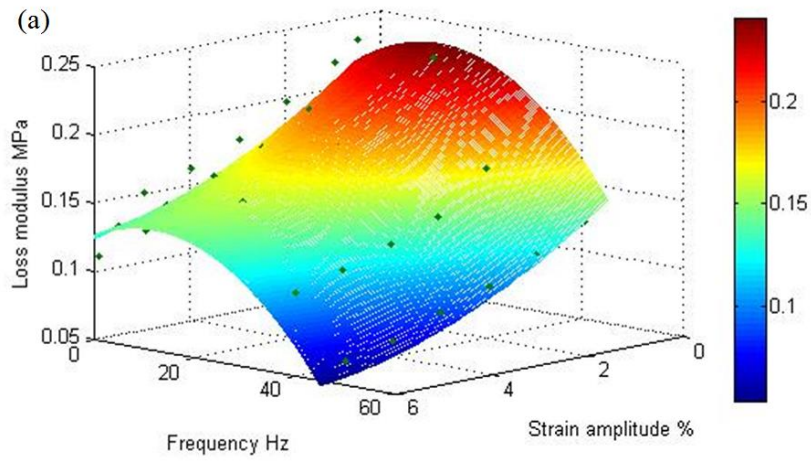


Figure 6.3 Experimental results of loss modulus when (a) $B = 0$, (b) $B = 500\text{mT}$.

Table 6.1 Parameters of stiffness and damping.

$K_I (B = 0)$ N/m	$K_I' (B = 0)$ N·s/m	$K_I'' (B = 0)$ N·s ² /m	$K_I^* (B = 0)$ N/m ²	$K_I^{**} (B = 0)$ N/m ³
2680940	2262.62	-4.75572	-24667300	221363000
$K_I (B = 0.5T)$ N/m	$K_I' (B = 0.5T)$ N·s/m	$K_I'' (B = 0.5T)$ N·s ² /m	$K_I^* (B = 0.5T)$ N/m ²	$K_I^{**} (B = 0.5T)$ N/m ³
4131550	3028.96	-6.97805	-52978300	438218000
$C_I (B = 0)$ N·s/m	$C_I' (B = 0)$ N·s ² /m	$C_I'' (B = 0)$ N·s ³ /m	$C_I^* (B = 0)$ N·s/m ²	$C_I^{**} (B = 0)$ N·s/m ³
740.282	408062	-3.39443	-4758770	30987400
$C_I (B = 0.5T)$ N·s/m	$C_I' (B = 0.5T)$ N·s ² /m	$C_I'' (B = 0.5T)$ N·s ³ /m	$C_I^* (B = 0.5T)$ N·s/m ²	$C_I^{**} (B = 0.5T)$ N·s/m ³
797.505	663845	-3.96701	-9594550	65007000

The relationship between K_I and K_2 can be determined on the basis of guaranteeing the static load capacity and avoiding any waste or any failure of MRE material, as expressed in Equation (6.3), namely. Consequently, it can be deduced from the mechanical properties of MRE that all the parameters of stiffness and damping $K_{1,2}$, $K_{1,2}'$, $K_{1,2}''$, $K_{1,2}^*$, $K_{1,2}^{**}$, $C_{1,2}$, $C_{1,2}'$, $C_{1,2}''$, $C_{1,2}^*$ and $C_{1,2}^{**}$ have the same relationship.

$$M_1 K_2 = (M_1 + M_2) K_1 \quad (6.3)$$

6.2.2 Steady state response of system

In order to observe the steady state behaviour of the system, numerical simulations are carried out using the expressions derived above. According to the standard form of motion equations, a specific group of parameters is selected for simulation. The response of the vibration isolation system for this selection is shown in Figure 6.4 and the Poincare map is shown in Figure 6.5.

Applying the method of averaging, the steady state responses are represented as

$$\mathbf{x}(t) = \mathbf{u}(t) \cos \Omega t + \mathbf{v}(t) \sin \Omega t \quad (6.4)$$

where $\mathbf{u}(t) = \begin{bmatrix} u_1(t) \\ u_2(t) \end{bmatrix}$, $\mathbf{v}(t) = \begin{bmatrix} v_1(t) \\ v_2(t) \end{bmatrix}$ are assumed to be slow functions of time t . The motivation for this assumption is that \mathbf{F} is zero, then Equation (6.2) its solutions in the form of the Equation (6.4) with $\mathbf{u}(t)$ and $\mathbf{v}(t)$ constants. The velocity is expressed by

$$\dot{\mathbf{x}}(t) = -\Omega\mathbf{u}(t)\sin\Omega t + \Omega\mathbf{v}(t)\cos\Omega t. \quad (6.5)$$

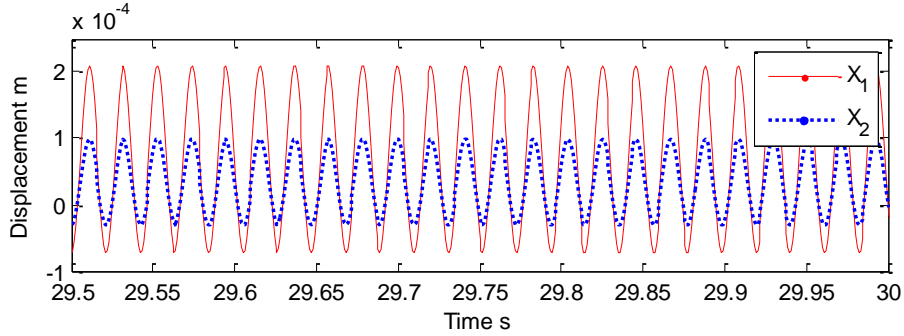


Figure 6.4 Response of the system ($M_1 = 30\text{kg}$, $M_2 = 5\text{kg}$ and $F_0 = 300\text{N}$).

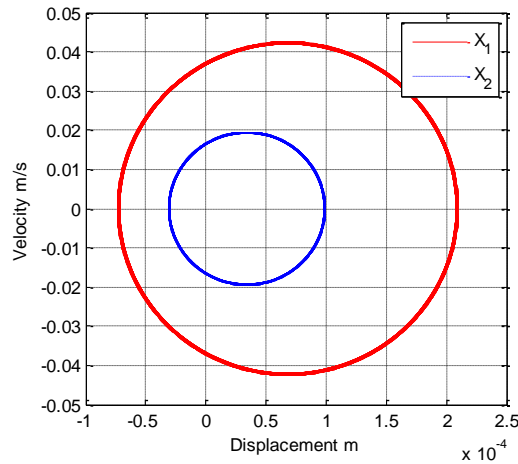


Figure 6.5 Poincaré maps of the system ($M_1 = 30\text{kg}$, $M_2 = 5\text{kg}$ and $F_0 = 300\text{N}$).

Differentiating Equation (6.4)(6.5) with respect to the time t , we obtain

$$\dot{\mathbf{x}}(t) = \dot{\mathbf{u}}(t)\cos\Omega t - \Omega\mathbf{u}(t)\sin\Omega t + \dot{\mathbf{v}}(t)\sin\Omega t + \Omega\mathbf{v}(t)\cos\Omega t. \quad (6.6)$$

Substituting Equation (6.6) into Equation (6.5), the resulting equation is

$$\dot{\mathbf{u}}(t)\cos\Omega t + \dot{\mathbf{v}}(t)\sin\Omega t = 0. \quad (6.7)$$

Also, differentiating Equation (6.6)

$$\ddot{\mathbf{x}}(t) = -\Omega\dot{\mathbf{u}}(t)\sin\Omega t - \Omega^2\mathbf{u}(t)\cos\Omega t + \Omega\dot{\mathbf{v}}(t)\cos\Omega t - \Omega^2\mathbf{v}(t)\sin\Omega t \quad (6.8)$$

Substituting the expressions about $\ddot{\mathbf{x}}, \dot{\mathbf{x}}, \mathbf{x}$ into Equation (6.2), we have

$$\begin{aligned} & (\Omega\mathbf{M}\dot{\mathbf{v}} - \Omega^2\mathbf{M}\mathbf{u} + \Omega\mathbf{C}\mathbf{v} + \mathbf{K}\mathbf{u})\cos\Omega t - (\Omega\mathbf{M}\dot{\mathbf{u}} + \Omega^2\mathbf{M}\mathbf{v} + \Omega\mathbf{C}\mathbf{u} - \mathbf{K}\mathbf{v})\sin\Omega t \\ & = \mathbf{F}(\mathbf{u}, \mathbf{v}, t) \end{aligned} \quad (6.9)$$

Adding $(-\sin\Omega t) \times$ Equation (6.9) and $(\mathbf{M}\Omega\cos\Omega t) \times$ Equation (6.7), we can obtain

$$\begin{aligned} & \Omega\mathbf{M}\dot{\mathbf{u}} + (\Omega^2\mathbf{M}\mathbf{u} - \Omega\mathbf{C}\mathbf{v} - \mathbf{K}\mathbf{u})\cos\Omega t \sin\Omega t + (\Omega^2\mathbf{M}\mathbf{v} + \Omega\mathbf{C}\mathbf{u} - \mathbf{K}\mathbf{v})\sin^2\Omega t \\ & = \mathbf{F}(\mathbf{u}, \mathbf{v}, t)(-\sin\Omega t) \end{aligned} \quad (6.10)$$

With a similar manipulation, we can also obtain

$$\begin{aligned} & \Omega\mathbf{M}\dot{\mathbf{v}} - (\Omega^2\mathbf{M}\mathbf{u} - \Omega\mathbf{C}\mathbf{v} - \mathbf{K}\mathbf{u})\cos^2\Omega t - (\Omega^2\mathbf{M}\mathbf{v} + \Omega\mathbf{C}\mathbf{u} - \mathbf{K}\mathbf{v})\sin\Omega t \cos\Omega t \\ & = \mathbf{F}(\mathbf{u}, \mathbf{v}, t)\cos\Omega t \end{aligned} \quad (6.11)$$

According to the assumption expressed in Equation (6.4),

$$\begin{aligned} X_1 &= u_1 \cos\Omega t + v_1 \sin\Omega t \\ X_2 &= u_2 \cos\Omega t + v_2 \sin\Omega t \end{aligned} \quad (6.12)$$

the nonlinear term $\mathbf{F}(\mathbf{u}, \mathbf{v}, t)$ in Equation (6.2) can be expressed as

$$\mathbf{F} = \begin{bmatrix} F_0 \cos\Omega t + M_1 g - C_1^* [\Delta v \cos\Omega t - \Delta u \sin\Omega t][\Delta u \cos\Omega t + \Delta v \sin\Omega t] \\ -C_1^{**} [\Delta v \cos\Omega t - \Delta u \sin\Omega t][\Delta u \cos\Omega t + \Delta v \sin\Omega t]^2 \\ -\left(C_1' + C_1''\Omega^2\right)[\Delta v \cos\Omega t - \Delta u \sin\Omega t] - \left(K_1'\Omega + K_1''\Omega^2\right)[\Delta u \cos\Omega t + \Delta v \sin\Omega t] \\ -K_1^* [\Delta u \cos\Omega t + \Delta v \sin\Omega t]^2 - K_1^{**} [\Delta u \cos\Omega t + \Delta v \sin\Omega t]^3 \\ \\ M_2 g + C_1^* [\Delta v \cos\Omega t - \Delta u \sin\Omega t][\Delta u \cos\Omega t + \Delta v \sin\Omega t] \\ +C_1^{**} [\Delta v \cos\Omega t - \Delta u \sin\Omega t][\Delta u \cos\Omega t + \Delta v \sin\Omega t]^2 \\ +\left(C_1' + C_1''\Omega^2\right)[\Delta v \cos\Omega t - \Delta u \sin\Omega t] + \left(K_1'\Omega + K_1''\Omega^2\right)[\Delta u \cos\Omega t + \Delta v \sin\Omega t] \\ +K_1^* [\Delta u \cos\Omega t + \Delta v \sin\Omega t]^2 + K_1^{**} [\Delta u \cos\Omega t + \Delta v \sin\Omega t]^3 \\ -C_2^* [-u_2 \sin\Omega t + v_2 \cos\Omega t][u_2 \cos\Omega t + v_2 \sin\Omega t] \\ -C_2^{**} [-u_2 \sin\Omega t + v_2 \cos\Omega t][u_2 \cos\Omega t + v_2 \sin\Omega t]^2 \\ -\left(C_2' + C_2''\Omega^2\right)[v_2 \cos\Omega t - u_2 \sin\Omega t] - \left(K_2'\Omega + K_2''\Omega^2\right)[u_2 \cos\Omega t + v_2 \sin\Omega t] \\ -K_2^* [u_2 \cos\Omega t + v_2 \sin\Omega t]^2 - K_2^{**} [u_2 \cos\Omega t + v_2 \sin\Omega t]^3 \end{bmatrix} \quad (6.13)$$

where $\Delta u = u_1 - u_2, \Delta v = v_1 - v_2$.

Then Equation (6.10) is integrated from 0 to $2\pi/\Omega$ by assuming that \mathbf{u}, \mathbf{v} remain constant. The final result is

$$\mathbf{M}\dot{\mathbf{u}} = \frac{1}{2\Omega}(\mathbf{K} - \Omega^2\mathbf{M})\mathbf{v} + \frac{1}{2\Omega}\begin{bmatrix} Q_1 \\ Q_2 \end{bmatrix}. \quad (6.14)$$

With a similar manipulation, we can also obtain

$$\mathbf{M}\dot{\mathbf{v}} = \frac{1}{2\Omega}(\Omega^2\mathbf{M} - \mathbf{K})\mathbf{u} + \frac{1}{2\Omega}\begin{bmatrix} Q_3 \\ Q_4 \end{bmatrix} \quad (6.15)$$

where

$$\begin{aligned} Q_1 &= -C_1\Omega\Delta u - (C_1' + C_1''\Omega^2)\Delta u + (K_1'\Omega + K_1''\Omega^2)\Delta v - \frac{8C_1^*}{3\pi}\Delta u\Delta v + \frac{8K_1^*}{3\pi}\Delta v^2 \\ &+ \left(\frac{3K_1^{**}}{4}\Delta v - \frac{C_1^{**}}{4}\Delta u\right)(\Delta u^2 + \Delta v^2) \\ Q_2 &= C_1\Omega\Delta u - (C_2' + C_2''\Omega^2)u_2 + (K_2'\Omega + K_2''\Omega^2)v_2 - \frac{8C_2^*}{3\pi}u_2v_2 + \frac{8K_2^*}{3\pi}v_2^2 \\ &- C_2\Omega u_2 + (C_1' + C_1''\Omega^2)\Delta u - (K_1'\Omega + K_1''\Omega^2)\Delta v + \frac{8C_1^*}{3\pi}\Delta u\Delta v - \frac{8K_1^*}{3\pi}\Delta v^2 \\ &+ \left(\frac{C_1^{**}}{4}\Delta u - \frac{3K_1^{**}}{4}\Delta v\right)(\Delta u^2 + \Delta v^2) + \left(\frac{3K_2^{**}}{4}v_2 - \frac{C_2^{**}}{4}u_2\right)(u_2^2 + v_2^2) \\ Q_3 &= F_0 - C_1\Omega\Delta v - (C_1' + C_1''\Omega^2)\Delta v - (K_1'\Omega + K_1''\Omega^2)\Delta u - \frac{8C_1^*}{3\pi}\Delta u\Delta v - \frac{8K_1^*}{3\pi}\Delta u^2 \\ &- \left(\frac{3K_1^{**}}{4}\Delta u + \frac{C_1^{**}}{4}\Delta v\right)(\Delta u^2 + \Delta v^2) \\ Q_4 &= C_1\Omega\Delta v - (C_2' + C_2''\Omega^2)v_2 - (K_2'\Omega + K_2''\Omega^2)u_2 - \frac{8C_2^*}{3\pi}u_2v_2 - \frac{8K_2^*}{3\pi}u_2^2 \\ &- C_2\Omega v_2 + (C_1' + C_1''\Omega^2)\Delta v + (K_1'\Omega + K_1''\Omega^2)\Delta u + \frac{8C_1^*}{3\pi}\Delta u\Delta v + \frac{8K_1^*}{3\pi}\Delta u^2 \\ &+ \left(\frac{3K_1^{**}}{4}\Delta u + \frac{C_1^{**}}{4}\Delta v\right)(\Delta u^2 + \Delta v^2) - \left(\frac{3K_2^{**}}{4}u_2 + \frac{C_2^{**}}{4}v_2\right)(u_2^2 + v_2^2) \end{aligned} \quad (6.16)$$

Equations (6.14) and (6.15) represent a set of first order, ordinary differential equations. For the periodic steady state vibration, the conditions are given as

$$\dot{\mathbf{u}} = \dot{\mathbf{v}} = \mathbf{0}. \quad (6.17)$$

Substituting Equations (6.14) and (6.15) into condition Equation (6.17), a set of four non-linear algebraic equations for u_1, v_1, u_2, v_2 are obtained, namely

$$\begin{cases} (K_1 - \Omega^2 M_1)v_1 - K_1 v_2 + Q_1 = 0 & -K_1 v_1 + (K_1 + K_2 - \Omega^2 M_2)v_2 + Q_2 = 0 \\ (\Omega^2 M_1 - K_1)u_1 + K_1 u_2 + Q_3 = 0 & K_1 u_1 + (\Omega^2 M_2 - K_1 - K_2)u_2 + Q_4 = 0 \end{cases} \quad (6.18)$$

6.3 Efficiency analysis of vibration isolation system

6.3.1 Analysis of dynamical characteristic

A very important aspect of vibration analysis is the natural frequencies of mechanical systems, as vibration isolators are believed to be effective when the excitation frequency is well above $\sqrt{2}\omega_0$, as stated in Section 2.5.2, where ω_0 is the natural frequency of isolators. The calculation of natural frequencies can provide guidelines for the dynamic design of isolator. In many handbooks on vibration^[118], we can obtain the expressions of natural frequencies for two-stage linear vibration systems as

$$\omega_{1,2} = \sqrt{\frac{1}{2} \left[\frac{K_2}{M_2} + \frac{K_1}{M_1} \left(1 + \frac{M_1}{M_2} \right) \right] \pm \sqrt{\left[\frac{K_2}{M_2} + \frac{K_1}{M_1} \left(1 + \frac{M_1}{M_2} \right) \right]^2 - \frac{4K_1 K_2}{M_1 M_2}}}. \quad (6.19)$$

Substituting Equation (6.3) into Equation (6.19), the natural frequencies of the corresponding linear system in Figure 6.1 can be expressed as

$$\omega_{1,2} = \sqrt{\frac{K_1}{M_1} \left(1 + \frac{M_1}{M_2} \right) \left(1 \pm \sqrt{\frac{M_1}{M_1 + M_2}} \right)}. \quad (6.20)$$

When $M_1 = 30\text{kg}$, $K_1 = 2680940$ and K_2 is designed following Equation (6.3), we can see the influence of M_2 on natural frequencies of system from Figure 6.6. The first natural frequency ω_1 increases from 34 Hz to 36.5 Hz with M_2 from 1kg to 30kg, and the second natural frequency ω_2 decreases from 370 Hz to 90 Hz with M_2 .

In order to determine the stability of a periodic solution, a small perturbation of the solutions of Equation (6.18) is introduced and written as

$$\begin{cases} u_1(t) = u_{10} + u_{11}(t), & v_1(t) = v_{10} + v_{11}(t) \\ u_2(t) = u_{20} + u_{21}(t), & v_2(t) = v_{20} + v_{21}(t) \end{cases} \quad (6.21)$$

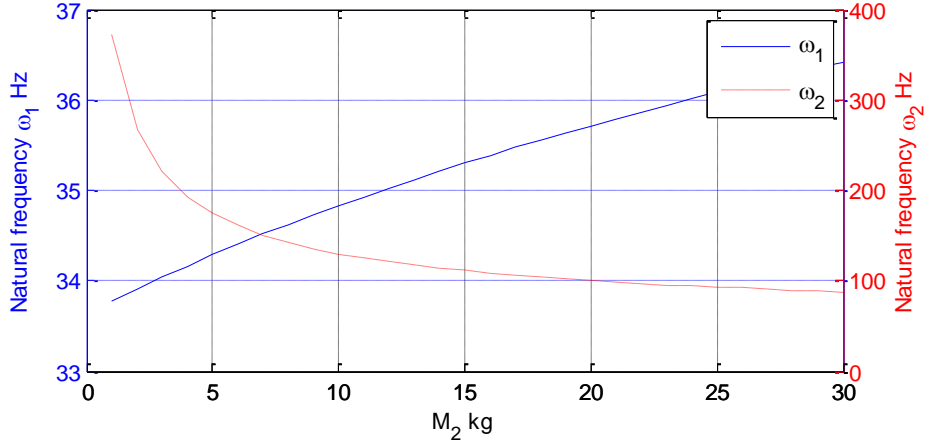


Figure 6.6 The influence of M_2 on natural frequencies of system.

where $u_{10}, v_{10}, u_{20}, v_{20}$ are the steady state solutions of Equation (6.18), and $u_{11}(t), v_{11}(t), u_{21}(t)$ and $v_{21}(t)$ are small perturbations. Substituting Equation (6.21) into Equations (6.14) and (6.15), expanding the resulting equations in Taylor series with respect to u_{11}, v_{11}, u_{21} and v_{21} , and using conditions in Equation (6.17), the perturbed equations are obtained by keeping the linear parts, which is a linear system in the form of

$$\dot{\mathbf{x}} = \mathbf{A}\mathbf{x} \quad (6.22)$$

where

$$\mathbf{x} = [u_{11}(t), u_{21}(t), v_{11}(t), v_{21}(t)]^T \quad (6.23)$$

And

$$\mathbf{A} = \frac{1}{2\Omega} \begin{bmatrix} \mathbf{M} & \mathbf{0} \\ \mathbf{0} & \mathbf{M} \end{bmatrix}^{-1} \left(\begin{bmatrix} \mathbf{0} & (\mathbf{K} - \Omega^2\mathbf{M}) \\ (\Omega^2\mathbf{M} - \mathbf{K}) & \mathbf{0} \end{bmatrix} + \begin{bmatrix} \left. \begin{array}{cccc} \frac{\partial Q_1}{\partial u_{11}|_0} & \frac{\partial Q_1}{\partial u_{21}|_0} & \frac{\partial Q_1}{\partial v_{11}|_0} & \frac{\partial Q_1}{\partial v_{21}|_0} \\ \frac{\partial Q_2}{\partial u_{11}|_0} & \frac{\partial Q_2}{\partial u_{21}|_0} & \frac{\partial Q_2}{\partial v_{11}|_0} & \frac{\partial Q_2}{\partial v_{21}|_0} \\ \frac{\partial Q_3}{\partial u_{11}|_0} & \frac{\partial Q_3}{\partial u_{21}|_0} & \frac{\partial Q_3}{\partial v_{11}|_0} & \frac{\partial Q_3}{\partial v_{21}|_0} \\ \frac{\partial Q_4}{\partial u_{11}|_0} & \frac{\partial Q_4}{\partial u_{21}|_0} & \frac{\partial Q_4}{\partial v_{11}|_0} & \frac{\partial Q_4}{\partial v_{21}|_0} \end{array} \right| \end{bmatrix} \right) \quad (6.24)$$

By obtaining the eigenvalues of the coefficient matrix in Equation (6.24), the stability of periodic solutions can be determined. If the real part of all the eigenvalues is negative, then the periodic solution is stable; otherwise, it is unstable. If a real eigenvalue changes sign, it is a saddle-node-type bifurcation and may result in jump phenomena. If we have a pair of complex conjugate eigenvalues whose real part changes sign, it is a Hopf bifurcation and quasi-periodic vibrations will result.

6.3.2 Analysis of isolation characteristic

The effectiveness of an isolator can be assessed by examining the transmissibility of the vibrating system. Transmissibility is defined as the ratio of the force transmitted to the foundation to the applied force, in the direction of the applied loads. In order to investigate the isolation transmissibility of the two-stage vibration system, the transmitted force F_B can be expressed as

$$F_B = C_2 \dot{X}_2 + \frac{C_2'}{\Omega} \dot{X}_2 + C_2'' \Omega \dot{X}_2 + \frac{C_2^*}{\Omega} X_2 \dot{X}_2 + \frac{C_2^{**}}{\Omega} X_2^2 \dot{X}_2 + K_2 X_2 + K_2' \Omega X_2 + K_2'' \Omega^2 X_2 + K_2^* X_2^2 + K_2^{**} X_2^3 \quad (6.25)$$

According to Equation (6.12), the steady state response can be expressed as

$$X_2 = A_2 \cos(\Omega t + \varphi_2) \quad (6.26)$$

where $\varphi_2 = \tan^{-1}(-v_2/u_2)$ is the phase between exciting force $F_0 \cos \Omega t$ and the steady state response X_2 . Substituting Equation (6.26) into Equation (6.25), we obtain the transmitting force F_B , as

$$F_B = -F_B^0 + F_B' \cos(\Omega t + \varphi + \Delta') + F_B'' \cos(2\Omega t + 2\varphi + \Delta'') + F_B''' \cos(3\Omega t + 3\varphi + \Delta''') \quad (6.27)$$

$$\text{where } F_B^0 = \frac{K_2^* A_2^2}{2}, \quad F_B'' = \frac{A_2^2}{2} \sqrt{K_2^{*2} + C_2^{*2}}, \quad F_B''' = \frac{A_2^3}{4} \sqrt{K_2^{**2} + C_2^{**2}},$$

$$F_B' = A_2 \sqrt{\left(C_2 \Omega + C_2' + C_2'' \Omega^2 + \frac{C_2^{**} A_2^2}{4} \right)^2 + \left(K_2 + K_2' \Omega + K_2'' \Omega^2 + \frac{3K_2^{**} A_2^2}{4} \right)^2},$$

$$\Delta' = \tan^{-1} \left(\left(C_2 \Omega + C_2' + C_2'' \Omega^2 + \frac{C_2^{**} A_2^2}{4} \right) / \left(K_2 + K_2' \Omega + K_2'' \Omega^2 + \frac{3K_2^{**} A_2^2}{4} \right) \right),$$

$\Delta'' = \tan^{-1}\left(\frac{C_2^*}{K_2^*}\right)$, and $\Delta''' = \tan^{-1}\left(\frac{C_2^{**}}{K_2^{**}}\right)$. Then the transmissibility of isolation system is

defined as the magnitude of the force ratio, which can be expressed as

$$Tr = \|F_B/F_0\|. \quad (6.28)$$

From this expression, it is obvious that a decrease in transmissibility leads to a reduction in the vibration transmitted to the foundation. In order to obtain the best isolation characteristic, the analysis focusses on how to reduce the vibration transmissibility.

6.4 Numerical results and discussions

6.4.1 Influence of linear parameters

In all the numerical calculations, the exciting frequency Ω is taken as an independent variable. r_1 and r_2 denote the response amplitudes of X_1 and X_2 , respectively, namely

$$r_1 = \sqrt{u_1^2 + v_1^2} \quad r_2 = \sqrt{u_2^2 + v_2^2}. \quad (6.29)$$

When the nonlinear parameters $K_{1,2}' = K_{1,2}'' = K_{1,2}^* = K_{1,2}^{**} = C_{1,2}' = C_{1,2}'' = C_{1,2}^* = C_{1,2}^{**} = 0$, the vibration system turns into a linear dynamical system. As illustrated in Section 6.2.1, for safety design of static load capacity we have to guarantee the relationship between stiffness K_1 and stiffness K_2 .

$$K_2 \geq \frac{(M_1 + M_2)}{M_1} K_1. \quad (6.30)$$

The steady responses of X_1 and X_2 are studied to assess the vibration attenuation of this corresponding linear dynamical system. As shown in Figure 6.7, we can see the influence of stiffness K_2 on response amplitudes of X_1 and X_2 . When M_1 is 30kg, M_2 is 5kg, K_1 is 2680940N/m and C_1 is 740N.s/m, the resonance frequencies of both X_1 and X_2 shift to the right with increasing stiffness K_2 and the peak values of vibration amplitude reduce for both X_1 and X_2 . However, the amplitudes of vibration response are not sensitive to the stiffness ratio of K_2 to K_1 with further increasing frequencies higher than resonance frequency. As stated previously, the vibration effectiveness of isolation can be obtained by ensuring that the excitation frequency is well above $\sqrt{2}\omega_0$, where ω_0 is the natural frequency of the isolator. Therefore, both the lower resonance frequency and the smaller peak of vibration amplitude are desirable characteristics for

isolation. In this two-stage isolation system, increasing the stiffness K_2 can reduce the peaks of vibration amplitude, but at the same time result in a right shift of resonance frequency, which should be avoided to improve the effectiveness of isolation by lowering the natural frequency of isolators. Besides considering saving MRE material, it also makes perfect sense to design the stiffness K_2 as expressed by Equation (6.3).

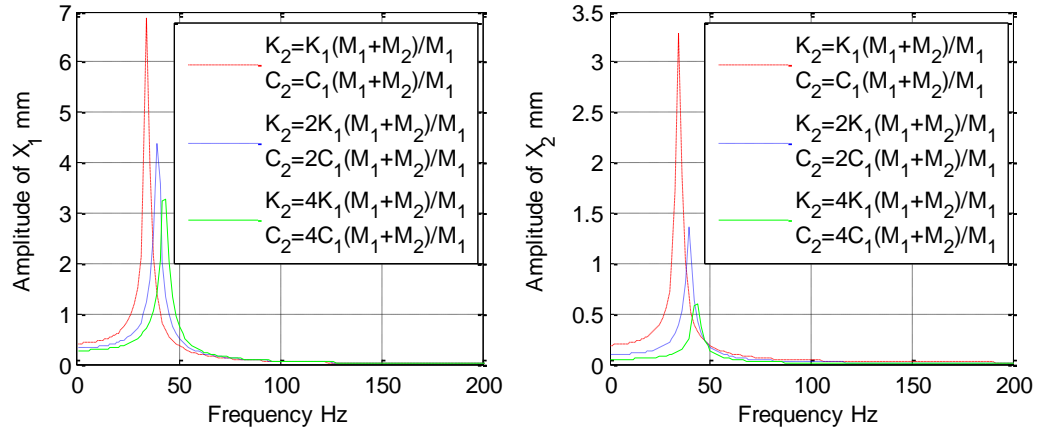


Figure 6.7 The effect of stiffness K_2 on the amplitude of vibration response ($F_0 = 300\text{N}$, $M_1 = 30\text{kg}$, $M_2 = 5\text{kg}$, $K_1 = 2680940\text{N/m}$ and $C_1 = 740\text{N.s/m}$).

Figure 6.8 shows the effect of the mass ratio M_1 / M_2 on the system response. When M_1 is 30kg, K_1 is 2680940N/m, C_1 is 740N.S/m and the stiffness K_2 and C_2 are designed according to Equation (6.3), an observable decrease of resonance frequency can be obtained by increasing this mass ratio. However, simultaneously the peaks of vibration amplitude increase obviously, as shown in Figure 6.8. When the excitation frequencies are higher than resonance frequency, the mass ratio M_1 / M_2 barely affects the vibration amplitude of the system. Therefore, as a desirable characteristic of isolation smaller peaks of vibration amplitude can be obtained by decreasing the mass ratio of M_1 to M_2 , although the resonance frequency slightly increases at the same time in this two-stage isolation system.

The numerical results of transmissibility are investigated to evaluate the effectiveness of isolation in the corresponding linear vibration system. Figure 6.9 shows the influence of stiffness K_2 on transmissibility of isolation system. When M_1 is 30kg, M_2 is 5kg, K_1 is 2680940N/m and C_1 is 740N.s/m, increasing of stiffness K_2 can shift natural frequencies to the right and increase the force transmissibility values at frequencies higher than the resonance frequency, but the peak of transmissibility does not change much. Therefore, it can be concluded that a lower stiffness K_2 can improve the isolation characteristics, because the lower

stiffness K_2 can reduce both the resonance frequency and also reduce the force transmissibility at higher frequencies.

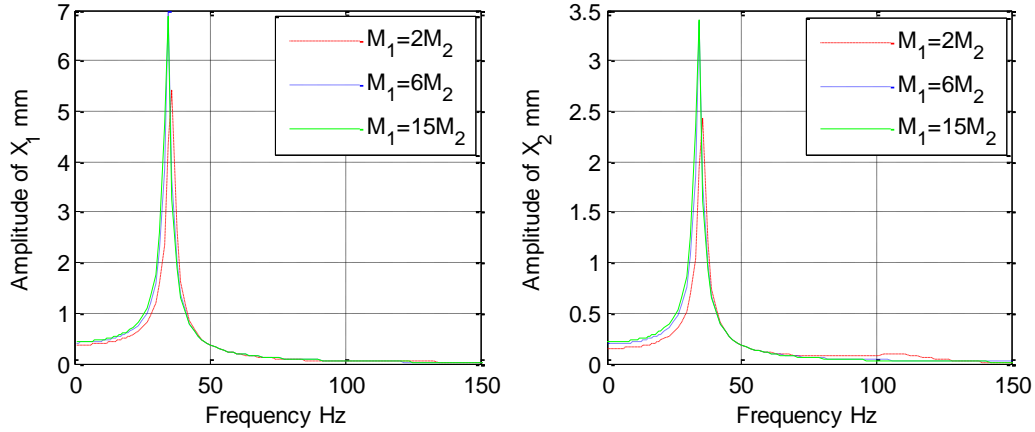


Figure 6.8 The effect of mass M_2 on the amplitude of vibration response ($F_0 = 300\text{N}$, $M_1 = 30\text{kg}$, $K_1 = 2680940\text{N/m}$, $C_1 = 740\text{N.s/m}$, $K_2 = K_1(M_1 + M_2)/M_1$ and $C_2 = C_1(M_1 + M_2)/M_1$).

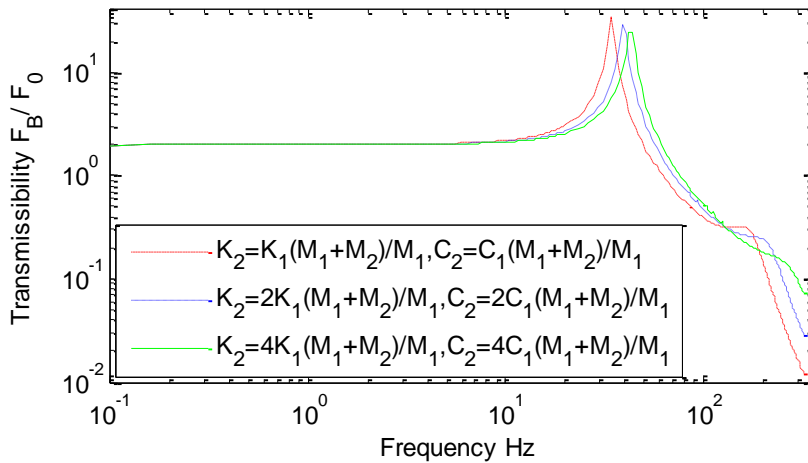


Figure 6.9 The effect of stiffness K_2 on the transmissibility of system ($F_0 = 300\text{N}$, $M_1 = 30\text{kg}$, $M_2 = 5\text{kg}$, $K_1 = 2680940\text{N/m}$ and $C_1 = 740\text{N.S/m}$).

When M_1 is 30kg, K_1 is 2680940N/m, C_1 is 740N.s/m and the stiffness K_2 and C_2 are selected according to Equation (6.3), it can be seen in Figure 6.10 that increasing mass M_2 slightly shifts the first natural frequency of system to the left and obviously shifts the second natural frequency to the right, which is in accordance with the discussion on natural frequency of system in Section 6.3.1. As mass M_2 increases, the force transmissibility increases slightly at frequencies lower than the first natural frequency, and the transmissibility increases obviously when excitation frequencies are above the second natural frequency. Increasing the mass ratio

M_1 / M_2 slightly increases the peak of force transmissibility at resonance frequency and significantly decreases the transmissibility at frequencies between the two natural frequencies. Overall a lower mass ratio M_1 / M_2 can effectively reduce the force transmissibility at high frequencies; hence, appropriately increasing the mass M_2 is helpful to reduce the force transmissibility in this isolation system.

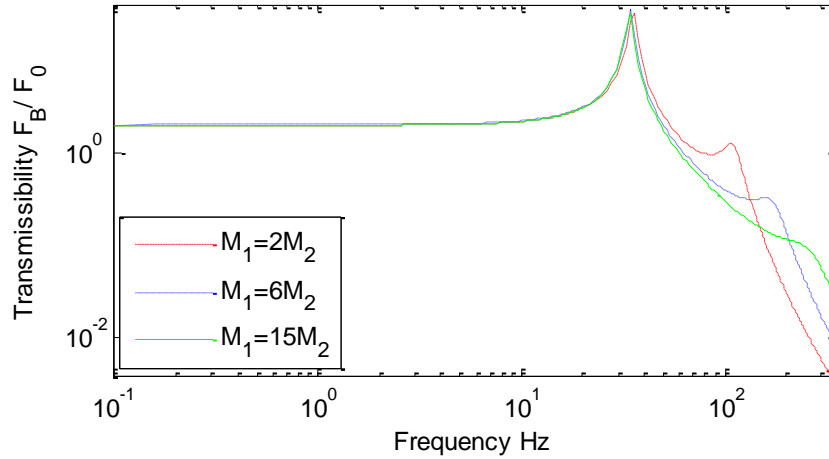


Figure 6.10 The effect of mass M_2 on the transmissibility of system ($F_0 = 300\text{N}$, $M_1 = 30\text{kg}$, $K_1 = 2680940\text{N/m}$, $C_1 = 740\text{N.S/m}$, $K_2 = K_1(M_1 + M_2)/M_1$ and $C_2 = C_1(M_1 + M_2)/M_1$).

6.4.2 The influence of non-linearity

Solving Equation (6.1) is essential to assess the performance of dynamic isolators and to explore the influence of nonlinearity on the isolation characteristic. However, it is impossible to obtain the exact analytical solutions of the system response when damping or stiffness is nonlinear. Alternatively, direct numerical integration is employed with the fourth order Runge-Kutta method to investigate the dynamical behaviour and isolation transmissibility.

If the nonlinear parameters $K_{1,2}' = K_{1,2}'' = K_{1,2}^* = K_{1,2}^{**} = C_{1,2}' = C_{1,2}'' = C_{1,2}^* = C_{1,2}^{**} = 0$, the vibration system is a linear isolation system; if the parameters $K_{1,2}' = K_{1,2}'' = K_{1,2}^* = K_{1,2}^{**} = C_{1,2} = C_{1,2}'' = C_{1,2}^* = C_{1,2}^{**} = 0$ and the storage and loss moduli of the MRE material are linear and this material turns into a linear viscoelastic material. As shown in Figure 6.11, the influence of non-linearity on vibration response of this two-stage isolation system is investigated by comparing with a corresponding linear vibration system and a corresponding linear viscoelastic material. All the non-linear parameters are chosen from Table 6.1 with magnetic intensity $B = 0$, and the stiffness and damping are designed following the relationship in Equation (6.3). From Figure 6.11, a slight right shift of the resonance frequency occurs with the non-linearity of MRE

isolator in this two-stage vibration system when comparing with either the linear isolator or the linear viscoelastic material. It can also be noticed that the MRE isolator can work much better than the linear isolator on reducing the peaks of transmitted vibration, but the MRE isolator cannot lower the transmitted vibration as much as the linear viscoelastic material. Furthermore, the amplitude of steady response changes dramatically at 74 Hz, because the negative damping happens when frequencies are higher than 74 Hz which will never happen in reality because the loss modulus of MRE must be a positive value. Therefore, this model has a limited working frequency range to guarantee its efficiency considering the frequency range where the experimental results are used to develop mathematical modelling.

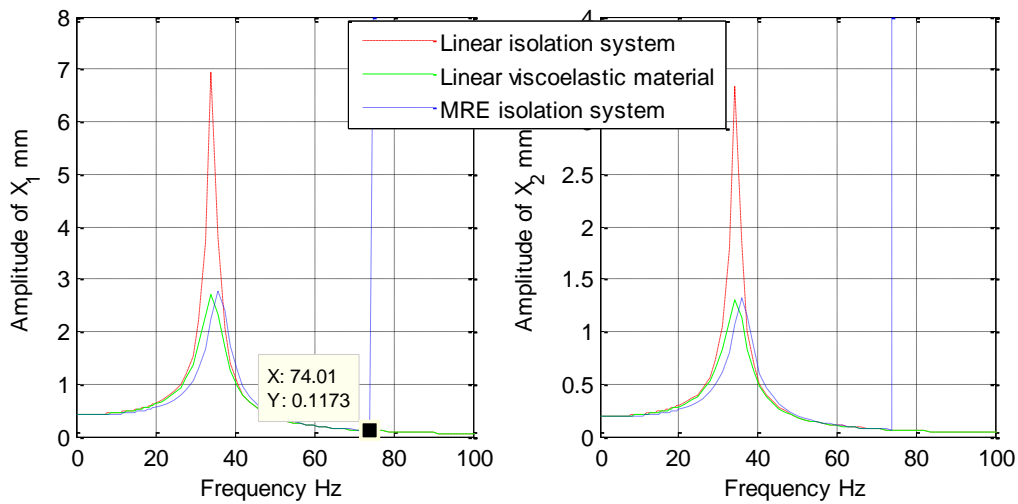


Figure 6.11 The vibration responses of different systems ($F_0 = 300\text{N}$, $M_1 = 30\text{kg}$ and $M_2 = 5\text{kg}$).

In Figure 6.12, the non-linear parameters for MRE isolation system in a field-on state are chosen from Table 6.1 when magnetic intensity $B = 500$ mT, and the stiffness and damping are also designed following the relationship in Equation (6.3). It can be seen that the application of a magnetic field of 500 mT can shift the resonance frequency to the right noticeably and reduces the peak of vibration amplitude simultaneously. In this two-stage vibration system, the lower resonance frequency and the smaller peak value of response amplitude can be obtained as desirable characteristics for isolation by employing a magnetic field of 500 mT when frequencies are lower than 40 Hz and removing the magnetic field when frequencies are higher than 40 Hz. That is because with the application of magnetic field the adaptive MRE isolator can have a higher stiffness, which is helpful to attenuate the vibration amplitude at low frequencies in this vibration system, and at high frequencies this isolator works with a low stiffness to improve the isolation efficiency.

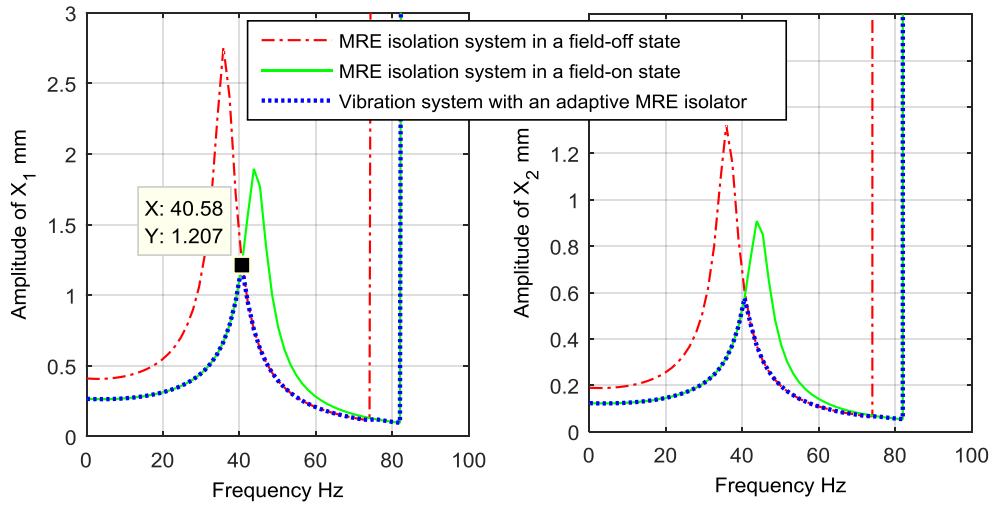


Figure 6.12 The vibration response of system with MRE isolators ($F_0 = 300\text{N}$, $M_1 = 30\text{kg}$ and $M_2 = 5\text{kg}$).

From Figure 6.13 we can see the comparison between conventional isolators and adaptive MRE isolators. The resonance frequency of this adaptive MRE isolator shifts to the right compared with either the linear isolator or the linear viscoelastic material. In addition the peak of vibration amplitude can be reduced much more with an adaptive MRE isolator than the linear isolator or the linear viscoelastic material. Therefore, the vibration isolation can be effectively improved over the full frequency range by applying a magnetic field of 500 mT at frequencies below 40 Hz and removing this magnetic field at frequencies above 40 Hz.

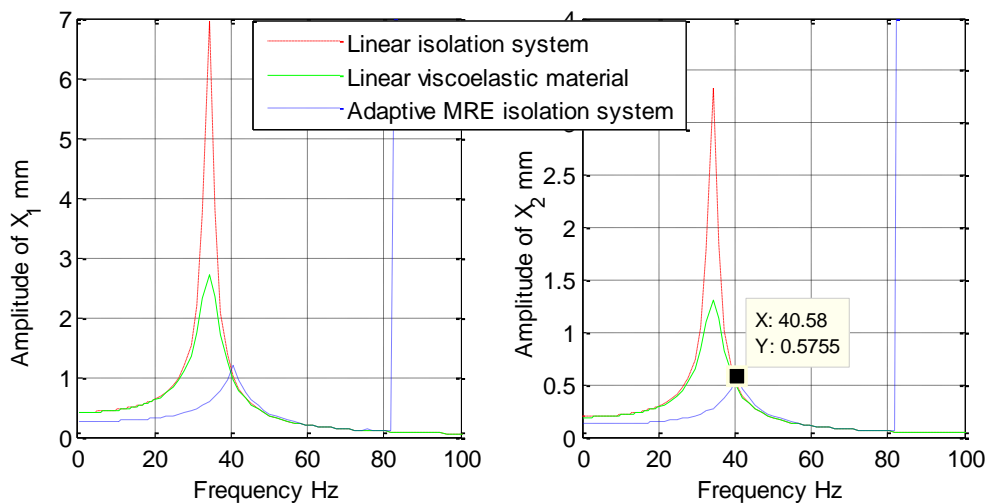


Figure 6.13 The vibration response of different systems ($F_0 = 300\text{N}$, $M_1 = 30\text{kg}$ and $M_2 = 5\text{kg}$).

The force transmissibility of the selected systems is investigated to evaluate the effectiveness of MRE isolators. The numerical results of Equation (6.28) are obtained as vibration transmissibility. As shown in Figure 6.14, the resonance frequency is a bit higher in the MRE isolation system than it is in either the linear isolation system or the linear viscoelastic material, and the peak of transmissibility in the MRE isolation system is lower than it is in the linear isolation system, but for the linear viscoelastic material the peak of transmissibility is even lower. It can also be noted that the MRE isolation system becomes unstable at frequencies above 74 Hz, because the expression of damper force in Equation (5.9) results in negative damping coefficients when frequencies are higher than 74 Hz, a limitation of modelling results from the frequency range during testing of mechanical properties characterisation for MRE. From the fact in Section 5.3.2 that the equivalent damping coefficient of MRE structure drastically decreases with increasing frequency, it can be deduced that at frequencies higher than 74 Hz the damping coefficient will be very low and close to zero; hence, the isolation characteristic in the MRE vibration system will be even better than either the linear isolation system or the linear viscoelastic material, as the general knowledge of vibration isolation is that low damping coefficients play a more important role in improving the isolation characteristic as driving frequency increases. Besides, the discussion in Section 5.3.2 shows that the equivalent stiffness of MRE isolator increases with frequency. Therefore, in this two-stage vibration system although the numerical results show instability of MRE isolation system at frequencies above 74 Hz, due to the limitation of mathematical modelling, there is a good reason to deduce that comparing with the linear isolation system or the linear viscoelastic material MRE isolation system will have better characteristics for vibration isolation at those high frequencies.

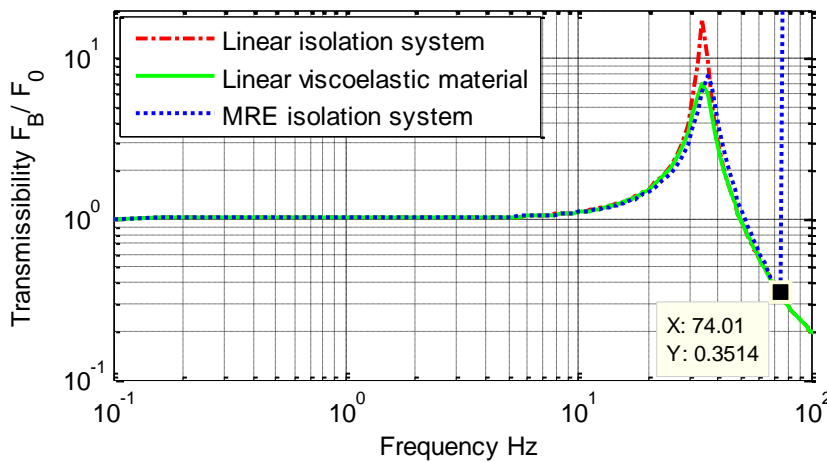


Figure 6.14 The force transmissibility of different systems ($F_0 = 300\text{N}$, $M_1 = 30\text{kg}$ and $M_2 = 5\text{kg}$).

From Figure 6.15 it can be seen that the resonance frequency can be effectively shifted to the right with the application of a magnetic field of 500 mT from 36 Hz to 45 Hz, but the transmissibility remains the same. The isolation performance can be improved by applying a magnetic field of 500 mT at frequencies below 40 Hz and removing the magnetic field at frequencies above 40 Hz. In this two-stage vibration system, the lower resonance frequency and the smaller peak value of transmissibility can be obtained as desirable isolation characteristics with a switchable magnetic field. Thus, the application of magnetic field enables the adaptive MRE isolator to have a higher stiffness and, thus, attenuate the transmissibility at low frequencies, and at high frequencies removing this magnetic field allows the adaptive MRE isolator to work with a low stiffness to improve the isolation efficiency.

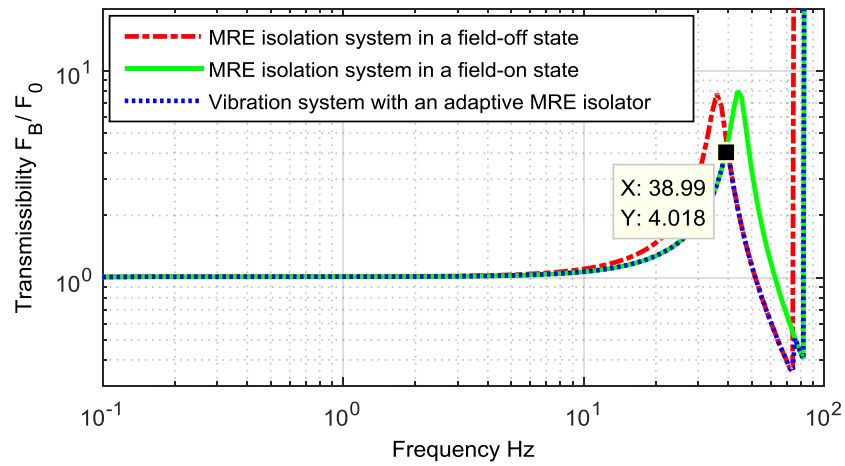


Figure 6.15 The transmissibility of system with MRE isolators ($F_0 = 300\text{N}$, $M_1 = 30\text{kg}$ and $M_2 = 5\text{kg}$).

Figure 6.16 shows the comparison between conventional isolators and adaptive MRE isolators. The adaptive MRE isolator has a higher resonance frequency and a lower peak value of isolation transmissibility when compared with either the linear isolator or the linear viscoelastic material. Therefore, a better isolation performance can be obtained by switching on a magnetic field of 500 mT when frequencies are lower than 40 Hz and switching off this magnetic field when frequencies are higher than 40 Hz. In addition, as discussed previously in this section although the simulation shows an instability in MRE isolation system at frequencies above 74 Hz, because the model of this two-stage vibration system has a limitation of working frequency to guarantee its efficiency considering the frequency domain where the experimental results are used to develop this mathematical model, it can be still deduced that the MRE isolation system will have a lower isolation transmissibility at frequencies higher than 74 Hz.

compared with the linear isolation system or the linear viscoelastic material. This is based on the results and discussions in Section 5.3.2 that the equivalent damping of MRE isolators decreases with frequencies and the equivalent stiffness increases which can result in an improved isolation performance at frequencies higher than resonance frequency.

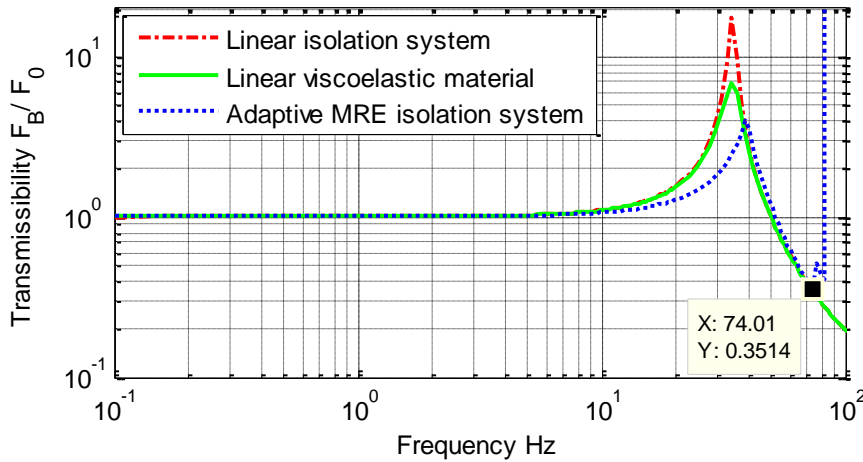


Figure 6.16 The force transmissibility of different systems ($F_0 = 300\text{N}$, $M_1 = 30\text{kg}$ and $M_2 = 5\text{kg}$).

6.5 Summary

In this chapter, a two-stage vibration system incorporating non-linear damping and non-linear stiffness is selected to investigate the use of MRE in isolation system. Firstly the study presents analytical expressions to describe the dynamical behaviour of this two-stage system that allows a simulation of steady response and an assessment of stability. Finally, direct numerical integration is employed to investigate the dynamical behaviour and isolation characteristics of this system. The steady vibration responses and force transmissibility curves of different systems are compared in frequency domain to evaluate the efficiency of adaptive MRE isolators.

In isolation systems, both lower resonance frequency and smaller peak of vibration amplitude or transmissibility are desirable characteristics. In this two-stage isolation system, appropriately increasing the mass of M_2 and decreasing the stiffness of K_2 can effectively lower the resonance frequency and reduce the peak of force transmissibility. However, considering keeping isolators compact and saving MRE material, we cannot increase the mass M_2 or reduce the stiffness K_2 ad infinitum, since the corresponding bearing capacity must be guaranteed for the safety of dynamic designs.

Comparing with the corresponding linear isolator and linear viscoelastic material, it is hard for MRE isolators to improve the efficiency of vibration control by lowering the resonance frequency. As an alternative way to improve the isolation characteristic, reduction of the peak value of vibration amplitude or force transmissibility can be obtained by controlling the magnetic field applied to an MRE isolator. With a switchable magnetic field, at low frequencies the application of magnetic field enables the adaptive MRE isolator to have a higher stiffness thus attenuate the vibration and the transmissibility, and at high frequencies removing this magnetic field allows the adaptive MRE isolator to work with a lower stiffness to improve the isolation efficiency.

Guidelines for designing MRE isolators: considering the related requirement for bearing capacity, the MRE isolator is designed with the lowest allowable stiffness to support the equipment; referring to the intersection point on curves of transmissibility in a field-off state and field-on state, the frequency for switching magnetic field is determined for MRE isolators; at low frequencies the isolator works in a field-on state, at high frequencies the isolator works in a field-off state.

Chapter 7 MRE Vibration Absorption Systems

7.1 Introduction

At present, the vibration absorber is the main application of MRE and the range of working frequencies can be effectively broadened for MRE absorbers by adjusting the magnetic field. As the stiffness of MRE material can be controlled with magnetic fields, when the excitation frequency varies MRE absorbers can be accordingly retuned. Compared with the commercialisation and industrialisation of MRF the application of MRE is still on a very early stage. Thus it is essential to develop reliable mechanical models for MRE to describe its dynamical behaviour accurately with the consideration of the dependence on strain, frequency and magnetic field.

The aim of this chapter is to study the dynamics of vibration absorption systems with MRE absorbers. At first, the general form of motion equations is established for this vibration absorption system, and the dynamical characteristics are analysed with analytical expressions. Secondly, the steady state vibration response and the transmissibility of absorption system are investigated by direct numerical integration. The performance of vibration control can be improved with MRE absorbers by adjusting the magnetic field accordingly as excitation frequency varies, from the perspective of both vibration response and force transmissibility^[113]. The results and discussions in this chapter can provide useful guidelines for the dynamic design of MRE absorbers.

7.2 Equations of motion

7.2.1 Standard form of equations of motion

The absorption system can be considered as a two DOF vibration system, which refers to the auxiliary absorber and the primary system with a spring and a damper, as shown in Figure 7.1. X_1 and X_2 are displacements of the absorber and the compressor. M_1 is the auxiliary mass coupled by a non-linear damper and a non-linear spring to a primary system with properties M_2 , K_2 and C_2 . The primary system is excited by force of amplitude of F_0 and angular frequency of Ω and it is assumed that the masses in this system only have vertical displacements.

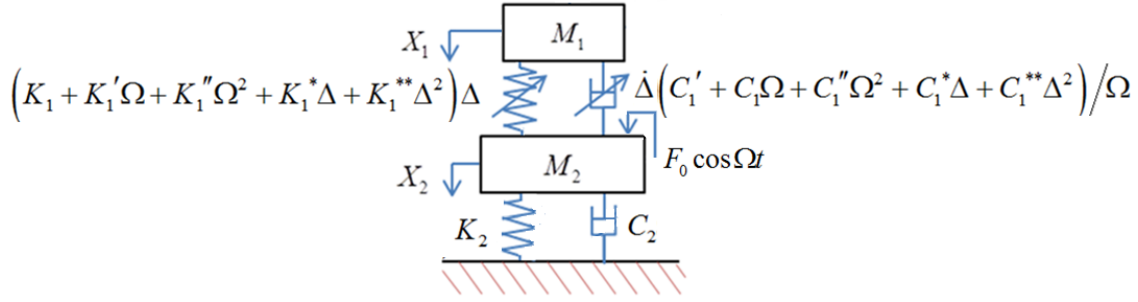


Figure 7.1 Vibration system with an MRE absorber.

Considering the mathematical modelling in Section 5.3, the governing differential equations of displacements are

$$\begin{aligned}
 M_1 \ddot{X}_1 + \left(C_1 + \frac{C_1'}{\Omega} + C_1'' \Omega + \frac{C_1^*}{\Omega} \Delta + \frac{C_1^{**}}{\Omega} \Delta^2 \right) \dot{\Delta} + \left(K_1 + K_1' \Omega + K_1'' \Omega^2 + K_1^* \Delta + K_1^{**} \Delta^2 \right) \Delta &= M_1 g \\
 M_2 \ddot{X}_2 + C_2 \dot{X}_2 + K_2 X_2 &= F_0 \cos \Omega t + M_2 g + \left(C_1 + \frac{C_1'}{\Omega} + C_1'' \Omega + \frac{C_1^*}{\Omega} \Delta + \frac{C_1^{**}}{\Omega} \Delta^2 \right) \dot{\Delta} + \left(K_1 + K_1' \Omega + K_1'' \Omega^2 + K_1^* \Delta + K_1^{**} \Delta^2 \right) \Delta
 \end{aligned} \tag{7.1}$$

where $\Delta = X_1 - X_2$ is the relative displacement of mass M_1 with respect of mass M_2 and $\dot{\Delta}$ is the relative velocity, $C_{1,2}$ and $K_{1,2}$ are the linear damping and stiffness coefficients of the absorber and the compressor, respectively; K_1' , K_1'' are coefficients of stiffness which proportionally and quadratically depend on frequency, respectively; K_1^* , K_1^{**} are coefficients of stiffness which proportionally and quadratically depend on strain, respectively; C_1' , C_1'' are coefficients of damping which anti-proportionally and proportionally depend on frequency, respectively; C_1^* , C_1^{**} are coefficients of damping which proportionally and quadratically depend on strain, respectively.

The motion equations can be also rewritten in matrix form:

$$\mathbf{M} \ddot{\mathbf{x}} + \mathbf{C} \dot{\mathbf{x}} + \mathbf{K} \mathbf{x} = \mathbf{F} \tag{7.2}$$

where

$$\ddot{\mathbf{x}} = \begin{bmatrix} \ddot{X}_1 \\ \ddot{X}_2 \end{bmatrix}, \quad \dot{\mathbf{x}} = \begin{bmatrix} \dot{X}_1 \\ \dot{X}_2 \end{bmatrix}, \quad \mathbf{x} = \begin{bmatrix} X_1 \\ X_2 \end{bmatrix}.$$

The mass, damping and stiffness matrices are expressed by

$$\mathbf{M} = \begin{bmatrix} M_1 & 0 \\ 0 & M_2 \end{bmatrix}, \mathbf{C} = \begin{bmatrix} C_1 & -C_1 \\ -C_1 & C_1 + C_2 \end{bmatrix}, \mathbf{K} = \begin{bmatrix} K_1 & -K_1 \\ -K_1 & K_1 + K_2 \end{bmatrix}$$

respectively, and the force vector

$$\mathbf{F} = \begin{bmatrix} M_1 g - \frac{C_1'}{\Omega} \dot{\Delta} - C_1'' \Omega \dot{\Delta} - \frac{C_1^*}{\Omega} \Delta \dot{\Delta} - \frac{C_1^{**}}{\Omega} \Delta^2 \dot{\Delta} - K_1' \Omega \Delta - K_1'' \Omega^2 \Delta - K_1^* \Delta^2 - K_1^{**} \Delta^3 \\ F_0 \cos \Omega t + M_2 g + \frac{C_1'}{\Omega} \dot{\Delta} + C_1'' \Omega \dot{\Delta} + \frac{C_1^*}{\Omega} \Delta \dot{\Delta} + \frac{C_1^{**}}{\Omega} \Delta^2 \dot{\Delta} + K_1' \Omega \Delta + K_1'' \Omega^2 \Delta + K_1^* \Delta^2 + K_1^{**} \Delta^3 \end{bmatrix}$$

Table 7.1 Parameters of designed stiffness and damping.

$K_I (B = 0)$ N/m	$K_I' (B = 0)$ N·s/m	$K_I'' (B = 0)$ N·s ² /m	$K_I^* (B = 0)$ N/m ²	$K_I^{**} (B = 0)$ N/m ³
536188	452.524	-0.95094	-4933460	44272600
$K_I (B = 0.5T)$ N/m	$K_I' (B = 0.5T)$ N·s/m	$K_I'' (B = 0.5T)$ N·s ² /m	$K_I^* (B = 0.5T)$ N/m ²	$K_I^{**} (B = 0.5T)$ N/m ³
826310	605.792	-1.39561	-10595650	87643500
$C_I (B = 0)$ N·s/m	$C_I' (B = 0)$ N·s ² /m	$C_I'' (B = 0)$ N·s ³ /m	$C_I^* (B = 0)$ N·s/m ²	$C_I^{**} (B = 0)$ N·s/m ³
148.056	81612	-0.67889	-951754	6197480
$C_I (B = 0.5T)$ N·s/m	$C_I' (B = 0.5T)$ N·s ² /m	$C_I'' (B = 0.5T)$ N·s ³ /m	$C_I^* (B = 0.5T)$ N·s/m ²	$C_I^{**} (B = 0.5T)$ N·s/m ³
159.501	132769	-0.79340	-1918910	13001400

As the discussion in Section 5.3, the parameters of designed stiffness and damping can be obtained by combining the geometrical design of the structure and the dynamical properties of MRE materials. The shear strain limitation of static load capacity is defined as 1% for the safe dynamic design of MRE absorber, the primary mass $M_2 = 30$ kg, the primary stiffness $K_2 = 5.5 \times 10^6$ N/m and the excitation force $F_0 = 300$ N. According to Equation (5.8), the calculation of equivalent stiffness and damping are based upon experimental results of mechanical property characterisation for MRE in Figure 6.2 and Figure 6.3. The parameters of designed stiffness and

designed damping for an auxiliary mass $M_1 = 3 \text{ kg}$ are listed in Table 7.1, when a magnetic field of 500 mT is applied the parameters change as per the discussion in Section 5.2.

Ensuring the static load capacity and avoiding any waste or any failure of MRE material, the stiffness K_1 has to be in proportion to the auxiliary mass M_1 , as expressed in Equation (7.3). From the mechanical properties of MRE it can be deduced that all the parameters of stiffness and damping $K_1, K_1', K_1'', K_1^*, K_1^{**}, C_1, C_1', C_1'', C_1^*$ and C_1^{**} have the same relationship.

$$\begin{aligned} M_1 &= 3n \text{ kg} \\ K_1 &= 536188n \text{ N/m} \end{aligned} \quad (n = 1, 2, 3, \dots) \quad (7.3)$$

7.2.2 Steady state response of system

Numerical simulations of Equation (7.1) are used to observe the steady state behaviour of this vibration absorption system. A specific group of parameters is selected for simulation according to the standard form of motion equations. The response of the absorption system for this selection is shown in Figure 7.2 Response of the system ($M_1 = 3 \text{ kg}, M_2 = 30 \text{ kg}, K_2 = 5.5 \times 10^6 \text{ N/m}$ and $F_0 = 300 \text{ N}$). and the Poincare map is shown in Figure 7.3.

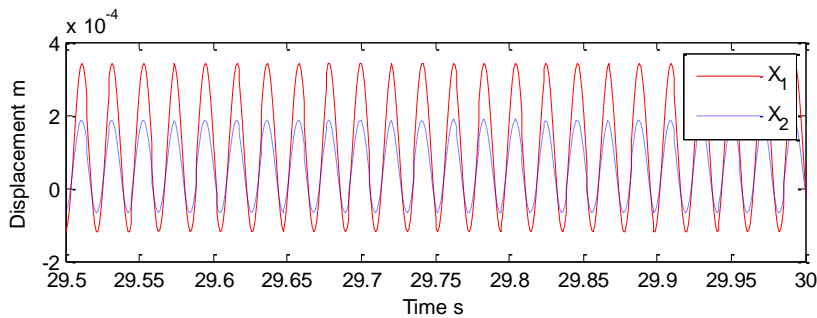


Figure 7.2 Response of the system ($M_1 = 3 \text{ kg}, M_2 = 30 \text{ kg}, K_2 = 5.5 \times 10^6 \text{ N/m}$ and $F_0 = 300 \text{ N}$).

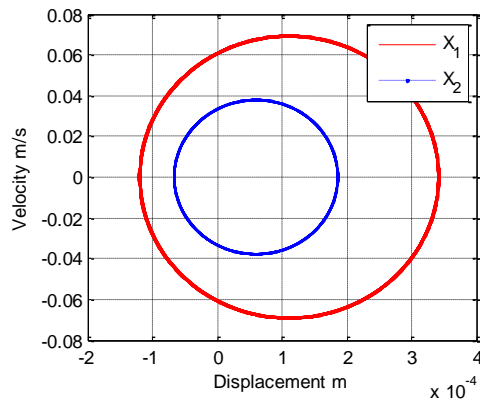


Figure 7.3 Poincare maps of the system ($M_1 = 3 \text{ kg}, M_2 = 30 \text{ kg}, K_2 = 5.5 \times 10^6 \text{ N/m}$ and $F_0 = 300 \text{ N}$).

The steady state responses can be represented as Equation (7.4) when applying the method of averaging,

$$\mathbf{x}(t) = \mathbf{u}(t)\cos\Omega t + \mathbf{v}(t)\sin\Omega t \quad (7.4)$$

where $\mathbf{u}(t) = \begin{bmatrix} u_1(t) \\ u_2(t) \end{bmatrix}$, $\mathbf{v}(t) = \begin{bmatrix} v_1(t) \\ v_2(t) \end{bmatrix}$ are assumed to be slow functions of time t . The

motivation for this assumption is that \mathbf{F} is zero when Equation (7.2) has a solution in the form of Equation (7.4) with $\mathbf{u}(t)$ and $\mathbf{v}(t)$ constants. Applying the same progress as in Section 6.2.2, we obtain

$$\begin{aligned} & \Omega M\dot{\mathbf{u}} + (\Omega^2 M\mathbf{u} - \Omega C\mathbf{v} - \mathbf{K}\mathbf{u})\cos\Omega t \sin\Omega t + (\Omega^2 M\mathbf{v} + \Omega C\mathbf{u} - \mathbf{K}\mathbf{v})\sin^2\Omega t \\ & = \mathbf{F}(\mathbf{u}, \mathbf{v}, t)(-\sin\Omega t) \end{aligned} \quad (7.5)$$

and

$$\begin{aligned} & \Omega M\dot{\mathbf{v}} - (\Omega^2 M\mathbf{u} - \Omega C\mathbf{v} - \mathbf{K}\mathbf{u})\cos^2\Omega t - (\Omega^2 M\mathbf{v} + \Omega C\mathbf{u} - \mathbf{K}\mathbf{v})\sin\Omega t \cos\Omega t \\ & = \mathbf{F}(\mathbf{u}, \mathbf{v}, t)\cos\Omega t \end{aligned} \quad (7.6)$$

According to the assumption expressed in Equation (7.4),

$$\begin{aligned} X_1 &= u_1 \cos\Omega t + v_1 \sin\Omega t \\ X_2 &= u_2 \cos\Omega t + v_2 \sin\Omega t \end{aligned} \quad (7.7)$$

and the nonlinear term $\mathbf{F}(\mathbf{u}, \mathbf{v}, t)$ in Equation (7.5) and Equation (7.6) can be expressed as

$$\mathbf{F} = \begin{bmatrix} M_1 g - C_1^* [\Delta v \cos\Omega t - \Delta u \sin\Omega t] [\Delta u \cos\Omega t + \Delta v \sin\Omega t] \\ -C_1^{**} [\Delta v \cos\Omega t - \Delta u \sin\Omega t] [\Delta u \cos\Omega t + \Delta v \sin\Omega t]^2 \\ -[C_1' + C_1''\Omega^2] [\Delta v \cos\Omega t - \Delta u \sin\Omega t] - K_1^* [\Delta u \cos\Omega t + \Delta v \sin\Omega t]^2 \\ -K_1^{**} [\Delta u \cos\Omega t + \Delta v \sin\Omega t]^3 - [K_1'\Omega + K_1''\Omega^2] [\Delta u \cos\Omega t + \Delta v \sin\Omega t] \\ F_0 \cos\Omega t + M_2 g + C_1^* [\Delta v \cos\Omega t - \Delta u \sin\Omega t] [\Delta u \cos\Omega t + \Delta v \sin\Omega t] \\ +C_1^{**} [\Delta v \cos\Omega t - \Delta u \sin\Omega t] [\Delta u \cos\Omega t + \Delta v \sin\Omega t]^2 \\ +[C_1' + C_1''\Omega^2] [\Delta v \cos\Omega t - \Delta u \sin\Omega t] + K_1^* [\Delta u \cos\Omega t + \Delta v \sin\Omega t]^2 \\ +K_1^{**} [\Delta u \cos\Omega t + \Delta v \sin\Omega t]^3 + [K_1'\Omega + K_1''\Omega^2] [\Delta u \cos\Omega t + \Delta v \sin\Omega t] \end{bmatrix} \quad (7.8)$$

where $\Delta u = u_1 - u_2$, $\Delta v = v_1 - v_2$.

Then Equation (7.5) and Equation (7.6) are integrated from 0 to $2\pi/\Omega$ by assuming that \mathbf{u} and \mathbf{v} remain constant. The final result is

$$\mathbf{M}\dot{\mathbf{u}} = \frac{1}{2\Omega}(\mathbf{K} - \Omega^2\mathbf{M})\mathbf{v} + \frac{1}{2\Omega} \begin{bmatrix} Q_1 \\ Q_2 \end{bmatrix} \quad (7.9)$$

$$\mathbf{M}\dot{\mathbf{v}} = \frac{1}{2\Omega}(\Omega^2\mathbf{M} - \mathbf{K})\mathbf{u} + \frac{1}{2\Omega} \begin{bmatrix} Q_3 \\ Q_4 \end{bmatrix} \quad (7.10)$$

where

$$\begin{aligned} Q_1 &= -C_1\Omega\Delta u - (C_1' + C_1''\Omega^2)\Delta u + (K_1'\Omega + K_1''\Omega^2)\Delta v \\ &\quad - \frac{8C_1^*}{3\pi}\Delta u\Delta v + \frac{8K_1^*}{3\pi}\Delta v^2 + \left(\frac{3K_1^{**}}{4}\Delta v - \frac{C_1^{**}}{4}\Delta u\right)(\Delta u^2 + \Delta v^2) \\ Q_2 &= C_1\Omega\Delta u - C_2\Omega u_2 + (C_1' + C_1''\Omega^2)\Delta u - (K_1'\Omega + K_1''\Omega^2)\Delta v \\ &\quad + \frac{8C_1^*}{3\pi}\Delta u\Delta v - \frac{8K_1^*}{3\pi}\Delta v^2 + \left(\frac{C_1^{**}}{4}\Delta u - \frac{3K_1^{**}}{4}\Delta v\right)(\Delta u^2 + \Delta v^2) \\ Q_3 &= C_1\Omega\Delta v - (C_1' + C_1''\Omega^2)\Delta v - (K_1'\Omega + K_1''\Omega^2)\Delta u \\ &\quad - \frac{8C_1^*}{3\pi}\Delta u\Delta v - \frac{8K_1^*}{3\pi}\Delta u^2 - \left(\frac{3K_1^{**}}{4}\Delta u + \frac{C_1^{**}}{4}\Delta v\right)(\Delta u^2 + \Delta v^2) \\ Q_4 &= F_0 + C_1\Omega\Delta v - C_2\Omega v_2 + (C_1' + C_1''\Omega^2)\Delta v + (K_1'\Omega + K_1''\Omega^2)\Delta u \\ &\quad + \frac{8C_1^*}{3\pi}\Delta u\Delta v + \frac{8K_1^*}{3\pi}\Delta u^2 + \left(\frac{3K_1^{**}}{4}\Delta u + \frac{C_1^{**}}{4}\Delta v\right)(\Delta u^2 + \Delta v^2) \end{aligned} \quad (7.11)$$

Equations (7.9) and (7.10) represent a set of first order, ordinary differential equations. For the periodic steady state vibration, the conditions are given as

$$\dot{\mathbf{u}} = \dot{\mathbf{v}} = \mathbf{0}. \quad (7.12)$$

Substituting Equations (7.9) and (7.10) into the initial condition Equation (7.12), a set of four non-linear algebraic equations for u_1, u_2, v_1, v_2 is obtained

$$\begin{aligned} (K_1 - \Omega^2 M_1)v_1 - K_1 v_2 + Q_1 &= 0 & -K_1 v_1 + (K_1 + K_2 - \Omega^2 M_2)v_2 + Q_2 &= 0 \\ (\Omega^2 M_1 - K_1)u_1 + K_1 u_2 + Q_3 &= 0 & K_1 u_1 + (\Omega^2 M_2 - K_1 - K_2)u_2 + Q_4 &= 0 \end{aligned} \quad (7.13)$$

7.3 Efficiency analysis of vibration absorption system

7.3.1 Analysis of dynamical characteristic

It is necessary to analyse the natural frequencies of dynamical systems. Practical consideration makes it important to avoid any resonance. The calculation of natural frequencies can provide guidelines for the dynamic design of absorbers. From many handbooks on vibration^[118], we can obtain the expressions of natural frequencies in absorption systems as

$$\omega_{1,2} = \sqrt{\frac{\omega_a^2(1+\mu) + \omega_0^2}{2} \pm \sqrt{\left[\frac{\omega_a^2(1+\mu) - \omega_0^2}{2}\right]^2 + \mu\omega_a^2\omega_0^2}} \quad (7.14)$$

where $\omega_a = \sqrt{K_1/M_1}$ is the natural frequency of the auxiliary system on its own, $\omega_0 = \sqrt{K_2/M_2}$ is the natural frequency of the primary system on its own and $\mu = M_1/M_2$.

When $M_2 = 30\text{kg}$, $K_2 = 5.5 \times 10^6 \text{N/m}$, M_1 and K_1 are designed following Equation (7.3), we can see the influence of M_1 on the natural frequencies of composite system in Figure 7.4. The first natural frequency ω_1 decreases from 65Hz to 42Hz with M_1 from 1kg to 30kg, and the second natural frequency ω_2 increases from 75Hz to 110Hz with M_1 .

The analysis of stability for this absorption system is similar to that of Section 6.3.1. By obtaining the eigenvalues of the coefficient matrix in Equation (7.15), the stability of periodic solutions can be determined. When the real part of all eigenvalues is negative, then the periodic solution is stable; otherwise, it is unstable.

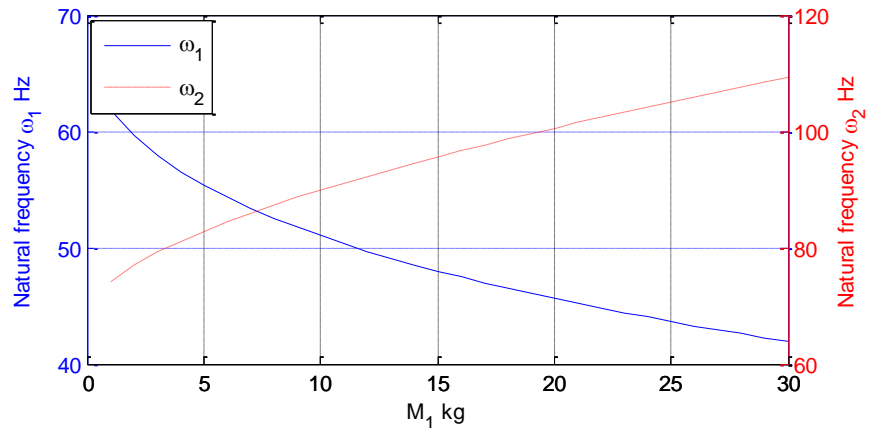


Figure 7.4 The influence of M_1 on natural frequencies of this composite system.

$$\mathbf{A} = \frac{1}{2\Omega} \begin{bmatrix} \mathbf{M} & \mathbf{0} \\ \mathbf{0} & \mathbf{M} \end{bmatrix}^{-1} \left(\begin{bmatrix} \mathbf{0} & (\mathbf{K} - \Omega^2 \mathbf{M}) \\ (\Omega^2 \mathbf{M} - \mathbf{K}) & \mathbf{0} \end{bmatrix} + \begin{bmatrix} \left. \frac{\partial Q_1}{\partial u_{11}} \right|_0 & \left. \frac{\partial Q_1}{\partial u_{21}} \right|_0 & \left. \frac{\partial Q_1}{\partial v_{11}} \right|_0 & \left. \frac{\partial Q_1}{\partial v_{21}} \right|_0 \\ \left. \frac{\partial Q_2}{\partial u_{11}} \right|_0 & \left. \frac{\partial Q_2}{\partial u_{21}} \right|_0 & \left. \frac{\partial Q_2}{\partial v_{11}} \right|_0 & \left. \frac{\partial Q_2}{\partial v_{21}} \right|_0 \\ \left. \frac{\partial Q_3}{\partial u_{11}} \right|_0 & \left. \frac{\partial Q_3}{\partial u_{21}} \right|_0 & \left. \frac{\partial Q_3}{\partial v_{11}} \right|_0 & \left. \frac{\partial Q_3}{\partial v_{21}} \right|_0 \\ \left. \frac{\partial Q_4}{\partial u_{11}} \right|_0 & \left. \frac{\partial Q_4}{\partial u_{21}} \right|_0 & \left. \frac{\partial Q_4}{\partial v_{11}} \right|_0 & \left. \frac{\partial Q_4}{\partial v_{21}} \right|_0 \end{bmatrix} \right) \quad (7.15)$$

7.3.2 Analysis of absorption characteristic

The effectiveness of an absorber can be assessed by examining the amplitude of vibration response, and a good absorption characteristic leads to a profound reduction in the vibration response of the primary system. If the auxiliary mass is small relative to the mass of the primary system, the effectiveness of the absorber is dependent on accurate tuning. Nominally the absorber is tuned to the frequency of the excitation, so the natural frequency $\omega_{1,2}$ that is close to the driving frequency is of interest. The ratio of $\omega_{1,2}$ to ω_a is a measure of sensitivity of the tuning required to avoid resonance, and the tuning for a primary system with high natural frequency is more sensitive compare to that for a primary system with low natural frequency. When the driving frequency is above the natural frequency of the primary system ω_0 , it is preferable to tune the absorber to a frequency slightly lower than the driving frequency to avoid the resonance that lies above ω_0 . Likewise when the driving frequency is less than ω_0 , it is better to tune the absorber to a frequency slightly greater than the driving frequency.

In order to obtain the best absorption characteristic, the analysis focusses on how to reduce the amplitude of vibration response in the primary system. In this thesis, transmissibility is defined as the ratio of the amplitude of motion of primary mass to the static deflection of the primary system. According to Equation (7.7), the steady response of the primary mass can be expressed as

$$X_2 = A_2 \cos(\Omega t + \varphi_2) \quad (7.16)$$

where $\varphi_2 = \tan^{-1}(-v_2/u_2)$ is the phase between excitation and the steady state response.

Then the transmissibility of the absorption system is defined as the ratio of vibration amplitude A_2 to the static deflection $A_{st} = F_0 / K_2$, it can be expressed as Equation (7.17). From

this expression, a decrease in transmissibility results from a reduction in the amplitude of the vibration response in primary system.

$$Tr = \|A_2/A_{st}\| \quad (7.17)$$

7.4 Numerical results and discussions

7.4.1 Influence of linear parameters

In all the numerical calculations, the exciting frequency Ω is taken as an independent variable. r_1 and r_2 denote the response amplitudes of X_1 and X_2 , respectively

$$r_1 = \sqrt{u_1^2 + v_1^2} \quad r_2 = \sqrt{u_2^2 + v_2^2} . \quad (7.18)$$

When the nonlinear parameters $K_1' = K_1'' = K_1^* = K_1^{**} = C_1' = C_1'' = C_1^* = C_1^{**} = 0$, the vibration system is a linear absorption system. As discussed in Section 7.3.2 absorbers are tuned to the excitation frequency, the auxiliary mass M_1 and the stiffness K_1 are designed following the relationship in Equation (7.3). The steady responses of X_1 and X_2 are studied to explore the influence of linear parameters on the vibration attenuation of the corresponding linear absorption systems.

Figure 7.5 shows the effect of the auxiliary mass M_1 on the system response, the stiffness K_1 changes with the mass M_1 due to the tuning progress of absorbers and the design rule in Equation (7.3). There are two peaks in the vibration amplitude, at natural frequencies ω_1 and ω_2 respectively. The vibration of primary mass M_2 is effectively attenuated at frequencies between the ω_1 and ω_2 where the vibration amplitude of X_2 is reduced. When M_2 is 30kg and K_2 is 5500000N/m, from the vibration amplitude of X_2 we can observe that as the auxiliary mass M_1 decreases, the peak of amplitude at ω_1 decreases and the peak of amplitude at ω_2 increases, but the range of working frequencies which are between the two natural frequencies ω_1 and ω_2 narrows down. Thus the effectiveness of absorbers depends on an accurate tuning very much when the auxiliary mass M_1 is relatively small. Comparing the vibration amplitude of X_2 with the vibration amplitude of X_1 , we can see that at working frequencies between natural frequencies ω_1 and ω_2 the absorber effectively reduce the vibration amplitude of X_2 for the primary system, simultaneously the motion of the absorbers becomes very large as the vibration amplitude of X_1 is even larger than the vibration amplitude of X_2 at frequencies between ω_1 and ω_2 . From the vibration amplitude of X_1 , as the auxiliary mass decreases the motion of absorbers

at frequencies between the two natural frequencies ω_1 and ω_2 becomes larger, so it is necessary to limit the vibration of the auxiliary mass by damping for avoiding failure.

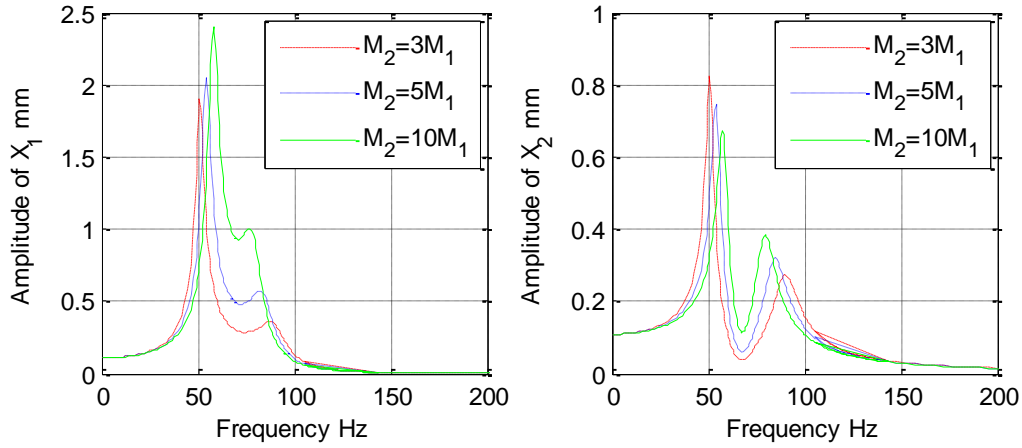


Figure 7.5 The effect of mass M_1 on the amplitude of vibration response ($F_0 = 300\text{N}$, $M_2 = 30\text{kg}$ and $K_2 = 5500000\text{N/m}$).

The effect of the damping C_1 of the absorber on the vibration response of the system can be seen in Figure 7.6. When M_2 is 30kg, K_2 is 5500000N/m and C_2 is 1500N.s/m, increasing the damping C_1 reduces the vibration amplitudes for both X_1 and X_2 at the two natural frequencies ω_1 and ω_2 . However, the vibration amplitude for X_2 increases with damping at the natural frequency of the absorber ω_a . Therefore, an increase of damping C_1 can effectively attenuates the vibrations of the auxiliary mass M_1 thus mitigate the risk of any failure of absorbers, as well as reduce the vibrations of the primary mass M_2 at the two natural frequencies ω_1 and ω_2 . However, at the natural frequency of the absorber ω_a , increasing damping C_1 cannot help in obtaining a better absorption performance but deteriorates the absorption efficiency, as the vibration amplitudes of X_2 increases with damping C_1 at the natural frequency ω_a . Additionally, damping C_1 cannot either broaden or narrow the range of working frequencies for the absorber.

In order to evaluate the absorption efficiency, we alternatively investigate the numerical results of Equation (7.17) obtained as vibration transmissibility. In Figure 7.7 we can see the influence of auxiliary mass M_1 on transmissibility of the absorption system. Because of the tuning process of absorbers and the design rule in Equation (7.3) the stiffness K_1 and the mass M_1 of the absorber change together. When M_2 is 30kg and K_2 is 5500000N/m, increasing the auxiliary mass M_1 can effectively broaden the range of working frequencies. For example when it is required to reduce the transmissibility lower than 1 between the two natural frequencies of this composite system ω_1 and ω_2 , there is a frequency range where the transmissibility is below

1, if the excitation frequency is in this range the transmissibility can be effectively controlled. From Figure 7.7 it can be seen that as the auxiliary mass M_1 increases, the range of working frequencies becomes wider, which is another piece of evidence that when the auxiliary mass M_1 is relatively small the effectiveness of absorbers depends on accurate tuning. The absorption performance is better because the transmissibility decreases with the increasing auxiliary mass M_1 in the range of working frequency, in addition a larger auxiliary mass M_1 results in a lower transmissibility at the second natural frequency of this composite system ω_2 , however, increasing the auxiliary mass M_1 will slightly increase the transmissibility at the first natural frequency of this composite system ω_1 .

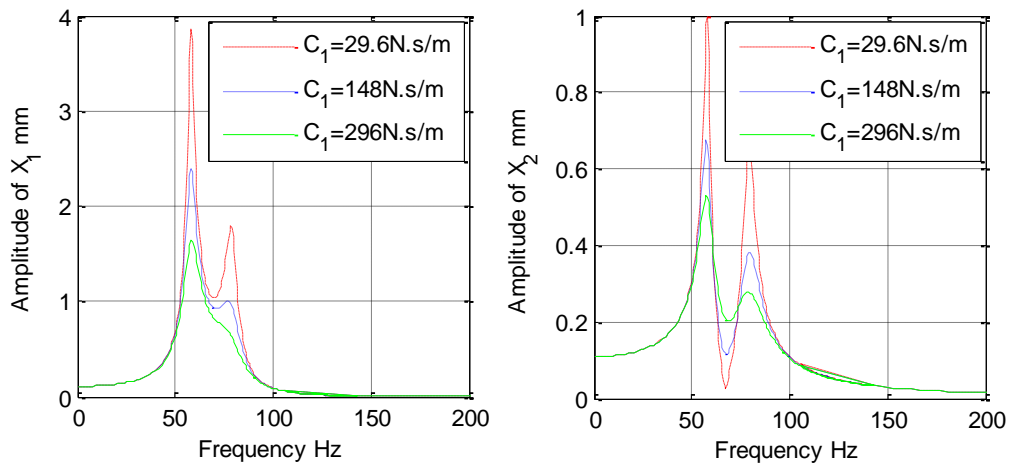


Figure 7.6 The effect of damping C_1 on the amplitude of vibration response ($F_0 = 300\text{N}$, $M_2 = 30\text{kg}$, $K_2 = 5500000\text{N/m}$ and $C_2 = 1500\text{N.s/m}$).

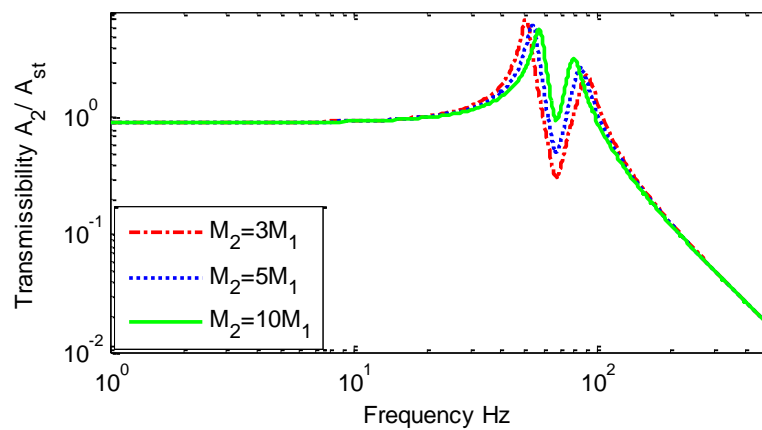


Figure 7.7 The effect of mass M_1 on the transmissibility ($F_0 = 300\text{N}$, $M_2 = 30\text{kg}$ and $K_2 = 5500000\text{N/m}$).

From Figure 7.8, we can see how the damping C_1 of absorbers influences the transmissibility of this composite system when M_2 is 30kg, K_2 is 5500000N/m and C_2 is 1500N.s/m. The two peaks of transmissibility at natural frequencies of this composite system ω_1 and ω_2 significantly decrease with the increasing damping C_1 . However, increasing the damping C_1 degrades the transmissibility at the natural frequency of the absorber ω_a , so in the range of working frequencies lowering the damping C_1 is an effective way to improve the absorption characteristic. This suggests that increasing the damping C_1 can help to reduce the transmissibility at the two natural frequencies ω_1 and ω_2 , but it is necessary to lower the damping C_1 for a better absorption performance in the range of working frequencies.

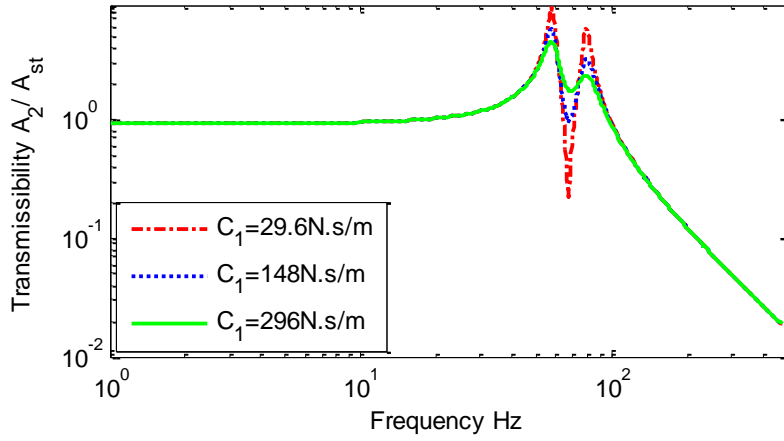


Figure 7.8 The effect of damping C_1 on the transmissibility ($F_0 = 300\text{N}$, $M_2 = 30\text{kg}$, $K_2 = 5500000\text{N/m}$ and $C_2 = 1500\text{N.S/m}$).

7.4.2 The influence of non-linearity

It is important to solve Equation (7.1) for both assessing the performance of dynamic absorbers and exploring the influence of nonlinearity on the absorption characteristics. However, the exact analytical solutions of the system response are impossible to get when the dynamical system is nonlinear. As an alternative to investigate the dynamical behaviour and vibration transmissibility direct numerical integration is employed with the fourth order Runge-Kutta method.

The vibration system turns into a linear absorption system when the nonlinear parameters $K_1' = K_1'' = K_1^* = K_1^{**} = C_1' = C_1'' = C_1^* = C_1^{**} = 0$, the MRE material turns to be a linear viscoelastic material when the parameters $K_1' = K_1'' = K_1^* = K_1^{**} = C_1 = C_1'' = C_1^* = C_1^{**} = 0$ because the storage modulus and loss modulus are linear. By comparing with a corresponding linear vibration system and a corresponding linear viscoelastic material, the influence of non-

linearity on vibration response of this absorption system is investigated, as shown in Figure 7.9. The non-linear parameters are as per Table 7.1. When M_2 is 30kg, K_2 is 5500000N/m and C_2 is 1500N.s/m we can see the MRE absorber amplifies the vibration of both the auxiliary mass M_1 and primary mass M_2 at the two natural frequencies ω_1 and ω_2 compared to linear absorbers and linear viscoelastic materials. This may cause the failure of absorbers and primary systems. From the amplitude of X_2 , it can be seen that the absorption system with corresponding linear viscoelastic material has the lowest vibration amplitude at the two natural frequencies of this composite system. The application of MRE absorbers results in an improved absorption performance in the range of working frequency as the vibration amplitude of X_2 in the primary system can be effectively reduced at frequencies in a range around the natural frequency of absorber ω_a . From the vibration of both the absorber and the primary system, it can be seen that at 91.7 Hz the vibration amplitudes of both X_1 and X_2 increase dramatically, because in this modelling of MRE absorbers the form of damping force allows negative damping to occur at frequencies higher than 91.7 Hz, which is the limitation of this mathematical modelling as illustrated in Section 5.3.2 that the equivalent damping coefficient of MRE structure dramatically decreases with frequencies. But the instability due to negative damping will never occur in reality, as the loss modulus of MRE material must be a positive value although the damping gets close to zero with increasing frequencies.

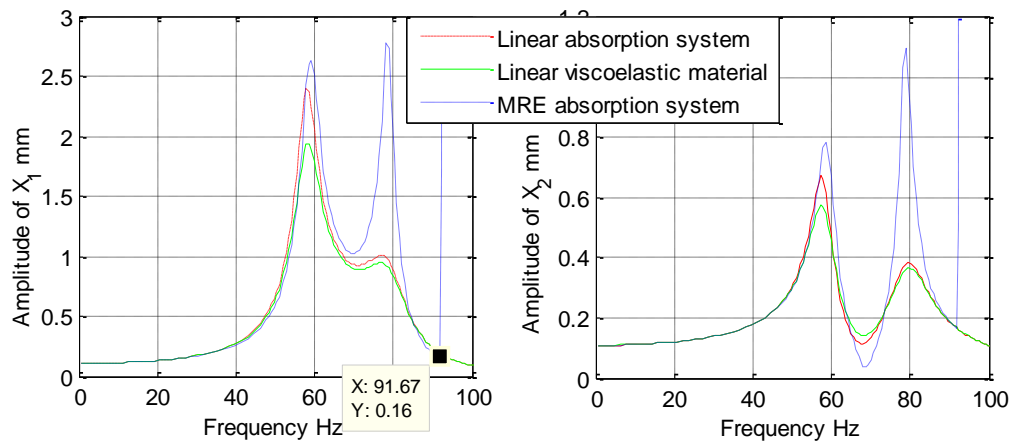


Figure 7.9 The vibration responses of different systems ($M_2 = 30\text{kg}$, $K_2 = 5500000\text{N/m}$ and $C_2 = 1500\text{N.s/m}$).

Figure 7.10 shows the performances of the MRE absorber before retuning and after retuning. In this MRE absorption system the non-linear parameters for a field-on state are chosen from Table 7.1 when magnetic intensity $B = 500\text{ mT}$, and the stiffness and damping are also designed following the relationship in Equation (7.3). From the vibration amplitude of X_2

we can see that without any application of magnetic field the natural frequency of the MRE absorber ω_a is 69 Hz, where the vibration of the primary mass M_2 can be effectively attenuated by this absorber, while a field-on state shifts the natural frequency of the MRE absorber ω_a from 69 Hz to 80 Hz. Additionally the peaks of vibration amplitude at the two natural frequencies of this composite system ω_1 and ω_2 can be obviously reduced with retuning the MRE absorber as well, which contributes to the mitigation of potential failures. From the vibration amplitude of X_1 it can be seen that retuning MRE absorber also results in a significant reduction of the vibration amplitude of the auxiliary mass M_1 at the two natural frequencies of this composite system ω_1 and ω_2 . Therefore, the potential risks of failure for both auxiliary system and primary system can be mitigated by retuning the MRE absorber, and the frequency range for vibration control which is around the natural frequency of the absorber ω_a can effectively shift by 16% with an adaptive MRE absorber, which is a potential way to broaden the frequency range for vibration control.

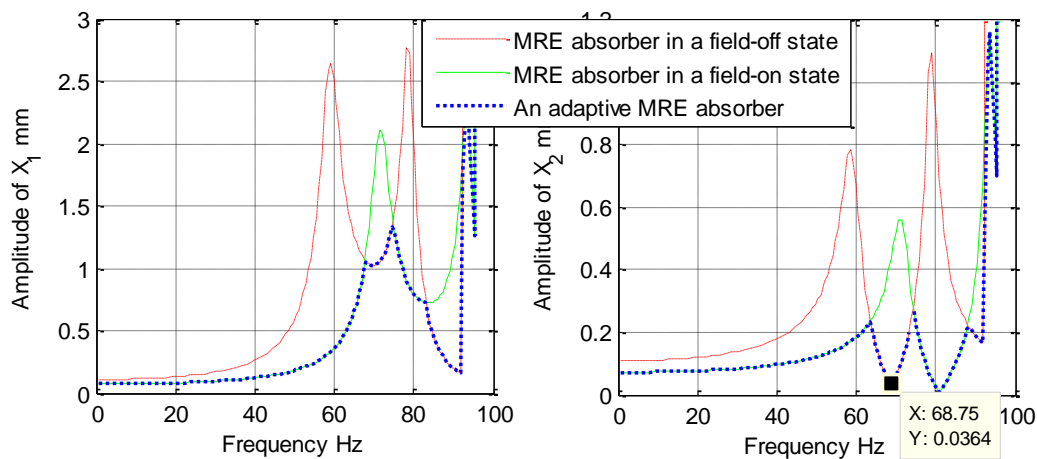


Figure 7.10 The vibration responses of MRE absorption systems ($M_2 = 30\text{kg}$, $K_2 = 5500000\text{N/m}$ and $C_2 = 1500\text{N.s/m}$).

In Figure 7.11 it is the comparison of vibration responses among a linear absorption system, a linear viscoelastic material and an adaptive MRE absorption system. From the vibration amplitude of X_2 it can be seen that the adaptive MRE absorber provides an improved performance for vibration control at working frequencies, which are around the natural frequency of the absorber ω_a , because at frequencies around ω_a the vibration amplitude of the primary mass M_2 can be reduced more with the adaptive MRE absorber than with the corresponding linear absorber and the corresponding linear viscoelastic material. Furthermore, the natural frequency ω_a can be effectively retuned with an adaptive MRE absorber, in this adaptive MRE absorption system ω_a is shifted from 69 Hz to 80 Hz through an application of

magnetic field of 500 mT. The adaptive capability enables MRE absorbers to have a broader frequency range where the vibration of primary system can be successfully absorbed. Additionally comparing with the corresponding linear absorber and the corresponding linear viscoelastic material the better absorption characteristic of adaptive MRE absorbers can reduce potential failures of the primary system. From the vibration response of X_1 , an adaptive MRE absorber can obviously reduce the first peak of vibration amplitude for the auxiliary mass M_1 and slightly increase the second peak compared with the corresponding linear absorber and the corresponding linear viscoelastic material. As the vibration amplitude at the first natural frequency of this composite system is much larger than the vibration amplitude at the second natural frequency, the potential failure of auxiliary system is more sensitive to the first peak of vibration amplitude, therefore the adaptive MRE absorber can also mitigate the risk of potential failure for auxiliary system by reducing the first peak of vibration amplitude of the auxiliary mass M_1 .

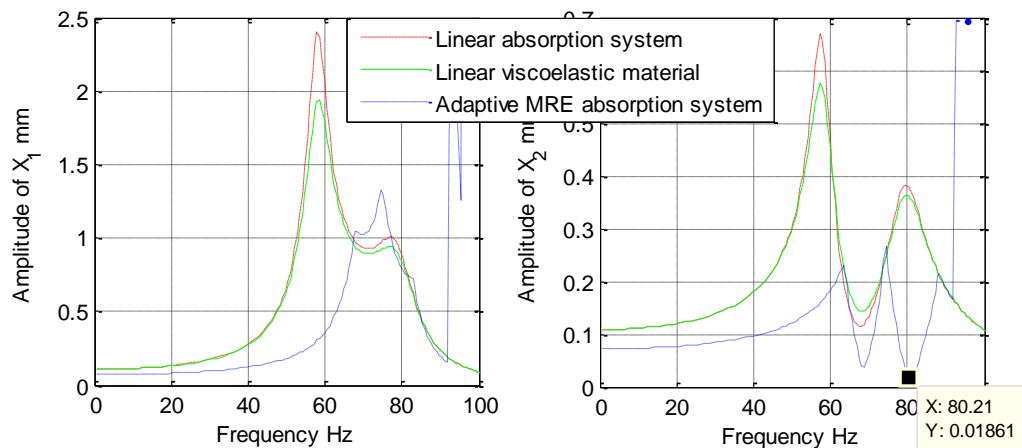


Figure 7.11 The vibration responses of different systems ($M_2 = 30\text{kg}$, $K_2 = 5500000\text{N/m}$ and $C_2 = 1500\text{N.s/m}$).

In order to evaluate the effectiveness of the MRE absorber, the transmissibility of selected systems is studied with the numerical results of Equation (7.17). From Figure 7.12, it can be seen that at frequencies around the natural frequency of the absorber ω_a the transmissibility in the MRE absorption system is lower than it is in either the corresponding linear system or the corresponding linear viscoelastic material. Thus in the frequency range for vibration control, which is around the natural frequency ω_a the MRE absorber is more effective in reducing the transmissibility than the linear absorber and the linear viscoelastic material. However, at the two natural frequencies of this composite system ω_1 and ω_2 the transmissibility is higher in the MRE absorption system than it is in either the corresponding linear system or

the corresponding linear viscoelastic material. The natural frequencies ω_a in the three systems are almost the same. It can be noted that the transmissibility of MRE absorption system increases dramatically at 91.7 Hz, thus the MRE absorption system becomes unstable at frequencies above 91.7 Hz. In the mathematical model for MRE absorber, the expression of damper force in Equation (5.9) results in negative damping coefficients at frequencies above 91.7 Hz which undermines the stability of system. Regardless of this limitation of modelling due to the testing conditions of mechanical properties characterisation for MRE, negative damping can never occur because the loss modulus of MRE material cannot be a negative value.

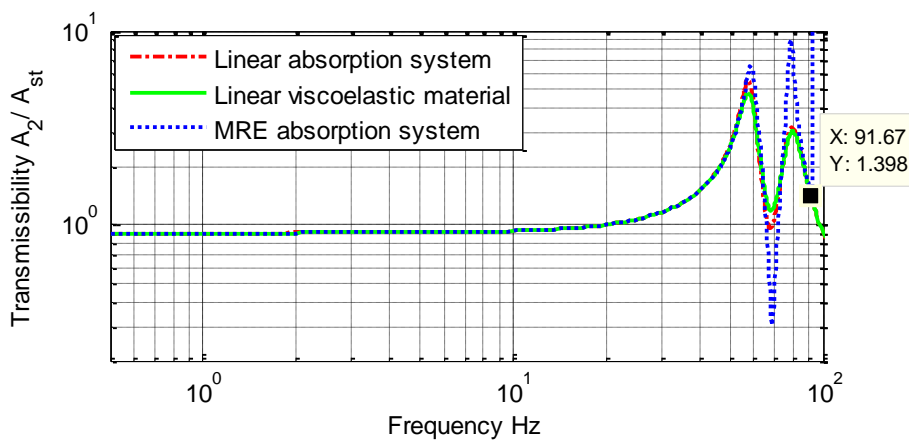


Figure 7.12 The transmissibility of different systems ($M_2 = 30\text{kg}$, $K_2 = 5500000\text{N/m}$ and $C_2 = 1500\text{N.s/m}$).

Figure 7.13 shows that with the application of a magnetic field of 500 mT the MRE absorber can shift the natural frequencies ω_a from 69 Hz to 80 Hz. In this way an adaptive MRE absorber is effective in broadening the working frequency range for vibration control by retuning the natural frequency of the absorber ω_a with a controllable magnetic field. Additionally, the peaks of transmissibility curve can also be reduced obviously with an adaptive MRE absorber, which can contribute to avoiding potential failures for primary system. Therefore, in this vibration system, the wider range of working frequency and the smaller peak value of transmissibility can be obtained as desirable absorption characteristics with an adaptive MRE absorber by controlling the applied magnetic field.

It can be seen from Figure 7.14 that an improved absorption performance at working frequencies around the natural frequency of the absorber ω_a can be obtained with an adaptive MRE absorber, since at frequencies around the natural frequency ω_a the adaptive MRE absorber can more effectively reduce the transmissibility of the system than the corresponding linear absorber or the corresponding linear viscoelastic material. Without any application of magnetic

field the natural frequency of absorbers ω_a is 69 Hz, whilst with the application of a magnetic field of 500 mT the natural frequency ω_a can be shifted by 16% through the adaptive MRE absorber. This capability of retuning the natural frequency ω_a will enable MRE absorbers to have a wider frequency range for effectively reducing the transmissibility of system. Comparing with the corresponding linear absorber or the corresponding linear viscoelastic material, the adaptive MRE absorber can also obviously reduce the two peaks of the transmissibility at the two natural frequencies of this composite system ω_1 and ω_2 , which is beneficial to mitigation of potential failure for primary system. Therefore, the adaptive MRE absorber can provide an improved performance for vibration control with a larger reduction of vibration transmissibility and a broader frequency range of effective vibration control when comparing with the corresponding linear absorber or the corresponding linear viscoelastic material.

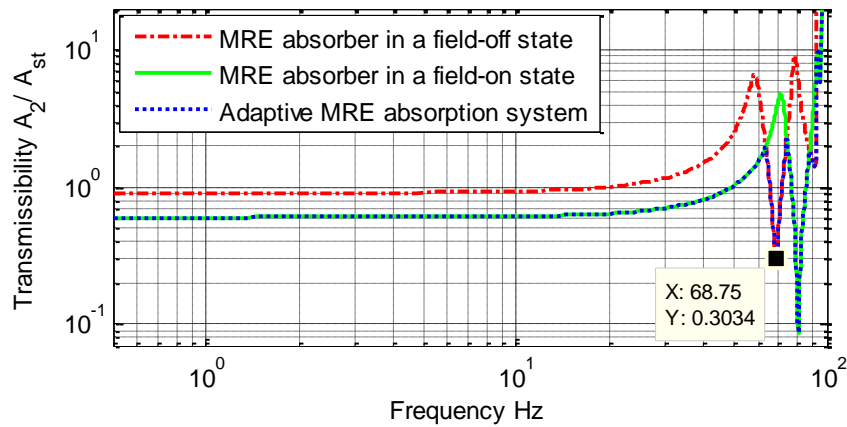


Figure 7.13 The transmissibility of MRE absorption systems ($M_2 = 30\text{kg}$, $K_2 = 5500000\text{N/m}$ and $C_2 = 1500\text{N.s/m}$).

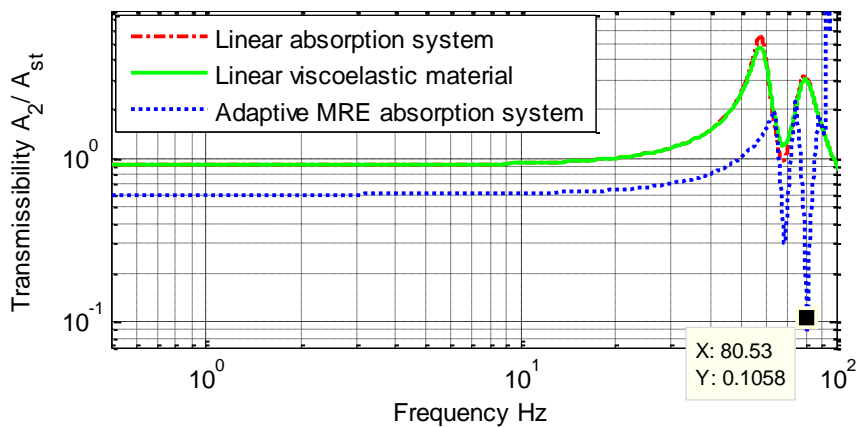


Figure 7.14 The transmissibility of different absorption systems ($M_2 = 30\text{kg}$, $K_2 = 5500000\text{N/m}$ and $C_2 = 1500\text{N.s/m}$).

7.5 Summary

A vibration system with a nonlinear absorber is selected in this chapter to investigate the use of MRE in absorption systems. At first, the equations of motion for this absorption system are presented for the dynamic analysis that enables a simulation of steady response and an assessment of stability. Then, the dynamical behaviour and absorption performance of this system is investigated with the method of direct numerical integration, and the efficiency of adaptive MRE absorbers is evaluated with comparisons of the vibration amplitudes and the transmissibility for different systems in frequency domain.

In absorption systems, the desirable characteristics are a broader frequency range for effective vibration control and smaller peaks of vibration amplitude or transmissibility. In this selected system, because of the tuning process of absorbers and the safe design of bearing capacity the auxiliary mass M_I and the stiffness K_I have to be designed under the standards expressed by Equation (7.3). As the mass of M_I and the stiffness K_I increase, the frequency range for vibration absorption can be effectively widened, which results in an improved absorption characteristic, and the vibration of absorbers can be obviously reduced, which mitigates the potential risks of failure. However, the mass M_I and the stiffness K_I cannot be increased ad infinitum considering keeping absorbers compact and saving MRE material. Increasing the damping C_I can reduce the vibration and transmissibility at the two natural frequencies ω_1 and ω_2 , which contributes to avoiding potential failures; but in the frequency range of effective absorption the vibration and transmissibility increase with the damping C_I . Therefore, it is necessary to balance a better absorption performance with better mitigation for potential failures.

Comparing with traditional absorbers or linear viscoelastic materials, both the absorption characteristic and the mitigation of failures for the system can be improved with adaptive MRE absorbers. By retuning the MRE absorber with a controllable magnetic field, the peak value of vibration amplitude or force transmissibility can be effectively reduced and the frequency range for effective absorption can be broadened.

Guidelines for designing MRE absorbers: according to the related requirement for bearing capacity, the MRE absorber are tuned to the driving frequency; considering the natural frequency of the primary system, the frequency range of effective vibration absorption can be determined to broaden to lower frequencies or higher frequencies; referring to the intersection point on curves of transmissibility in a field-off state and field-on state, the frequency for

switching magnetic field is determined for MRE absorbers; at low frequencies the isolator works in a field-off state, at high frequencies the isolator works in a field-on state.

Chapter 8 **Nonlinear MRE Isolation Systems with a Flexible Base**

8.1 Introduction

The mechanical properties of MRE can be adjusted through a controllable external magnetic field, which makes MRE very suitable as a smart spring for vibration isolations, and the adaptive isolator is another main application of MRE. Due to the dependence of mechanical properties on strain, frequency and magnetic field, a non-linear mathematical model is necessary to describe its unique dynamical behaviour. Investigations on the dynamics of MRE isolation systems are necessary for applications in vibration control. Vibration on board ships might be caused by the propeller, engine, ancillary machinery and effects of the sea. The frequency of random vibrations is between 0.01Hz in very calm seas and 1.5Hz in bad weather and the frequency of periodic vibrations is between 3Hz and 80Hz. On ships, the entire driveshaft, which is liable to respond to the excitation from the propeller or propulsion system, and thus may excite the structure of the double bottom; the entity made up of an engine and the structure of the double bottom may respond to excitations caused by the functioning of the engine and make the structure of hull vibrate.

In this chapter, the effectiveness of MRE isolators is examined in a vibration isolation system with a beam as a flexible base^[111]. Firstly, the standard form of motion equations is formulated for this isolation system to obtain the overall steady state response, and the dynamical characteristics of system are analysed with analytical expressions. This is followed by an analysis of the resulting vibratory power flow with an originally derived analytical expression. Furthermore, the vibratory energy transmission and isolation transmissibility are investigated by direct numerical integration and compared for different parameters. Finally by comparing with traditional isolators, the improved isolation characteristic of adaptive MRE isolators demonstrates the potential for vibration isolation.

8.2 Equation of motion

8.2.1 Standard form of equations of motion

Figure 8.1 illustrates schematically a dynamical interaction system comprising a machine, an isolator and a simply supported beam. During operation, it is assumed that the machine is excited by sinusoidal loadings. This study predicts the resultant motions of the beam and assesses the interactions between many components with an emphasis on the nonlinear behaviour. The uniform simply supported beam is of length L , mass density per unit length ρ and bending stiffness EI , and this beam is assumed to be symmetric (port-starboard) about the longitudinal X -axis. M denotes the mass of the machine, F_0 and Ω are the amplitude and angular frequency of the harmonic excitation, respectively.

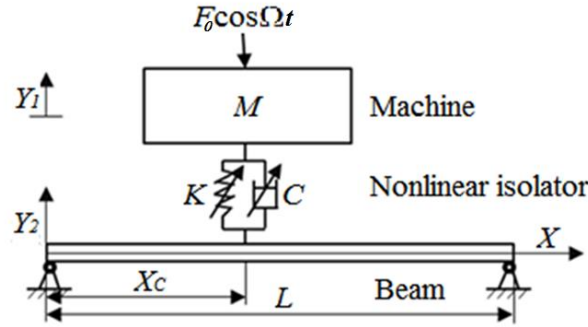


Figure 8.1 Dynamic interaction system comprising a machine, an isolator and a beam.

The governing equations describing the nonlinear interactive system are as follows:

$$\begin{aligned}
 M\ddot{Y}_1 + F(\Omega, S, \dot{S}) &= F_0 \cos \Omega t \\
 EI \frac{\partial^4 Y_2}{\partial X^4} + \rho \frac{\partial^2 Y_2}{\partial t^2} &= F(\Omega, S, \dot{S}) D(X - X_c) \\
 Y_2|_{X=0,L} &= 0, \quad \frac{\partial^2 Y_2}{\partial X^2} \Big|_{X=0,L} = 0 \\
 F(\Omega, S, \dot{S}) &= \left(C + \frac{C'}{\Omega} + C''\Omega + \frac{C^*}{\Omega} S + \frac{C^{**}}{\Omega} S^2 \right) \dot{S} + (K + K'\Omega + K''\Omega^2 + K^* S + K^{**} S^2) S \\
 S(t) &= Y_1(t) - Y_2(X_c, t)
 \end{aligned} \tag{8.1}$$

where $D()$ denotes a delta function, Y_1 and Y_2 are the absolute displacements of the mass and the beam at the point X_c , respectively. $F(\Omega, S, \dot{S})$ represents the restoring force of the MRE nonlinear isolator where S and \dot{S} are relative displacement and velocity, $K, K', K'', K^*, K^{**}, C, C', C'', C^*$ and C^{**} are introduced as parameters of stiffness and damping for this nonlinear isolator.

Here, the natural vibration of a linear uniform dry simply supported beam is examined, which is governed by the following equations

$$EI \frac{\partial^4 Y_2}{\partial X^4} + \rho \frac{\partial^2 Y_2}{\partial t^2} = 0$$

$$Y_2|_{X=0,L} = 0, \quad \frac{\partial^2 Y_2}{\partial X^2} \Big|_{X=0,L} = 0 \quad (8.2)$$

By solving the characteristic equations of the system, the natural frequencies Ω_n and the corresponding mode functions $\Phi_n(X)$ are obtained as follows:

$$\Omega_n = \frac{n^2 \pi^2}{L^2} \sqrt{\frac{EI}{\rho}} \quad n = 1, 2, \dots \quad (8.3)$$

$$\Phi_n(X) = \sin \frac{n\pi X}{L}$$

These natural modes satisfy orthogonal relations, namely

$$\int_0^L \rho \Phi_i(X) \Phi_j(X) dX = \frac{\rho L}{2} \delta_{ij} \quad i, j = 1, 2, \dots \quad (8.4)$$

$$\int_0^L EI \Phi_i''(X) \Phi_j''(X) dX = \frac{\rho L}{2} \Omega_i^2 \delta_{ij}$$

where $()'' = \partial^2()/\partial X^2$ and δ_{ij} represents the Kronecker delta. These natural mode functions $\Phi_i(X)$ ($i=1,2,\dots$) form a series of complete and orthogonal functions defined in the domain $(0,L)$. Obviously, these functions are continuous and sufficiently differentiable within the defined domain and independent of any external forces.

This beam is assumed to have no discontinuity or multi-values of the displacement at any point during its motion, so the dynamic displacement $Y_2(X,t)$ of the beam satisfying Equation (8.1) is a single-value and differentiable function of X defined in the domain $X \in (0,L)$. Therefore, the dynamic displacement $Y_2(X,t)$ of the beam can be represented using an arbitrary series of complete functions defined in the domain $X \in (0,L)$. Here the series of the mode functions $\Phi_i(X)$ are chosen^[114]. Thus

$$Y_2(X,t) = \sum_1^N \Phi_n(X) Q_n(t) \quad (8.5)$$

where $Q_n(t)$ ($n=1,2,\dots$) is a time-dependent generalised coordinate and N is the maximum number of modes adopted in the analysis to achieve a prescribed accuracy of solution.

Substituting Equation (8.5) into Equation (8.1), then pre-multiplying $\Phi_n(X)$ on both sides, integrating with respect to X from 0 to L and using the orthogonal relations driven by Equation (8.4) as well as considering the delta function $D(X-X_c)$ in the integration, we obtain

$$\ddot{Q}_n + \Omega_n^2 Q_n = F(\Omega, S, \dot{S}) \Phi_n(X_c) / M_n \quad (n=1,2,\dots). \quad (8.6)$$

Here M_n , K_n and Ω_n are generalised mass, stiffness and natural frequency, respectively.

$$\begin{aligned} M_n &= \int_0^L \rho \Phi_n^2(X_c) dX \\ K_n &= \int_0^L EI \Phi_n''^2(X_c) dX \quad n = 1, 2, \dots \\ \Omega_n &= \sqrt{K_n / M_n} \end{aligned} \quad (8.7)$$

Equation (8.6) is a set of differential equations with $N+2$ unknown variables $Q_n(t)$ ($n=1,2,\dots$) and $S(t)$ to be determined by solving Equation (8.6) and Equation (8.1).

8.2.2 Steady state response of system

The harmonic balance method is an effective numerical tool to study nonlinear dynamical problems in the frequency domain. The general idea of this method is to represent each time history by its frequency content and then a set of equations can be obtained by balancing the terms with the same frequency components to find the solutions of these equations through an iterative procedure. Considering it is difficult to know the frequency components in vibration systems in reality, calculating sufficient orders for approximate solutions is necessary for obtaining precise solutions with the harmonic balance method. In this thesis, the relative displacement $S(t)$, the generalised coordinates $Q_n(t)$ and the nonlinear coupling force $F(\Omega, S, \dot{S})$ are represented as Fourier expansions to the first order as a first approximation in the harmonic balance method. Herein it is assumed that the first approximation is adequate for weak nonlinear systems, and the approximation belonging to higher orders are very small and can be neglected compared with the first approximation. Without loss of generality, we can arbitrarily choose $S = 0$ as a reference position in the Fourier expansion of the relative displacement S , namely

$$\begin{aligned} S(t) &= \Delta_1 \cos(\Omega t + \varphi) \\ Q_n(t) &= Q_{n0} + Q_{n1} \cos \Omega t + Q_{n2} \sin \Omega t \\ F(t) &= R_0 + R_1 \cos(\Omega t + \varphi) + R_2 \sin(\Omega t + \varphi) \end{aligned} \quad (8.8)$$

where φ is a phase angle, Δ_1 , Q_{n0} , Q_{n1} and Q_{n2} are coefficients of amplitudes to be determined. It is not necessary to include phase angle φ in Equation (8.8), but it is a convenient parameter for the derivation of the power flow absorption later on. R_0 , R_1 and R_2 are the Fourier coefficients defined by

$$\begin{aligned} R_0 &= \frac{1}{2\pi} \int_{-\pi}^{\pi} F(\theta) d\theta \\ R_1 &= \frac{1}{\pi} \int_{-\pi}^{\pi} F(\theta) \cos \theta d\theta \\ R_2 &= \frac{1}{\pi} \int_{-\pi}^{\pi} F(\theta) \sin \theta d\theta \end{aligned} \quad (8.9)$$

where $\theta = \Omega t + \varphi$. Substituting Equation (8.8) into Equations (8.1) and (8.9) and omitting the lengthy derivation of the integration, we find that the detailed expressions for R_0 , R_1 and R_2 are given by

$$\begin{aligned} R_0 &= \frac{K^* \Delta_1^2}{2} + \frac{4K^{**} \Delta_1^3}{3\pi} \\ R_1 &= K \Delta_1 + K' \Omega \Delta_1 + K'' \Omega^2 \Delta_1 + \frac{8}{3\pi} K^* \Delta_1^2 + \frac{3}{4} K^{**} \Delta_1^3 \\ R_2 &= -C \Omega \Delta_1 - C' \Delta_1 - C'' \Omega^2 \Delta_1 - \frac{1}{4} C^{**} \Delta_1^3 \end{aligned} \quad (8.10)$$

The substitution of Equation (8.10) into Equation (8.1) and Equation (8.6) gives

$$\begin{aligned} & -M \Omega^2 \Delta_1 \cos \theta + R_0 + R_1 \cos \theta + R_2 \sin \theta \\ & = F_0 \cos \Omega t - M \sum_1^N \Phi_n(X_C) \ddot{Q}_n(t) \end{aligned} \quad (8.11)$$

which when combined with Equation (8.8) and (8.10) yield

$$\begin{aligned} (R_1 - M \Omega^2 \Delta_1) \cos \varphi + R_2 \sin \varphi &= F_0 + M \Omega^2 \sum_1^N \Phi_n(X_C) Q_{n1} \\ (R_1 - M \Omega^2 \Delta_1) \sin \varphi - R_2 \cos \varphi &= -M \Omega^2 \sum_1^N \Phi_n(X_C) Q_{n2} \end{aligned} \quad (8.12)$$

The coefficients of the same harmonics (i.e. $\sin \Omega t$, $\cos \Omega t$) and constant terms in Equation (8.6) are equated, resulting in

$$\begin{aligned}
Q_{n0} &= \frac{\Phi_n(X_C)R_0}{M_n\Omega_n^2} = \frac{\Phi_n(X_C)}{M_n\Omega_n^2} \left(\frac{K_3\Delta_1^2}{2} + \frac{4K_4\Delta_1^3}{3\pi} \right) \\
(\Omega_n^2 - \Omega^2)Q_{n1} - R_1\Phi_n(X_C)\cos\varphi - R_2\Phi_n(X_C)\sin\varphi &= 0 \\
(\Omega_n^2 - \Omega^2)Q_{n2} + R_1\Phi_n(X_C)\sin\varphi - R_2\Phi_n(X_C)\cos\varphi &= 0
\end{aligned} \tag{8.13}$$

To solve the coupled nonlinear algebraic equations, we express Equations (8.12) and (8.13) in the matrix form, namely

$$\begin{aligned}
M \sum_{n=0}^N \Phi_n(X_C) \mathbf{Q}_n + \mathbf{G} \mathbf{Y} &= \mathbf{F}_n \quad (n=1,2,\dots,N) \\
\mathbf{A}_n \mathbf{Q}_n + \mathbf{B}_n \mathbf{Y} &= \mathbf{0} \quad (n=1,2,\dots,N)
\end{aligned} \tag{8.14}$$

where

$$\begin{aligned}
\mathbf{A}_n &= \begin{bmatrix} \Omega_n^2 - \Omega^2 & 0 \\ 0 & \Omega_n^2 - \Omega^2 \end{bmatrix} \quad \mathbf{B}_n = \begin{bmatrix} -R_1\Phi_n(X_C) & -R_2\Phi_n(X_C) \\ -R_2\Phi_n(X_C) & R_1\Phi_n(X_C) \end{bmatrix} \\
\mathbf{G} &= \begin{bmatrix} M\Omega^2\Delta_1 - R_1 & -R_2 \\ -R_2 & R_1 - M\Omega^2\Delta_1 \end{bmatrix} \\
\mathbf{Q}_n &= \begin{Bmatrix} Q_{n1} \\ Q_{n2} \end{Bmatrix} \quad \mathbf{F}_n = \begin{Bmatrix} -F_0 \\ 0 \end{Bmatrix} \quad \mathbf{Y} = \begin{Bmatrix} \cos\varphi \\ \sin\varphi \end{Bmatrix}
\end{aligned} \tag{8.15}$$

To aid calculation, Equation (8.15) is written as

$$\begin{aligned}
\mathbf{A}_n &= (\Omega_n^2 - \Omega^2) \mathbf{I}_0 \\
\mathbf{B}_n &= R_1\Phi_n(X_C) \mathbf{I}_1 - R_2\Phi_n(X_C) \mathbf{I}_2 \\
\mathbf{G} &= (R_1 - M\Omega^2\Delta_1) \mathbf{I}_1 - R_2 \mathbf{I}_2
\end{aligned} \tag{8.16}$$

where the matrices \mathbf{I}_0 , \mathbf{I}_1 and \mathbf{I}_2 are given by

$$\mathbf{I}_0 = \begin{bmatrix} 1 & 0 \\ 0 & 1 \end{bmatrix} \quad \mathbf{I}_1 = \begin{bmatrix} -1 & 0 \\ 0 & 1 \end{bmatrix} \quad \mathbf{I}_2 = \begin{bmatrix} 0 & 1 \\ 1 & 0 \end{bmatrix} \tag{8.17}$$

The set of Equations (8.14) is of nonlinear form and the exact analytical solutions are impossible to obtain. Many numerical methods can be used as alternatives to solve such nonlinear system problems, e.g. a Newton–Raphson iteration process. This method is adopted to solve the resulting nonlinear equations by combining the two coupled nonlinear Equations (8.14).

$$\mathbf{F}(\Delta_1, \Omega)\mathbf{Y} = \mathbf{F}_n, \quad (8.18)$$

where

$$\mathbf{F}(\Delta_1, \Omega) = \mathbf{G} - M \sum_{n=1}^N \Phi_n(X_C) \mathbf{A}_n^{-1} \mathbf{B}_n. \quad (8.19)$$

Equation (8.18) is a nonlinear vector equation where the vector $\mathbf{F}(\Delta_1, \Omega)$ depends nonlinearly on the displacement Δ_1 and requires solving iteratively. The solution at each excitation frequency Ω is determined using the Newton–Raphson iteration method.

8.3 Efficiency analysis of vibration isolation system

8.3.1 Analysis of isolation characteristics

The effectiveness of an isolator can be assessed by examining the transmissibility of the vibrating system. Transmissibility is defined as the ratio of the force transmitted to the foundation to the applied force in the direction of the applied loads. In order to investigate the isolation transmissibility of the vibration system, the transmitted force $F(t)$ can be expressed as Equation (8.20) following Equation (8.8),

$$F(t) = \left(\frac{K^* \Delta_1^2}{2} + \frac{4K^{**} \Delta_1^3}{3\pi} \right) + \left(-C\Omega\Delta_1 - C'\Delta_1 - C''\Omega^2\Delta_1 - \frac{1}{4}C^{**}\Delta_1^3 \right) \sin \theta \\ + \left(K\Delta_1 + K'\Omega\Delta_1 + K''\Omega^2\Delta_1 + \frac{8}{3\pi}K^*\Delta_1^2 + \frac{3}{4}K^{**}\Delta_1^3 \right) \cos \theta \quad (8.20)$$

Then the transmissibility of isolation system can be defined as the magnitude of the force ratio, which can be expressed as

$$Tr = \left\| \sqrt{R_1^2 + R_2^2} / F_0 \right\|. \quad (8.21)$$

From this expression, it is obvious that a decrease in transmissibility leads to a reduction in the vibration transmitted to the beam. In order to obtain the best isolation performance, the analysis focusses on how to reduce the vibration transmissibility.

8.3.2 Power flow analysis

By accounting for both force and motion characteristics, the vibratory power flow can describe the dynamical behaviour of vibration systems well and also serve as a cost function for

evaluating the efficiency of vibration control^[115,116]. Various power flow analysis methods have been successfully developed to model complex vibration systems and to predict power generation, dissipation and transmission. Once the nonlinear dynamic displacement variables are obtained the associated vibratory power flow can be calculated from the inner product of the force and the corresponding velocity response^[117].

The instantaneous input power P_{in} is defined by the cyclic force $F_0 \cos \Omega t$ and the velocity response $\dot{Y}_1(t)$ of the machine.

$$P_{in} = F_0 \cos \Omega t \cdot \dot{Y}_1(t). \quad (8.22)$$

The time-averaged input power $\langle P_{in} \rangle$ is defined by

$$\langle P_{in} \rangle = \frac{1}{T} \int_0^T F_0 \cos \Omega t \cdot \dot{Y}_1(t) dt \quad (8.23)$$

where $T = 2\pi/\Omega$.

Aiming at characterisation of vibratory energy transmission from the machine to the ship, the instantaneous transmitted power P_{out} is calculated from the inner product of the transmitted force $F(S, \dot{S})$ and the velocity response $\dot{Y}_2(t)$ of the flexible base

$$P_{out} = F(S, \dot{S}) \cdot \dot{Y}_2(X_C, t). \quad (8.24)$$

The time-averaged transmitted power $\langle P_{out} \rangle$ transmitted through the mounting to the ship is calculated by

$$\langle P_{out} \rangle = \frac{1}{T} \int_0^T P_{out} dt. \quad (8.25)$$

The power flow isolation can be used to assess the effectiveness of power flow control, which is intended for isolating vibratory energy or minimising its transmission to foundation through an isolation system. By using the power generation and transmission equations described previously, the instantaneous power P_{iso} dissipated by the nonlinear isolator can be derived from the product of the transmitted force $F(S, \dot{S})$ and the relative velocity response $\dot{S}(t)$

$$P_{iso} = \dot{S}(t) \cdot F(S, \dot{S}). \quad (8.26)$$

The time-averaged dissipated power $\langle P_{iso} \rangle$ can be expressed as

$$\langle P_{iso} \rangle = \frac{1}{T} \int_0^T P_d dt \quad (8.27)$$

where $\dot{S}(t) = -\Omega\Delta_1 \sin(\Omega t + \varphi)$.

8.4 Numerical results and discussions

8.4.1 The influence of linear parameters

The effectiveness of isolation can be guaranteed by ensuring that the excitation frequency is well above $\sqrt{2}\omega_0$, where $\omega_0 = \sqrt{K/M}$ is the natural frequency of the isolator. Both lower resonance frequency and smaller vibration transmission are desirable characteristics for isolation. In order to investigate the dynamical behaviour and isolation efficiency for this interactive isolation system as illustrated in Figure 8.1, numerical simulations are undertaken with the system parameters as follows: the beam: $L = 20$ m, $\rho = 200$ kg/m; the machine: $M = 60$ kg; mounting position: $X_C = 5$ m; exiting force: $F_0 = 600$ N. And it is assumed that the first three elastic modes of the beam are covering the frequency bandwidth of interest. The time-averaged power flow for different isolation systems are calculated in the frequency domain to investigate the effects of elastic supporting structure.

The parameters of stiffness and damping in MRE isolators can be designed as per the discussion in Section 5.3, by combining the geometrical design of structure and the dynamical properties of material. It is obvious a lower stiffness of the isolator may lead to a better isolation characteristic, but considering guaranteeing load capacities and saving MRE materials, the stiffness of isolators cannot be lowered ad infinitum. The static load capacity of this MRE isolator is designed by a shear strain limitation of 2% for the safe dynamic design. The equivalent stiffness and damping can be calculated according to Equation (5.9) with the experimental results of mechanical properties characterisation for MRE in Figure 6.2 and Figure 6.3. The parameters of designed stiffness and designed damping are listed in Table 8.1.

Numerical simulations are carried out to investigate the dynamical behaviour of the system excited by a sinusoidal force. According to the equations of motion in Equation (8.1), a group of parameters is selected for the observation of steady response. When the nonlinear parameters $K' = K'' = K^* = K^{**} = C' = C'' = C^* = C^{**} = 0$, the vibration isolation system is linear. It can be seen from Figure 8.2 that the response of the system with elastic base is not simple harmonic and it is necessary to identify the frequency components.

Table 8.1 Parameters of designed stiffness and damping.

$K (B = 0)$ N/m	$K' (B = 0)$ N·s/m	$K'' (B = 0)$ N·s ² /m	$K^* (B = 0)$ N/m ²	$K^{**} (B = 0)$ N/m ³
5361880	4525.24	-9.51144	-49334600	442726000
$K (B = 0.5T)$ N/m	$K' (B = 0.5T)$ N·s/m	$K'' (B = 0.5T)$ N·s ² /m	$K^* (B = 0.5T)$ N/m ²	$K^{**} (B = 0.5T)$ N/m ³
8263100	6057.92	-13.9561	-105957000	876436000
$C (B = 0)$ N·s/m	$C' (B = 0)$ N·s ² /m	$C'' (B = 0)$ N·s ³ /m	$C^* (B = 0)$ N·s/m ²	$C^{**} (B = 0)$ N·s/m ³
1480.56	816124	-6.78886	-9517540	61974800
$C (B = 0.5T)$ N·s/m	$C' (B = 0.5T)$ N·s ² /m	$C'' (B = 0.5T)$ N·s ³ /m	$C^* (B = 0.5T)$ N·s/m ²	$C^{**} (B = 0.5T)$ N·s/m ³
1595.01	1327690	-7.93402	-19189100	130014000

The Fourier transform is employed to analyse the frequency components in frequency domain, as shown in Figure 8.3, it is obvious when L is 20 m, ρ is 200 kg/m, M is 60 kg and X_C is 5 m, the vibration response of system with an elastic base has more than one peak in the spectrum, namely at 22Hz and 25Hz, respectively. In this system, when a natural frequency of the beam is 22 Hz, we can see from Figure 8.3 that the corresponding elastic mode of the beam is active at 25 Hz which is in the neighbourhood of the natural frequency 22 Hz.

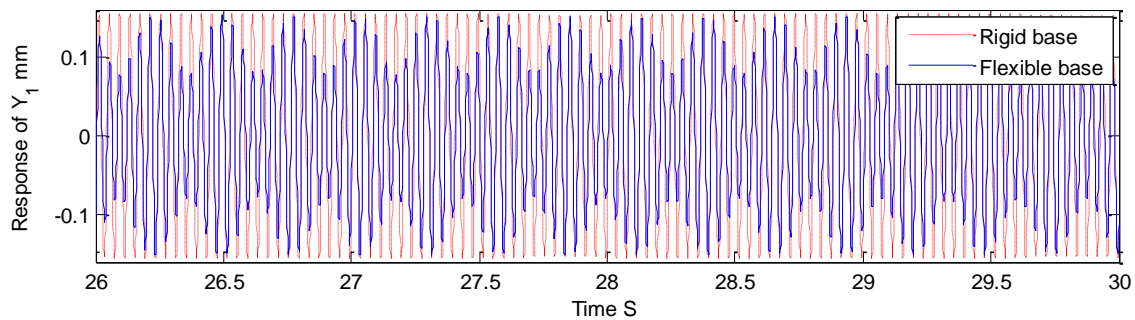


Figure 8.2 Response of different systems ($F_0 = 600$ N, $EI = 6 \times 10^9$ Nm² and $\Omega = 25$ Hz).

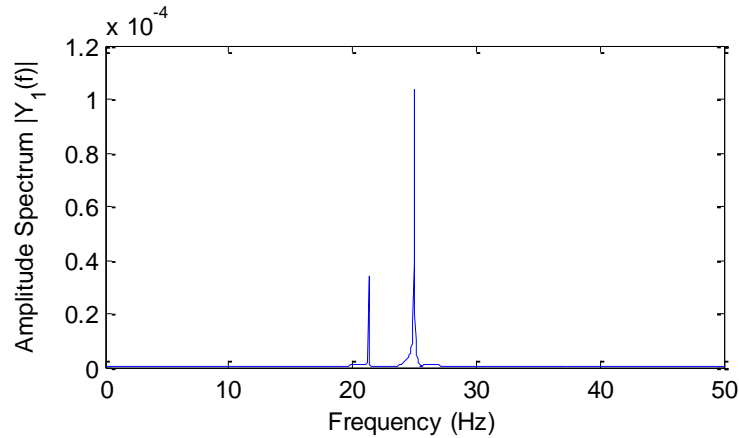


Figure 8.3 Amplitude Spectrum of $Y_1(t)$ ($F_0 = 600$ N, $EI = 6 \times 10^9$ Nm² and $\Omega = 25$ Hz).

Figure 8.4 (a) and (b) show the effects of the base on the vibration response in the presented system by comparing a rigid base with a flexible base within this isolation system and illustrating the influence of the bending stiffness EI of this beam on the amplitude of vibration response. The numerical results reveal that comparing with the rigid base the isolation system mounted on the beam has a more complex dynamical behaviour. As shown in Figure 8.4 (a), there are four peaks on the curve of amplitude of Y_2 at the frequencies $\omega = \omega_0, \omega_1, \omega_2, \omega_3$. These peaks correspond to the rigid mode at frequency ω_0 and three elastic modes at frequencies $\omega_1, \omega_2, \omega_3$ respectively. Therefore, it is important to consider the elastic effect in designing an effective isolation system. As the bending stiffness EI increases in the isolation system with a flexible base, the three natural frequencies $\omega_1, \omega_2, \omega_3$ shift to the right and the peaks of vibration amplitude at natural frequencies $\omega_1, \omega_2, \omega_3$ decline dramatically. It can be seen in Figure 8.4 (b), for the system with a rigid base the curve of vibration amplitude of Y_1 is unimodal, while for the system with a flexible base there are more than one peaks on the curve because of the elastic modes. When the natural frequencies of the elastic modes are lower than the frequency of the rigid mode, the peaks at natural frequencies will be noticeable. For example, in Figure 8.4 (a) when EI is 6×10^9 Nm² or EI is 2.4×10^{10} Nm² the first natural frequency ω_1 is lower than ω_0 and the curve of vibration amplitude of Y_1 has two obvious peaks, which is another evidence indicating the importance of considering the elastic effect in designing an effective isolation system especially when the base is comparatively soft.

In Figure 8.5 we can see the influences of the base on the transmissibility of this isolation system. It can be observed from the numerical results that in the isolation system with a flexible base there might be more than one peak on the curve of transmissibility due to the corresponding elastic modes, especially when the corresponding natural frequencies are lower

than the frequency of the rigid mode. As shown in Figure 8.5 the first natural frequency ω_1 of the elastic mode is lower than ω_0 , when EI is $6 \times 10^9 \text{ Nm}^2$ and EI is $2.4 \times 10^{10} \text{ Nm}^2$ and there are three and two peaks respectively on the curve of transmissibility. In the comparison with the main peak at ω_0 , the other peaks corresponding to higher natural frequencies can be neglected. In the isolation system it can be also seen that with a flexible base the increasing bending stiffness EI can effectively shift the three natural frequencies $\omega_1, \omega_2, \omega_3$ to the right.

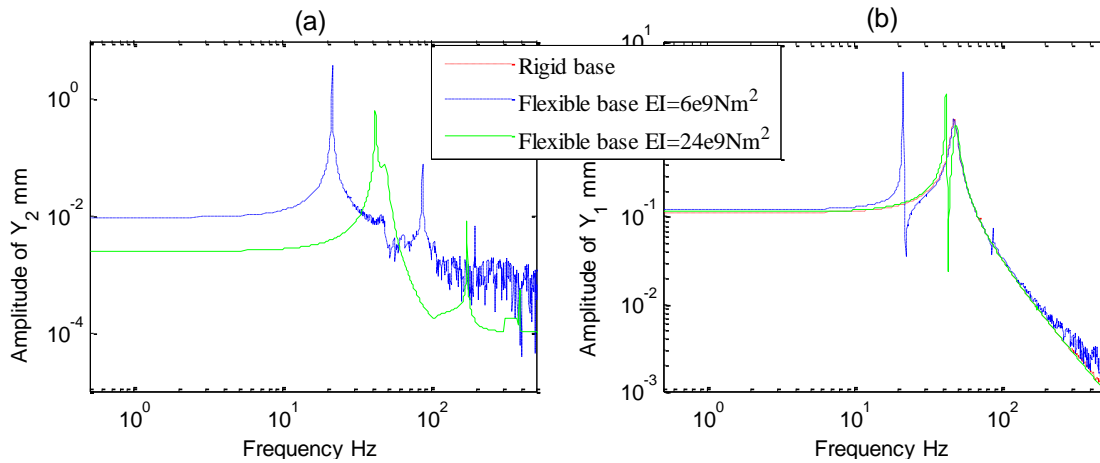


Figure 8.4 (a) The influence of base on the vibration amplitude of Y_2 and (b) the vibration amplitude of Y_1 ($L = 20 \text{ m}$, $\rho = 4 \times 10^3 \text{ kg/m}$, $M = 60 \text{ kg}$ and $F_0 = 600 \text{ N}$).

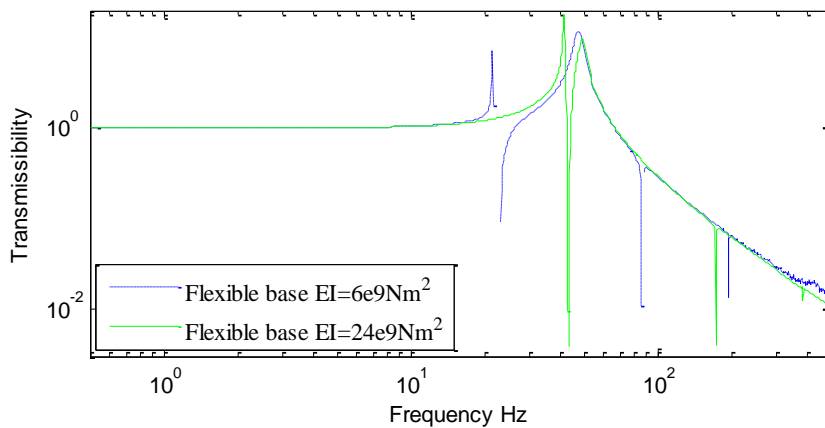


Figure 8.5 The influence of base on the transmissibility ($L = 20 \text{ m}$, $\rho = 4 \times 10^3 \text{ kg/m}$, $M = 60 \text{ kg}$ and $F_0 = 600 \text{ N}$).

The influences of the base on the input vibratory power and the vibratory power transmission are also discussed to assess the isolation performance. From the numerical results in Figure 8.6 it can be seen that in the isolation system with a rigid base the curve of input power is unimodal, whilst in the system with a flexible base the curve of input power $\langle P_{in} \rangle$

might own more than one peak, because of the peaks corresponding to the elastic modes, especially when the corresponding natural frequencies are lower than the frequency of the rigid mode. In addition, in the isolation system with a flexible base the three natural frequencies ω_1 , ω_2 , ω_3 shift to the right with the increasing bending stiffness EI . In Figure 8.6 when EI is $6 \times 10^9 \text{ Nm}^2$ and EI is $2.4 \times 10^{10} \text{ Nm}^2$ the first natural frequency ω_1 of the elastic mode is lower than ω_0 , and there are three and two obvious peaks respectively on the curve of input power, while the other peaks corresponding to natural frequencies higher than the frequency ω_0 of the rigid mode can be neglected compared with the main peak at ω_0 .

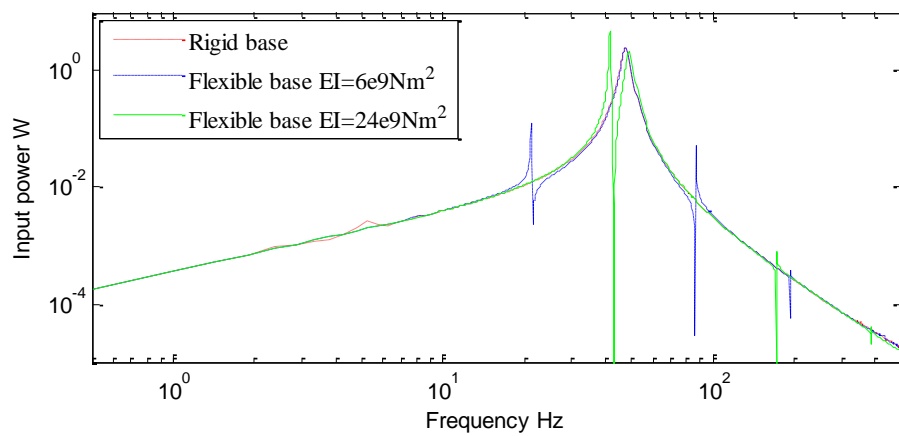


Figure 8.6 The influence of base on the input power ($L = 20 \text{ m}$, $\rho = 4 \times 10^3 \text{ kg/m}$, $M = 60 \text{ kg}$ and $F_0 = 600 \text{ N}$).

In Figure 8.7 the transmitted power $\langle P_{out} \rangle$ increases dramatically at the natural frequencies of elastic modes. The three natural frequencies ω_1 , ω_2 , ω_3 increase with the bending stiffness EI and the peaks of transmitted power decrease with bending stiffness EI . Therefore, it can be concluded that the simplified rigid model underestimates the vibration response and power at frequencies around ω_1 , ω_2 , ω_3 , especially when the base is comparatively soft. Increasing the bending stiffness EI thus the elastic natural frequencies is beneficial in reducing vibration transmission from the mounted machine to the base.

Figure 8.8 displays the influence of base on the isolated vibratory power, which has trends similar to that of transmissibility in Figure 8.5. With a rigid base the curve of isolated power $\langle P_{iso} \rangle$ is unimodal and with a flexible base there might be more than one peak on the curve of isolated power. Especially when the natural frequencies of elastic modes are lower than the frequency of the rigid mode, the corresponding peaks become obvious compared with the

main peak at ω_0 . When the natural frequencies of elastic modes are well higher than the frequency ω_0 of the rigid mode, the corresponding peaks can be neglected.

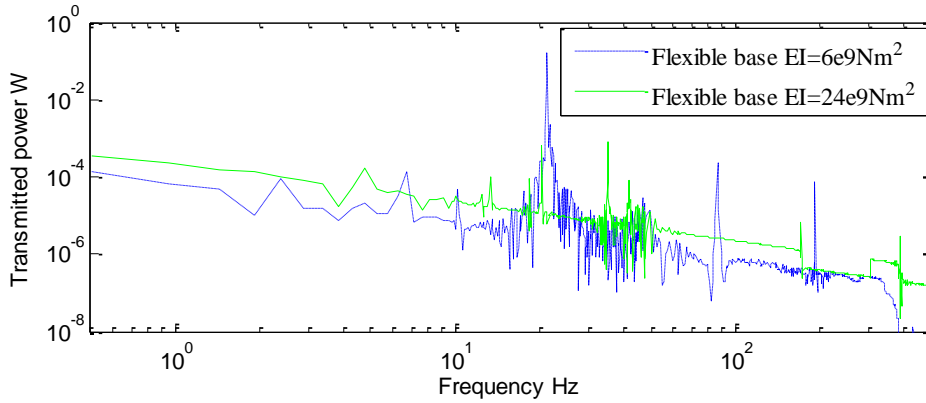


Figure 8.7 The influence of base on the power transmission ($L = 20$ m, $\rho = 4 \times 10^3$ kg/m, $M = 60$ kg and $F_0 = 600$ N).

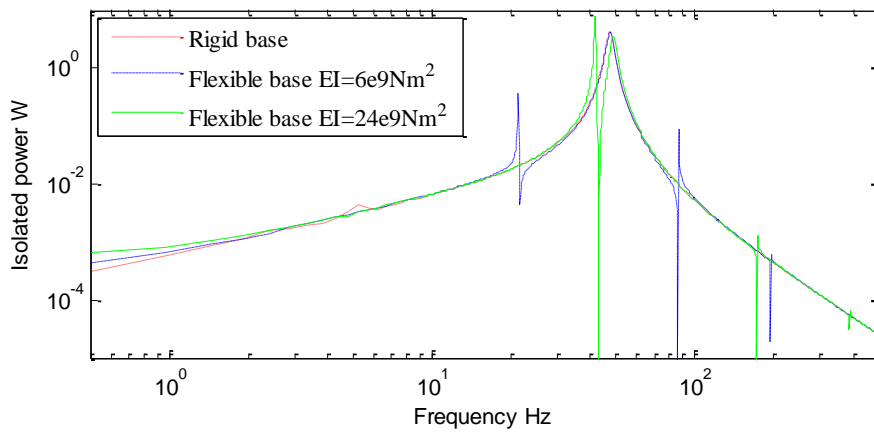


Figure 8.8 The influence of base on the isolated vibratory power ($L = 20$ m, $M = 60$ kg, $F_0 = 600$ N and $\rho = 4 \times 10^3$ kg/m).

The vibration responses of Y_1 and Y_2 around the natural frequencies of elastic modes can be used to investigate the influence of base flexibility on the dynamical behaviour. As shown in Figure 8.9, when L is 20 m, ρ is 200 kg/m, M is 60 kg and X_C is 5 m, the first elastic mode is at $\omega_1 = 22$ Hz if the bending stiffness EI is 6×10^9 Nm². The vibration transmission can be better understood through comparison at frequencies around the first elastic mode. It can be seen in Figure 8.9 (a) and (b) that the dynamical response of Y_1 at 20 Hz is greater than it is at 23 Hz, while at 20 Hz the vibration amplitude of Y_1 is 0.33 mm and it is 0.12 mm at 23 Hz. In Figure 8.9 (c) we can see that at 20 Hz the vibration amplitude of Y_2 is 0.13 mm which is lower than it is at 23 Hz where the amplitude is 0.20 mm. Therefore, at frequencies in the vicinity of

the elastic modes the vibration transmitted to the base increases, as illustrated in Figure 8.3 that the elastic mode of this beam wakes up within the neighbourhood of corresponding natural frequency. This is also in agreement with the discussion of power transmission in Figure 8.7, where the transmitted power obviously increases around the natural frequencies of the simply-supported beam.

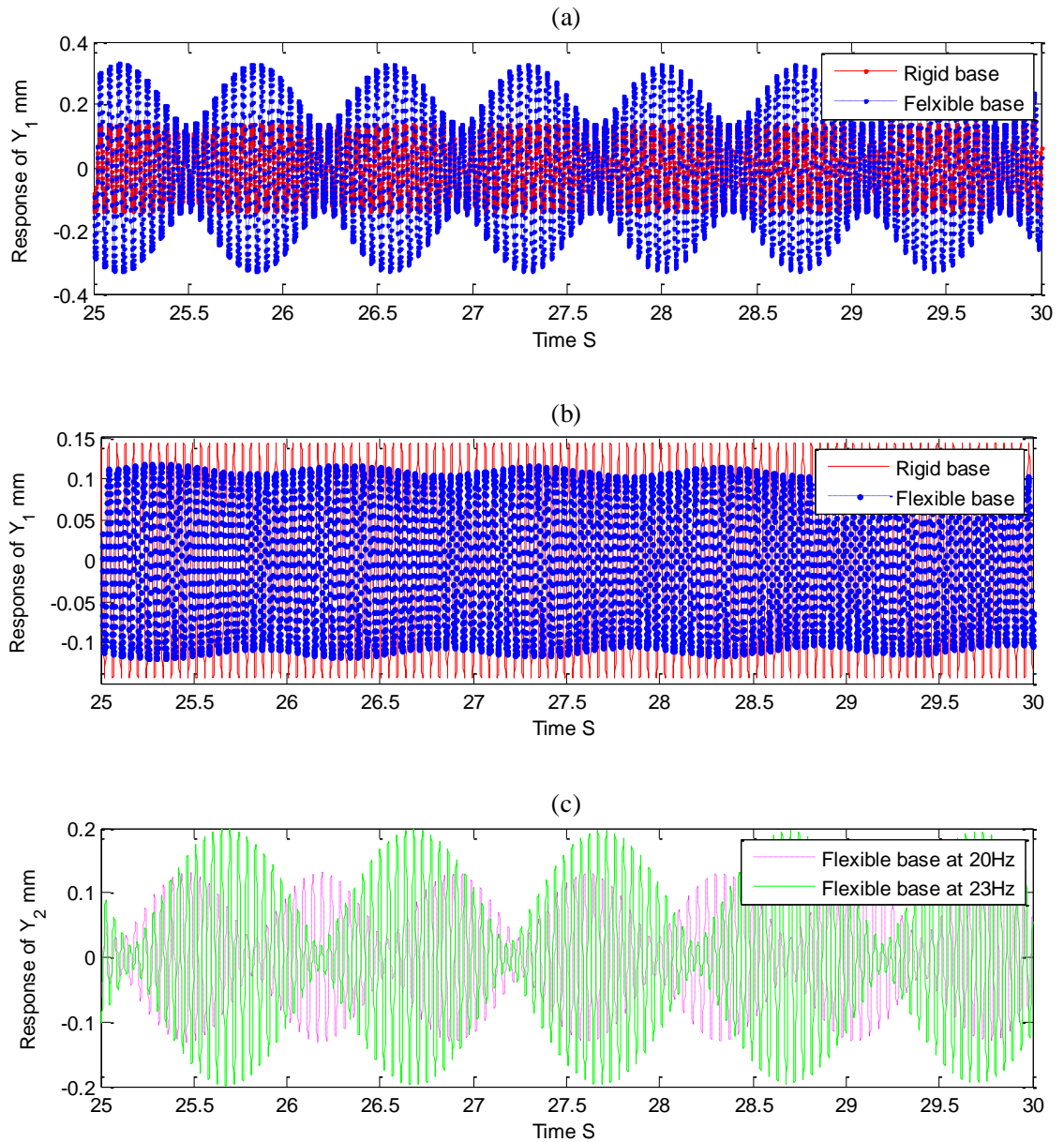


Figure 8.9 Response of Y_1 in different systems (a) at 20 Hz and (b) at 23 Hz, (c) response of Y_2 at different frequencies ($L = 20$ m, $\rho = 4 \times 10^3$ kg/m, $M = 60$ kg and $F_0 = 600$ N).

8.4.2 The influence of non-linearity

Solving Equation (8.1) for the isolation system can be used to investigate the influence of nonlinearities on the performance of vibration control. But when the dynamical system is nonlinear, the exact analytical solutions of vibration responses are impossible to get. The direct numerical integration can be employed as an alternative to investigate the dynamical behaviour and isolation performance with the fourth order Runge-Kutta method.

When the nonlinear parameters $K' = K'' = K^* = K^{**} = C' = C'' = C^* = C^{**} = 0$, the vibration system turns into a linear isolation system; while the parameters $K' = K'' = K^* = K^{**} = C = C'' = C^* = C^{**} = 0$ the MRE material turns to be a linear viscoelastic material because both the storage modulus and loss modulus are linear. L is 20 m, ρ is 4×10^3 kg/m, M is 60 kg, EI is 6×10^9 Nm² and F_0 is 600 N. In Figure 8.10 we can see the comparison of vibration responses among various systems. The natural frequency ω_0 of MRE isolators is a bit higher than that of either corresponding linear isolators or systems with corresponding linear viscoelastic materials. The amplitude of Y_1 in MRE isolation systems is slightly lower than that in the two corresponding linear systems. Whilst in MRE isolation systems the peak of vibration amplitudes at ω_0 is lower than that in corresponding linear isolation systems, but is not lower than that in systems with corresponding linear materials. It can be also noted that at 74 Hz the vibration responses of both Y_1 and Y_2 increase dramatically, which reflects the limitation of mathematical modelling illustrated in Section 5.3.2. Because in this modelling of MRE isolators the form of damping force allows negative damping to occur at frequencies higher than 74 Hz, but the instability due to negative damping will never occur in reality, as the loss modulus of MRE material must be a positive value although the damping becomes close to zero with increasing frequencies.

All the parameters of stiffness and damping for MRE isolation system in a field-on state are from Table 8.1 when the magnetic flux density $B = 0.5$ T. As shown in Figure 8.11 (a) there is an overall decline in the amplitude of Y_1 with the application of magnetic field, whilst the natural frequency ω_0 of isolators shifts to the right. Furthermore the peak of vibration amplitude can be effectively reduced with an adaptive MRE isolator, the switch-point at 54 Hz is determined by the intersection of curves of vibration amplitude in a field-off state and in a field-on state. At lower frequencies the MRE isolator works in a field-on state because a higher stiffness helps to reduce the resultant vibration, and at higher frequencies the isolator works in a field-off state as a lower stiffness can improve the isolation performance. In Figure 8.11 (b) there is no obvious difference of the vibration amplitude among the three isolation systems.

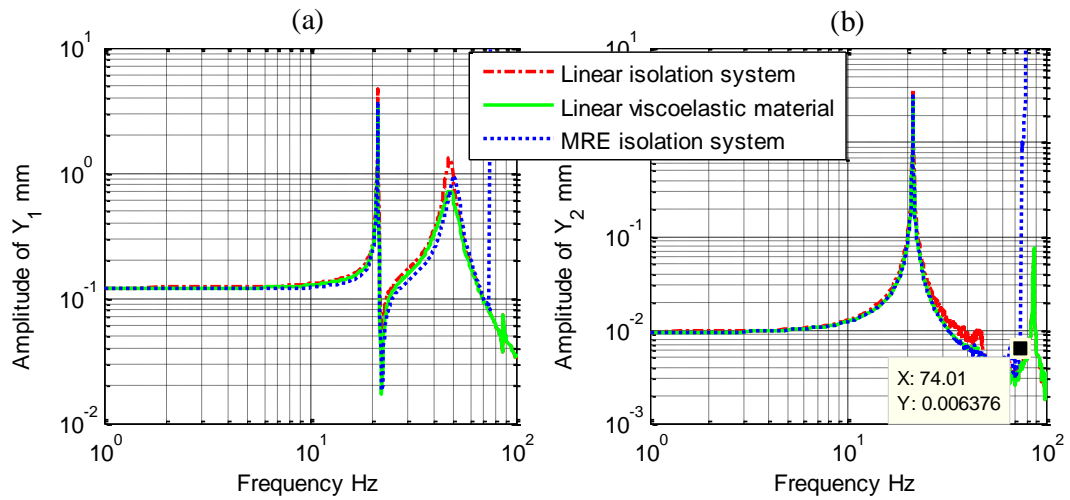


Figure 8.10 The vibration amplitude of (a) Y_1 and (b) Y_2 in different vibration systems ($L = 20$ m, $\rho = 4 \times 10^3$ kg/m, $M = 60$ kg, EI is 6×10^9 Nm² and $F_0 = 600$ N).

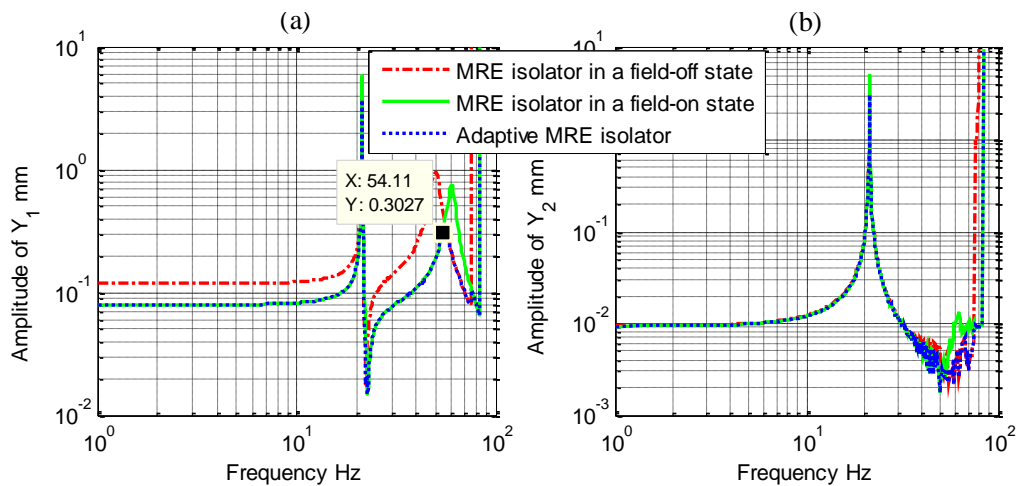


Figure 8.11 The vibration amplitude of (a) Y_1 and (b) Y_2 in MRE isolation systems ($\rho = 4 \times 10^3$ kg/m, $L = 20$ m, $M = 60$ kg, EI is 6×10^9 Nm² and $F_0 = 600$ N).

The comparison of vibration amplitudes among various systems is illustrated in Figure 8.12. As shown in Figure 8.12 (a), with a field-on state below 54 Hz and a field-off state above 54 Hz, the adaptive MRE isolator can globally reduce the vibration response of Y_1 and effectively lower the peak value of vibration amplitude of Y_1 , when compared with the corresponding linear isolation system and the system with corresponding linear viscoelastic material. In Figure 8.12 (b), it can be seen that comparing with the other two corresponding systems the adaptive MRE isolator can make no difference on the vibration amplitude of Y_2 , except in the vicinity of the natural frequency ω_0 of the isolators when the vibration amplitude of Y_2 can be effectively reduced with an adaptive MRE isolator. Additionally, in the

mathematical modelling illustrated in Section 5.3.2 the form of damping force results in a negative damping in this isolation system when frequencies are higher than 74 Hz, but the corresponding instability will never occur in reality, because the loss modulus of MRE material must be a positive value although the damping becomes very close to zero.

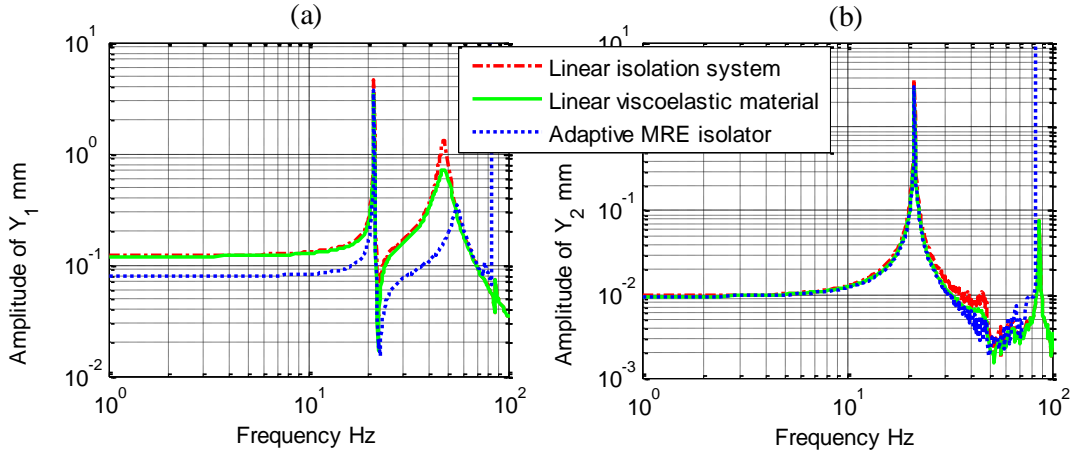


Figure 8.12 The vibration amplitude of (a) Y_1 and (b) Y_2 in different isolation systems ($\rho = 4 \times 10^3$ kg/m, $L = 20$ m, $M = 60$ kg, EI is 6×10^9 Nm² and $F_0 = 600$ N).

The performance of vibration control can be evaluated with the numerical results of transmissibility in Section 8.3. In Figure 8.13 we can see when L is 20 m, ρ is 4×10^3 kg/m, M is 60 kg, EI is 6×10^9 Nm² and F_0 is 600 N, the MRE isolator slightly shifts the natural frequency ω_0 to the right compared with the corresponding linear isolation system and the system with corresponding linear viscoelastic material. At frequencies below ω_1 the MRE isolator can hardly make any difference on transmissibility with corresponding linear isolation system or linear viscoelastic material. At frequencies between ω_0 and ω_1 the MRE isolator can reduce the transmissibility more than the two corresponding isolation systems and at frequencies above ω_0 the MRE isolator cannot obviously improve the isolation performance compared with the other two linear systems. Because of the limitation of mathematical modelling on damping force as illustrated in Section 5.3.2, in this MRE isolation system the instability happens when frequencies are higher than 74 Hz due to negative damping. But in reality this instability will never occur as the loss modulus of MRE material cannot be a negative value. It can be seen from Figure 8.13 that the reduction of transmissibility in the MRE isolation system increases with frequencies, as the equivalent damping decreases with increasing frequency in this mathematical modelling which can benefit the isolation performance at high frequency.

The parameters of stiffness and damping when the magnetic flux density B is 0.5 T in Table 8.1 are taken for the simulation of the MRE isolation system in a field-on state, and the transmissibility in different MRE isolation systems are shown in Figure 8.14. The resonant frequency of MRE isolators increases with the application of magnetic field as the equivalent stiffness increases. The isolation performance can be effectively improved with an adaptive MRE isolator by reducing the transmissibility over the full frequency range. When frequencies are below 54 Hz the adaptive MRE isolator works in a field-on state, as a higher stiffness can help to reduce the resultant vibration at low frequencies. At high frequencies a lower stiffness can improve the effectiveness of isolation, so the MRE isolator works in a field-off state.

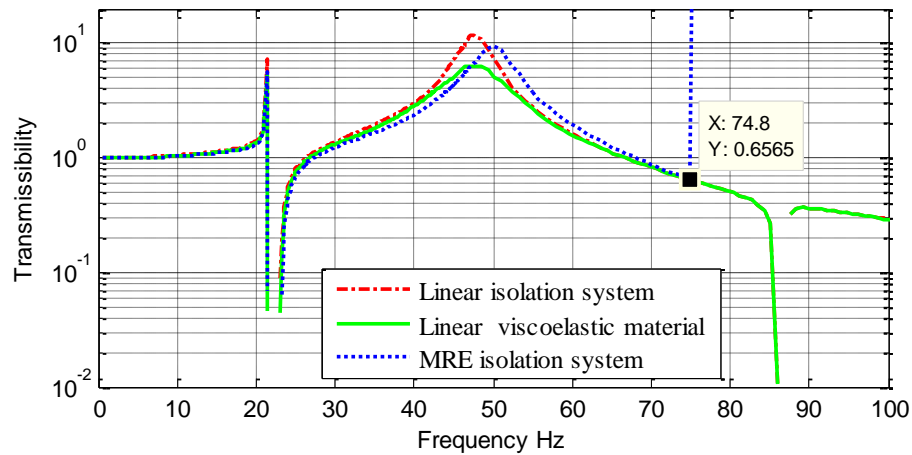


Figure 8.13 The transmissibility in different vibration systems ($L = 20$ m, $\rho = 4 \times 10^3$ kg/m, $M = 60$ kg, EI is 6×10^9 Nm² and $F_0 = 600$ N).

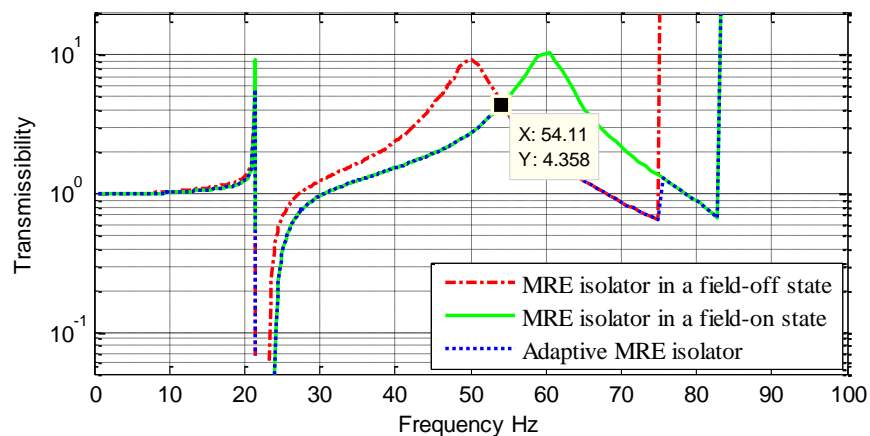


Figure 8.14 The transmissibility in different MRE isolation systems ($L = 20$ m, $\rho = 4 \times 10^3$ kg/m, $M = 60$ kg, EI is 6×10^9 Nm² and $F_0 = 600$ N).

As shown in Figure 8.15, the force transmissibility can be effectively reduced by the adaptive MRE isolator over the full frequency range. When comparing with the two corresponding isolation systems, the main peaks of transmissibility at resonant frequencies around 50 Hz can be significantly reduced with the adaptive MRE isolator by switching from a field-on state to a field-off state: at frequencies between the first natural frequency of elastic mode ω_1 and the resonant frequency ω_0 , with the adaptive MRE isolator we can obtain a substantial reduction of transmissibility. However, at frequencies below ω_1 or above ω_0 , the performance of vibration control cannot be obviously improved with an adaptive MRE isolator than the two corresponding linear systems from the perspective of the force transmissibility.

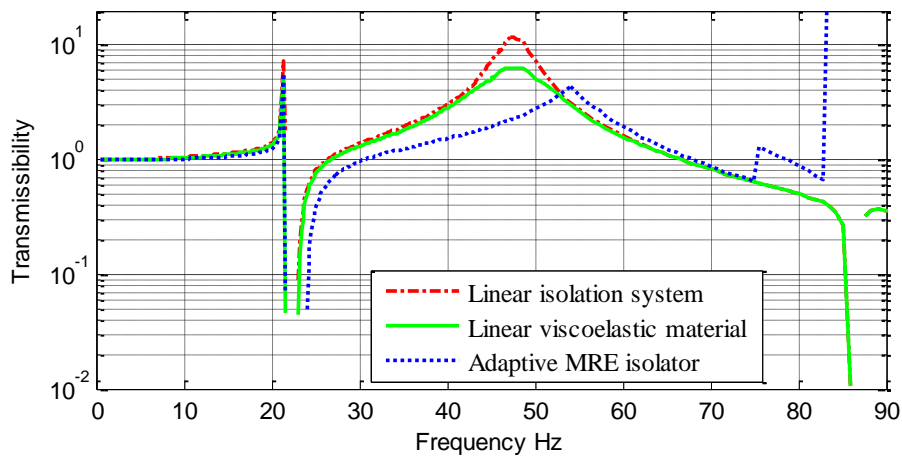


Figure 8.15 The transmissibility in different isolation systems ($L = 20$ m, $\rho = 4 \times 10^3$ kg/m, $M = 60$ kg, EI is 6×10^9 Nm² and $F_0 = 600$ N).

The numerical results of Section 8.3 are investigated to assess the vibratory power generation, dissipation and transmission in this dynamical system and evaluate the effectiveness of isolation. When L is 20 m, ρ is 4×10^3 kg/m, M is 60 kg, EI is 6×10^9 Nm² and F_0 is 600 N, as shown in Figure 8.16, compared with the corresponding linear isolation system and the system with corresponding linear viscoelastic material, the MRE isolation system slightly shifts the natural frequency ω_0 to the right. It can be seen that at frequencies below ω_0 both the power input through the machine $\langle P_{in} \rangle$ and the power isolated by the isolator $\langle P_{iso} \rangle$ in this MRE isolation system are at the same level as they are in the system with corresponding linear viscoelastic material, and higher than they are in the corresponding linear isolation system. Whilst at frequencies above ω_0 the input power $\langle P_{in} \rangle$ and the isolated power $\langle P_{iso} \rangle$ in the MRE isolation system is much lower than they are in the two corresponding isolation systems. In this MRE isolation system a negative damping occurs when frequencies are higher than 74 Hz,

which results from the limitation of mathematical modelling on damping force illustrated in Section 5.3.2. But the loss modulus of MRE material cannot be a negative value, so the corresponding instability will never occur in reality. From the comparison in Figure 8.16, it can be seen that as the frequency increases the reductions of both the input power and the isolated power by the MRE isolator also increase, because the equivalent damping decreases with increasing frequency in this mathematical modelling which can help to improve the isolation performance at high frequencies.

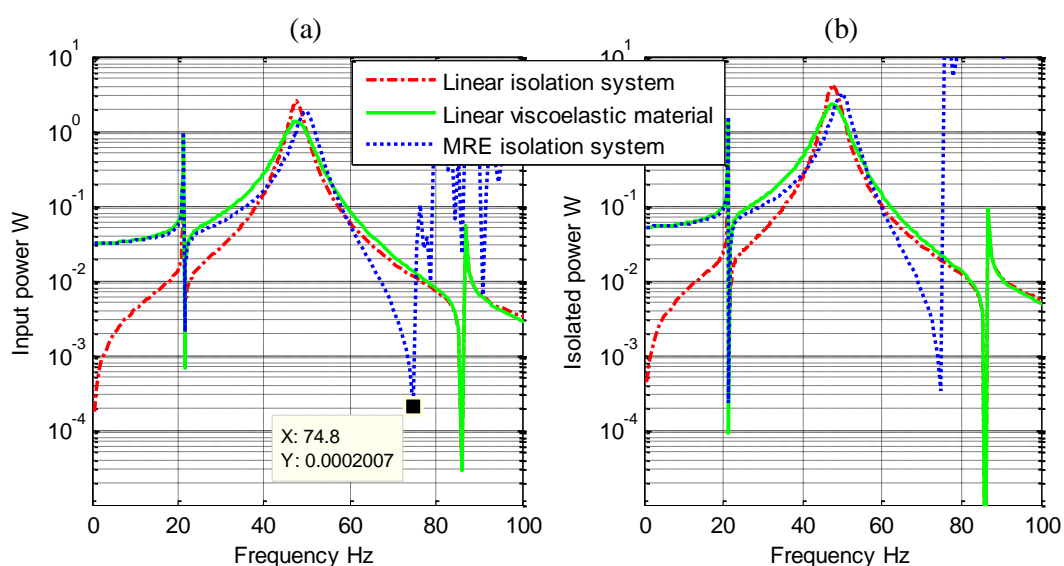


Figure 8.16 (a) The input power and (b) the isolated power in different vibration systems ($L = 20$ m, $\rho = 4 \times 10^3$ kg/m, $M = 60$ kg, EI is 6×10^9 Nm² and $F_0 = 600$ N).

In Figure 8.17 it can be seen that at frequencies below ω_0 50 Hz the power $\langle P_{out} \rangle$ transmitted to the base in the MRE isolation system is lower than that in the two corresponding isolation systems, but at higher frequencies the MRE isolator can make no improvement on the transmitted power $\langle P_{out} \rangle$. The instability reflected in Figure 8.17 will never occur, because the loss modulus of MRE material can never be a negative value although the limitation of mathematical modelling allows a negative damping to happen above 74 Hz.

The power input through the machine $\langle P_{in} \rangle$ and the power isolated by the isolator $\langle P_{iso} \rangle$ for different MRE isolation systems are shown in Figure 8.18. The parameters of stiffness and damping when the magnetic flux density B is 0.5 T in Table 8.1 are taken for the simulation of the MRE isolation system in a field-on state. The application of magnetic field can shift the resonant frequency of MRE isolators to higher frequency range by increasing the stiffness of MRE material, and the application of magnetic field has no effect on the natural frequencies of

the beam. The isolation performance can be effectively improved with an adaptive MRE isolator by reducing the input power $\langle P_{in} \rangle$. Because at low frequencies a higher stiffness can help to reduce the resultant vibration, the adaptive MRE isolator works in a field-on state when frequencies are below 54 Hz. At high frequencies a lower stiffness can help to improve the isolation efficiency, so the isolator works in a field-off state. Therefore the power $\langle P_{in} \rangle$ input through the machine can be effectively controlled with the adaptive MRE isolator over the full frequency range.

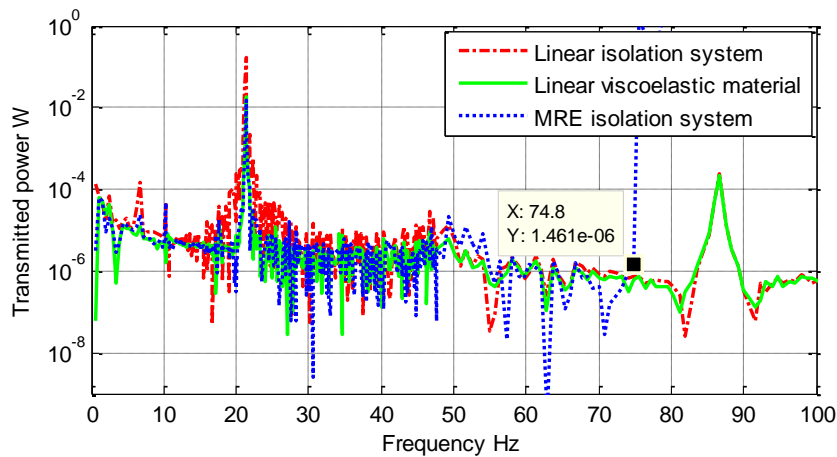


Figure 8.17 The power transmitted to the base in different isolation systems ($L = 20$ m, $\rho = 4 \times 10^3$ kg/m, $M = 60$ kg, EI is 6×10^9 Nm² and $F_0 = 600$ N).

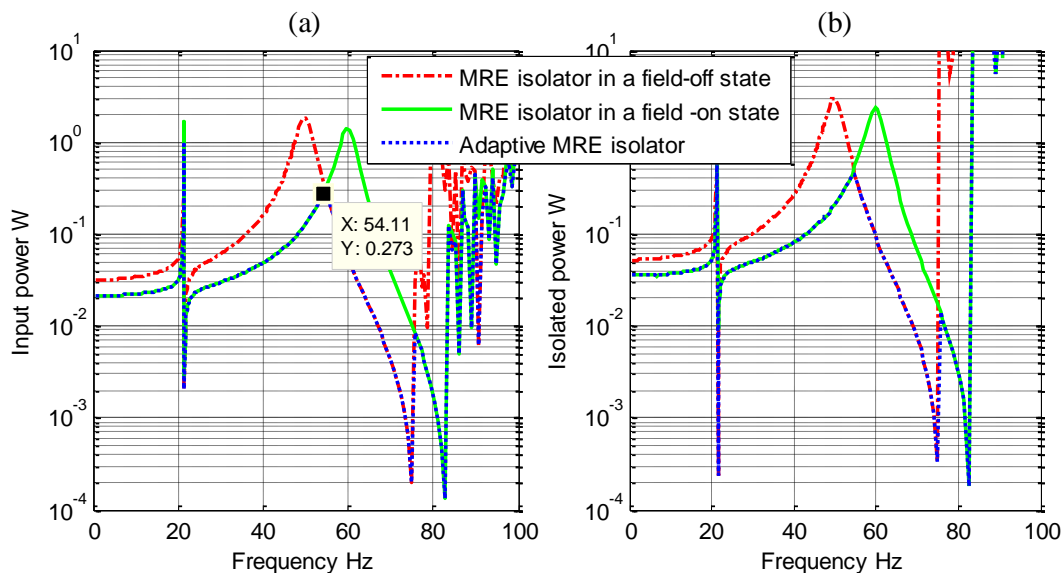


Figure 8.18 (a) The input power and (b) the isolated power in different MRE vibration systems ($L = 20$ m, $\rho = 4 \times 10^3$ kg/m, $M = 60$ kg, EI is 6×10^9 Nm² and $F_0 = 600$ N).

The time-averaged power $\langle P_{out} \rangle$ transmitted to the base in different MRE isolation systems is compared in Figure 8.19. It can be noted that in the neighbourhood of resonance frequency ω_0 the application of magnetic field can influence the output power flow $\langle P_{out} \rangle$, which can be mitigated by turning on the magnetic field below 54 Hz and removing this magnetic field above 54 Hz. However, there is no significantly global difference of the transmitted power $\langle P_{out} \rangle$ in the entire bandwidth range considered amongst the MRE isolation systems.

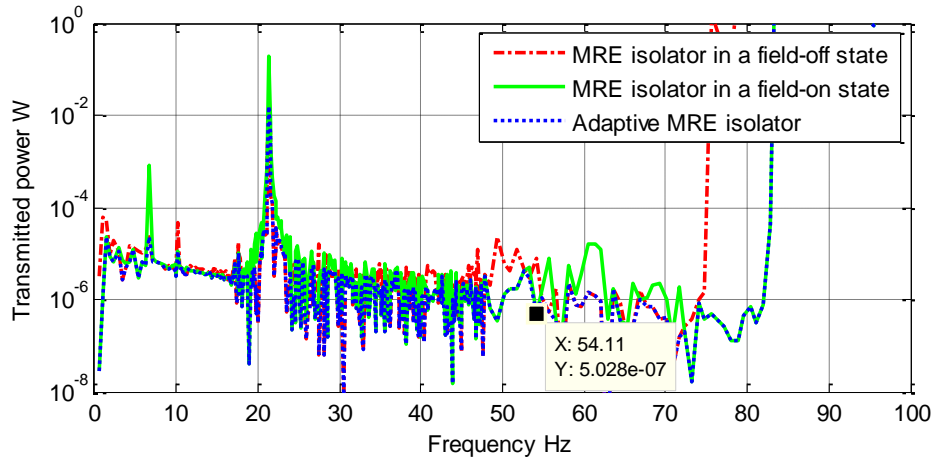


Figure 8.19 The power transmitted to the base in different MRE isolation systems ($L = 20$ m, $\rho = 4 \times 10^3$ kg/m, $M = 60$ kg, EI is 6×10^9 Nm² and $F_0 = 600$ N).

As shown in Figure 8.20, the power input through the machine $\langle P_{in} \rangle$ and the power isolated by the isolator $\langle P_{iso} \rangle$ can be effectively reduced by the adaptive MRE isolator over the full frequency range. When comparing with the two corresponding isolation systems around 50 Hz the natural frequency ω_0 of the isolator, the main peaks of input power $\langle P_{in} \rangle$ and isolated power $\langle P_{iso} \rangle$ can be significantly reduced with the adaptive MRE isolator by switching from a field-on state to a field-off state. At the high frequency range, the adaptive MRE isolator can also have a substantial reduction of both the input power $\langle P_{in} \rangle$ and the isolated power $\langle P_{iso} \rangle$ because the damping of MRE isolators declines with increasing frequency, which can result in an improved isolation characteristic at high frequencies. But in the very low frequency range, the efficiency of vibration control we obtain with an adaptive MRE isolator is not better than that we get from the corresponding linear isolator from the perspective of the power input through the machine $\langle P_{in} \rangle$ and the power isolated by the isolator $\langle P_{iso} \rangle$.

The numerical results in Figure 8.21 reveal that at frequencies below 54 Hz a better performance of vibration control can be obtained with an adaptive MRE isolator as the power $\langle P_{out} \rangle$ transmitted to the beam can be effectively reduced. However, above 54 Hz the adaptive

MRE isolator can hardly further lower the transmitted power flow compared with the corresponding conventional isolator and the isolator with corresponding linear viscoelastic material.

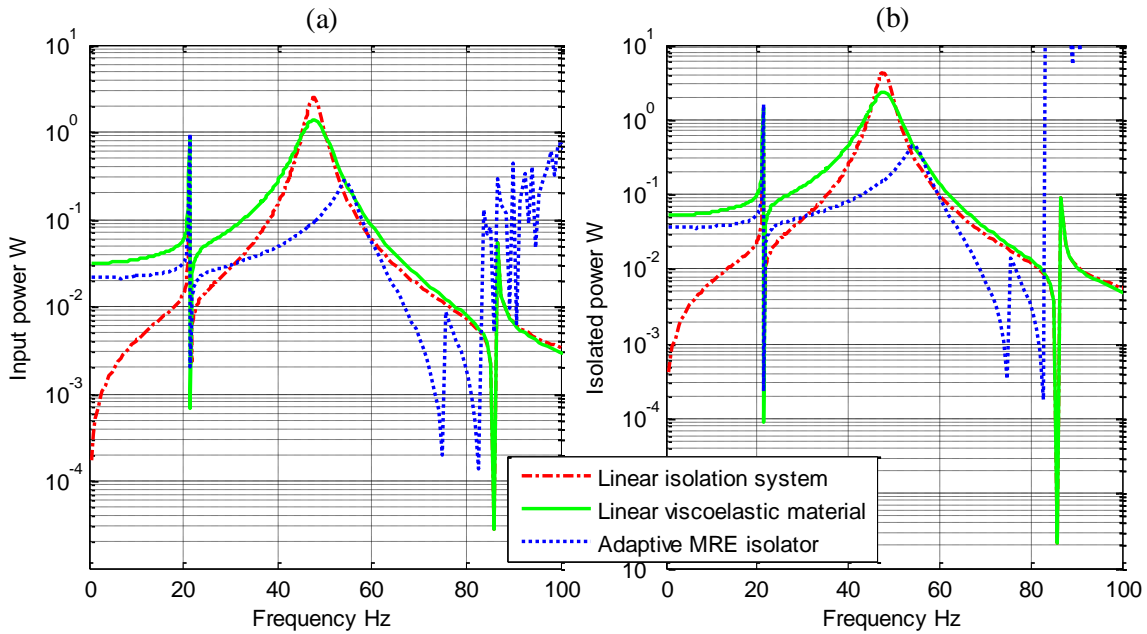


Figure 8.20 (a) The input power and (b) the isolated power in different vibration systems ($L = 20$ m, $\rho = 4 \times 10^3$ kg/m, $M = 60$ kg, EI is 6×10^9 Nm² and $F_0 = 600$ N).

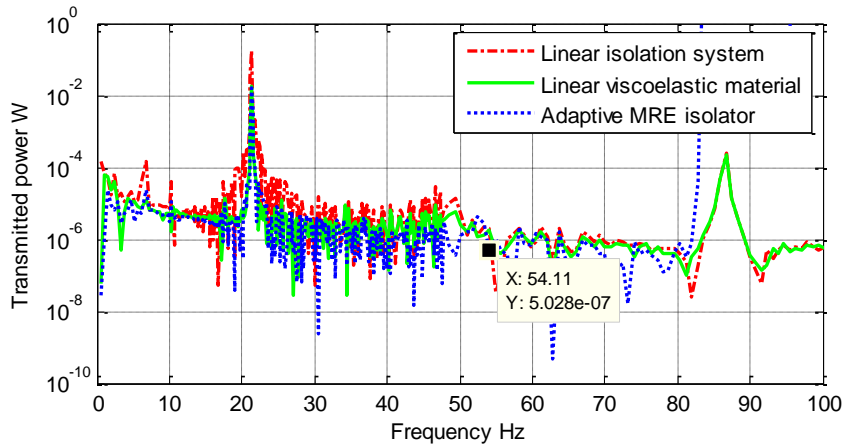


Figure 8.21 The power transmitted to the base in different isolation systems ($L = 20$ m, $\rho = 4 \times 10^3$ kg/m, $M = 60$ kg, EI is 6×10^9 Nm² and $F_0 = 600$ N).

8.5 Summary

In this chapter, an isolation system with an MRE isolator and a flexible beam is investigated to explore the application of MRE in vibration control. Firstly the equations of motion are

employed to analyse the steady response and the vibration power flow of this isolation system. Secondly, the numerical simulation of vibration response and power flow is used to study the dynamical behaviour and isolation performance in frequency domain. Both the lower resonance frequency and smaller vibration response or power transmissibility are desirable characteristics for vibration isolation. Lastly the effectiveness of adaptive MRE isolators is examined by comparing with the corresponding conventional isolators and the isolators with linear viscoelastic material.

In this selected isolation system, we have a rigid mode of the isolator and a few elastic modes of the flexible base. When the frequencies of the elastic modes are lower than the frequency of the rigid mode, the peaks on the curve of vibration amplitude or vibration power at natural frequencies will be notable, which indicates the importance of considering the elastic effect in designing an effective isolation system especially when the base is comparatively soft. For a safe design the elastic dynamic characteristics of the supporting structure need to be considered when the excitation frequencies are in the vicinity of the elastic natural frequencies. At these frequencies the vibration transmitted to the base dramatically increases, as the elastic mode wakes up in the neighbourhood of corresponding natural frequency.

The lower resonance frequency and the smaller vibration transmission are two desirable characteristics for isolation. Although a lower stiffness of the isolator may improve the isolation performance, the stiffness of isolators cannot be lowered ad infinitum to guarantee load capacities and save MRE materials. Finally, the effectiveness of isolation is estimated for the adaptive MRE isolator by comparing with the corresponding linear isolation system and the system with corresponding linear viscoelastic material. Numerical results show that with a magnetic field-on state at low frequencies and a magnetic field-off state at high frequencies, the adaptive MRE isolator can effectively reduce the vibration response and vibration power over the full frequency range. Therefore, by retuning the MRE isolator with a switchable magnetic field, the performance of vibration control can be improved from the perspective of dynamical behaviour and vibratory energy transmission.

Chapter 9 **Conclusions**

The MRE is composed of magnetisable particles dispersed in an elastic medium, and under an applied magnetic field this material has a variable capability of field-dependent modulus within the pre-yield regime. Therefore, the mechanical properties of MRE make this material well suited to vibration control. Modelling and simulation is a necessary step towards the application of MRE. The main contribution of this work is divided into three parts:

1. A nonlinear mathematical model is built up to present the dynamic behaviour of MRE based upon a comprehensive experimental investigation on the influence of frequencies, strains and magnetic fields on the mechanical properties. The methodology of modelling can be also used to describe the dynamic behaviour for other materials in a certain range continuously with a comparatively low requirement of calculation on parameter identification.
2. An MRE structure is developed with a high bearing capacity and a good controllability of stiffness to benefit vibration control systems. The extension of this mathematical model to MRE structures is examined by comparing the predictions of structural stiffness and damping with experimental results of dynamic tests.
3. The performance evaluation of vibration control for MRE devices in terms of dynamical behaviour, transmissibility and vibratory energy transmission can provide guidelines for the dynamic design of MRE isolators and absorbers. Comparing with traditional devices, the efficiency of vibration control can be effectively improved with MRE devices in isolation systems and absorption systems.

9.1 Mechanical properties of MRE

Comparing with the MRF, the MRE have better thermal stability and mechanical properties; thus, can be considered as a good solution to overcome many disadvantages of the MRF, such as deposition, environmental contamination and sealing problems. The MR effect of MRE is the variation capability of dynamic stiffness within a pre-yield regime under applied magnetic field, this material is widely applied for adaptive devices of vibration control. The main experimental results are as follows:

1. The presence of magnetic field in solidification can not only improve both the storage modulus and the loss modulus, but also enhance the frequency- strain- and magnetic field dependent properties of MRE.
2. The storage modulus of MRE increases with frequency, and the dependence of loss modulus on frequency is determined by the matrix material. In this study, at low frequencies (<10Hz) the loss modulus increases with frequency and at high frequencies (>10Hz) the loss modulus decreases. Consequently, the stiffness increases with an increase of excitation frequency and the damping decreases. In vibration absorption systems, a variable stiffness can result in a better absorption performance by broadening the range of frequencies for which the dynamic absorber is effective. In vibration isolation systems, the lower level of damping at high frequencies and the higher level of damping at low frequencies are desirable to improve isolation efficiency.
3. Both the storage modulus and loss modulus of MRE decrease with increasing strain, as a result stiffness and damping decrease as the strain increases. The dependence of mechanical properties on the strain undermines the bearing capacity of MRE; thus, limiting its applications, thereby, the dynamic design is important for vibration control devices to guarantee the safety.
4. The storage modulus and the loss modulus of MRE increase with the magnetic flux density and remain constant when magnetic saturation occurs. The MR effect increases with magnetic flux density and can reach as high as 37% under magnetic field of 400mT. The stiffness and damping of MRE vibration control devices can be continuously, rapidly and reversibly adjusted by employing external magnetic field.

9.2 Mathematical modelling for MRE

The MRE is a nonlinear viscoelastic material, considering its dependence on mechanical properties of strain and frequency the current research on modelling is still insufficient to describe the complex dynamic behaviour of MRE and to provide guidelines for dynamical analysis of vibration systems.

1. The comprehensive experimental research of MRE in this thesis enables a nonlinear mathematical model to develop from Kelvin-Voigt model, whereby the spring and the damping forces are expressed in the form of polynomials with frequency and strain as independently continuous variables. With a low requirement of calculation on parameter identification and a full use of gathered information on the mechanical properties, the

methodology of modelling can be also applied to other materials to continuously describe their dynamical behaviour in a certain range of strain and frequency.

2. An MRE structure is developed with a good bearing capacity and good controllability of stiffness for application to vibration control systems. Considering the structural dynamic design and the nonlinear mathematical model, the dynamical properties of MRE structure on a large scale are predicted, and the predicted results are compared with the experimental results to validate the extension of this mathematical model of MRE structure.

9.3 Applications for vibration control

Compared with the industrialisation and commercialisation of MRF the current applications of MRE on vibration control are still on a very exploratory stage. Performance evaluation of vibration control is essential for the application of MRE, and herein a two-stage isolation system, an absorption system and an isolation system with a flexible base are investigated. Aiming at providing guidelines for the dynamic design of MRE devices, this nonlinear mathematical model is employed to investigate the dynamical behaviour, transmissibility and vibratory energy transmission in MRE vibration control systems. Comparing with traditional devices the effectiveness of vibration control can be further improved with MRE devices by controlling an external magnetic field.

1. For MRE absorbers the range of frequencies for effective absorption can be broadened, as the natural frequencies of MRE absorbers cannot only be precisely tuned to the excitation frequency for an optimum performance but also be retuned with a controllable magnetic field to suit time-varying excitation frequencies.
2. For MRE isolators the vibration transmissibility and energy transmission can be effectively reduced by employing magnetic fields at low frequencies where the high stiffness can help to reduce the vibration and removing magnetic fields at high frequencies where the low stiffness can improve the isolation performance.

Chapter 10 Recommendations for future work

The outcomes of the work in this thesis highlight the importance of considering the dependence of mechanical properties on frequencies, strains and magnetic fields for mathematical modelling of MRE as a step towards its application. To achieve a more integral research on this subject, future work is recommended and major challenges are foreseen as described briefly below.

1. Develop mathematical models for MRE.

In the light of the experimental results of mechanical characterisation, a mathematical model is developed from Kelvin-Voigt model to continuously describe the dynamical behaviour of MRE. Herein the dependence of mechanical properties on frequencies, strains and magnetic fields are investigated from 1 Hz to 60 Hz, from 0 to 6% and from 0 to 400 mT. Because of the propeller, engine, ancillary machinery and effects of the sea, the frequency of vibration on board ships might be between 0.01Hz and 80Hz, a wider range of frequencies, strains and magnetic fields is more desirable for developing this mathematical model of MRE.

2. Dynamical design MRE devices for vibration control.

A wide variation of stiffness from a field-off state to a field-on state is essential for MRE vibration control devices, which requires a large MR effect and, consequently, a soft matrix, but the soft materials undermines the bearing capacity and the durability of MRE. A strong magnetic field is also of benefit to the variation of stiffness, but the resultant power consumption cannot be neglected. Therefore, a trade-off between a high MR effect and other criteria needs to be considered carefully, and the dynamic designs need to enable MRE structures to improve the mechanical properties. Compact designs for the MRE devices emphasize that mass and the volume of electromagnets need to be taken into account for dynamic designs. Besides the electromagnets produce temperature influence while generating magnetic field, and MRE material becomes softer with the increasing temperature.

3. Experimental validation of modelling for MRE.

Although the extension of this model to MRE structures has been validated in this thesis, it is necessary to manufacture the MRE devices and verify their performances on vibration control. The extension of mathematical models and the efficiency of modelling methodology

can be examined by comparing the predicted values with the experimental results. From the perspective of effectiveness and economy, a valid methodology of performance evaluation without manufacturing and testing MRE devices is important for the dynamic design of vibration control devices.

List of Publications

Journal Publications

- **Mathematical Modelling on mechanical properties of MRE**
G. Zhu, Y.P. Xiong, S. Daley, R.A. Sheno
Smart Materials and Structures, (in revision)

Conference Publications

- **Magnetorheological elastomer materials and structures with vibration energy control for marine application**
G. Zhu, Y.P. Xiong, S. Daley, R.A. Sheno
Analysis and Design of Marine Structure V, P. 197-204, 2015.
- **Experimental Study and Mathematical Modelling on Dependent Shear Properties of MRE Material**
G. Zhu, Y.P. Xiong, S. Daley, R.A. Sheno
14th International Conference on Electrorheological Fluids and Magnetorheological Suspensions, Granada, Spain, 07-11 July 2014.
- **Mathematical Modelling and Dynamical Analysis of a Magnetorheological Elastomer Tuneable Absorber**
G. Zhu, Y.P. Xiong, S. Daley, R.A. Sheno
Vibration Engineering and Technology of Machinery-IX, Nanjing, China, 21-23 August 2013.
- **Dynamical Analysis of a Two-stage Nonlinear MRE Vibration Isolation System**
G. Zhu, Y.P. Xiong, S. Daley, R.A. Sheno
19th International Congress on Sound and Vibration, Vilnius, Lithuania, 7-13 July 2012.

Conference Posters

- **Smart materials and structures with hybrid nonlinear vibration control for marine applications**
G. Zhu, Y.P. Xiong, S. Daley, R.A. Shenoi
FSI Away Day Conference, University of Southampton, January 2012
- **Dynamical Analysis of Nonlinear MRE Properties Applied to Vibration Control**
G. Zhu, Y.P. Xiong, S. Daley, R.A. Shenoi
FSI Away Day Conference, University of Southampton, January 2013
- **Experimental Study and Mathematical Modelling on Mechanical Properties of MRE**
G. Zhu, Y.P. Xiong, S. Daley, R.A. Shenoi
FSI Away Day Conference, University of Southampton, July 2015

Research Reports

- **Innovative magnetic materials and smart structures with hybrid vibration control for marine application**
G. Zhu, Y.P. Xiong, S. Daley, R.A. Shenoi
The Lloyd's Register Educational Trust University Technology Centre (LRET UTC) Annual Report, 2012
- **Magnetorheological materials and structures with hybrid vibration control for marine application**
G. Zhu, Y.P. Xiong, S. Daley, R.A. Shenoi
The Lloyd's Register Educational Trust University Technology Centre (LRET UTC) Annual Report, 2014

References

- [1] S. Daley, F.A. Johnson, J.B. Pearson, R. Dixon, Active vibration control for marine applications, *Control Engineering Practice*, 12(4), 465–474, (2004).
- [2] Y.P. Xiong, J.T. Xing, W.G. Price, X. P. Wang, Hybrid active and passive control of vibratory power flow in flexible isolation system, *Shock and Vibration*, 7(3), 139-148, (2000).
- [3] A. Sheno, A. Waddams, A. Sinha, Smart Materials and the Marine Environment: A state of the art review, Available from: <https://connect.innovateuk.org>, (2009).
- [4] J. Rabinow, The magnetic fluid clutch, *American Institute of Electrical Engineers, Transactions*, 67(2), 1308-1315, (1948).
- [5] J.D. Carlson, M.R. Jolly, MR fluid, foam and elastomer devices, *Mechatronics*, 10(4), 555-569, (2000).
- [6] Y. Shen, M.F. Golnaraghi, G.R. Heppler, Analytical and experimental study of the response of a suspension system with a magnetorheological damper, *Journal of intelligent material systems and structures*, 16(2), 135-147, (2005).
- [7] W.M. Stewart, J.M. Ginder, L.D. Elie, Method and apparatus for reducing brake shudder, *United States Patent*, U.S. 5,816,587. (1998).
- [8] Y. Li, J. Li, W. Li, B. Samali, Development and characterization of a magnetorheological elastomer based adaptive seismic isolator, *Smart Materials and Structures*, 22(3), 035005, (2013).
- [9] G. Zhu, Y.P. Xiong, S. Daley, R.A Sheno, Magnetorheological elastomer materials and structures with vibration energy control for marine application, *Analysis and Design of Marine Structure V*, 197-204, (2015).
- [10] N. Hoang, N. Zhang, H. Du, An adaptive tunable vibration absorber using a new magnetorheological elastomer for vehicular powertrain transient vibration reduction, *Smart Materials and Structures*, 20(1), 015019, (2011).
- [11] Y. Shen, M.F. Golnaraghi, G.R. Heppler. Experimental research and modeling of magnetorheological elastomers. *Journal of Intelligent Material Systems and Structures*, 15(1), 27-35, (2004).

- [12] Y. Wang, Y. Hu, X. Gong, W. Jiang, P. Zhang, Z. Chen, Preparation and Properties of Magnetorheological Elastomers Based on Silicon/Polystyrene Blend Matrix, *Journal of Applied Polymer Science*, 103(5), 3143-3149, (2007).
- [13] L. Chen, X. Gong, W. Jiang, J. Yao, H. Deng, W. Li, Investigation on magnetorheological elastomers based on natural rubber, *Journal of Material Science*, 42(14), 5483-5489,(2007).
- [14] S.A. Demchuk, V.A. Kuz'min, Viscoelastic properties of magnetorheological elastomers in the regime of dynamic deformation, *Journal of Engineering Physics and Thermophysics*, 75(2), 396-400, (2002).
- [15] J. Wu, X. Gong, Y. Fan, H. Xia, Improving the Magnetorheological Properties of Polyurethane Magnetorheological Elastomer through Plasticization, *Journal of Applied Polymer Science*, 123(4), 2476–2484 (2012).
- [16] V.V. Sorokin, E. Ecker, G.V. Stepanov, M. Shamonin, G.J. Monkman, E.Y. Kramarenko, A.R. Khokhlov, Experimental study of the magnetic field enhanced Payne effect in magnetorheological elastomers, *Soft matter*, 10(43), 8765-8776, (2014).
- [17] M. Lokander, T. Reitberger, Oxidation of natural rubber-based magnetorheological elastomers. *Polymer degradation and stability*, 86(3), 467-471, (2004).
- [18] H.M. Yin, L.Z. Sun, Magnetoelasticity of chain-structured ferromagnetic composites, *Applied Physics Letters*, 86(26), 261901, (2005).
- [19] G. Stepanov, D. Borin, S. Odenbach, Magnetoreological effect of magneto-active elastomers containing large particles, *Journal of Physics: Conference Series*, 149(1),012098, (2009).
- [20] M. Lokander, B. Stenberg, Performance of isotropic magnetorheological rubber materials, *Polymer Testing*, 22(3), 245-251, (2003).
- [21] J.H. Yoon, I.H. Yang, U.C. Jeong, K.H. Chung, J.Y. Lee, J.E. Oh, Investigation on Variable Shear Modulus of Magnetorheological Elastomer Based on Natural Rubber due to Change of Fabrication Design, *Polymer Engineering and Science*, 53(5), 992-1000, (2013).
- [22] L.C. Davis, Model of magnetorheological elastomers. *Journal of Applied Physics*, 85(6), 3348-3351, (1999).
- [23] J. Kaleta, M. Krolewicz, D. Lewandowski, Magnetomechanical properties of anisotropic and isotropic magnetorheological composites with thermoplastic elastomer matrices, *Smart Materials and Structures*, 20(8), 085006, (2011).

- [24] M.R. Jolly, J.D. Carlson, B.C. Muñoz, The magnetoviscoelastic response of elastomer composites consisting of ferrous particles embedded in a polymer matrix. *Journal of Intelligent Material Systems and Structures*, 7(6), 613-622, (1996).
- [25] Z. Varga, G. Filipcsei, M. Zrínyi, Magnetic field sensitive functional elastomers with tuneable elastic modulus, *Polymer*, 47(1), 227-233, (2006).
- [26] J. Wu, X. Gong, Y. Fan, H. Xia, Physically crosslinked poly(vinyl alcohol) hydrogels with magnetic field controlled modulus, *Journal of Soft Matter*, 7(13), 6205–6212, (2011).
- [27] J.L. Leblanc, Rubber–filler interactions and rheological properties in filled compounds, *Progress in polymer science*, 27(4): 627-687, (2002).
- [28] M. Lokander, B. Stenberg, Improving the magnetorheological effect in isotropic magnetorheological rubber materials, *Polymer testing*, 22(6), 677-680, (2003).
- [29] Y. Wang, Y. Hu, L. Chen, X. Gong, W. Jiang, P. Zhang, Z. Chen, Effects of rubber/magnetic particle interactions on the performance of magnetorheological elastomers, *Journal of Polymer Testing*, 25(2), 262-267, (2006).
- [30] W. Jiang, J. Yao, X. Gong, L. Chen, Enhancement in magnetorheological effect of magnetorheological elastomers by surface modification of iron particles, *Chinese Journal of Chemical Physics*, 21(1), 87-92, (2008).
- [31] R. Li, L.Z. Sun, Dynamic mechanical behaviour of magneto-rheological nanocomposites filled with carbon nanotubes, *Applied Physics Letters*, 99(13), 131912, (2011).
- [32] S.S. Demchuk, V.A.Kuzmin, Viscoelastic properties of magnetorheological elastomers in the regime of dynamic deformation, *Journal of Engineering Physics and Thermophysics*, 75(2), 104-107, (2002).
- [33] A. Lion, C. Kardelky, The Payne effect in finite viscoelasticity: constitutive modelling based on fractional derivative and intrinsic time scales, *International Journal of Plasticity*, 20(7), 1313-1345, (2004).
- [34] A.S. Khan, O. Lopez-Pamies, Time and temperature dependent response and relaxation of a soft polymer, *International Journal of Plasticity*, 18(10): 1359-1372, (2002).
- [35] W. Luo, X. Hu, C. Wang, Q. Li, Frequency-and strain-amplitude-dependent dynamical mechanical properties and hysteresis loss of CB-filled vulcanized natural rubber, *International Journal of Mechanical Sciences*, 52(2), 168-174, (2010).
- [36] H.J. Jung, S.J. Lee, D.D. Jang, Dynamic characterization of magneto-rheological elastomers in shear mode, *IEEE Transactions on Magnetics*, 45(10), 3930-3933, (2009).

- [37] T. F. Tian, W. H. Li, G. Alici, H. Du, Y. M. Deng, Microstructure and magnetorheology of graphite-based MR elastomers, *Rheol Acta*, 50(9-10), 825-836, (2011).
- [38] Alexander Lion, A constitutive model for carbon black filled rubber: Experimental investigations and mathematical representation, *Continuum Mechanics and Thermodynamics*, 8(3), 153-169, (1996).
- [39] L. Mullins, Softening of Rubber by Deformation, *Rubber chemistry and technology*, 42(1), 339-362, (1969).
- [40] L. Laiarinandrasana, R. Piques, A. Robisson, Visco-hyperelastic model with internal state variable coupled with discontinuous damage concept under total Lagrangian formulation. *International Journal of Plasticity*, 19(7), 977-1000, (2003).
- [41] T. Shiga, A. Okada, T. Kurauchi, Magnetorheological behavior of composite gels, *Journal of Applied Polymer Science*, 58(4), 787-792, (1995).
- [42] G.Y. Zhou, Shear properties of a magnetorheological elastomer, *Smart materials and structures*, 12(1), 139, (2003).
- [43] K. Danas, S.V. Kankanala, N. Triantafyllidis, Experiments and modelling of Iron-particle-filled magnetorheological elastomers, *Journal of Mechanics and Physics of Solid*, 60(1), 120-138, (2012).
- [44] S.A. Demchuk, V.A. Kuzmin, Viscoelastic properties of magnetorheological elastomers in the regime of dynamic deformation, *Journal of Engineering and Thermophysics*, 75(2), 396-400, (2002).
- [45] H. Bose, R. Roder, Magnetorheological Elastomers with High Variability of their Mechanical Properties, *Journal of Physics: Conference Series*, 149(1), 012090, (2009).
- [46] Z. Varga, G. Filipcsei, M. Zrínyi, Smart composites with controlled anisotropy, *Polymer*, 46(18), 7779-7787, (2005).
- [47] W.H. Li, X.Z. Zhang, A study of the magnetorheological effect of bimodal particle based magnetorheological elastomers, *Smart Materials and Structures*, 19(3), 035002, (2010).
- [48] M.R. Jolly, J.D. Carlson, B.C. Munoz, A model of the behavior of magnetorheological materials, *Smart Material Structures*, 5(5), 607-614, (1996).
- [49] L.C. Davis, Model of Magnetorheological Elastomers, *Applied Physics*, 85(6), 3348-3351, (1999).
- [50] Y. Han, W. Hong, L.A.E. Faidley, Field-stiffening effect of magneto-rheological elastomers, *International Journal of Solids and Structures*, 50(14), 2281-2288, (2013).

- [51] X. Gong, Y. Xu, S. Xuan, C. Guo, L. Zong, The investigation on the nonlinearity of plasticine-like magnetorheological material under oscillatory shear rheometry, *Journal of the Society of Rheology*, 56(6), 1375-1391, (2012).
- [52] K.M. Popp, M. KroGer, W. Li, X. Zhang, P. B. Kosasih, MRE Properties under Shear and Squeeze Modes and Applications, *Journal of Intelligent Material Systems and Structures*, 21(15), 1471-1477, (2010).
- [53] W. Zhang, X. Gong, S. Xuan, W. Jiang, Temperature-Dependent Mechanical Properties and Model of Magnetorheological Elastomers, *Industrial & Engineering Chemistry Research*, 50(11), 6704–6712, (2011).
- [54] G. Liao, X. Gong, S. Xuan, C. Guo, L. Zong, Magnetic-Field-Induced Normal Force of Magnetorheological Elastomer under Compression Status, *Industrial & Engineering Chemistry Research*, 51(8), 3322–3328,(2012).
- [55] N. Kchit, P. Lancon, G. Bossis, Thermoresistance and Giant Magnetoresistance of Magnetorheological Elastomers, *Journal of Physics D: Applied Physics*, 42(10), 105506, (2009).
- [56] A. Boczkowska, S. Awietjan, Microstructure and properties of magnetorheological elastomers, *INTECH Open Access Publisher*, (2012).
- [57] S.J. Jang, M.J. Brennan, E. Rustighi, H.J. Jung, A simple method for choosing the parameters of a two degree-of-freedom tuned vibration absorber, *Journal of Sound and Vibration*, 331(21),4658-4667, (2012).
- [58] L. Chen, S. Jerrams, A rheological model of the dynamic behavior of magnetorheological elastomers, *Journal of Applied Physics*, 110(1), 013513, (2011).
- [59] L.C. Davis, Model of magnetorheological elastomers, *Journal of Applied Physics*, 85(6), 3348-3351, (1999).
- [60] L. Chen, X.L. Gong, W.H. Li, Microstructures and viscoelastic properties of anisotropic magnetorheological elastomers, *Smart Materials and Structures*, 16(6), 2645, (2007).
- [61] W.H. Li, G.Z. Yao, G. Chen, Testing and steady state modelling of a linear MR damper under sinusoidal loading, *Smart Materials and Structures*, 9(1), 95-102, (2000).
- [62] D. Roylance, Engineering viscoelasticity, *Department of Materials Science and Engineering–Massachusetts Institute of Technology, Cambridge MA*, 2139, 1-37, (2001).
- [63] W.H. Li, Y. Zhou, T.F. Tian, Viscoelastic properties of MR elastomers under harmonic loading, *Rheologica Acta*, 49(7), 733-740, (2010).
- [64] D. Roylance, Engineering viscoelasticity, *Department of Materials Science and Engineering–Massachusetts Institute of Technology, Cambridge MA*, 2139, 1-37, (2001).

- [65] W.H. Li, H.J. Du, G.Chen, S.H. Yeo, N.Q. Guo, Nonlinear viscoelastic properties of MR fluids under large-amplitude-oscillatory-shear, *Rheologica. Acta*, 42(3), 280–286, (2003).
- [66] J.T. Zhu, Z.D. Xu, Y.Q. Guo, Magnetoviscoelasticity parametric model of an MR elastomer vibration mitigation device, *Smart materials and structures*, 21(7), 075034, (2012).
- [67] J. Yang, H. Du, W. Li, Y. Li, J. Li, Experimental study and modeling of a novel magnetorheological elastomer isolator, *Smart Materials and Structures*, 22(11), 117001, (2013).
- [68] S. Daley, J. Wang, A geometric approach to the design of remotely located vibration control systems. *Journal of Sound and Vibration*, 318(4), 702-714, (2008).
- [69] Y. Li, J. Li, W. Li, H. Du, A state-of-the-art review on magnetorheological elastomer devices, *Smart Materials and Structures*, 23(12), 123001, (2014).
- [70] J.M. Ginder, M.E. Nichols, L.D. Elie, Controllable-stiffness components based on magnetorheological elastomers. *SPIE's 7th Annual International Symposium on Smart Structures and Materials*, International Society for Optics and Photonics, 418-425, (2000).
- [71] J.M. Ginder, W.F. Schlotter, M.E. Nichols, Magnetorheological elastomers in tuneable vibration absorbers. *SPIE's 8th Annual International Symposium on Smart Structures and Materials*, International Society for Optics and Photonics, 103-110, (2001).
- [72] H.X. Deng, X.L. Gong, L.H. Wang, Development of an adaptive tuned vibration absorber with magnetorheological elastomer, *Smart materials and structures*, 15 (5), N111, (2006).
- [73] H.X. Deng, X.L. Gong, Adaptive tuned vibration absorber based on magnetorheological elastomer, *Journal of Intelligent Material Systems and Structures*, 18(12), 1205–1210, (2007).
- [74] S.S. Sun, Y. Chen, J. Yang, T.F. Tian, H.X. Deng, W.H. Li, H. Du, G. Alici, The development of an adaptive tuned magnetorheological elastomer absorber working in squeeze mode, *Smart Materials and Structures*. 23(7), 075009, (2014).
- [75] A.A. Lerner, K.A. Cunefare, Performance of MRE-based vibration absorbers, *Journal of Intelligent Material Systems and Structures*, 19, 551-563, (2007).
- [76] N. Hoang, N. Zhang, W.H. Li, Development of a torsional dynamic absorber using a magnetorheological elastomer for vibration reduction of a powertrain test rig, *Journal of Intelligent Material Systems and Structures*, 24(16), 2036-2044, (2013).

- [77] H. Deng, X. Gong, Application of Magnetorheological elastomers to vibration absorber, *Communications in Nonlinear Science and Numerical Simulation*, 13(9), 1938-1947, (2008).
- [78] G.J. Liao, X.L. Gong, C.J. Kang, S.H. Xuan, The design of an active-adaptive tuned vibration absorber based on magnetorheological elastomers and its vibration attenuation performance, *Smart Materials and Structures*, 20(7), 075015, (2011).
- [79] Y.K. Kim, J.H. Koo, K.S. Kim, S.H. Kim, Suppressing harmonic vibration of a miniature cryogenic cooler using an adaptive tuned vibration absorber based on magneto-rheological elastomers, *Review of Science Instruments*, 82(3), 035103, (2011).
- [80] Z. Xu, X. Gong, G. Liao, An active-damping-compensated magnetorheological elastomer adaptive tuned vibration absorber. *Journal of Intelligent Material Systems and Structures*, 21(10), 1039-1047, (2010).
- [81] R.A. Ibrahim, Recent advances in nonlinear passive vibration isolators, *Journal of Sound and Vibration*, 314(3), 371-452, (2008).
- [82] T.J. Royston, R. Singh, Optimization of passive and active non-linear vibration mounting systems based on vibratory power transmission. *Journal of Sound and Vibration*, 194(3), 295-316, (1996).
- [83] S. Daley, J. Hätönen, D.H. Owens, Active vibration isolation in a “smart spring” mount using a repetitive control approach. *Control Engineering Practice*, 14(9), 991-997, (2006).
- [84] C. Liu, X. Jing, S. Daley, F. Li, Recent advances in micro-vibration isolation, *Mechanical Systems and Signal Processing*, 56(57), 55-80, (2015).
- [85] J.R. Watson, Method and apparatus for varying the stiffness of a suspension bushing, *United States Patent*, U.S. 5,609,353, (1997).
- [86] G.H. Hitchcock, F. Gordaninejad, A. Fuchs, Controllable MRE vibration isolator, *United States Patent*, US 7,086,507 B2, (2006).
- [87] P.R. Marur, Magneto-rheological Elastomer-based Vehicle Suspension, *United States Patent*, U.S. 0087985 A1, (2013).
- [88] M. Behrooz, X. Wang, F. Gordaninejad, Modeling of a new semi-active/passive magnetorheological elastomer isolator, *Smart Materials and Structures*, 23(4), 045013, (2014).
- [89] H. Du, W. Li, N. Zhang, Semi-active variable stiffness vibration control of vehicle seat suspension using an MR elastomer isolator, *Smart Materials and Structures*, 20(10), 105003, (2011).

- [90] S. Opie, W. Yim, Design and Control of a Real-Time Variable Modulus Vibration Isolator, *Journal of Intelligent Material Systems and Structures*, 22(10), 113-125, (2011).
- [91] S.H. Eem, H.J. Jung, J.H. Koo, Application of MR Elastomer for Improving Seismic Protection of Base-Isolated Structures, *IEEE Transaction on Magnetics*, 47(10), 2901-2904, (2011).
- [92] S.H. Eem, H.J. Jung, J.H. Koo, Seismic performance evaluation of an MR elastomer-based smart base isolation system using real-time hybrid simulation, *Smart Materials and Structures*, 22(5), 055003, (2013).
- [93] Y. Li, J. Li, T. Tian, W. Li. A highly adjustable magnetorheological elastomer base isolator for applications of real-time adaptive control, *Smart Materials and Structures*, 22(9), 095020, (2013).
- [94] W.J. Choi, Y.P. Xiong, R.A. Shenoi, Vibration characteristics of sandwich beams with steel skins and magnetorheological cores, *Advances in Structural Engineering*, 13(5), 837-844, (2010) .
- [95] M. Yalcintas, H. Dai, Vibration suppression capabilities of magnetorheological materials based adaptive structures, *Smart Materials and Structures*, 13(1), 1, (2004).
- [96] Y.Q. Ni, Z.G. Ying, Z.H. Chen, Magneto-rheological elastomer (MRE) based composite structures for micro-vibration control, *Earthquake Engineering and Engineering Vibration*, 9(3), 345-356, (2010).
- [97] S.K. Dwivedy, N. Mahendra, K.C. Sahu, Parametric instability regions of a soft and magnetorheological elastomer cored sandwich beam, *Journal of Sound and Vibration*, 325(4), 686–704, (2009).
- [98] B. Nayak, S.K. Dwivedy, K.S.R.K. Murthy, Multi-frequency excitation of magnetorheological elastomer-based sandwich beam with conductive skins, *International Journal of Non-Linear Mechanics*, 47(5), 448–460, (2012).
- [99] X. Wang, F. Gordaninejad, A New magnetorheological fluid-elastomer mount: phenomenological modelling and experimental study, *Smart Materials and Structures*, 18(9), 095045, (2009).
- [100] D. York, X. Wang, F. Gordaninejad, A New Magnetorheological Mount for Vibration Control, *Journal of Vibration and Acoustics*, 133(3), 031003, (2011).
- [101] R.B. Anderson, Isoelastic magneto-rheological elastomer isolator, *United States Patent*, US 8152145 B2, (2012).

- [102]W. Zhang, X.L. Gong, S.H. Xuan, Y.G. Xu, High-Performance Hybrid Magnetorheological Materials: Preparation and Mechanical Properties, *Industrial & Engineering Chemistry Research*, 49(24), 12471-12476, (2010).
- [103]X. Gong, Y. Fan, S. Xuan, Y. Xu, C. Peng, Control of the Damping Properties of Magnetorheological Elastomers by Using Polycaprolactone as a Temperature-Controlling Component, *Industrial & Engineering Chemistry Research*, 51(18), 6395–6403, (2012).
- [104] An overview of silicone rubber, Available from: <http://www.thefreelibrary.com>.
- [105] Shin-Etsu Chemical Company, Characteristic Properties of Silicone Rubber Compounds, Available from: <http://www.shinetsusilicone-global.com>.
- [106]W. Zhang, X. Gong, T. Sun, Y. Fan, W. Jiang, Effect of Cyclic Deformation on Magnetorheological Elastomers, *Chinese Journal of Chemical Physics*, 23(2), 226-230, (2010).
- [107]Y. Zhou, S. Jerrams, L. Chen, Multi-axial fatigue in magnetorheological elastomers using bubble inflation, *Materials and Design*, 50, 68-71, (2013).
- [108]W. Zhang, X.L. Gong, W.Q. Jiang, Y.C. Fan, Investigation of the durability of anisotropic magnetorheological elastomers based on mixed rubber, *Smart Materials and Structures*, 19(8), 085008, (2010).
- [109]J.H. Koo, F. Khan, D.D. Jang, Dynamic characterization and modelling of magnetorheological elastomers under compressive loadings, *Smart Materials and Structures*, 19(11), 117002, (2010).
- [110]M. Kallio, *The elastic and damping properties of magnetorheological elastomers*, VTT Technical Research Centre of Finland, (2005).
- [111]G. Zhu, Y.P. Xiong, S. Daley, R.A. Shenoi, Experimental Study and Mathematical Modelling on Dependent Shear Properties of MRE Material, *14th International Conference on Electrorheological Fluids and Magnetorheological Suspensions*, Granada, Spain, 07-11 July 2014.
- [112]G. Zhu, Y.P. Xiong, S. Daley, R.A. Shenoi, Dynamical Analysis of a Two-stage Nonlinear MRE Vibration Isolation System, *ICSV2013*, Vilnius, Lithuania, 7-13 July 2012.
- [113]G. Zhu, Y.P. Xiong, S. Daley, R.A. Shenoi, Mathematical Modelling and Dynamical Analysis of a Magnetorheological Elastomer Tuneable Absorber, *VETOMAC-IX*, Nanjing, China, 21-23 August 2013.

- [114]R.E.D. Bishop, D.C. Johnson, *The Mechanics of Vibration*, Cambridge University Press, Cambridge, (1960).
- [115]Y.P. Xiong, J.T. Xing, W.G. Price, A general linear mathematical model of power flow analysis and control for integrated structure-control systems, *Journal of Sound and Vibration*, 267, 301–334, (2003).
- [116]Y.P. Xiong, J.T. Xing, W.G. Price, Power flow analysis of complex coupled systems by progressive approaches, *Journal of Sound and Vibration*, 239, 275–295, (2001).
- [117]Y.P. Xiong, J.T. Xing, W.G. Price, Interactive power flow characteristics of an integrated equipment nonlinear isolator travelling flexible ship excited by sea waves, *Journal of sound and vibration*, 287(1), 245-276, (2005).
- [118]C.M. Harris, A.G. Piersol, *Harris' Shock and Vibration Handbook*, The McGraw-Hill Companies, USA, (2002).

Appendices

Appendix I



ELASTOSIL® M 4644 A/B

RTV-2 SILICONE RUBBER / MOLD MAKING

Product description

Pourable, addition-curing, two-component silicone rubber that vulcanizes at room temperature.

Special features

- good flow
- fast and non-shrink cure at room temperature which can be accelerated considerably by the application of heat
- medium Shore A hardness (approx. 40)
- good transparency of the cured rubber
- high tear strength
- outstanding resistance to casting resins, particularly polyurethanes and epoxies, for very long service life of the molds

Application

High-performance silicone mold-making compound which is particularly suitable for reproducing models with undercuts in polyurethane or epoxy resins.

Main field of application:
Vacuum casting for rapid prototyping.

Processing

Important note:
The platinum catalyst is in component A.

Important:
A and B components may only be used together if they have the same batch number.

Comprehensive instructions are given in our leaflet "ELASTOSIL® - PROCESSING RTV-2 SILICONE

RUBBERS".

Detailed information on other mold-making compounds in the ELASTOSIL® M range is contained in our brochure "ELASTOSIL® M. Mold-Making Compounds For Maximum Precision".

Storage

The 'Best use before end' date of each batch is shown on the product label.

Storage beyond the date specified on the label does not necessarily mean that the product is no longer usable. In this case however, the properties required for the intended use must be checked for quality assurance reasons.

Additional information

Please visit our website www.wacker.com.

Safety notes

Components of the addition-curing grade ELASTOSIL® M 4644 A/B contain only constituents that over many years have proved to be neither toxic nor aggressive. Special handling precautions are therefore not required, i.e., only the general industrial hygiene regulations apply.

Comprehensive instructions are given in the corresponding Material Safety Data Sheets. They are available on request from WACKER subsidiaries or may be printed via WACKER web site <http://www.wacker.com>.

Product data

Typical general characteristics	Inspection Method	Value
Product data (uncured)		
Component A		
Color		translucent
Density at 23 °C		1,08 g/cm ³
Viscosity at 23 °C, after stirring	ISO 3219	70000 mPa s
Component B		
Color		colorless
Density at 23 °C		0,97 g/cm ³
Viscosity at 23 °C, after stirring	ISO 3219	500 mPa s
Product data (catalyzed A + B)		
Mix ratio (pbw)	A : B	10 : 1
Viscosity at 23 °C	ISO 3219	50000 mPa s
Pot life at 23 °C, up to 150000 mPa s		80 min
Cure time, tack-free		12 h
Product data (cured)		
Color		translucent
Density at 23 °C in water	ISO 2781	1,07 g/cm ³
Hardness Shore A	ISO 868	40
Tensile strength	ISO 37	5,50 N/mm ²
Elongation at break	ISO 37	400 %
Tear strength	ASTM D 624 B	> 25 N/mm
Linear shrinkage		≤ 0,1 %

Vulcanizate after 24 h at 23 °C

These figures are only intended as a guide and should not be used in preparing specifications.

Appendix II

SIGMA-ALDRICH[®]

sigma-aldrich.com

3050 Spruce Street, Saint Louis, MO 63103, USA

Website: www.sigmaaldrich.com

Email USA: techserv@sial.com

Outside USA: eurtechserv@sial.com

Product Specification

Product Name:
Silicone oil - viscosity 100 cSt (25 °C)

Product Number: 378364
CAS Number: 63148-62-9
MDL: MFCD00132673
Formula: (-Si(CH₃)₂O-)_n

TEST	Specification
Appearance (Color)	Colorless
Appearance (Form)	Viscous Liquid
Infrared spectrum	Conforms to Structure
Viscosity 95.0 - 105.0 cSt	

Specification: PRD.1.ZQ5.10000024985

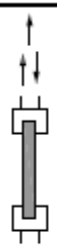
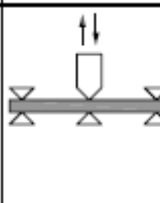
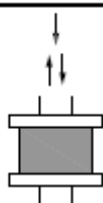
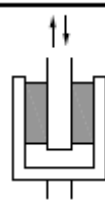
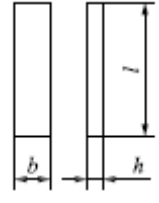
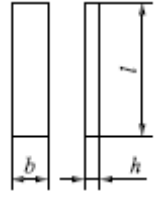
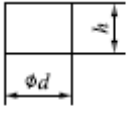
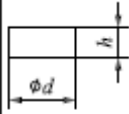
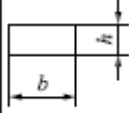
Appendix III

BS ISO 4664-1:2011
ISO 4664-1:2011(E)

7.5 Small-sized test apparatus

The basic principles of dynamic testing using a small-sized test apparatus and the forced-vibration non-resonance method are given in Table 2.

Table 2 — Test conditions and test pieces for small-sized test apparatus

		Mode of deformation				Comments
		Tension	Bending	Compression	Shear	
Type of test piece and mode of deformation (strain)						The bending method is usually applied to relatively stiff and inextensible materials such as rubber/fibre composite materials.
↑ and ↓ = Mean static strain ↑↓ = Dynamic strain						
Test piece shapes and dimensions		 $h = 1 \text{ mm to } 3 \text{ mm}$ $b = 4 \text{ mm to } 12 \text{ mm}$ $l = 20 \text{ mm to } 80 \text{ mm}$ The distance between holders is preferably 2,5 to 5 times the width b .	 The distance between the bending support points is preferably 16 times the thickness h . $h = 1 \text{ mm to } 3 \text{ mm}$	 $h:d = \text{about } 1:1,5$ $h = 1 \text{ mm to } 5 \text{ mm}$	 $d \geq 4h$ $h \leq 12 \text{ mm}$ Rectangular column  $b = \text{length of each side}$ $b \geq 4h$ $h \leq 12 \text{ mm}$	For the tension and bending methods, the measured dimensions of the test piece shall include the thickness, width, and distance between the grips or distance between the bending support points. For the compression and shear methods, they shall include the thickness, width, and diameter or lengths of the sides. Each dimensional tolerance shall be maintained to within $\pm 1\%$.
Test conditions	Mean strain, %	1 to 10	0	1 to 10	0	For bench analysis, values will depend on the machine parameters.
	Strain amplitude, %	$\pm 0,5, \pm 1, \pm 2$ Can also be a continuous scan				The maximum tolerance of the detector should preferably be within $\pm 1\%$.
	Frequency, Hz	1, 5, 10, 15, 30, 50, 100, 150, 200 Can also be a continuous scan				The maximum tolerance on the frequency shall be within $\pm 2\%$.
	Test temperature, °C	Select from ISO 23529, although smaller intervals can be necessary in transition regions where properties are changing rapidly. Can also be a continuous temperature scan. A rate of 1 °C/min is recommended.				The maximum tolerance of the detector should preferably be within $\pm 1\text{ °C}$.
Parameters required		M^* , M' , M'' , $\tan \delta$				For dynamic tests with small-sized apparatus, the effect of temperature is frequently depicted graphically.

Appendix IV

Energy Method (for loss angle determination)

This method uses the ratio of the area of the hysteresis loop and the area of an ellipse bounded by the force (load) and displacement amplitudes of the hysteresis loop, as shown below.

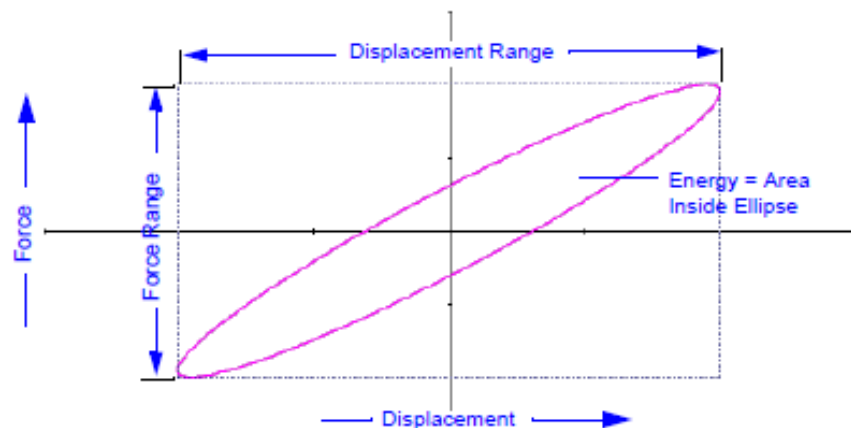


Figure 9-2. Hysteresis Loop with Ellipse Area (90° out-of-phase) - Energy Method

Using this method, WaveMatrix uses the following formula to calculate the loss angle:

$$\text{Loss Angle} = \text{Arcsine} \left(\frac{\text{energy}}{\pi \cdot \frac{\text{displacement range}}{2} \cdot \frac{\text{force range}}{2}} \right)$$

Where:

energy = the area enclosed by the hysteresis loop (integral of force with respect to displacement)



The measured waveforms must be sinusoidal otherwise the hysteresis loop will not be an ellipse as assumed.

The numerical integration used to calculate the energy term in this method reduces the effects of measurement noise and takes into account waveform distortion due to a nonlinear specimen or the presence of harmonics of the basic waveform frequency.

Appendix V

Experimental data for equivalent stiffness

KN/m	65 μm	130 μm	195 μm	260 μm	325 μm	390 μm
1Hz	223.2	204.9	195.8	192.2	189.1	185.0
5 Hz	242.3	214.5	204.9	200.6	197.3	192.7
10 Hz	241.8	222.1	210.7	205.8	201.4	197.3
20 Hz	252.7	229.2	217.8	213.3	208.4	203.6
30 Hz	253.2	231.0	219.8	214.6	209.0	204.1
40 Hz	255.8	233.0	221.7	215.3	210.3	205.4
50 Hz	256.1	234.6	222.4	216.6	211.2	206.1

Expectation of equivalent stiffness

KN/m	65 μm	130 μm	195 μm	260 μm	325 μm	390 μm
1Hz	229.9	213.1	200.5	191.9	187.5	187.2
5 Hz	234.8	218.0	205.3	196.8	192.4	192.1
10 Hz	240.1	223.3	210.6	202.1	197.7	194.4
20 Hz	248.1	231.3	218.6	210.1	205.7	205.4
30 Hz	252.6	235.8	223.1	214.6	210.2	209.9
40 Hz	253.6	236.8	224.1	215.6	210.2	210.9
50 Hz	251.1	234.3	221.7	213.1	208.7	208.4

Errors

%	65 μm	130 μm	195 μm	260 μm	325 μm	390 μm
1Hz	3.00	4.00	2.40	0.15	0.84	1.18
5 Hz	3.09	1.63	0.19	0.18	2.48	0.31
10 Hz	0.70	0.54	0.05	1.80	1.84	1.47
20 Hz	1.82	0.92	0.37	1.50	1.30	0.88
30 Hz	0.24	2.08	1.50	0	0.57	2.84
40 Hz	0.86	1.63	1.08	0.14	0.05	2.68
50 Hz	1.95	0.13	0.31	1.62	1.18	1.12

Experimental data for equivalent damping

KN·s/m	65 μm	130 μm	195 μm	260 μm	325 μm	390 μm
1Hz	4.446	3.728	3.349	3.198	2.947	2.669
5 Hz	1.136	0.927	0.826	0.759	0.698	0.657
10 Hz	0.625	0.541	0.492	0.447	0.419	0.395
20 Hz	0.285	0.247	0.228	0.206	0.199	0.178
30 Hz	0.158	0.137	0.129	0.117	0.106	0.099
40 Hz	0.109	0.103	0.086	0.078	0.071	0.066
50 Hz	0.064	0.055	0.048	0.042	0.036	0.032

Expectation of equivalent damping

KN·s/m	65 μm	130 μm	195 μm	260 μm	325 μm	390 μm
1Hz	4.458	3.890	3.415	3.031	2.739	2.539
5 Hz	1.138	1.005	0.901	0.793	0.714	0.654
10 Hz	0.588	0.532	0.484	0.446	0.417	0.397
20 Hz	0.297	0.269	0.245	0.226	0.211	0.191
30 Hz	0.166	0.147	0.131	0.118	0.108	0.102
40 Hz	0.119	0.105	0.093	0.083	0.076	0.071
50 Hz	0.070	0.059	0.050	0.042	0.036	0.032

Errors

%	65 μm	130 μm	195 μm	260 μm	325 μm	390 μm
1Hz	0.27	4.35	1.97	5.22	7.06	4.87
5 Hz	0.18	8.41	9.08	4.48	2.29	0.46
10 Hz	5.92	1.66	1.63	0.22	0.48	0.51
20 Hz	4.21	8.90	7.45	9.71	6.03	7.30
30 Hz	5.06	7.30	1.55	0.85	1.89	3.03
40 Hz	9.17	1.94	8.14	6.41	7.04	7.58
50 Hz	9.37	7.27	4.17	0	0	0